

Научном већу Института за физику Београд

ИНСТИТУТ ЗА ФИЗИКУ			
ПРИМЉЕНО: 06. 02. 2020			
Рад.јед.	б р о ј	Арх.шифра	Прилог
0801	157/2		

МОЛБА

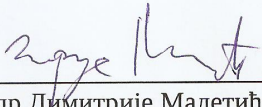
за покретање поступка реизбора у звање виши научни сарадник

Молим Научно веће Института за физику Београд да, у складу са Правилником о поступку, начину вредновања и квантитативном исказивању научноистраживачких резултата истраживача, покрене поступак за мој реизбор у звање виши научни сарадник.

У прилогу достављам:

1. Мишљење руководиоца лабораторије са предлогом комисије која ће писати извештај.
2. Стручну биографију.
3. Преглед научне активности.
4. Елементе за квалитативну анализу.
5. Елементе за квантитативну анализу.
6. Списак објављених радова и других публикација.
7. Податке о цитираности.
8. Копије објављених радова и других публикација.
9. Решење о претходном избору у звање.
10. Прилоге.

У Београду, 06. фебруара 2020.


др Димитрије Малетић
виши научни сарадник
Институт за физику Београд

ИНСТИТУТ ЗА ФИЗИКУ

ПРИМЉЕНО: 06. 02. 2020			
Рад.јед.	б р о	Арх.шифра	Прилог
0801	157/1		

Научном већу Института за физику Београд

Мишљење руководиоца лабораторије о reizбору др Димитрија Малетића у звање виши научни сарадник

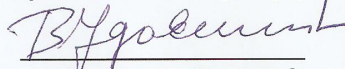
Др Димитрије Малетић је запослен у Нискофонској лабораторији за нуклеарну физику Института за физику Београд, Универзитета у Београду. Бави се истраживањима у областима физике космичког зрачења, физике високих енергија и нуклеарне физике. С обзиром да испуњава све предвиђене услове у складу са Правилником о поступку, начину вредновања и квантитативном исказивању научноистраживачких резултата истраживача МПНТР, сагласан сам са покретањем поступка за reizбор др Димитрија Малетића у звање виши научни сарадник.

За састав комисије за reizбор др Димитрија Малетића у звање виши научни сарадник предлагем:

1. Др Владимир Удовичић, виши научни сарадник, Институт за физику Београд.
2. Др Дејан Јоковић, виши научни сарадник, Институт за физику Београд.
3. Проф. др Марија Димитријевић Ђирић, ванредни професор, Физички Факултет Универзитета у Београду.

У Београду, 06. фебруара 2020.

Руководилац лабораторије



др Владимир Удовичић
виши научни сарадник
Институт за физику Београд

2. Стручна биографија кандидата

Димитрије Малетић је рођен 21.02.1976. године у Вуковару, р. Хрватска. Завршио је гимназију у Вуковару 1994. године. Основне студије на Физичком факултету Универзитета у Београду на смеру Теоријска и експериментална физика завршио је 2003. године одбранивши дипломски рад под насловом *“Температурска калибрација сензора за контролни систем CMS ECAL гејекџора”* под руководством проф. др Јована Пузовића. Запошљава се 1. маја 2004. године у Групи за физику елементарних честица Лабораторије за физику (010) Института за нуклеарне науке Винча. Уписује последипломске магистарске студије, и почиње сарадњу са колегама на експерименту CMS у CERN-у, у Женеви, Швајцарска. Магистрира 2006. године на Физичком факултету Универзитета у Београду са темом *„Монте Карло симулација CMS ECAL Preshower гејекџора и поређење са експерименталним резултатима“* под руководством проф. др Петра Аџића. Учествоје у пројекту основног истраживања у периоду 2006-2009 под називом *„Физика високих енергија на детектору CMS“* под руководством проф. др Петра Аџића. 25. 09. 2006. године је изабран у звање истраживач сарадник у Институту Винча. Наставак рада обележава и веће ангажовање у CMS колаборацији, што резултира израдом докторске дисертације под називом *„Редукација фона двофотонског канала распада Хигс бозона (SM) на гејекџору CMS“*, под руководством проф. др Петра Аџића, која је 2009. године одбрањена на Физичком факултету Универзитета у Београду, а која је уједно представљена и CMS колаборацији, и добила статус CERN-ове тезе. У периоду израде докторске тезе блиско је сарађивао са проф. др Аристотелисом Киријакисом из NCSR Демокритос из Института за Нуклеарну и честичну физику у Атини, Грчка, који долази из института које је више пута кандидат посећивао у периоду 2004-2010. Вреди поменути и то да знања о Монте Карло симулацијама, вештачким неуронским мрежама, програмирању и GRID окружењу добро усваја и успешно користи при изради магистарске и докторске тезе. 28.12.2009 изабран је у звање Научни сарадник у Институту Винча. Договорно напушта Институт Винча и CMS колаборацију и 1. маја 2010. године се запошљава у Нискофонској лабораторији за Нуклеарну физику, у Институту за физику Београд, Универзитета у Београду. Учествоје на пројекту основних истраживања МПНТР у периоду 2010-2019 под називом *„Нуклеарне методе истраживања ретких догађаја и космичког зрачења“* под руководством проф. др Иштвана Бикита. Започиње рад на физици космичког зрачења под руководством проф. др Ивана Аничина. Придружује се SHINE колаборацији у CERN-у 2011-2013 године. Започиње рад на проблематици радона под руководством др Владимира Удовичића као и проблематици заштите животне средине. Придружује се MICE колаборацији 2015- и предводи групу сарадника из Института за физику Београд на MICE експерименту у Радерфорд Аплетон лабораторији у Енглеској.

Научне теме којима се кандидат до сада бавио су физика високих и средњих енергија која укључује рад на експериментима CMS, SHINE и MPD/NICA, акцелераторска физика јонизационог хлађења на експерименту MICE, физика космичког зрачења, нуклеарна физика која укључује изучавање особина радиоактивног гаса радона (ИФ, IAEA) и изучавање фонског зрачења које долази од природне радиоактивности, а интерес има и за заштиту од зрачења и заштиту животне средине. По бази SCOPUS има 79 радова са 7142 цитата и х-индекс 30. По Google Scholar има 115 радова са укупно 15806 цитата и х-индекс 40, а по бази <http://inspirehep.net> број цитата искључујући самоцитате је 6,687 и х-индекс је 24. Био је ментор за израду докторске дисертације Михаила Савића, одбрањене 2019. године на Физичком факултету Универзитета у Београду.

3. Преглед научне активности

Научноистраживачка активност кандидата обухвата:

- физику високих енергија на детектору CMS,
- изучавања особина атомских језгара на средњим енергијама на експериментима SHINE и NICA,
- акцелераторска физика јонизационог хлађења на MICE експерименту,
- физика космичког зрачења,
- изучавање динамике радона и фонског зрачења
- заштита животне средине.

3.1. Физика високих енергија на детектору CMS

Др Димитрије Малетић се бави физиком на CMS експерименту у периоду од 2003. до 2009. године. Од самог почетка доприноси развоју софтверског пакета за анализу, Монте Карло симулације и реконструкцију експерименталних догађаја Електромагнетског калориметра (ECAL) комплексног детектора CMS који се градио на Великом хадронском сударачу LHC у CERN-у. Значајан део његовог рада сумиран је у докторској дисертацији. У првом делу дисертације, после уводних делова, презентовано је обједињење, анализу и поређење резултата свог сложеног симулационог програма Preshower детектора и резултата реалног експеримента. Успео је да развије, анализира ефикасност, оптимизује и имплементира алгоритам за сепарацију фотона и неутралних пиона, базиран на Вештачким неуронским мрежама, користећи резултате ECAL barrel-а. Анализира добијене резултате из Монте Карло симулација, тј. симулација одговора детектора на упадне честице продукване у протон-протон сударима, са нагласком на детекцију неутралних пиона и фотона, као и анализа до тада једино доступних реалних догађаја из мерења космичког зрачења. Даље је успео да допринесе каснијим анализама података развојем алгоритама као и развојем CMSSW – (симулационог софтвера CMS детектора) – развојем алгоритма читавања и унапређењем описа нове геометрије Preshower детектора. Имплементацијом алгоритма и својим активним учешћем успео је да допринесе званичним анализама двофотонског канала распада Хигс бозона предвиђеног Стандардним моделом. Учествовао је у мерењима протон-протон судара, тј. прикупљању података ECAL детектора, а касније и окидачког система целог CMS детектора. Поред тога, заједно са колегама из института “Democritos” из Атине, радио на адаптирању више генератора догађаја за коришћење при симулацији и анализи аномалних спрезања ($Z\gamma\gamma$) на детектору CMS који би служили за проверу могућности њиховог детектовања, као и помоћ при анализама ових сигнала. Др Димитрије Малетић је у току истраживачког рада на детектору CMS показао способност да потпуно самостално и на ефикасан и брз начин решава сложене проблеме и задатке као и да своје знање успева да у кратком року пренесе другим члановима CMS колаборације и Београдске CMS групе.

3.2 Изучавања особина атомских језгара на средњим енергијама на експериментима SHINE и NICA

Искуство кандидата у Физици високих енергија и рад на CMS експерименту увелико је разлог зашто се укључио у нови експеримент у CERN-у, SHINE (SPS Heavy Ion and Neutrino experiment), као заменик пуководиоца Београдске групе. Првенствено увидећи потребу млађих колега за помоћ при раду на симулацијама и анализама експерименталних резултата овог експеримента, доста је времена и труда уложио како би колегама помогао да се докажу у новој средини. Поред помоћи млађим колегама у анализама, првенствено K0 и делта++ резонантним сигнаlima са експеримента судара снопа са фиксном метом, веома брзо је преузео вођење званичне реконструкције свих података SHINE (NA61) детектора у грид окружењу. Треба напоменути и покретање компјутерског кластера за потребе NA61 експеримента и потребе симулација у Нискофонској лабораторији у Институту за физику Београд. Интерес у анализи је показивао првенствено за податке мете која је реплика мете T2K експеримента у Јапану, коју види као веза експеримента и истраживаче делатност др Димитрија Малетића у циљу унапређења знања процеса хадронизације која се користи и у симулацијама космичког зрачења, којима се доста бавио у Нискофонској лабораторији Института за физику. Интерес који је имао за експерименте изучавања особина атомских језгара, са нагласком на понашања језгара у близини confinement-а заинтересовао га је за проблематику изучавања кварк-глуон плазме, односно скенирање/употпуњавање графикона такозваних фазних прелаза језгара. Изучавање ове интересантне проблематике наставља радом на MPD детектору NICA сударача у Обједињеном Институту за Нуклеарна истраживања Дубна, Русија, где се укључио у развој софтвера за анализу сигнала електромагнетског калориметра (EMC). Првенствено учествује у развоју софтверских алата за истраживање физике неутралних мезона и промтних фотона који настају у сударима снопова тешких јона.

3.3 Акцелераторска физика јонизационог хлађења на MICE експерименту

Од 2015. године кандидат предводи групу истраживача из Нискофонске лабораторије за нуклеарну физику Института за физику Београд у раду на MICE-у (Muon Ionisation Cooling Experiment). Бавио се анализама губитка енергије миона у метама од течног водоника (LH2) и литијум-хидрида (LiH), на којима је највећи број експерименталних догађаја измерено, и која је у центру проблематике јонизационог хлађења снопа миона. Такође се кандидат бавио развојем софтвера, везано за Монте Карло симулације и реконструкцију мерених догађаја. Учествовао је у оптимизацији симулација проласка честица кроз акцелераторске сегменте. Радио је на развоју програма који омогућују званичну симулацију и реконструкцију догађаја у грид компјутерском систему. Радио је на преласку продукције на „проширење“ грид система ка робустнијем дистрибутивном систему коришћењем Singularity container images. Учествовао у мерењима на MICE експерименту. Кандидат је одговоран за званичну продукцију MICE колаборације тј. за симулацију и реконструкцију експерименталних података.

3.4 Физика космичког зрачења

Кандидат је непосредно након одбрањене докторске дисертације фокус свог истраживачког интересовања усмерио, и већ дао значајан допринос у области космичког зрачења. Треба истаћи да је рад на симулацијама Космичког зрачења помогао да се продубе сазнања о овој проблематици. Такође, развој софтвера за аутоматску обраду података континуалног мониторинга интензитета

космичког зрачења и приказивања података on-line, омогућило је да се Нискофонска лабораторија стави на мапу светских станица за мониторинг космичког зрачења.

3.5 Изучавање динамике радона и фонског зрачења

Кандидат је активно укључен у проблематику радијационе физике, прецизније у истраживања везана за проблематику радона и торона, као доминантних извора природне радио-активности. Примена мултиваријантних метода у анализи динамике радона дала је нове резултате у истраживању. Учествоје у првом испитивању концентрација радона у кућама и становима у Републици Србији 2015-2016, као и у испитивању концентрација радона у Школама у Републици Србији 2019, оба везана за Националне пројекте под руководством Директората за радијациону и нуклеарну сигурност и безбедност Србије, а под покровитељством Међународне агенције за атомску енергију са седиштем у Бечу. Учествоје у изради прве Радонске мапе Србије, као и при укључивању ове мапе у Европску радонску мапу. Предмет интересовања др Димитрија Малетића је такође и нискофонска гама спектроскопија. Развојем неопходног и оригиналног софвера за off-line анализу података, и упоредна симулација космичког зрачења и природне радиоактивности доводи до постављање Нискофонске лабораторије у лидерски положај у стручности у области ниско-енергетског природног фона као и у области проучавања варијабилности фона природне радиоактивности и космогеног фона. Бавио се и динамиком, варијабилношћу и симулацијом продукције космогених радионуклида у атмосфери и у земљишту.

3.6 Заштита животне средине

Примена мултиваријантних метода у анализи концентрација неких од најзаступљенијих радионуклида у животној средини; радона-222 и олова-210 као и космогеног берилијума-7 дале су добре резултате, и следећи корак је био да се ове методе примене у изучавању динамике и концентрација опасних једињења у животној средини. Добијени резултати усмеравају и охрабрују интезивирање ових истраживања.

4. Елементи за квалитативну анализу

4.1 Научни ниво и значај резултата, утицај научних радова

Од прошлог избора у звање научног сарадника кандидат је објавио два рада у категорији M21a, један рад у категорији M21, седам радова у категорији M22 и четири рада у категорији M23.

Као пет најзначајнијих радова кандидата од свих објављених радова могу се узети:

1. Stojic Andreja M, **Maletic Dimitrije M**, Stanisic-Stojic Svetlana M, Mijic Zoran R, Sostaric Andrej I, Forecasting of VOC emissions from traffic and industry using classification and regression multivariate methods, SCIENCE OF THE TOTAL ENVIRONMENT, vol. 521, br. , str. 19-26, 2015. цитиран 18 пута.
2. Forkapic Sofija M, **Maletic Dimitrije M**, Vasin Jovica R, Bikit Kristina I, Mrdja Dusan S, Bikit Istvan S, Udovicic Vladimir I, Banjanac Radomir M, Correlation analysis of the natural radionuclides in soil and indoor radon in Vojvodina, Province of Serbia, JOURNAL OF ENVIRONMENTAL RADIOACTIVITY, vol. 166, br. , str. 403-411, 2017. цитиран 17 пута

3. D.Barney, W.Bialas, P.Kokkas, N.Manthos, **D.Maletic**, I.Papadopoulos, A.Peisert, S.Reynaud, P.Vichoudis, Detection of muons at 150 GeV/c with a CMS Preshower Prototype, Nucl Instrum Meth A, 564, 126-133, 2006. цитиран 6 пута

4. R. Banjanac, **D. Maletić**, D. Joković, N. Veselinović, A. Dragić, V. Udovičić, I. Aničin, On the omnipresent background gamma radiation of the continuous spectrum, Nucl Instrum Meth A, 745, 7-11, 2014. цитиран 2 пута

5. Savic Mihailo R, Dragic Aleksandar L, **Maletic Dimitrije M**, Veselinovic Nikola B, Banjanac Radomir M, Jokovic Dejan R, Udovicic Vladimir I, A novel method for atmospheric correction of cosmic-ray data based on principal component analysis, ASTROPARTICLE PHYSICS, vol. 109, br. , str. 1-11, 2019. није цитиран

Први рад спада у рад кандидата на заштити животне средине. Рад се бави концентрацијама Volatile organic compounds (VOC) који у атмосферу бивају испуштани од извора као што су саобраћај и индустрија. Кандидат је радио на моделовању зависности концентрација ових једињења од атмосферских параметара коришћењем мултиваријантних метода, тј. регресионом мултиваријантном анализом, као и могућношћу предикције концентрације ових једињења. Мултиваријантне методе које су коришћене налазе се имплементирани у скуп програма TMVA (Toolkit for multivariate analysis) унутар ROOT програмског пакета популарног у анализи података у физици високих енергија.

У другом раду је кандидат користио исте мултиваријантне методе као у првом раду за анализу корелација и моделирања концентрација радонама у животним просторима у зависности од састава земљишта и концентрација радионуклида у земљишту, и резултати се поклапају са резултатима других европских земаља, првенствено Велике Британије, чија су истраживања имала много већи број експерименталних резултата.

Трећи рад представља рад на тестовима сноповима, у H4 експерименталној хали у Превесену у близини Женева, и то Preshower детектора, који је инсталиран у затварачки део електромагнетског калориметра CMS детектора. Кандидат се бавио развојем целокупног програма за Монте Карло симулацију модула за тестирање базирану на популарном Geant4 програмском пакету за симулацију интеракција честица са материјом. Такође се бавио поређењем експерименталних података и симулацијом. Овај рад је издвојен јер је кандидат показао велику самосталност у раду на почетку своје каријере у великој колаборацији CMS. Резултати ових тестова дали су значајне резултате за оптимизацију првенствено електронике, као и софтвера за реконструкцију депоноване енергије и локализацију удара честица у овај детектор.

Четврти рад представља интересантно истраживање нискоенергетског фона зрачења и декомпозицију на фон на фон који долази од радионуклида из земље и грађевинског материјала лабораторије, и који се одбија од зидове лабораторије у којем су вршена мерења, и на космогени фон. Мерења су вршена коришћењем оловом заштићеног, сем са горње стране, HPGe детектора. Овај рад представља и детаљну анализу “тврдоће” меке компоненте фона, коришћењем различитог броја танких абсорбера од лакних метала. Кандидат се бавио детаљном Монте Карло симулацијом и поређењем са експерименталним резултатима.

Пети рад је један од радова чије је резултате Михаило Савић укључио у своју докторску тезу. Кандидат је радио са докторантом на разматрању примене разних модерних мултиваријантних метода. Кандидат је такође радио на методама обраде података, софтверу за аквизицију, развоју база података и припреми експерименталних резултата који долазе од континуалног мониторинга флукса миона коришћењем пластичних сцинтилатора у Нискофонској лабораторији Института за физику Београд.

4.2 Параметри квалитета часописа сумарно

Укупан фактор утицаја (ИФ) свих радова кандидата је 227.4 а од претходног избора у звање 70.4.

Додатни библиометријски показатељи у вези са објављеним радовима кандидата од избора у претходно звање дати су у доњој табели. Она садржи импакт факторе (ИФ) радова, М бодове радова по српској категоризацији научноистраживачких резултата, као и импакт фактор нормализован по импакту цитирајућег чланка (СНИП). У табели су дате укупне вредности, као и вредности свих фактора усредњених по броју чланака и по броју аутора по чланку, за радове објављене у категоријама М20.

	ИФ	М	СНИП
Укупно	70.44	75	22.56
Усредњено по чланку	5.03	5.77	1.61
Усредњено по аутору	3.24	7.46	1.55

4.3 Награде

- Награда за најбољи постер међународна конференција РАД 2014.

У прилогу изглед странице са објављеним добитницима награда на сајту конференције.

- Иако не спада у награде, интересантно је поменути да кандидат има забележена достигнућа на сајту Research gate, и то да су током 9 недеља његове публикације биле најчитаније од свих аутора из институција р. Србије, и 40 недеља најчитаније публикације од аутора из Института за физику Београд.

У прилогу стилизована листа достигнућа на сајту Research gate.

4.4 Ангажованост у формирању научних кадрова

После избора у вишег научног сарадника:

- кандидат је био ментор Михаилу Савићу при изради докторске тезе на Физичком факултету, Универзитета у Београду, одбрањене 4. јула 2019. године.

У прилогу.

Пре избора у вишег научног сарадника:

- помагао је у изради теза - налази се поменут у захвалници докторских дисертација за: Дејана Јоковића, под називом: *“Детекција и спектроскопија миона из Космичког зрачења пластичним сцинтилационим детекторима”*, на Физичком факултету, Универзитета у Београду и Радомира Бањанца, под називом: *„Временски променеиве комбинације фона у Нискофонској њодземној лабораторији“* на Физичком факултету, Универзитета у Београду.

Био је ментор два одбрањена дипломска рада, (по старом систему – у еквиваленцији мастер рада) Радована Ковачевића и Биљане Савић на Физичком факултету, Универзитет у Београду.

2004.-2005. Држао је експерименталне вежбе из предмета: Физика језгра и честица.

2005.-2006. Држао је рачунске вежбе из предмета: Нуклеарна физика, Физика језгра и честица.

2007.-2008. Држао је рачунске вежбе из предмета: Нуклеарна физика, Физика језгра и честица и експерименталне вежбе из предмета: Нуклеарна физика

Ментор два матурска рада за ученике Математичке гимназије у Београду. Један од кандидата потом уписао Физички факултет у Београду.

Сарадња са Центром за таленте Земун. Ментор рада Наталије Ђорђевић, ученице 1 разреда Девете београдске гимназије, која је освојила 3. место на републичкој смотри за таленте 2014 године.

Радио је на популаризација науке

После избора у вишег научног сарадника:

20. новембар 2015. одржао је колоквијум на Департману за физику, ПМФ Нови Сад.
У прилогу.

Пре избора у вишег научног сарадника:

2008. Учешће на Фесивалу науке.

2009. и 2010. Члан локалног организационог комитета и предавач на Masterclass-у одржаном на Физичком факултету у Београду.

2009. Предавање по позиву о CERN-у на семинару за професоре физике, у Новом Саду.

2009. Предавање по позиву на скупу “CERN у Димитровграду”.

2009. “*Serbian and Montenegrin Teachers Programme 2009*”. Посета професора физике из Србије и Црне Горе CERN-у. Члан организационог одбора и предавач “*Physics with the CMS ECAL*”

2012. “Novi Sad University Students” посета студената Универзитета у Новом саду ЦЕРН-у. Водич посете CERN-овом компјутерском центру.

2010-2014. Посета професора Физике и студената Физичког факултета ИФ-у. Упознавање са Нискофонском лабораторијом.

2014 аутор текстова у часопису “Млади физичар”

4.5 Нормирање броја коауторских радова, патената и техничких решења

Сви радови са више од седам коаутора нормирани су у складу са Правилником.

Након нормирања према Правилнику, број М бодова које је кандидат остварио након претходног избора у звање са 114.5 смањује се на 80.08, а током каријере са 552.5 на 151.7.

Нормирање не утиче на значајан начин на број бодова за реизбор кандидата.

4.6 Руковођење пројектима, потпројектима и пројектним задацима

После избора у вишег научног сарадника:

- Води учешће сарадника Института за физику Београд у МІСЕ коалборацији, корисници Trans-nacionalni access fund, EuCARD2 део ЕУ програма FP7.

У прилогу.

- Руководи учешћем сарадника из Института за физику Београд у билатералном пројекту на експерименту MPD/NICA у Обједињеном институту за нуклеарна страживања у Дубни, Русија. Учешће финансирано од стране МПНТР, преко Заједничког комитета за сарадњу са ОИНИ Дубна и р. Србије, чији је кандидат члан задужен за сарадњу у области физике високих енергија.

У прилогу.

- Пројектни задатак израде радонске мапе Србије и обраду података за Европску мапу радона.

У прилогу.

Пре избора у вишег научног сарадника:

- 2011. Пројектни задатак покретања on-line обраде података континуалног мониторинга Београдске мионске станице.
- 2012. Пројектни задатак покретања компјутерског кластера добијеног на поклон од CERN-а на ИФ-у за потребе SHINE колаборације и Нискофонске лабораторије.

4.7 Активност у научним и научно-стручним друштвима

После избора у вишег научног сарадника:

2017- Члан Заједничког комитета за сарадњу са ОИНИ Дубна и р. Србије, задужен за сарадњу у области физике високих енергија

У прилогу.

Фебруар 2019 – Члан Joint MICE Experiment Management Office (МИМО)

У прилогу.

Рецензент је у међународним часописима: *Nuclear Technology and Radiation Protection, Fuel, Environmental Pollution, Atmospheric Pollution Research, Building and Environment*
У прилогу.

2017. Рецензирао је билатерални пројекат са Мађарском

Пре избора у вишег научног сарадника:

2012-2014. Представник Института за физику у одсеку Физике језгра, елементарних честица и основних интеракција одељења Друштва Физичара Србије за Научна истраживања и високо образовање (НИВО ДФС)

2012. Члан локалној организационој одбора једнодневне научне скупине одржане у згради САНУ њод називом: “100 година од ојкрића ајомској језира”.

Рецензент је у међународним часописима: *Nuclear Technology and Radiation Protection, Applied Radiation and Isotopes*

4.8 Конкретан допринос кандидата у реализацији радова у научним центрима у земљи и иностранству

2004-2010. Члан Београдске CMS групе. (Рад на експерименту CMS у CERN-у)

2011-2013. Члан Београдског SHINE тима (Рад на експерименту NA61 у CERN-у)

2015- Води учешће сарадника Института за физику Београд у MICE коалборацији.

2016-2017 Учесник билатералног пројекта са р. Белорусијом: RADON MAPS PREPARING AND DOSE ASSESSMENT OF THE PUBLIC EXPOSURE TO RADON IN BELARUS AND SERBIA

2018- Учесник у раду на IAEA регионалном пројекту: RER9153 – Enhancing the Regional Capacity to Control Long Term Risks to the Public due to Radon in Dwellings and Workplaces.

Активности везане за радон у Србији и регионале пројекте IAEA;

1. SRB/9/003 “Enhancing the Regulatory Infrastructure and Legislative System” Expert Mission to assist Serbia in designing a National Radon Survey. Belgrade, 2-4 February 2015
2. RER/9/136. “Reducing Public Exposure to Radon by Supporting the Implementation and Further Development of National Strategies” Expert Mission to assist Serbia On Measures To Reduce Radon Levels In Buildings. Belgrade, 15-16 November 2016
3. SRB/9/006 Planning and kick-off meeting. Belgrade, Serbia. 22nd February 2018
4. RER/9/153-1706076 "Enhancing the Regional Capacity to Control Long Term Risk to the Public due to Radon in Dwelings and Workplaces", Regional Workshop on Database and Statistical Analysis, Harmonization of Protocols and Procedures for the Measurement of Radon, Bosnia & Hercegovina, Sarajevo, 12-14 June 2018
5. RER9153 – Enhancing the Regional Capacity to Control Long Term Risks to the Public due to Radon in Dwellings and Workplaces: Regional Workshop on Development of Radon Maps and the Definition of Radon-Prone Areas (EVT1807175), Vilnius, Lithuania, 09-11 July 2019.

4.9 Уводна предавања на конференцијама и друга предавања

18. Septembar 2017 COOL 2017 conference in Gustav-Stresemann-Institut, Bonn

1) „Measurement of phase-space density evolution in MICE“. 50 минутно предавање.

2) „Recent results from MICE on multiple Coulomb scattering and energy loss“. 40 минутно предавање.

У прилогу.

Интересантно је поменути:

7. Mart 2017 - MICE Project Board Review, „Bulk production of Monte Carlo“

У прилогу.

5. Елементи за квантитативну анализу

Остварени резултати у периоду након одлуке Научног већа о предлогу за стицање претходног научног звања:

Категорија	М бодова по раду	Број радова	Укупно М бодова	Нормирани број М бодова
M21a	10	2	20	10.37
M21	8	1	8	0.3
M22	5	7	35	26.86
M23	3	4	12	7.15
M32	1.5	2	3	2.44
M33	1	28	28	25.72
M34	0.5	17	8.5	7.24

Поређење са минималним квантитативним условима за реизбор у звање виши научни сарадник (половина од минималног броја за избор у звање виши научни сарадник):

Минимални број М бодова		Остварено, М бодова без нормирања	Остварено, нормирани број М бодова
Укупно	25	114.5	80.08
M10+M20+M31+M32+M33+M41+M42+M90	20	106	72.84
M11+M12+M21a+M21+M22+M23	15	75	44

6. Списак објављених радова и других публикација

6.1 Радови у међународним часописима изузетних вредности (M21a)

Радови објављени након претходног избора у звање:

1. Bogomilov, M., Tsenov, R., Vankova-Kirilova, G.,..., Maletic, D.,..., *et al.* Demonstration of cooling by the Muon Ionization Cooling Experiment. *Nature* **578**, 53–59, 2020.
2. Stojic Andreja M, Maletic Dimitrije M, Stanisic-Stojic Svetlana M, Mijic Zoran R, Sostaric Andrej I, Forecasting of VOC emissions from traffic and industry using classification and regression multivariate methods, *SCIENCE OF THE TOTAL ENVIRONMENT*, vol. 521, br. , str. 19-26, 2015.

Радови објављени пре претходног избора у звање:

3. N. Abgrall, A. Aduszkiewicz, ..., D. Maletić, ..., W. Zipper, Measurements of production properties of K0S mesons and Λ hyperons in proton-carbon interactions at 31 GeV/c, *Phys Rev C*, 89, 025205, 2014.
4. Khachatryan V,...,Adzic Petar R, Djordjevic Milos P, Krpic Dragomir K, Maletic Dimitrije, Milosevic Jovan, Puzovic Jovan M, Measurement of the charge ratio of atmospheric muons with the CMS detector, *Phys Lett B*, 692, 83-104, 2010.
5. Chatrchyan S,...,Adzic Petar R,Djordjevic Milos P,Jovanovic Dragoslav,Krpic Dragomir K,Maletic Dimitrije,Puzovic Jovan M,Smiljkovic Nebojsa,..., Measurement of the muon stopping power in lead tungstate, *J Instrum*, 5, P03007, 2010.
6. Chatrchyan S,..., Adzic Petar R, Djordjevic Milos P, Jovanovic Dragoslav, Krpic Dragomir K, Maletic Dimitrije, Puzovic Jovan M, Smiljkovic Nebojsa, Alignment of the CMS silicon tracker during commissioning with cosmic rays, *J Instrum*, 5, T03009, 2010.
7. Chatrchyan S,...,Adzic Petar R,Djordjevic Milos P,Jovanovic Dragoslav,Krpic Dragomir K,Maletic Dimitrije,Puzovic Jovan M,Smiljkovic Nebojsa, Performance of the CMS cathode strip chambers with cosmic rays, *J Instrum*, 5, T03018, 2010.
8. Adzic Petar R, Almeida N, Andelin D, Anicin Ivan V,..., Djordjevic Milos P,..., Drndarevic Snezana L,..., Jovanovic Dragoslav,..., Krpic Dragomir K,..., Maletic Dimitrije,..., Milenovic Predrag,..., Puzovic Jovan M, Radiation hardness qualification of PbWO4 scintillation crystals for the CMS Electromagnetic Calorimeter, *J Instrum*, 5, P03010, 2010.
9. Chatrchyan S,..., Adzic Petar R, Djordjevic Milos P, Jovanovic Dragoslav, Krpic Dragomir K, Maletic Dimitrije, Puzovic Jovan M, Smiljkovic Nebojsa, Performance study of the CMS barrel resistive plate chambers with cosmic rays, *J Instrum*, 5, T03017, 2010
10. Chatrchyan S,..., Adzic Petar R, Djordjevic Milos P, Jovanovic Dragoslav, Krpic Dragomir K, Maletic Dimitrije, Puzovic Jovan M, Smiljkovic Nebojsa, Time reconstruction and performance of the CMS electromagnetic calorimeter, *J Instrum*, 5, T03011, 2010.

11. Chatrchyan S,..., Adzic Petar R, Djordjevic Milos P, Jovanovic Dragoslav, Krpic Dragomir K, Maletic Dimitrije, Puzovic Jovan M, Smiljkovic Nebojsa, Performance of CMS muon reconstruction in cosmic-ray events, J Instrum, 5, T03022, 2010.
12. Chatrchyan S,...,Adzic Petar R, Djordjevic Milos P, Jovanovic Dragoslav, Krpic Dragomir K, Maletic Dimitrije, Puzovic Jovan M, Smiljkovic Nebojsa, Performance of CMS hadron calorimeter timing and synchronization using test beam, cosmic ray, and LHC beam data, J Instrum, 5, T03013, 2010.
13. Chatrchyan S,..., Adzic Petar R, Djordjevic Milos P, Jovanovic Dragoslav, Krpic Dragomir K, Maletic Dimitrije, Puzovic Jovan M, Smiljkovic Nebojsa, Commissioning of the CMS High-Level Trigger with cosmic rays, J Instrum, 5, T03005 , 2010.
14. Chatrchyan S,..., Adzic Petar R, Djordjevic Milos P, Jovanovic Dragoslav, Krpic Dragomir K, Maletic Dimitrije, Puzovic Jovan M, Smiljkovic Nebojsa, Performance of the CMS drift-tube chamber local trigger with cosmic rays, J Instrum, 5, T03015, 2010.
15. Chatrchyan S,..., Adzic Petar R, Djordjevic Milos P, Jovanovic Dragoslav, Krpic Dragomir K, Maletic Dimitrije, Puzovic Jovan M, Smiljkovic Nebojsa,..., Milenovic Predrag, Commissioning and Performance of the CMS Pixel Tracker with Cosmic Ray Muons, J Instrum, 5, T03007, 2010.
16. Chatrchyan S,..., Adzic Petar R, Djordjevic Milos P, Jovanovic Dragoslav, Krpic Dragomir K, Maletic Dimitrije, Puzovic Jovan M, Smiljkovic Nebojsa, Performance of the CMS Level-1 trigger during commissioning with cosmic ray muons and LHC beams, J Instrum, 5, T03002, 2010.
17. Chatrchyan S,..., Adzic Petar R, Djordjevic Milos P, Jovanovic Dragoslav, Krpic Dragomir K, Maletic Dimitrije, Puzovic Jovan M, Smiljkovic Nebojsa,..., Milenovic Predrag, Calibration of the CMS drift tube chambers and measurement of the drift velocity with cosmic rays, J Instrum, 5, T03016, 2010.
18. Chatrchyan S,..., Adzic Petar R, Djordjevic Milos P, Jovanovic Dragoslav, Krpic Dragomir K, Maletic Dimitrije, Puzovic Jovan M, Smiljkovic Nebojsa, Precise mapping of the magnetic field in the CMS barrel yoke using cosmic rays, J Instrum, 5, T03021, 2010.
19. Chatrchyan S,..., Adzic Petar R, Djordjevic Milos P, Jovanovic Dragoslav, Krpic Dragomir K, Maletic Dimitrije, Puzovic Jovan M, Smiljkovic Nebojsa, Commissioning and performance of the CMS silicon strip tracker with cosmic ray muons, J Instrum, 5, T03008, 2010.
20. Chatrchyan S,...,Adzic Petar R, Djordjevic Milos P, Jovanovic Dragoslav, Krpic Dragomir K, Maletic Dimitrije, Puzovic Jovan M, Smiljkovic Nebojsa, Commissioning of the CMS experiment and the cosmic run at four tesla, J Instrum, 5,T03001, 2010.
21. Chatrchyan S,..., Adzic Petar R, Djordjevic Milos P, Jovanovic Dragoslav, Krpic Dragomir K, Maletic Dimitrije, Puzovic Jovan M, Smiljkovic Nebojsa, Performance of the CMS drift tube chambers with cosmic rays, J Instrum, 5, T03015, 2010.

22. Chatrchyan S,..., Adzic Petar R, Djordjevic Milos P, Jovanovic Dragoslav, Krpic Dragomir K, Maletic Dimitrije, Puzovic Jovan M, Smiljkovic Nebojsa, Identification and filtering of uncharacteristic noise in the CMS hadron calorimeter, *J Instrum*, 5, T03014, 2010.
23. Chatrchyan S,..., Adzic Petar R, Djordjevic Milos P, Jovanovic Dragoslav, Krpic Dragomir K, Maletic Dimitrije, Puzovic Jovan M, Smiljkovic Nebojsa, Performance and operation of the CMS electromagnetic calorimeter, *J Instrum*, 5, T03010, 2010.
24. Chatrchyan S,..., Adzic Petar R, Djordjevic Milos P, Jovanovic Dragoslav, Krpic Dragomir K, Maletic Dimitrije, Puzovic Jovan M, Smiljkovic Nebojsa, Alignment of the CMS muon system with cosmic-ray and beam-halo muons, *J Instrum*, 5, T03020, 2010.
25. Chatrchyan S,..., Adzic Petar R, Djordjevic Milos P, Jovanovic Dragoslav, Krpic Dragomir K, Maletic Dimitrije, Puzovic Jovan M, Smiljkovic Nebojsa, Aligning the CMS muon chambers with the muon alignment system during an extended cosmic ray run, *J Instrum*, 5, T03019, 2010.
26. Chatrchyan S,..., Adzic Petar R, Djordjevic Milos P, Jovanovic Dragoslav, Krpic Dragomir K, Maletic Dimitrije, Puzovic Jovan M, Smiljkovic Nebojsa, Performance of the CMS hadron calorimeter with cosmic ray muons and LHC beam data, *J Instrum*, 5, T03012, 2010.
27. Chatrchyan S,..., Adzic Petar R, Djordjevic Milos P, Jovanovic Dragoslav, Krpic Dragomir K, Maletic Dimitrije, Puzovic Jovan M, Smiljkovic Nebojsa, Fine synchronization of the CMS muon drift-tube local trigger using cosmic rays, *J Instrum*, 5, T03004, 2010.
28. Chatrchyan S,..., Adzic Petar R, Djordjevic Milos P, Jovanovic Dragoslav, Krpic Dragomir K, Maletic Dimitrije, Puzovic Jovan M, Smiljkovic Nebojsa,..., Milenovic Predrag, CMS data processing workflows during an extended cosmic ray run, *J Instrum*, 5, T03006, 2010.
29. Khachatryan V,..., Adzic Petar R, Djordjevic Milos P, Krpic Dragomir K, Maletic Dimitrije, Milosevic Jovan, Puzovic Jovan M, First Measurement of Bose-Einstein Correlations in Proton-Proton Collisions at $\sqrt{s}=0.9$ and 2.36 TeV at the LHC, *Phys Rev Lett*, 105, 032001, 2010.
30. ...,Adzic Petar R, Djordjevic Milos P, Krpic Dragomir K, Maletic Dimitrije, Milosevic Jovan Z, Puzovic Jovan M,..., Milenovic Predrag, Search for Dijet Resonances in 7 TeV pp Collisions at CMS, *Phys Rev Lett*, 105, 211801, 2010.
31. Khachatryan V,..., Adzic Petar R, Djordjevic Milos P, Krpic Dragomir K, Maletic Dimitrije, Milosevic Jovan, Puzovic Jovan M, Transverse-Momentum and Pseudorapidity Distributions of Charged Hadrons in pp Collisions at $\sqrt{s}=7$ TeV, *Phys Rev Lett*, 105, 022002, 2010.
32. David G. d'Enterria et al. (with D. Maletic) CMS Collaboration, CMS physics technical design report: Addendum on high density QCD with heavy ions, *J Phys G*, 34, 2307-2455, 2007.
33. G.L. Bayatian et al. (with D. Maletic) CMS Collaboration, CMS technical design report, volume II: Physics performance, *J Phys G*, 34, 995-1579, 2007.

6.2 Радови у врхунским међународним часописима (M21)

Радови објављени након претходног избора у звање:

34. Adams D,..., Jokovic Dejan R, ..., Maletic Dimitrije M, ..., Savic Mihailo R, ..., First particle-by-particle measurement of emittance in the Muon Ionization Cooling Experiment, EUROPEAN PHYSICAL JOURNAL C, vol. 79, br. 3, 2019.

Радови објављени пре претходног избора у звање:

35. R. Banjanac, A. Dragić, V. Udovičić, D. Joković, D. Maletić, N. Veselinović, M. Savić, Variations of gamma-ray background in the Belgrade shallow underground low-level laboratory, Appl Radiat Isotopes, 87, 70, 2014.

36. R. Banjanac, D. Maletić, D. Joković, N. Veselinović, A. Dragić, V. Udovičić, I. Aničin, On the omnipresent background gamma radiation of the continuous spectrum, Nucl Instrum Meth A, 745, 7-11, 2014.

37. N. Abgrall, O. Andreeva, ..., D. Maletić, ..., W. Zipper, NA61/SHINE facility at the CERN SPS: beams and detector system, J Instrum, 9, 06005, 2014.

38. M. Krmar, J. Hansman, N. Jovančević, N. Lalović, J. Slivka, D. Joković, D. Maletić, A method to estimate a contribution of Ge(n,n') reaction to the low-energy part of gamma spectra of HPGe detectors, Nucl Instrum Meth A, 709, 8-11, 2013.

39. Abgrall N,...,Grabez Bojana S,...,Maletic Dimitrije,...,Puzovic Jovan M,...,Savic Mihailo, Pion emission from the T2K replica target: Method, results and application, Nucl Instrum Meth A, 701, 99-114, 2013.

40. Khachatryan V,..., Adzic Petar R, Djordjevic Milos P, Krpic Dragomir K, Maletic Dimitrije, Milosevic Jovan, Puzovic Jovan M, Observation of long-range, near-side angular correlations in proton-proton collisions at the LHC, JHEP, 1009, 091, 2010.

41. Khachatryan V,...,Adzic Petar R, Djordjevic Milos P, Maletic Dimitrije, Puzovic Jovan M,..., Milenovic Predrag, Transverse-momentum and pseudorapidity distributions of charged hadrons in pp collisions at root s=0.9 and 2.36 TeV, JHEP, 1002, 041, 2010.

42. R. Adolphi et al. (with D. Maletic) CMS Collaboration, The CMS experiment at the CERN LHC, J Instrum 3, S08004, 2008.

43. P. Adzic et al.(with D. Maletic) CMS Electromagnetic Calorimeter Group, Intercalibration of the barrel electromagnetic calorimeter of the CMS experiment at start-up, J Instrum 3, P10007, 2008.

44. P. Adzic et al.(with D. Maletic) CMS Electromagnetic Calorimeter Group, Energy resolution of the barrel of the CMS electromagnetic calorimeter, J Instrum, 2, P04004, 2007.

45. D.Barney, W.Bialas, P.Kokkas, N.Manthos, D.Maletic, I.Papadopoulos, A.Peisert, S.Reynaud, P.Vichoudis, Detection of muons at 150 GeV/c with a CMS Preshower Prototype, Nucl Instrum Meth A, 564, 126-133, 2006.

46. P. Milenovic, J. Puzovic, D. Jovanovic, D. Maletic, G. Dissertori, P. Adzic, Performance of the CMS-ECAL Safety System for Super Modules SM0 and SM1, Nucl Instrum Meth A, 554, 427-436, 2005.

6.3 Радови у истакнутим међународним часописима (M22)

Радови објављени након претходног избора у звање:

47. Knezevic David, Jovancevic Nikola, Sukhovej Anatoly M, Dragic Aleksandar L, Mitsyna Ludmila V, Revay Zsolt, Stieghorst Christian, Stephan Oberstedt, Krmar Miodrag D, Arsenic Ilija D, Maletic Dimitrije M, Jokovic Dejan R. Study of gamma ray transitions and level scheme of Mn-56(25) using the Mn-55(25)(n(th),2 gamma) reaction, NUCLEAR PHYSICS A, vol. 992, 2019.

48. Savic Mihailo R, Dragic Aleksandar L, Maletic Dimitrije M, Veselinovic Nikola B, Banjanac Radomir M, Jokovic Dejan R, Udovicic Vladimir I, A novel method for atmospheric correction of cosmic-ray data based on principal component analysis, ASTROPARTICLE PHYSICS, vol. 109, br. , str. 1-11, 2019.

49. Savic Mihailo R, Veselinovic Nikola B, Dragic Aleksandar L, Maletic Dimitrije M, Jokovic Dejan R, Banjanac Radomir M, Udovicic Vladimir I, Rigidity dependence of Forbush decreases in the energy region exceeding the sensitivity of neutron monitors, ADVANCES IN SPACE RESEARCH, vol. 63, br. 4, str. 1483-1489, 2019.

50. Bogomilov M, ..., Jokovic Dejan R, Maletic Dimitrije M, Savic Mihailo R, ..., Lattice design and expected performance of the Muon Ionization Cooling Experiment demonstration of ionization cooling, PHYSICAL REVIEW ACCELERATORS AND BEAMS, vol. 20, br. 6, 2017.

51. Perisic Mirjana D, Maletic Dimitrije M, Stanisic-Stojic Svetlana M, Rajsic Slavica F, Stojic Andreja M, Forecasting hourly particulate matter concentrations based on the advanced multivariate methods, INTERNATIONAL JOURNAL OF ENVIRONMENTAL SCIENCE AND TECHNOLOGY, vol. 14, br. 5, str. 1047-1054, 2017.

52. Forkapic Sofija M, Maletic Dimitrije M, Vasin Jovica R, Bikit Kristina I, Mrdja Dusan S, Bikit Istvan S, Udovicic Vladimir I, Banjanac Radomir M, Correlation analysis of the natural radionuclides in soil and indoor radon in Vojvodina, Province of Serbia, JOURNAL OF ENVIRONMENTAL RADIOACTIVITY, vol. 166, br. , str. 403-411, 2017.

Радови објављени пре претходног избора у звање:

53. Dimitrije M. Maletić, Vladimir I. Udovičić, Radomir M. Banjanac, Dejan R. Joković, Aleksandar L. Dragić, Nikola B. Veselinović, Jelena Filipović, Correlative and multivariate analysis of increased radon concentration in underground laboratory, Radiation Protection Dosimetry, 162, 1-2, 148-151, 2014.
54. D. Maletić, V. Udovičić, R. Banjanac, D. Joković, A. Dragić, N. Veselinović, J. Filipović, Comparison of multivariate classification and regression methods for the indoor radon measurements, Nucl Technol Radiat, 29, 17-23, 2014.
55. V. Udovičić, J. Filipović, A. Dragić, R. Banjanac, D. Joković, D. Maletić, B. Grabež, N. Veselinović Daily and seasonal radon variability in the underground low-background laboratory in Belgrade, Serbia, Radiation Protection Dosimetry, doi: 10.1093/rpd/ncu109, 2014.
56. A. Dragić, V. Udovičić, R. Banjanac, D. Joković, D. Maletić, N. Veselinović, M. Savić, J. Puzović, I. Aničin, The new set-up in the Belgrade low-level and cosmic-ray laboratory, Nucl Technol Radiat, 26, 181-192, 2011.
57. Khachatryan V,..., Adzic Petar R, Djordjevic Milos P, Krpic Dragomir K, Maletic Dimitrije, Milosevic Jovan, Puzovic Jovan M,..., CMS tracking performance results from early LHC operation, Eur Phys J C, 70, 1165-1192, 2010.
58. Khachatryan V,...,Adzic Petar R, Djordjevic Milos P, Krpic Dragomir K, Maletic Dimitrije, Milosevic Jovan, Puzovic Jovan M,..., First measurement of the underlying event activity at the LHC with root s=0.9 TeV, Eur Phys J C, 70, 555-572, 2010.
59. S. Abdullin et al. (with D.Maletic) CMS HCAL/ECAL Collaborations, The CMS barrel calorimeter response to particle beams from 2 to 350 GeV/c, Eur Phys J C, 60, 359-373, 2009.
60. P. Adzic et al., (with D. Maletic) ECAL/CMS Collaboration, Results of the first performance tests of the CMS electromagnetic calorimeter, Eur Phys J C, 44S02, 1-10, 2006.

6.4 Радови у међународним часописима (M23)

Радови објављени након претходног избора у звање:

61. Asfandiyarov R,..., Maletic Dimitrije M,..., Savic Mihailo R,..., MAUS: the MICE analysis user software, JOURNAL OF INSTRUMENTATION, vol. 14, 2019.
62. Udovicic Vladimir I, Maletic Dimitrije M, Banjanac Radomir M, Jokovic Dejan R, Dragic Aleksandar L, Veselinovic Nikola B, Zivanovic Jelena Z, Savic Mihailo R, Forkapic Sofija M, Multiyear Indoor Radon Variability in a Family House - a Case Study in Serbia, NUCLEAR TECHNOLOGY & RADIATION PROTECTION, vol. 33, br. 2, str. 174-179. 2018.

63. Udovicic Vladimir I, Maletic Dimitrije M, Eremic-Savkovic Maja M, Pantelic Gordana K, Ujic Predrag N, Celikovic Igor T, Forkapic Sofija M, Nikezic Dragoslav R, Markovic Vladimir MM, Arsic Vesna, Ilic Jovana, First steps towards national radon action plan in Serbia, NUKLEONIKA, vol. 61, br. 3, str. 361-365, 2016.

64. Filipovic Jelena Z, Maletic Dimitrije M, Udovicic Vladimir I, Banjanac Radomir M, Jokovic Dejan R, Savic Mihailo R, Veselinovic Nikola B, The use of multivariate analysis of the radon variability in the underground laboratory and indoor environment, NUKLEONIKA, vol. 61, br. 3, str. 357-360, 2016.

Радови објављени пре претходног избора у звање:

65. Maletic Slavica B, Maletic Dimitrije, Petronijevic Ivan M, Dojcilovic Jablan R, Popovic Dusan M (2014) Dielectric and infrared properties of SrTiO₃ single crystal doped by 3d (V, Mn, Fe, Ni) and 4f (Nd, Sm, Er) ions, Chinese Physics B, 23, 026102, 2014.

66. V. Udovičić, N. Veselinović, D. Joksimović, R. Banjanac, D. Maletić, D. Joković, D. Lukić, Plasma focus studies in Serbia, Journal of Modern Physics, 5, 82-88, 2014.

67. R. Banjanac, V. Udovičić, A. Dragić, D. Joković, D. Maletić, N. Veselinović, B. Grabež, Daily variations of gamma-ray background and radon concentration, Romanian Journal of Physics, 58, S14-S21, 2013.

68. A. Dragić, I. Aničin, R. Banjanac, V. Udovičić, D. Joković, D. Maletić, J. Puzović, Forbush decreases – clouds relation in the neutron monitor era, Astrophysics and Space Science Transactions, 7, 315-318, 2011.

6.5 Предавања по позиву с међународних скупова штампана у изводу (M32)

Радови објављени након претходног избора у звање:

69. Vladimir Udovičić, Dimitrije Maletić, Maja Eremić Savković, Sofija Forkapić, From motivation through the national radon survey to European Indoor Radon Map, 2nd International Workshop on the European Atlas of Natural Radiation IWEANR 2017, Verbania, Italy, 6-9 November 2017.

70. Vladimir Udovičić, Dimitrije Maletić, Maja Eremić Savković, Gordana Pantelić, Predrag Ujić, Igor Čeliković, Sofija Forkapić, Dragoslav Nikezić, Vladimir Marković, Vesna Arsić, SAMPLING DESIGN OF THE FIRST NATIONAL INDOOR RADON SURVEY IN SERBIA, International Workshop on the European Atlas of Natural Radiation, Verbania, Italy, 9-13 November 2015.

6.6 Саопштења са међународних скупова штампана у целини (M33)

Радови објављени након претходног избора у звање:

71. Drielsma, F. and Maletic, D., Measurement of Phase Space Density Evolution in MICE, Proceedings, International Workshop on Beam Cooling and Related Topics (COOL'17): Bonn, Germany, September 18-22, 2018.

72. Vladimir Udovičić, Dimitrije Maletić, Aleksandar Dragić, Radomir Banjanac, Dejan Joković, Mihailo Savić, Nikola Veselinović, AN OVERVIEW OF THE RADON RESEARCH IN THE INSTITUTE OF PHYSICS BELGRADE, Proceedings of 11th Symposium of the Croatian Radiation Protection Association, Osijek, Croatia, April 5 - 7, 2017.
73. N. Veselinović A. Dragić, M. Savić, D. Maletić, D. Joković, R. Banjanac, V. Udovičić, Utilization of a shallow underground laboratory for studies of the energy dependent CR solar modulation, XXV European Cosmic Ray Symposium, Torino, Sept. 4-9, 2016.
74. M. Savic, A. Dragic, N. Veselinovic, V. Udovicic, R. Banjanac, D. Jokovic, D. Maletic, Effect of pressure and temperature corrections on muon flux variability at ground level and underground, XXV European Cosmic Ray Symposium, Torino, Sept. 4-9, 2016.
75. Ajtic Jelena V, Maletic Dimitrije M, Stratimirovic Djordje I, Blesic Suzana M, Nikolic Jelena D, Djurdjevic Vladimir S, Todorovic Dragana J, Predictability of Lead-210 in Surface Air Based on Multivariate Analysis, RAD 2015: THE THIRD INTERNATIONAL CONFERENCE ON RADIATION AND APPLICATIONS IN VARIOUS FIELDS OF RESEARCH, vol. , br. , str. 317-322, 2015.
76. Banjanac Radomir M, Udovicic Vladimir I, Jokovic Dejan R, Maletic Dimitrije M, Veselinovic Nikola B, Savic Mihailo R, Dragic Aleksandar L, Anicin Ivan V, Background Spectrum Characteristics of the HPGE Detector Long-Term Measurement in the Belgrade Low-Background Laboratory, RAD 2015: THE THIRD INTERNATIONAL CONFERENCE ON RADIATION AND APPLICATIONS IN VARIOUS FIELDS OF RESEARCH, vol. , br. , str. 151-153, 2015.
77. Maletic Dimitrije M, Banjanac Radomir M, Jokovic Dejan R, Udovicic Vladimir I, Dragic Aleksandar L, Savic Mihailo R, Veselinovic Nikola B, Correlative and Periodogram Analysis of Dependence of Continuous Gamma Spectrum in the Shallow Underground Laboratory on Cosmic Ray and Climate Variables, RAD 2015: THE THIRD INTERNATIONAL CONFERENCE ON RADIATION AND APPLICATIONS IN VARIOUS FIELDS OF RESEARCH, vol. , br. , str. 47-50, 2015.
78. Savic Mihailo R, Maletic Dimitrije M, Jokovic Dejan R, Veselinovic Nikola B, Banjanac Radomir M, Udovicic Vladimir I, Dragic Aleksandar L, Pressure and temperature effect corrections of atmospheric muon data in the Belgrade cosmic-ray station, 24TH EUROPEAN COSMIC RAY SYMPOSIUM (ECRS), vol. 632, 2015.
79. Veselinovic Nikola B, Dragic Aleksandar L, Maletic Dimitrije M, Jokovic Dejan R, Savic Mihailo R, Banjanac Radomir M, Udovicic Vladimir I, Anicin Ivan V, Cosmic Rays Muon Flux Measurements at Belgrade Shallow Underground Laboratory, EXOTIC NUCLEI AND NUCLEAR/PARTICLE ASTROPHYSICS (V). FROM NUCLEI TO STARS, vol. 1645, br. , str. 421-425, 2015.
80. V. Udovičić, D. Maletić, M. Eremić Savković, G. Pantelić, P. Ujić, I. Čeliković, S. Forkapić, D. Nikezić, V. M. Marković, V. Arsić, NATIONAL PROGRAMME FOR THE CONTROL OF PUBLIC EXPOSURE TO RADON IN SERBIA, V International Congress BIOMEDICINE AND GEOSCIENCES – INFLUENCE OF ENVIRONMENT ON HUMAN HEALTH, Hotel Crowne Plaza, Belgrade, March 3-4, 32-39, 2015.

81. N. Veselinović, A. Dragić, D. Maletić, D. Joković, M. Savić, R. Banjanac, V. Udovičić and I. Aničin, Cosmic rays muon flux measurements at Belgrade shallow underground laboratory, Exotic Nuclei and Nuclear/Particle Astrophysics (V). From Nuclei to Stars, 13–26 July 2014, Sinaia, Romania. AIP Conf. Proc. 1645, 421-425, 2015.

82. Dimitrije Maletić, Radomir Banjanac, Dejan Joković, Vladimir Udovičić, Aleksandar Dragić, Mihailo Savić, Nikola Veselinović, CORRELATIVE AND PERIODOGRAM ANALYSIS OF DEPENDENCE OF CONTINUOUS GAMMA SPECTRUM IN THE SHALLOW UNDERGROUND LABORATORY ON COSMIC RAY AND CLIMATE VARIABLES, PROCEEDINGS OF THIRD INTERNATIONAL CONFERENCE ON RADIATION AND DOSIMETRY IN VARIOUS FIELDS OF RESEARCH RAD2015, JUNE 8 – 12, 47-50, 2015.

83. Radomir Banjanac, Vladimir Udovičić, Dejan Joković, Dimitrije Maletić, Nikola Veselinović, Mihailo Savić, Aleksandar Dragić, Ivan Aničin, BACKGROUND SPECTRUM CHARACTERISTICS OF THE HPGE DETECTOR LONG-TERM MEASUREMENT IN THE BELGRADE LOW-BACKGROUND LABORATORY, PROCEEDINGS OF THIRD INTERNATIONAL CONFERENCE ON RADIATION AND DOSIMETRY IN VARIOUS FIELDS OF RESEARCH RAD2015, JUNE 8 – 12, 151-153, 2015.

Радови објављени пре претходног избора у звање:

84. Dimitrije Maletić, Jelena Ajtić, Vladimir Đurđević, Dragana Todorović, Jelena Nikolić, Radomir Banjanac, and Vladimir Udovičić, Multivariate analysis of climate variables, teleconnection indices and activities of Lead-210 and Beryllium-7 in surface air in Belgrade, Serbia, Proceedings - The Second International Conference on Radiation and Dosimetry in Various Fields of Research, RAD 2014, May 27-30, 2014, Niš, Serbia, pp. 13-16., 2014.

85. R. Banjanac, V. Udovičić, J. Filipović, D. Joković, D. Maletić, M. Savić, N. Veselinović, P.Kolarž, A. Dragić, Relation between daily gamma-ray background and radon variability in the underground low-level laboratory in Belgrade, Proceedings - The Second International Conference on Radiation and Dosimetry in Various Fields of Research, RAD 2014, May 27-30, 2014, Niš, Serbia, pp.99-102, 2014.

86. Vladimir Udovičić, Dimitrije Maletić, Radomir Banjanac, Dejan Joković, Bojana Grabež, Nikola Veselinović, Jelena Filipović, Comprehensive analysis of long-term variations of low radon concentration in underground laboratory, Proceedings - The Second International Conference on Radiation and Dosimetry in Various Fields of Research, RAD 2014, May 27-30, 2014, Niš, Serbia, pp.35-38, 2014.

87. R. Banjanac, A. Dragić, V. Udovičić, D. Joković, D. Maletić, N. Veselinović, M. Savić, Comparative study of gamma-ray background and radon concentration inside ground level and underground low-level laboratories, Proceedings of the VII Hungarian Radon Forum, Veszprém, Hungary p.9-12, 2013.

88. D. Joković, V. Udovičić, R. Banjanac, D. Maletić, A. Dragić, N. Veselinović, B. Grabež, J. Nikolov, A simple Monte Carlo simulation method for estimating radon induced background of germanium detectors, Proceedings of the VII Hungarian Radon Forum, Veszprém, Hungary p.95-97, 2013.

89. V. Udovičić, A. Dragić, R. Banjanac, D. Joković, D. Maletić, N. Veselinović, J. Filipović, Influence of ventilation systems on indoor radon variability, Proceedings of the VII Hungarian Radon Forum, Veszprém, Hungary p.179-183, 2013.
90. A. Dragić, I. Aničin, R. Banjanac, V. Udovičić, D. Joković, D. Maletić, M. Savić, N. Veselinović, J. Puzović, Neutrons produced by muons at 25 mwe, 23rd European Cosmic Ray Symposium, Moscow, Russia (2012); Journal of Physics: Conference Series, 409, 012054, 2013.
91. I. Aničin, D. Maletić, A. Dragić, R. Banjanac, D. Joković, N. Veselinović, V. Udovičić, M. Savić, J. Puzović, Stopped cosmic ray muons in plastic scintillators on the surface and at the depth of 25 m.w.e., 23rd European Cosmic Ray Symposium, Moscow, Russia (2012); Journal of Physics: Conference Series, 409, 012142, 2013.
92. D. Maletić, V. Udovičić, R. Banjanac, A. Dragić, D. Joković, M. Savić, N. Veselinović, J. Puzović, Semi-empirical simulation of natural background in underground laboratory, Proceedings of the 3rd International Conference on Environmental Protection, Veszprém, Hungary, p. 83-88, 2012
93. P. Adzic, F. Beaudette, G. Dissertori, R.G. Garrido, G. Leshev, A. Lister, D. Maletic, P. Milenovic, R. Ofierzynski, J. Puzovic, A. Sytin, S. Zelepoukine, The detector control system for the electromagnetic calorimeter of the CMS experiment at the LHC, 10th International Conference on Accelerator and Large Experimental Physics Control Systems (ICALPCS 2005), Geneva, Switzerland, Europhysics Conference Abstracts, 29J, MO3_4-10, 2005.

6.7 Саопштења са међународних скупова штампана у изводу (М34)

Радови објављени након претходног избора у звање:

94. Vladimir Udovičić, Nikola Veselinovic, Dimitrije Maletic, Radomir Banjanac, Aleksandar Dragic, Dejan Jokovic, Mihailo Savic, David Knezevic, Maja Eremic Savkovic, RADON VARIABILITY DUE TO FLOOR LEVEL IN THE TWO TYPICAL RESIDENTIAL BUILDINGS IN SERBIA, BOOK of ABSTRACTS, 3 rd International Conference "Radon in the Environment 2019" 27-31 May 2019, Kraków, Poland. 2019.
95. Maja Eremic-Savkovic, Vladimir Udovicic, Dimitrije Maletic, Aleksandar Djordjevic, PILOT STUDY ON MITIGATION SOLUTIONS FOR BUILDINGS WITH AN ELEVATED RADON LEVELS IN SERBIA, BOOK of ABSTRACTS, 3 rd International Conference "Radon in the Environment 2019" 27-31 May 2019, Kraków, Poland, 2019.
96. Vladimir Udovičić, Dimitrije Maletić, Maja Eremić Savković, Slađan Velinov, Bojana Spasić, Branko Markoski, FIRST SERBIAN INDOOR RADON MAP, III East European Radon Symposium TEERAS 2017, Sofia, Bulgaria, 15-19 May, 2017, Book of Abstracts 16. 2017.
97. Dimitrije Maletic, Vladimir Udovicic, Radomir Banjanac, Dejan Jokovic, Mihailo Savic, Nikola Veselinovic, Jelena Zivanovic, Aleksandar Dragic, Correlative, multivariate and periodicity analysis of the variations of low radon concentrations in an shallow underground laboratory, III East European Radon Symposium TEERAS 2017, Sofia, Bulgaria, 15-19 May, 2017, Book of Abstracts 48. 2017.

98. D. Maletic, V. Udovicic, M. E. Savkovic, G. Pantelic, P. Ujic, I. Celikovic, S. Forkapic, D. Nikezic, V. Markovic, V. Arsic, J. Ilic, REPRESENTATIVENESS OF THE FIRST NATIONAL INDOOR RADON SURVEY IN SERBIA, V. TERRESTRIAL RADIOISOTOPES IN ENVIRONMENT, International Conference on Environmental Protection, Veszprém-Hungary, May 17-20, (2016) Book of Abstracts, pp. 11, 2016.
99. D. Joković, R. Banjanac, D. Maletić, V. Udovičić, M. Keržlin, S. Stošić, M. Serdar, A STUDY ON RADIOACTIVITY OF ENVIRONMENTAL SAMPLES FROM THE VICINITY OF THE OBRENOVAC POWER PLANT, V. TERRESTRIAL RADIOISOTOPES IN ENVIRONMENT, International Conference on Environmental Protection, Veszprém-Hungary, May 17-20, (2016) Book of Abstracts, pp. 70, 2016.
100. Dimitrije Maletic, Dejan Jokovic, Radomir Banjanac, Vladimir Udovicic, Aleksandar Dragic, Nikola Veselinovic, Mihailo Savic, VARIATION OF MUON COSMIC RAY FLUX RECORDED BY BELGRADE COSMIC RAY STATION DURING DECEMBER 2015 AND COMPARISON WITH EUROPEAN NEUTRON FLUX MONITORS, BOOK OF ABSTRACTS OF FOURTH INTERNATIONAL CONFERENCE ON RADIATION AND DOSIMETRY IN VARIOUS FIELDS OF RESEARCH RAD2016, MAY 23 – 27, 306, 2016.
101. Dejan Joković, Nikola Veselinović, Radomir Banjanac, Dimitrije Maletić, Vladimir Udovičić, Mihailo Savić, Marija Keržlin, Slaviša Stošić, A STUDY ON NATURAL RADIOACTIVITY OF VARIOUS ENVIRONMENTAL SAMPLES FROM THE VICINITY OF THE OBRENOVAC POWER PLANT, BOOK OF ABSTRACTS OF FOURTH INTERNATIONAL CONFERENCE ON RADIATION AND DOSIMETRY IN VARIOUS FIELDS OF RESEARCH RAD2016, MAY 23 – 27, 429, 2016.
102. Vladimir Udovicic, Dimitrije Maletic, Maja Eremic Savkovic, Gordana Pantelic, Predrag Ujic, Igor Celikovic, Dragoslav Nikezic, Vladimir Markovic, Per Nilsson, Sofija Forkapic, Vesna Arsic, Jovana Ilic, FIRST NATIONAL INDOOR RADON SURVEY IN SERBIA, BOOK OF ABSTRACTS OF FOURTH INTERNATIONAL CONFERENCE ON RADIATION AND DOSIMETRY IN VARIOUS FIELDS OF RESEARCH RAD2016, MAY 23 – 27, 490, 2016.
103. Vladimir Udovicic, Dimitrije Maletic, Radomir Banjanac, Dejan Jokovic, Gordan Nisevic, Vesna Manic, Goran Manic, IN-FIELD INTERCOMPARISON INDOOR RADON MEASUREMENTS IN RADON-PRONE AREAS OF NISKA BANJA, SERBIA, BOOK OF ABSTRACTS OF FOURTH INTERNATIONAL CONFERENCE ON RADIATION AND DOSIMETRY IN VARIOUS FIELDS OF RESEARCH RAD2016, MAY 23 – 27, 497, 2016.
104. Vladimir Udovicic, Dimitrije Maletic, Maja Eremic Savkovic, Gordana Pantelic, Predrag Ujic, Igor Celikovic, Sofija Forkapic, Dragoslav Nikezic, Vladimir Markovic, Vesna Arsic, Jovana Ilic, Per Nilsson, Preliminary results of the first national indoor radon survey in Serbia, 8th Conference of Protection against Radon at Home and at Work, 12 - 14 of September 2016, Prague, Czech Republic, Book of Abstracts, pp. 61., 2016.
105. Vladimir Udovicic, Dimitrije Maletic, Jelena Zivanovic, Aleksandar Dragic, Radomir Banjanac, Dejan Jokovic, Sofija Forkapic, Long-term indoor radon measurements in a family house – a case study in Serbia, 8th Conference of Protection against Radon at Home and at Work, 12 - 14 of September 2016, Prague, Czech Republic, Book of Abstracts, pp. 79. 2016.

106. Jokovic, D., Maletic, D., Savic, M., Veselinovic, N., Banjanac, R., Udovicic, V., Dragic, A., Pressure and temperature correction of atmospheric muon data, 24th European Cosmic Ray Symposium, Kiel, Germany, September 1 - 5, 2014, Book of Abstracts, pp. 74., 2015.
107. Veselinovic, N., Dragic, A., Maletic, D., Jokovic, D., Savic, M., Banjanac, R., Udovicic, V., Anicin, I., Muon measurements at Belgrade shallow underground laboratory, 24th European Cosmic Ray Symposium, Kiel, Germany, September 1 - 5, 2014, Book of Abstracts, pp. 74., 2015.
108. Jelena Z. Filipović, Vladimir I. Udovičić, Dimitrije M. Maletić, Radomir M. Banjanac, Dejan R. Joković, Mihailo R. Savić, Nikola B. Veselinović, The Use of Multivariate Analysis and Modeling of the Radon Variation in Laboratory and Real Environment, 2nd INTERNATIONAL CONFERENCE „RADON in the ENVIRONMENT 2015”; KRAKÓW, POLAND, May 25-29. 2015, Book of Abstracts, pp. 66, 2015.
109. Vladimir Udovičić, Dimitrije Maletić, Maja Eremić Savković, Gordana Pantelić, Predrag Ujić, Sofija Forkapić, Nenad Stevanović, Vladimir M. Marković, Vesna Arsić, First Steps Towards a National Radon Action Plan in Serbia, 2nd INTERNATIONAL CONFERENCE „RADON in the ENVIRONMENT 2015”; KRAKÓW, POLAND, May 25-29. 2015, Book of Abstracts, pp. 75, 2015.
110. R. Banjanac, D. Joković, D. Maletić, V. Udovičić, N. Veselinović, M. Savić, A. Dragić, Long-term background measurements in the Belgrade low-level underground laboratory, 20th International Conference on Radionuclide Metrology and its Applications, June 8 – 11, 2015, Vienna, Austria, Book of Abstracts, pp. P-161., 2015.

Радови објављени пре претходног избора у звање:

111. D. Joković, R. Banjanac, D. Maletić, V. Udovičić, N. Veselinović, B. Grabež, A GEANT4 based method to estimate radon concentration inside lead castle of shielded germanium detectors, Book of Abstracts - The Second International Conference on Radiation and Dosimetry in Various Fields of Research, RAD 2014, May 27-30, 2014, Niš, Serbia, p. 246, 2014.
112. N. Veselinović, D. Maletić, D. Joković, R. Banjanac, V. Udovičić, M. Savić, J. Puzović, I.V. Aničin, A. Dragić, Some peculiarities of digital γ -ray spectroscopy with germanium detectors performed in presence of neutrons, GAMMA-2, Scientific Workshop on Nuclear Fission Dynamics and the Emission of Prompt Neutrons and Gamma Rays; Book of Abstracts p30, 2013.
113. R. Banjanac, A. Dragić, V. Udovičić, D. Joković, D. Maletić, N. Veselinović, M. Savić, Variations of gamma-ray background in the Belgrade shallow underground low-level laboratory, 19th International Conference on Radionuclide Metrology and its Applications, Antwerp, Belgium; Book of Abstracts p142, 2013.
114. V. Udovičić, J. Filipović, A. Dragić, R. Banjanac, D. Joković, D. Maletić, B. Grabež, Daily radon variability in the underground low-background laboratory in Belgrade, Serbia, 7th International Conference on Protection Against Radon at Home and at Work, Prague; Czech Republic, Book of Abstracts, p122, 2013.

115. V. Udovičić, A. Dragić, R. Banjanac, D. Joković, D. Maletić, B. Grabež, J. Filipović, Effects of the air conditioning system usage on the indoor radon variability, 7th International Conference on Protection Against Radon at Home and at Work, Prague; Czech Republic, Book of Abstracts, p70, 2013.

116. R. Banjanac, V. Udovičić, A. Dragić, D. Joković, D. Maletić, N. Veselinović, J. Puzović, Correlation of daily variation between gamma-ray background and radon concentration, 1st East European Radon Symposium, Cluj-Napoca, Romania; Book of Abstracts, p94, 2012.

Нема ИФ

Радови објављени пре претходног избора у звање:

117. K. Karafasoulis, A. Kyriakis and D. Maletic, *Neutral Pion rejection for isolated and unconverted photon candidates using CMS ECAL and Preshower detector*, CMS Analysis Note 2008/036, 2008.

6.8 Саопштења са скупова националног значаја штампана у целини (M63)

Радови објављени након претходног избора у звање:

118. Vladimir UDOVIČIĆ, Dimitrije MALETIĆ, Aleksandar DRAGIĆ, Radomir BANJANAC, Dejan JOKOVIĆ, Nikola VESELINOVIĆ, Mihailo SAVIĆ, David KNEZEVIĆ, Maja EREMIĆ-SAVKOVIĆ, DISTRIBUCIJA KONCENTRACIJE RADONA PO SPRATNOSTI STAMBENIH ZGRADA, XXX SIMPOZIЈUM ДЗЗСЦГ Дивчибаре 2- 4. октобар 2019. године, 2019.

119. Mihailo SAVIĆ, Vladimir UDOVIČIĆ, Dimitrije MALETIĆ, Aleksandar DRAGIĆ, Radomir BANJANAC, Dejan JOKOVIĆ, Nikola VESELINOVIĆ i David KNEZEVIĆ, PROCENA TEMPERATURSKOG PROFILA ATMOSFERE NA OSNOVU DETEKTOVANOG FLUKSA KOSMIČKIH MIJONA, XXX SIMPOZIЈUM ДЗЗСЦГ Дивчибаре 2- 4. октобар 2019. године, 2019.

120. Vladimir UDOVIČIĆ, Dimitrije MALETIĆ, Aleksandar DRAGIĆ, Radomir BANJANAC, Dejan JOKOVIĆ i Sofija FORKAPIĆ, STUDIЈA SLUČAJA SEZONSKE VARIЈACIЈE KONCENTRACIЈE RADONA U PORODIČNOЈ KUĆI U SRBIЈI, XXIX SIMPOZIЈUM DRUŠTVA ZA ZAŠTITU OD ZRAČENЈA SRBIЈE I CRNE GORE, Srebrno jezero, Srbija, 27.-29. Septembar 2017, Zbornik radova 179-182., 2017.

121. Sofija FORKAPIĆ, Dimitrije MALETIĆ, Jovica VASIN, Kristina BIKIT, Dušan MRĐA, Ištvan BIKIT, Vladimir UDOVIČIĆ, Radomir BANJANAC, KORIŠĆENЈE MULTIVARIЈANTNE ANALIZE ZA PREDVIĐANЈE GEOGENOG RADONSKOG POTENCIЈALA, XXIX SIMPOZIЈUM DRUŠTVA ZA ZAŠTITU OD ZRAČENЈA SRBIЈE I CRNE GORE, Srebrno jezero, Srbija, 27.-29. Septembar 2017, Zbornik radova 210-218., 2017.

122. Владимир УДОВИЧИЋ, Александар ДРАГИЋ, Радомир БАЊАНАЦ, Дејан ЈОКОВИЋ, Димитрије МАЛЕТИЋ, Никола ВЕСЕЛИНОВИЋ, Михаило САВИЋ, Давид КНЕЖЕВИЋ, НИСКОФОНСКА ЛАБОРАТОРИЈА ИНСТИТУТА ЗА ФИЗИКУ - ПРВИХ ДВАДЕСЕТ ГОДИНА, XXIX СИМПОЗИЈУМ ДРУШТВА ЗА ЗАШТИТУ ОД ЗРАЧЕЊА СРБИЈЕ И ЦРНЕ ГОРЕ, Сребрно језеро, Србија, 27.-29. Септембар 2017, Зборник радова 429-437. 2017.

123. Dimitrije MALETIĆ, Vladimir UDOVIČIĆ, Dejan JOKOVIĆ, Radomir BANJANAC, Aleksandar DRAGIĆ, Mihailo SAVIĆ, Nikola VESELINOVIĆ, MONTE KARLO SIMULACIJA FONА HPGE DETEKTORA OD RADIONUKLIDA, KOSMIČKOG I SKYSHINE ZRAČENJA. XXIX SIMPOZIЈUM DRUŠTVA ZA ZAŠTITU OD ZRAČENJA SRBIЈE I CRNE GORE, Srebarno jezero, Srbija, 27.-29. Septembar 2017, Zbornik radova 438-442. 2017.

124. Dimitrije MALETIĆ, Dejan JOKOVIĆ, Radomir BANJANAC, Nikola VESELINOVIĆ, Mihailo SAVIĆ, Aleksandar DRAGIĆ, Vladimir UDOVIČIĆ, KORIŠĆENJE MOBILNOG TELEFONA ZA TESTIRANJE I OPTIMIZACIJU LABORATORIJSKIH MERENJA FOTOMULTIPLIKATORIMA. XXVIII Simpozijum DZZSCG, Vršac, Zbornik radova (2015) 589-593, 2015.

125. Dimitrije MALETIĆ, Dejan JOKOVIĆ, Mihailo SAVIĆ, Aleksandar DRAGIĆ, Radomir BANJANAC, Vladimir UDOVIČIĆ, Nikola VESELINOVIĆ, AUTOMATSKA OBRADA PODATAKA KOSMIKE I EVALUACIЈA KONCENTRACIЈE RADONA NA INTERNET (WEB) SERVERU, XXVIII Simpozijum DZZSCG, Vršac, Zbornik radova (2015) 584-588. 2015.

126. Dimitrije MALETIĆ, Nikola VESELINOVIĆ, Dejan JOKOVIĆ, Vladimir UDOVIČIĆ, Radomir BANJANAC, Mihailo SAVIĆ, Aleksandar DRAGIĆ, MONTE KARLO SIMULACIЈA KREIRANJA KOSMOGENIH RADIONUKLIDA U LESU. XXVIII Simpozijum DZZSCG, Vršac, Zbornik radova (2015) 481-486, 2015.

127. Jelena FILIPOVIĆ, Vladimir UDOVIČIĆ, Dimitrije MALETIĆ, Radomir BANJANAC, Dejan JOKOVIĆ, Mihailo SAVIĆ, Nikola VESELINOVIĆ, KORELACIONA I REGRESIONA ANALIZA VARIЈABILNOSTI RADONA PRIMENOM MULTIVARIЈANTNIH METODA, XXVIII Simpozijum DZZSCG, Vršac, Zbornik radova (2015) 254-259, 2015.

128. Mihailo SAVIĆ, Dimitrije MALETIĆ, Dejan JOKOVIĆ, Nikola VESELINOVIĆ, Aleksandar DRAGIĆ, Radomir BANJANAC, Vladimir UDOVIČIĆ, ODREĐIVANJE TEMPERATURSKOG PROFILA ATMOSFERE MERENJEM INTENZITETA KOSMIČKOG ZRAČENJA NA POVRŠINI ZEMLJE, XXVIII Simpozijum DZZSCG, Vršac, Zbornik radova (2015) 577-583, 2015.

129. Radomir BANJANAC, Vladimir UDOVIČIĆ, Jelena FILIPOVIĆ, Dejan JOKOVIĆ, Dimitrije MALETIĆ, Gordan NIŠEVIĆ, KORELACIЈA VARIЈACIЈA FONА GAMA ZRAČENJA I RADONA U NISKOFONSKOЈ PODZEMNOЈ LABORATORIЈI U BEOGRADU, XXVIII Simpozijum DZZSCG, Vršac, Zbornik radova (2015) 248-253, 2015.

130. Radomir BANJANAC, Aleksandar DRAGIĆ, Vladimir UDOVIČIĆ, Dejan JOKOVIĆ, Dimitrije MALETIĆ, Nikola VESELINOVIĆ, Mihailo SAVIĆ. GLEDANJE U KUGLU-25 GODINA POSLE, XXVIII Simpozijum DZZSCG, Vršac, Zbornik radova (2015) 548-554, 2015.

131. Vladimir UDOVIČIĆ, Mihailo SAVIĆ, Dejan JOKOVIĆ, Dimitrije MALETIĆ, Radomir BANJANAC, Nikola VESELINOVIĆ, Marina ŽIKIĆ, MERENJE KONCENTRACIЈE RADONA I

PROCENA IZLOŽENOSTI U BOGOVINSKOJ PEĆINI, XXVIII Simpozijum DZZSCG, Vršac, Zbornik radova (2015) 207-211, 2015.

132. Vladimir UDOVIČIĆ, Dimitrije MALETIĆ, Maja EREMIĆ SAVKOVIĆ, Gordana PANTELIĆ, Predrag UJIĆ, Igor ČELIKOVIĆ, Sofija FORKAPIĆ, Dragoslav NIKEZIĆ, Vladimir MARKOVIĆ, Vesna ARSIĆ, Jovana ILIĆ, NACIONALNI PROGRAM MERENJA RADONA U SRBIJI, XXVIII Simpozijum DZZSCG, Vršac, Zbornik radova (2015) 173-180, 2015.

Радови објављени пре претходног избора у звање:

133. V. Udovičić, J. Filipović, A. Dragić, R. Banjanac, D. Joković, D. Maletić, B. Grabež, Z.S. Žunić, Merenje niskih koncentracija radona u podzemnoj niskofonskoj laboratoriji u Zemunu, XII Kongres fizičara Srbije, Vrnjačka Banja, Zbornik radova, p457-460, 2013.

134. V. Udovičić, N. Veselinović, A. Dragić, R. Banjanac, D. Joković, D. Maletić, D. Joksimović, Zavisnost prinosa neutrona od pritiska radnog gasa u uređaju plazma fokus, XII Kongres fizičara Srbije, Vrnjačka Banja, Zbornik radova, p260-263, 2013.

135. J. Puzović, B. Grabež, D. Maletić, D. Joković, M. Savić, D. Manić, NA61/SHINE eksperiment i detektorski sistem, XII Kongres fizičara Srbije, Vrnjačka Banja, Zbornik radova, p244-247, 2013.

136. D. Maletić, V. Udovičić, R. Banjanac, A. Dragić, D. Joković, N. Veselinović, B. Grabež, M. Savić, J. Puzović, I. Aničin, Semi-empirijska simulacija prirodnog fona u podzemnoj laboratoriji, XII Kongres fizičara Srbije, Vrnjačka Banja, Zbornik radova, p228-231, 2013.

137. D. Maletić, A. Dragić, R. Banjanac, D. Joković, N. Veselinović, V. Udovičić, B. Grabež, M. Savić, J. Puzović, I. Aničin, Polarizacija miona kosmičkog zračenja na površini Zemlje i u podzemnoj laboratoriji, XII Kongres fizičara Srbije, Vrnjačka Banja, Zbornik radova, p224-227, 2013.

138. D. Maletić, A. Dragić, R. Banjanac, D. Joković, N. Veselinović, V. Udovičić, B. Grabež, M. Savić, J. Puzović, I. Aničin, Paket programa za spektralnu i vremensku analizu podataka u digitalnoj nuklearnoj i spektroskopiji kosmičkog zračenja, XII Kongres fizičara Srbije, Vrnjačka Banja, Zbornik radova, p220-223, 2013.

139. A. Dragić, D. Maletić, D. Joković, R. Banjanac, N. Veselinović, V. Udovičić, I. Aničin, Vreme života miona kosmičkog zračenja zaustavljenih u olovu, XII Kongres fizičara Srbije, Vrnjačka Banja, Zbornik radova, p201-203, 2013.

140. A. Dragić, D. Maletić, R. Banjanac, D. Joković, V. Udovičić, B. Grabež, N. Veselinović, M. Savić, J. Puzović, I. Aničin, Produkcija neutrona mionima iz kosmičkog zračenja na dubini od 25 m.w.e, XII Kongres fizičara Srbije, Vrnjačka Banja, Zbornik radova, p197-200, 2013.

141. A. Dragić, D. Maletić, R. Banjanac, D. Joković, V. Udovičić, B. Grabež, N. Veselinović, M. Savić, J. Puzović, I. Aničin, Indeks devijacije DTR i kosmički zraci, XII Kongres fizičara Srbije, Vrnjačka Banja, Zbornik radova, p193-196, 2013.

142. A. Dragić, N. Veselinović, D. Maletić, D. Joković, R. Banjanac, V. Udovičić, I. Aničin, O vezi između intenziteta kosmičkog zračenja i klime na Zemlji, XII Kongres fizičara Srbije, Vrnjačka Banja, Zbornik radova, p189-192, 2013.
143. R. Banjanac, D. Maletić, D. Joković, N. Veselinović, A. Dragić, V. Udovičić, I. Aničin, O svuda prisutnom fonskom zračenju kontinuirang spektra, XII Kongres fizičara Srbije, Vrnjačka Banja, Zbornik radova, p181-184, 2013.
146. R. Banjanac, A. Dragić, V. Udovičić, D. Joković, D. Maletić, N. Veselinović, M. Savić, B. Grabež, I. Aničin, J. Puzović, Varijacije radona i kosmičkog zračenja kao izvori vremenske varijacije fona gama zračenja u niskofonskoj gama spektrometriji, XII Kongres fizičara Srbije, Vrnjačka Banja, Zbornik radova, p177-180, 2013.
147. D. Maletić, D. Joković, R. Banjanac, A. Dragić, V. Udovičić, N. Veselinović, I. Aničin, Kompozicija kosmičkog zračenja zaustavljenog u veto detektorima, XXVII Simpozijum DZZSCG, Vrnjačka Banja, Zbornik radova, p394-397, 2013.
148. D. Maletić, A. Dragić, D. Joković, R. Banjanac, V. Udovičić, N. Veselinović, I. Aničin Spektralna i vremenska analiza u digitalnoj spektroskopiji – razvoj softvera i primeri, XXVII Simpozijum DZZSCG, Vrnjačka Banja, Zbornik radova, p390-393, 2013.
149. V. Udovičić, A. Dragić, R. Banjanac, D. Joković, D. Maletić, B. Grabež, J. Filipović. Korelaciona analiza uticaja atmosfere na varijaciju koncentracije radona u različitim sredinama XXVII Simpozijum DZZSCG, Vrnjačka Banja, Zbornik radova, p171-174, 2013.
150. V. Udovičić, D. Maletić, A. Dragić, R. Banjanac, D. Joković, N. Veselinović, J. Filipović Primena različitih metoda u analizi vremenskih serija koncentracije radona, XXVII Simpozijum DZZSCG, Vrnjačka Banja, Zbornik radova, p167-170, 2013.
151. D. Joković, J. Nikolov, R. Banjanac, V. Udovičić, D. Maletić, A. Dragić, B. Grabež, Monte Karlo simulacija za procenu radonske aktivnosti unutar olovne zaštite germanijumskih detektora, XXVII Simpozijum DZZSCG, Vrnjačka Banja, Zbornik radova, p143-146, 2013.
152. R. Banjanac, A. Dragić, V. Udovičić, D. Joković, D. Maletić, N. Veselinović, I. Aničin, Kompozicija niskoenergijskog dela fonskog spektra gama zračenja u nadzemnoj i podzemnoj niskofonskoj laboratoriji, XXVII Simpozijum DZZSCG, Vrnjačka Banja, Zbornik radova, p126-129, 2013.
153. R. Banjanac, A. Dragić, V. Udovičić, D. Joković, D. Maletić, N. Veselinović, I. Aničin, Vremenski promenljive komponente fona gama zračenja i merenje malih aktivnosti, XXVII Simpozijum DZZSCG, Vrnjačka Banja, Zbornik radova, p122-125, 2013.
154. D. Maletić, R. Banjanac, A. Dragić, D. Joković, V. Udovičić, J. Puzović, Semiempirijska simulacija prirodnog fona sendvič detektora, XXVI Simpozijum DZZSCG, Tara, Zbornik radova, p335-339, 2011.
155. D. Joković, R. Banjanac, V. Udovičić, A. Dragić, D. Maletić, N. Veselinović, I. Aničin, Monte Karlo simulacija apsolutne efikasnosti detekcije od 46.5 keV za određivanje koncentracije Pb-210 u

postojećoj olovnoj zaštiti HPGe detektora, XXVI Simpozijum DZZSCG, Tara, Zbornik radova, p311-315, 2011.

156. V. Udovičić, A. Dragić, R. Banjanac, D. Joković, B. Grabež, Z.S. Žunić, Periodičnost koncentracije radona u niskofonskoj podzemnoj laboratoriji u Beogradu, XXVI Simpozijum DZZSCG, Tara, Zbornik radova, p155-159, 2011.

157. Đorđević M., Lazić D., Maletić D., Adžić P.R., Particle identification in the combined test beam ECAL/HCAL of the CMS detector using Cherenkov counters in the experimental line H2 at CERN, Journal of Research in Physics, 31/2, 48-51, 2007

158. Maletić D., Creation and distribution of 'Monarc' files during the 'LoadTest07' exercise within the CMS experiment, Journal of Research in Physics, 31/2, 52-56, 2007

159. Maletić D., Đorđević M., Adžić P.R., Algorithmic XML geometry description of the CMS ECAL Preshower detector, Journal of Research in Physics, 31/2, 44-47, 2007

160. Maletić D., Đorđević M., Adžić P.R., Aničin I.V., Drndarević S., Jovanović D., Krpić D., Milenović P., Puzović J., Background reduction of two photon Higgs decay based on unconverted photon reconstruction in the central part of the ECAL of CMS detector, Journal of Research in Physics, 31/2, 40-43, 2007

161. Adžić P.R., Aničin V., Đorđević M., Drndarević S., Krpić D., Maletić D., Milenović P., Jovanović D., Puzović J., Smiljković N., The CMS experiment and participation of the CMS Belgrade group, Journal of Research in Physics, 31/2, 16-21, 2007

6.9 магистарске и докторске тезе (М 70)

М 71

Радови објављени пре претходног избора у звање:

162. 2009. докторирао на Физичком Факултету Универзитета у Београду са темом:
“*Редуција фона двофотонског канала распада $H_{i\bar{i}}$ бозона (СМ) на гејекџору CMS*”

М 72

Радови објављени пре претходног избора у звање:

163. 2006. магистрирао на Физичком Факултету Универзитета у Београду са темом: “*Мониторинг Карло симулација CMS ECAL Preshower гејекџора и поређење са експерименталним резултатима*”

7. Подаци о цитираности кандидата

По бази SCOPUS кандидат има 79 радова са 7142 цитата и х-индекс 30.
SCOPUS: <https://www.scopus.com/authid/detail.uri?authorId=15728244200>

По Google Scholar има 115 радова са укупно 15806 цитата и х-индекс 40,
Google Scholar: <https://scholar.google.com/citations?user=zdY0NXwAAAAJ&hl=en>

а по бази <http://inspirehep.net> број цитата искључујући самоцитате је 6,687 и х-индекс је 24.



Generated on 2020-02-07

74 papers found, 68 of them citeable (published or arXiv)

Citation summary results	Citeable papers	Citeable papers excluding self cites	Citeable papers excluding RPP	Published only	Published only excluding self cites	Published only excluding RPP
Total number of papers analyzed:	68	68	68	52	52	52
Total number of citations:	13723	6687	13723	12789	6030	12789
Average citations per paper:	201.8	98.3	201.8	245.9	116	245.9
Breakdown of papers by citations:						
Renowned papers (500+)	4	4	4	3	3	3
Famous papers (250-499)	3	2	3	3	2	3
Very well-known papers (100-249)	7	3	7	7	3	7
Well-known papers (50-99)	13	5	13	13	5	13
Known papers (10-49)	19	21	19	18	21	18
Less known papers (1-9)	11	20	11	4	14	4
Unknown papers (0)	11	13	11	4	4	4
hHEP index [?]	31	24	31	30	23	30

Bogomilov, M., Tsenov, R., Vankova-Kirilova, G. *et al.* Demonstration of cooling by the Muon Ionization Cooling Experiment. *Nature* **578**, 53–59 (2020). <https://doi.org/10.1038/s41586-020-1958-9>

<https://www.nature.com/articles/s41586-020-1958-9>

Часопис забрањује дистрибуцију pdf-а или копија рада у наредних 6 месеци. Рад може да се преузме као Open access.

The screenshot shows a web browser displaying the article page on the Nature website. At the top, there is a cookie consent banner. Below it is the Nature logo and navigation icons for Search, E-alert, Submit, and Login. The article title is "Demonstration of cooling by the Muon Ionization Cooling Experiment", published on 05 February 2020. It is an Open Access article. The abstract begins with "The use of accelerated beams of electrons, protons or ions has furthered the development of nearly every scientific discipline. However, high-". On the right side, there is a "Download PDF" button, "Associated Content" section with a link to "Muon colliders come a step closer" by Robert D. Ryne, and a "Sections" menu with options for "Abstract", "High-quality muon beams", and "MICE cooling apparatus".

Demonstration of cooling | Open Access | Published: 05 February 2020

Demonstration of cooling by the Muon Ionization Cooling Experiment

MICE collaboration

Nature **578**, 53–59(2020) | [Cite this article](#)

145 Altmetric | [Metrics](#)

Abstract

The use of accelerated beams of electrons, protons or ions has furthered the development of nearly every scientific discipline. However, high-

[Download PDF](#)

Associated Content

Nature | News & Views

Muon colliders come a step closer

Robert D. Ryne

Sections

- [Abstract](#)
- [High-quality muon beams](#)
- [MICE cooling apparatus](#)



ScienceDirect



Outline



Get Access

Share

Export



Advanced

Science of The Total Environment

Volumes 521–522, 15 July 2015, Pages 19-26

Forecasting of VOC emissions from traffic and industry using classification and regression multivariate methods

Andreja Stojić^a  , Dimitrije Maletić^a  , Svetlana Stanišić Stojić^b  , Zoran Mijić^a  , Andrej Šoštarić^c  [Show more](#)<https://doi.org/10.1016/j.scitotenv.2015.03.098>[Get rights and content](#)

Highlights

- Receptor models were applied for the purpose of VOC source apportionment.
- MVA methods were used for forecasting contributions from traffic and industry.
- Forecast was based on inorganic pollutant concentrations and meteorological data.
- Predicted values were consistent with the results of receptor modeling.
- The highest forecast accuracy was achieved with relative error of only 6%.



First particle-by-particle measurement of emittance in the Muon Ionization Cooling Experiment

MICE Collaboration

D. Adams¹⁵, D. Adey^{25,34}, R. Asfandiyarov¹³, G. Barber¹⁸, A. de Bari⁶, R. Bayes¹⁶, V. Bayliss¹⁵, R. Bertoni⁴, V. Blackmore^{18,a}, A. Blondel¹³, J. Boehm¹⁵, M. Bogomilov¹, M. Bonesini⁴, C. N. Booth²⁰, D. Bowring²⁵, S. Boyd²², T. W. Bradshaw¹⁵, A. D. Bross²⁵, C. Brown^{15,23}, G. Charnley¹⁴, G. T. Chatzitheodoridis^{16,21}, F. Chignoli⁴, M. Chung¹⁰, D. Cline³⁰, J. H. Cobb¹⁹, D. Colling¹⁸, N. Collomb¹⁴, P. Cooke¹⁷, M. Courthold¹⁵, L. M. Cremaldi²⁸, A. DeMello²⁶, A. J. Dick²¹, A. Dobbs¹⁸, P. Dornan¹⁸, F. Drielsma¹³, K. Dumbell¹⁴, M. Ellis²³, F. Filthaut^{11,32}, P. Franchini²², B. Freemire²⁷, A. Gallagher¹⁴, R. Gamet¹⁷, R. B. S. Gardener²³, S. Gourlay²⁶, A. Grant¹⁴, J. R. Greis²², S. Griffiths¹⁴, P. Hanlet²⁷, G. G. Hanson²⁹, T. Hartnett¹⁴, C. Heidt²⁹, P. Hodgson²⁰, C. Hunt¹⁸, S. Ishimoto⁹, D. Jokovic¹², P. B. Jurj¹⁸, D. M. Kaplan²⁷, Y. Karadzhev¹³, A. Klier²⁹, Y. Kuno⁸, A. Kurup¹⁸, P. Kyberd²³, J.-B. Lagrange¹⁸, J. Langlands²⁰, W. Lau¹⁹, D. Li²⁶, Z. Li³, A. Liu²⁵, K. Long¹⁸, T. Lord²², C. Macwaters¹⁵, D. Maletic¹², B. Martlew¹⁴, J. Martyniak¹⁸, R. Mazza⁴, S. Middleton¹⁸, T. A. Mohayai²⁷, A. Moss¹⁴, A. Muir¹⁴, I. Mullacrane¹⁴, J. J. Nebrensky²³, D. Neuffer²⁵, A. Nichols¹⁵, J. C. Nugent¹⁶, A. Oates¹⁴, D. Orestano⁷, E. Overton²⁰, P. Owens¹⁴, V. Palladino⁵, M. Palmer²⁴, J. Pasternak¹⁸, V. Pec²⁰, C. Pidcott^{22,33}, M. Popovic²⁵, R. Preece¹⁵, S. Prestemon²⁶, D. Rajaram²⁷, S. Ricciardi¹⁵, M. Robinson²⁰, C. Rogers¹⁵, K. Ronald²¹, P. Rubinov²⁵, H. Sakamoto^{8,31}, D. A. Sanders²⁸, A. Sato⁸, M. Savic¹², P. Snopok²⁷, P. J. Smith²⁰, F. J. P. Soler¹⁶, Y. Song², T. Stanley¹⁵, G. Stokes¹⁴, V. Suezaki²⁷, D. J. Summers²⁸, C. K. Sung¹⁰, J. Tang², J. Tarrant¹⁵, I. Taylor²², L. Tortora⁷, Y. Torun²⁷, R. Tsenov¹, M. Tucker¹⁴, M. A. Uchida¹⁸, S. Virostek²⁶, G. Vankova-Kirilova¹, P. Warburton¹⁴, S. Wilbur²⁰, A. Wilson¹⁵, H. Witte²⁴, C. White¹⁴, C. G. Whyte²¹, X. Yang³⁰, A. R. Young²¹, M. Zisman²⁶

¹ Department of Atomic Physics, St. Kliment Ohridski University of Sofia, Sofia, Bulgaria

² Institute of High Energy Physics, Chinese Academy of Sciences, Beijing, China

³ Sichuan University, Chengdu, China

⁴ Dipartimento di Fisica G. Occhialini, Sezione INFN Milano Bicocca, Milan, Italy

⁵ Sezione INFN Napoli and Dipartimento di Fisica, Università Federico II, Complesso Universitario di Monte S. Angelo, Naples, Italy

⁶ Sezione INFN Pavia and Dipartimento di Fisica, Pavia, Italy

⁷ INFN Sezione di Roma Tre and Dipartimento di Matematica e Fisica, Università Roma Tre, Rome, Italy

⁸ Department of Physics, Graduate School of Science, Osaka University, Toyonaka, Osaka, Japan

⁹ High Energy Accelerator Research Organization (KEK), Institute of Particle and Nuclear Studies, Tsukuba, Ibaraki, Japan

¹⁰ UNIST, Ulsan, Korea

¹¹ Nikhef, Amsterdam, The Netherlands

¹² Institute of Physics, University of Belgrade, Belgrade, Serbia

¹³ DPNC, Section de Physique, Université de Genève, Geneva, Switzerland

¹⁴ STFC Daresbury Laboratory, Daresbury, Cheshire, UK

¹⁵ STFC Rutherford Appleton Laboratory, Harwell Oxford, Didcot, UK

¹⁶ School of Physics and Astronomy, The University of Glasgow, Kelvin Building, Glasgow, UK

¹⁷ Department of Physics, University of Liverpool, Liverpool, UK

¹⁸ Blackett Laboratory, Department of Physics, Imperial College London, London, UK

¹⁹ Department of Physics, University of Oxford, Denys Wilkinson Building, Oxford, UK

²⁰ Department of Physics and Astronomy, University of Sheffield, Sheffield, UK

²¹ SUPA and the Department of Physics, University of Strathclyde, Glasgow, UK

²² Department of Physics, University of Warwick, Coventry, UK

²³ Brunel University, Uxbridge, UK

²⁴ Brookhaven National Laboratory, Upton, NY, USA

²⁵ Fermilab, Batavia, IL, USA

²⁶ Lawrence Berkeley National Laboratory, Berkeley, CA, USA

²⁷ Illinois Institute of Technology, Chicago, IL, USA

²⁸ University of Mississippi, Oxford, MS, USA

²⁹ University of California, Riverside, CA, USA

³⁰ University of California, Los Angeles, CA, USA

³¹ Current address: RIKEN, Wako, Japan

³² Also at Radboud University, Nijmegen, The Netherlands

³³ Current address: Department of Physics and Astronomy, University of Sheffield, Sheffield, UK

³⁴ Current address: Institute of High Energy Physics, Chinese Academy of Sciences, Beijing, China

Received: 31 October 2018 / Accepted: 11 February 2019 / Published online: 21 March 2019

© The Author(s) 2019

Abstract The Muon Ionization Cooling Experiment (MICE) collaboration seeks to demonstrate the feasibility of ionization cooling, the technique by which it is proposed to cool the muon beam at a future neutrino factory or muon collider. The emittance is measured from an ensemble of muons assembled from those that pass through the experiment. A pure muon ensemble is selected using a particle-identification system that can reject efficiently both pions and electrons. The position and momentum of each muon are measured using a high-precision scintillating-fibre tracker in a 4 T solenoidal magnetic field. This paper presents the techniques used to reconstruct the phase-space distributions in the upstream tracking detector and reports the first particle-by-particle measurement of the emittance of the MICE Muon Beam as a function of muon-beam momentum.

1 Introduction

Stored muon beams have been proposed as the source of neutrinos at a neutrino factory [1,2] and as the means to deliver multi-TeV lepton-antilepton collisions at a muon collider [3,4]. In such facilities the muon beam is produced from the decay of pions generated by a high-power proton beam striking a target. The tertiary muon beam occupies a large volume in phase space. To optimise the muon yield for a neutrino factory, and luminosity for a muon collider, while maintaining a suitably small aperture in the muon-acceleration system requires that the muon beam be ‘cooled’ (i.e., its phase-space volume reduced) prior to acceleration. An alternative approach to the production of low-emittance muon beams through the capture of $\mu^+\mu^-$ pairs close to threshold in electron-positron annihilation has recently been proposed [5]. To realise the luminosity required for a muon collider using this scheme requires the substantial challenges presented by the accumulation and acceleration of the intense positron beam, the high-power muon-production target, and the muon-capture system to be addressed.

D. Cline, M. Zisman: Deceased.

^a e-mail: v.blackmore@imperial.ac.uk

A muon is short-lived, with a lifetime of $2.2\ \mu\text{s}$ in its rest frame. Beam manipulation at low energy ($\leq 1\ \text{GeV}$) must be carried out rapidly. Four cooling techniques are in use at particle accelerators: synchrotron-radiation cooling [6]; laser cooling [7–9]; stochastic cooling [10]; and electron cooling [11]. In each case, the time taken to cool the beam is long compared to the muon lifetime. In contrast, ionization cooling is a process that occurs on a short timescale. A muon beam passes through a material (the absorber), loses energy, and is then re-accelerated. This cools the beam efficiently with modest decay losses. Ionization cooling is therefore the technique by which it is proposed to increase the number of particles within the downstream acceptance for a neutrino factory, and the phase-space density for a muon collider [12–14]. This technique has never been demonstrated experimentally and such a demonstration is essential for the development of future high-brightness muon accelerators or intense muon facilities.

The international Muon Ionization Cooling Experiment (MICE) has been designed [15] to perform a full demonstration of transverse ionization cooling. Intensity effects are negligible for most of the cooling channels conceived for the neutrino factory or muon collider [16]. This allows the MICE experiment to record muon trajectories one particle at a time. The MICE collaboration has constructed two solenoidal spectrometers, one placed upstream, the other downstream, of the cooling cell. An ensemble of muon trajectories is assembled offline, selecting an initial distribution based on quantities measured in the upstream particle-identification detectors and upstream spectrometer. This paper describes the techniques used to reconstruct the phase-space distributions in the spectrometers. It presents the first measurement of the emittance of momentum-selected muon ensembles in the upstream spectrometer.

2 Calculation of emittance

Emittance is a key parameter in assessing the overall performance of an accelerator [17]. The luminosity achieved by a collider is inversely proportional to the emittance of the colliding beams, and therefore beams with small emittance are required.

A beam travelling through a portion of an accelerator may be described as an ensemble of particles. Consider a beam that propagates in the positive z direction of a right-handed Cartesian coordinate system, (x, y, z) . The position of the i^{th} particle in the ensemble is $\mathbf{r}_i = (x_i, y_i)$ and its transverse momentum is $\mathbf{p}_{Ti} = (p_{xi}, p_{yi})$; \mathbf{r}_i and \mathbf{p}_{Ti} define the coordinates of the particle in transverse phase space. The normalised transverse emittance, ε_N , of the ensemble approximates the volume occupied by the particles in four-dimensional phase space and is given by

$$\varepsilon_N = \frac{1}{m_\mu} \sqrt[4]{\det \mathcal{C}}, \tag{1}$$

where m_μ is the rest mass of the muon, \mathcal{C} is the four-dimensional covariance matrix,

$$\mathcal{C} = \begin{pmatrix} \sigma_{xx} & \sigma_{xp_x} & \sigma_{xy} & \sigma_{xp_y} \\ \sigma_{xp_x} & \sigma_{p_x p_x} & \sigma_{yp_x} & \sigma_{p_x p_y} \\ \sigma_{xy} & \sigma_{yp_x} & \sigma_{yy} & \sigma_{yp_y} \\ \sigma_{xp_y} & \sigma_{p_x p_y} & \sigma_{yp_y} & \sigma_{p_y p_y} \end{pmatrix}, \tag{2}$$

and $\sigma_{\alpha\beta}$, where $\alpha, \beta = x, y, p_x, p_y$, is given by

$$\sigma_{\alpha\beta} = \frac{1}{N-1} \left(\sum_i^N \alpha_i \beta_i - \frac{(\sum_i^N \alpha_i)(\sum_i^N \beta_i)}{N} \right), \tag{3}$$

and N is the number of muons in the ensemble.

The MICE experiment was operated such that muons passed through the experiment one at a time. The phase-space coordinates of each muon were measured. An ensemble of muons that was representative of the muon beam was assembled using the measured coordinates. The normalised transverse emittance of the ensemble was then calculated by evaluating the sums necessary to construct the covariance matrix, \mathcal{C} , and using Eq. 1.

3 The Muon Ionization Cooling Experiment

The muons for MICE came from the decay of pions produced by an internal target dipping directly into the circulating proton beam of the ISIS synchrotron at the Rutherford Appleton Laboratory (RAL) [18, 19]. The burst of particles resulting from one target dip is referred to as a ‘spill’. A transfer line of nine quadrupoles, two dipoles and a superconducting ‘decay solenoid’ selected a momentum bite and transported the beam into the experiment [20]. The small fraction of pions that remained in the beam were rejected during analysis using the time-of-flight hodoscopes, TOF0 and TOF1, and Cherenkov counters that were installed in the MICE Muon Beam line upstream of the cooling experiment [21, 22]. A ‘diffuser’ was installed at the upstream end of the experiment to vary the initial emittance of the beam by introducing a changeable amount of tungsten and brass, which are high- Z materials, into the beam path [20].

A schematic diagram of the experiment is shown in Fig. 1. It contained an absorber/focus-coil module sandwiched between two spectrometer-solenoid modules that provided a uniform magnetic field for momentum measurement. The focus-coil module had two separate windings that were operated with the same, or opposed, polarities. A lithium-hydride or liquid-hydrogen absorber was placed at the centre of the focus-coil module. An iron Partial Return Yoke (PRY) was installed around the experiment to contain the field produced by the solenoidal spectrometers (not shown in Fig. 1). The PRY was installed at a distance from the beam axis such that its effect on the trajectories of particles travelling through the experiment was negligible.

The emittance was measured upstream and downstream of the absorber and focus-coil module using scintillating-fibre tracking detectors [26] immersed in the solenoidal field provided by three superconducting coils E1, C, and E2. The

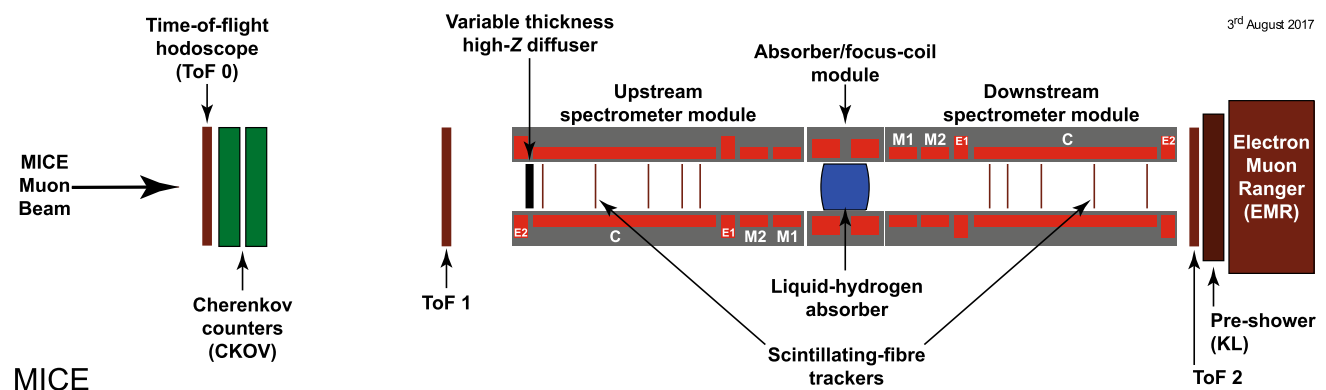


Fig. 1 Schematic diagram of the MICE experiment. The red rectangles represent the coils of the spectrometer solenoids and focus-coil module. The individual coils of the spectrometer solenoids are labelled E1, C, E2, M1 and M2. The various detectors (time-of-flight hodoscopes

(TOF0, TOF1) [23, 24], Cherenkov counters [25], scintillating-fibre trackers [26], KLOE-Light (KL) calorimeter [20, 27], and Electron Muon Ranger (EMR) [28, 29]) are also represented. The Partial Return Yoke (PRY) is not shown

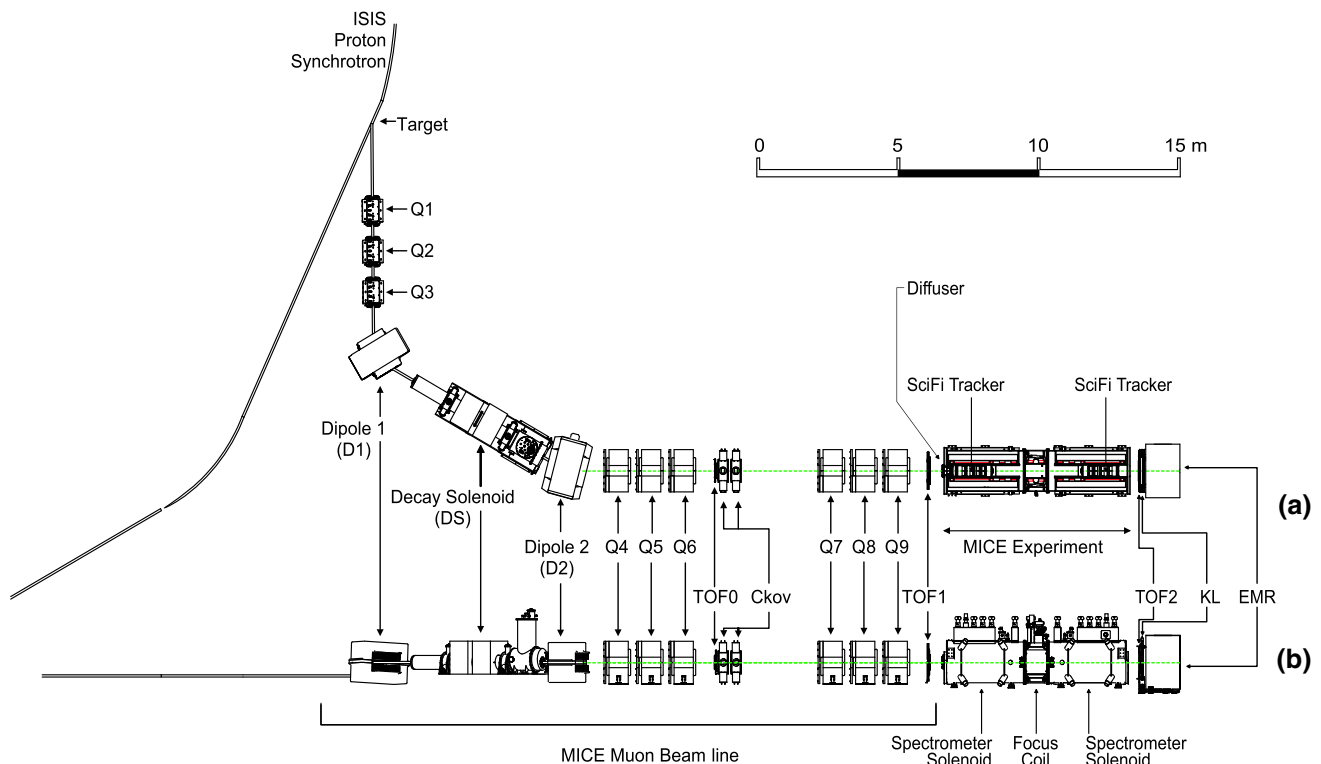


Fig. 2 **a** Top and **b** side views of the MICE Muon Beam line, its instrumentation, and the experimental configuration. A titanium target dipped into the ISIS proton synchrotron and the resultant spill of particles was captured with a quadrupole triplet (Q1–3) and transported

trackers were used to reconstruct the trajectories of individual muons at the entrance and exit of the absorber. The trackers were each constructed from five planar stations of scintillating fibres, each with an active radius of 150 mm. The track parameters were reported at the nominal reference plane: the surface of the scintillating-fibre plane closest to the absorber [30]. Hall probes were installed on the tracker to measure the magnetic-field strength in situ. The instrumentation up- and downstream of the spectrometer modules was used to select a pure sample of muons. The reconstructed tracks of the selected muons were then used to measure the muon-beam emittance at the upstream and downstream tracker reference planes. The spectrometer-solenoid modules also contained two superconducting ‘matching’ coils (M1, M2) that were used to match the optics between the uniform-field region and the neighbouring focus-coil module. The MICE coordinate system is such that the z axis is coincident with the beam direction, the y axis points vertically upward, and the x axis completes a right-handed co-ordinate system. This paper discusses the measurement of emittance using only the tracker and beam-line instrumentation upstream of the absorber. The diffuser was fully retracted for the data presented here, i.e. no extra material was introduced into the centre of the beam line, so that the incident particle distribution could be assessed.

through momentum-selecting dipoles (D1, D2). The quadrupole triplets (Q4–6, Q7–9) transported particles to the upstream spectrometer module. The time-of-flight of particles, measured between TOF0 and TOF1, was used for particle identification

4 MICE Muon beam line

The MICE Muon Beam line is shown schematically in Fig. 2. It was capable of delivering beams with normalised transverse emittance in the range $3 \lesssim \varepsilon_N \lesssim 10$ mm and mean momentum in the range $140 \lesssim p_\mu \lesssim 240$ MeV/ c with a root-mean-squared (RMS) momentum spread of ~ 20 MeV/ c [20] after the diffuser (Fig. 1).

Pions produced by the momentary insertion of a titanium target [18, 19] into the ISIS proton beam were captured using a quadrupole triplet (Q1–3) and transported to a first dipole magnet (D1), which selected particles of a desired momentum bite into the 5 T decay solenoid (DS). Muons produced in pion decay in the DS were momentum-selected using a second dipole magnet (D2) and focused onto the diffuser by a quadrupole channel (Q4–6 and Q7–9). In positive-beam running, a borated polyethylene absorber of variable thickness was inserted into the beam just downstream of the decay solenoid to suppress the high rate of protons that were produced at the target [31].

The composition and momentum spectra of the beams delivered to MICE were determined by the interplay between the two bending magnets D1 and D2. In ‘muon mode’, D2 was set to half the current of D1, selecting backward-going

muons in the pion rest frame. This produced an almost pure muon beam.

Data were taken in October 2015 in muon mode at a nominal momentum of 200 MeV/c, with ISIS in operation at 700 MeV. These data [32] are used here to characterise the properties of the beam accepted by the upstream solenoid with all diffuser irises withdrawn from the beam. The upstream E1-C-E2 coils in the spectrometer module were energised and produced a field of 4 T, effectively uniform across the tracking region, while all other coils were unpowered. Positively charged particles were selected due to their higher production rate in 700 MeV proton-nucleus collisions.

5 Simulation

Monte Carlo simulations were used to determine the accuracy of the kinematic reconstruction, to evaluate the efficiency of the response of the scintillating-fibre tracker, and to study systematic uncertainties. A sufficient number of events were generated to ensure that statistical uncertainties from the simulations were negligible in comparison to those of the data.

The beam impinging on TOF0 was modelled using G4beamline [33]. Particles were produced at the target using a parameterised particle-production model. These particles were tracked through the MICE Muon Beam line taking into account all material in and surrounding the beam line and using realistic models of the fields and apertures of the various magnets. The G4beamline simulation was tuned to reproduce the observed particle distributions at TOF0.

The MICE Analysis User Software (MAUS) [34] package was used to simulate the passage of particles from TOF0 through the remainder of the MICE Muon Beam line and through the solenoidal lattice. This simulation includes the response of the instrumentation and used the input distribution produced using G4beamline. MAUS was also used for offline reconstruction and to provide fast real-time detector reconstruction and data visualisation during MICE running. MAUS uses GEANT4 [35, 36] for beam propagation and the simulation of detector response. ROOT [37] was used for data visualisation and for data storage. The particles generated were subjected to the same trigger requirements as the data and processed by the same reconstruction programs.

6 Beam selection

Data were buffered in the front-end electronics and read out at the end of each spill [20]. For the reconstructed data presented here, the digitisation of analogue signals received from the detectors was triggered by a coincidence of signals in the PMTs serving a single scintillator slab in TOF1. Any slab in TOF1 could generate a trigger.

The following cuts were used to select muons passing through the upstream tracker:

- *One reconstructed space-point in TOF0 and TOF1* Each TOF hodoscope was composed of two perpendicular planes of scintillator slabs arranged to measure the x and y coordinates. A space-point was formed from the intersection of hits in the x and y projections. Figure 3a, b show the hit multiplicity in TOF0 plotted against the hit multiplicity in TOF1 for reconstructed data and reconstructed Monte Carlo respectively. The sample is dominated by events with one space-point in both TOF0 and TOF1. This cut removes events in which two particles enter the experiment within the trigger window.
- *Relative time-of-flight between TOF0 and TOF1, t_{rel} , in the range $1 \leq t_{\text{rel}} \leq 6 \text{ ns}$* The time of flight between TOF0 and TOF1, t_{01} , was measured relative to the mean positron time of flight, t_e . Figure 3c shows the relative time-of-flight distribution in data (black, circles) and simulation (filled histogram). All cuts other than the relative time-of-flight cut have been applied in this figure. The time-of-flight of particles relative to the mean positron time-of-flight is calculated as

$$t_{\text{rel}} = t_{01} - (t_e + \delta t_e),$$

where δt_e accounts for the difference in transit time, or path length travelled, between electrons and muons in the field of the quadrupole triplets [21]. This cut removes electrons from the selected ensemble as well as a small number of pions. The data has a longer tail compared to the simulation, which is related to the imperfect simulation of the longitudinal momentum of particles in the beam (see Sect. 7.1).

- *A single track reconstructed in the upstream tracker with a track-fit χ^2 satisfying $\frac{\chi^2}{N_{\text{DOF}}} \leq 4$* N_{DOF} is the number of degrees of freedom. The distribution of $\frac{\chi^2}{N_{\text{DOF}}}$ is shown in Fig. 3d. This cut removes events with poorly reconstructed tracks. Multi-track events, in which more than one particle passes through the same pixel in TOF0 and TOF1 during the trigger window, are rare and are also removed by this cut. The distribution of $\frac{\chi^2}{N_{\text{DOF}}}$ is broader and peaked at slightly larger values in the data than in the simulation.
- *Track contained within the fiducial volume of the tracker* The radius of the track measured by the tracker, R_{track} , is required to satisfy $R_{\text{track}} < 150 \text{ mm}$ to ensure the track does not leave and then re-enter the fiducial volume. The track radius is evaluated at 1 mm intervals between the stations. If the track radius exceeds 150 mm at any of these positions, the event is rejected.

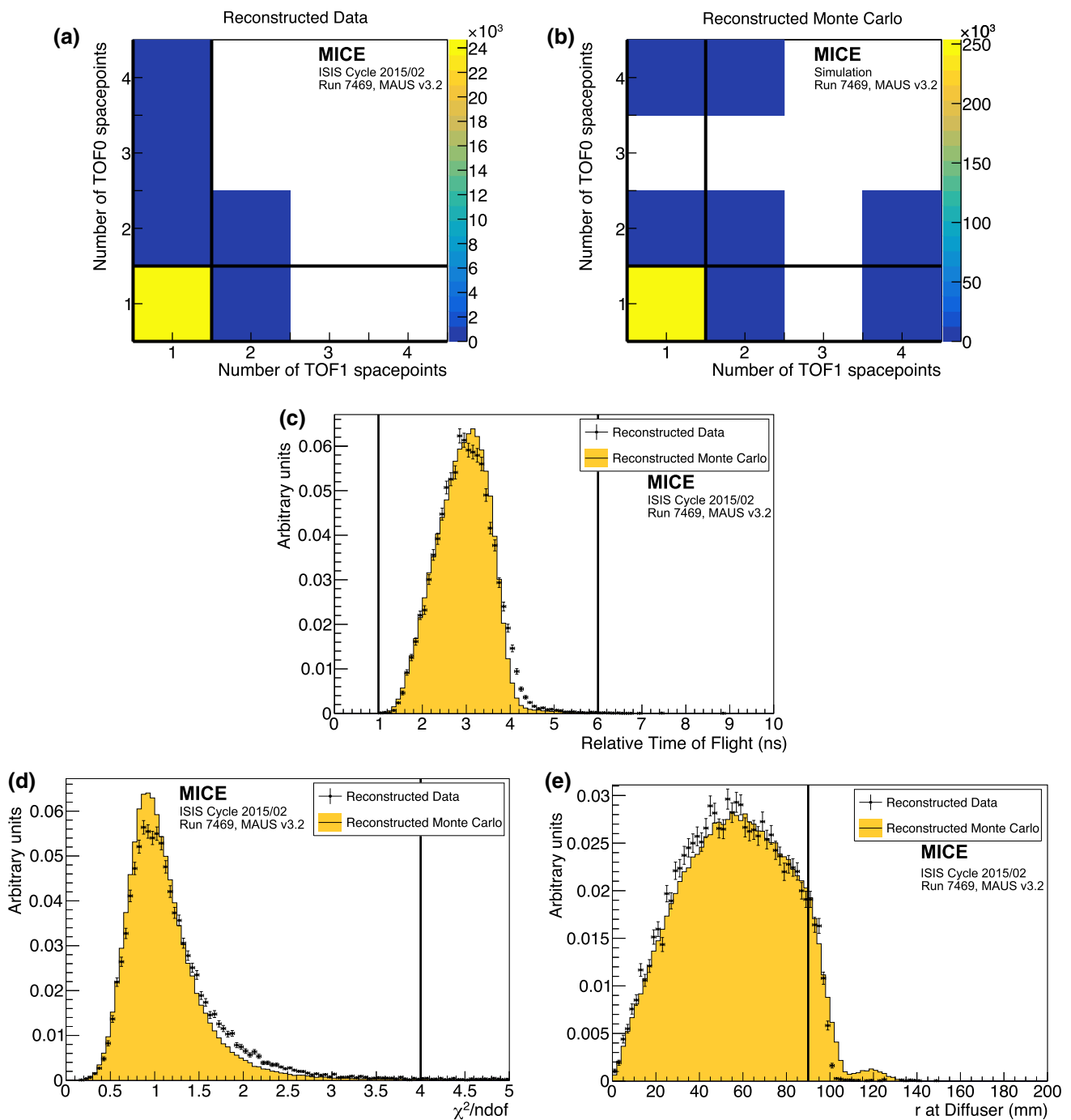


Fig. 3 Distribution of the quantities that were used to select the sample used to reconstruct the emittance of the beam: **a** the number of space-points in TOF0 plotted against the number of space-points in TOF1 for reconstructed data, and **b** reconstructed simulation; **c** distribution of the relative time-of-flight, t_{rel} ; **d** distribution of $\frac{\chi^2}{N_{DOF}}$; and **e** distribution

of R_{diff} . The 1D distributions show reconstructed data as solid (black) circles and reconstructed MAUS simulation as the solid (yellow) histogram. The solid (black) lines indicate the position of the cuts made on these quantities. Events enter these plots if all cuts other than the cut under examination are passed

– Extrapolated track radius at the diffuser, $R_{diff} \leq 90$ mm
Muons that pass through the annulus of the diffuser, which includes the retracted irises, lose a substantial amount of energy. Such muons may re-enter the track-

ing volume and be reconstructed but have properties that are no longer characteristic of the incident muon beam. The aperture radius of the diffuser mechanism (100 mm) defines the transverse acceptance of the beam injected

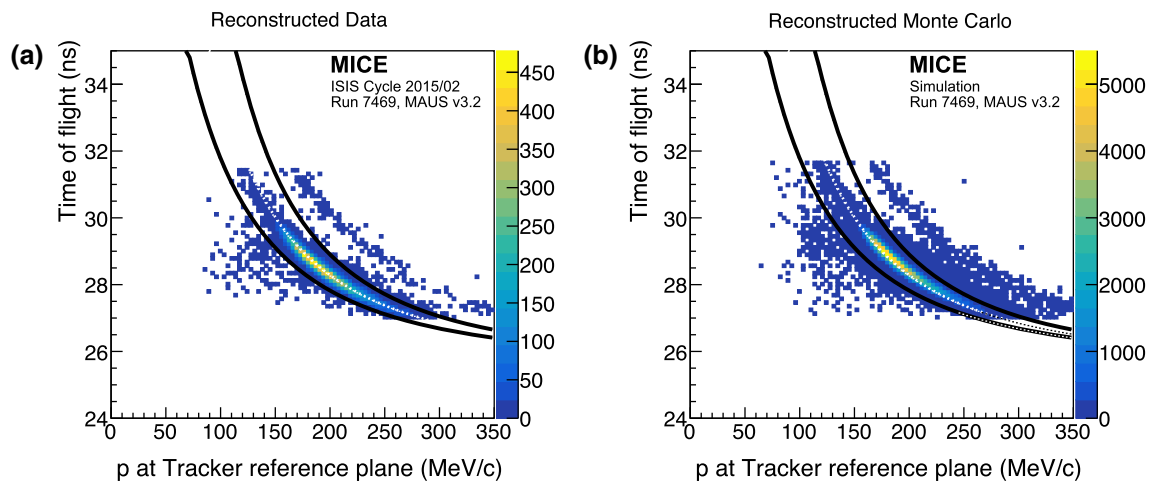


Fig. 4 Time of flight between TOF0 and TOF1 (t_{01}) plotted as a function of the muon momentum, p , measured in the upstream tracker. All cuts other than the muon hypothesis have been applied. Particles within the black lines are selected. The white dotted line is the trajectory of

a muon that loses the most probable momentum (20 MeV/c) between TOF1 and the tracker in **a** reconstructed data, and **b** reconstructed Monte Carlo

Table 1 The number of particles that pass each selection criterion. A total of 24,660 particles pass all of the cuts

Cut	No. surviving particles	Cumulative surviving particles
None	53 276	53 276
One space-point in TOF0 and TOF1	37 619	37 619
Relative time of flight in range 1–6 ns	37 093	36 658
Single reconstructed track with $\frac{\chi^2}{\text{N}_{\text{DOF}}} \leq 4$	40 110	30 132
Track within fiducial volume of tracker	52 039	29 714
Extrapolated track radius at diffuser ≤ 90 mm	42 592	25 310
Muon hypothesis	34 121	24 660
All	24 660	24 660

into the experiment. Back-extrapolation of tracks to the exit of the diffuser yields a measurement of R_{diff} with a resolution of $\sigma_{R_{\text{diff}}} = 1.7$ mm. Figure 3e shows the distribution of R_{diff} , where the difference between data and simulation lies above the accepted radius. These differences are due to approximations in modelling the outer material of the diffuser. The cut on R_{diff} accepts particles that passed at least $5.9\sigma_{R_{\text{diff}}}$ inside the aperture limit of the diffuser.

– *Particle consistent with muon hypothesis* Figure 4 shows t_{01} , the time-of-flight between TOF0 and TOF1, plotted as a function of p , the momentum reconstructed by the upstream tracking detector. Momentum is lost between TOF1 and the reference plane of the tracker in the material of the detectors. A muon that loses the most probable momentum, $\Delta p \simeq 20$ MeV/c, is shown as the dotted (white) line. Particles that are poorly reconstructed, or have passed through support material upstream of the tracker and have lost significant momentum, are excluded

by the lower bound. The population of events above the upper bound are ascribed to the passage of pions, or mis-reconstructed muons, and are also removed from the analysis.

A total of 24,660 events pass the cuts listed above. Table 1 shows the number of particles that survive each individual cut. Data distributions are compared to the distributions obtained using the MAUS simulation in Figs. 3 and 4. Despite minor disagreements, the agreement between the simulation and data is sufficiently good to give confidence that a clean sample of muons has been selected.

The expected pion contamination of the unselected ensemble of particles has been measured to be $\leq 0.4\%$ [22]. Table 2 shows the number of positrons, muons, and pions in the MAUS simulation that pass all selection criteria. The criteria used to select the muon sample for the analysis presented here efficiently reject electrons and pions from the Monte Carlo sample.

Table 2 The number of reconstructed electrons, muons, and pions at the upstream tracker that survive each cut in the Monte Carlo simulation. Application of all cuts removes almost all positrons and pions in the reconstructed Monte Carlo sample. In the Monte Carlo simulation, a total of 253,504 particles pass all of the cuts described in the text

Cut	e	μ	π	Total
None	14,912	432,294	1610	463,451
One space-point in TOF0 and TOF1	11,222	353,613	1213	376,528
Relative Time of flight in range 1–6 ns	757	369,337	1217	379,761
Single reconstructed track with $\frac{\chi^2}{\text{NDOF}} \leq 4$	10,519	407,276	1380	419,208
Track within fiducial volume of tracker	14,527	412,857	1427	443,431
Tracked radius at diffuser ≤ 90 mm	11,753	311,076	856	334,216
Muon hypothesis (above lower limit)	3225	362,606	411	367,340
Muon hypothesis (below upper limit)	12,464	411,283	379	424,203
Muon hypothesis (overall)	2724	358,427	371	361,576
All	22	253,475	5	253,504

7 Results

7.1 Phase-space projections

The distributions of x , y , p_x , p_y , p_z , and $p = \sqrt{p_x^2 + p_y^2 + p_z^2}$ are shown in Fig. 5. The total momentum of the muons that make up the beam lie within the range $140 \lesssim |p| \lesssim 260 \text{ MeV}/c$. The results of the MAUS simulation, which are also shown in Fig. 5, give a reasonable description of the data. In the case of the longitudinal component of momentum, p_z , the data are peaked to slightly larger values than the simulation. The difference is small and is reflected in the distribution of the total momentum, p . As the simulation began with particle production from the titanium target, any difference between the simulated and observed particle distributions would be apparent in the measured longitudinal and total momentum distributions. The scale of the observed disagreement is small, and as such the simulation adequately describes the experiment. The distributions of the components of the transverse phase space (x , p_x , y , p_y) are well described by the simulation. Normalised transverse emittance is calculated with respect to the means of the distributions (Eq. 2), and so is unaffected by this discrepancy.

The phase space occupied by the selected beam is shown in Fig. 6. The distributions are plotted at the reference surface of the upstream tracker. The beam is moderately well centred in the (x, y) plane. Correlations are apparent that couple the position and momentum components in the transverse plane. The transverse position and momentum coordinates are also seen to be correlated with total momentum. The correlation in the (x, p_y) and (y, p_x) plane is due to the solenoidal field, and is of the expected order. The dispersion and chromaticity of the beam are discussed further in Sect. 7.2.

7.2 Effect of dispersion, chromaticity, and binning in longitudinal momentum

Momentum selection at D2 introduces a correlation, dispersion, between the position and momentum of particles. Figure 7 shows the transverse position and momentum with respect to the total momentum, p , as measured at the upstream-tracker reference plane. Correlations exist between all four transverse phase-space co-ordinates and the total momentum.

Emittance is calculated in 10 MeV/ c bins of total momentum in the range $185 \leq p \leq 255 \text{ MeV}/c$. This bin size was chosen as it is commensurate with the detector resolution. Calculating the emittance in momentum increments makes the effect of the optical mismatch, or chromaticity, small compared to the statistical uncertainty. The range of $185 \leq p \leq 255 \text{ MeV}/c$ was chosen to maximise the number of particles in each bin that are not scraped by the aperture of the diffuser.

7.3 Uncertainties on emittance measurement

7.3.1 Statistical uncertainties

The statistical uncertainty on the emittance in each momentum bin is calculated as $\sigma_\varepsilon = \frac{\varepsilon}{\sqrt{2N}}$ [38–40], where ε is the emittance of the ensemble of muons in the specified momentum range and N is the number of muons in that ensemble. The number of events per bin varies from ~ 4000 for $p \sim 190 \text{ MeV}/c$ to ~ 700 for $p \sim 250 \text{ MeV}/c$.

7.4 Systematic uncertainties

7.4.1 Uncorrelated systematic uncertainties

Systematic uncertainties related to the beam selection were estimated by varying the cut values by an amount correspond-

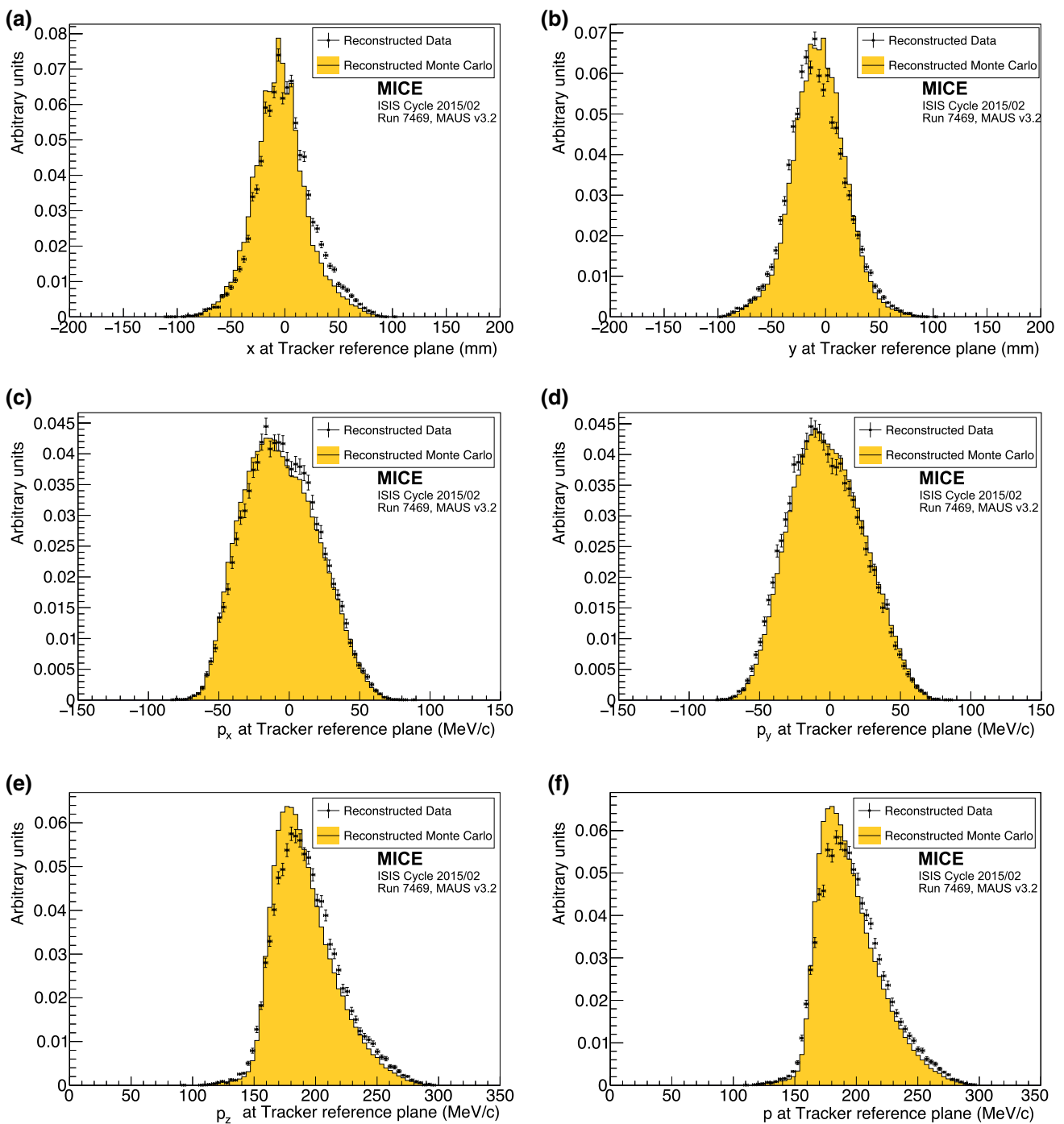


Fig. 5 Position and momentum distributions of muons reconstructed at the reference surface of the upstream tracker: **a** x , **b** y , **c** p_x , **d** p_y , **e** p_z , and **f** p , the total momentum. The data are shown as the solid circles while the results of the MAUS simulation are shown as the yellow histogram

ing to the RMS resolution of the quantity in question. The emittance of the ensembles selected with the changed cut values were calculated and compared to the emittance calculated using the nominal cut values and the difference taken as the uncertainty due to changing the cut boundaries. The overall uncertainty due to beam selection is summarised in Table 3. The dominant beam-selection uncertainty is in the

selection of particles that successfully pass within the inner 90 mm of the diffuser aperture.

Systematic uncertainties related to possible biases in calibration constants were evaluated by varying each calibration constant by its resolution. Systematic uncertainties related to the reconstruction algorithms were evaluated using the MAUS simulation. The positive and negative deviations

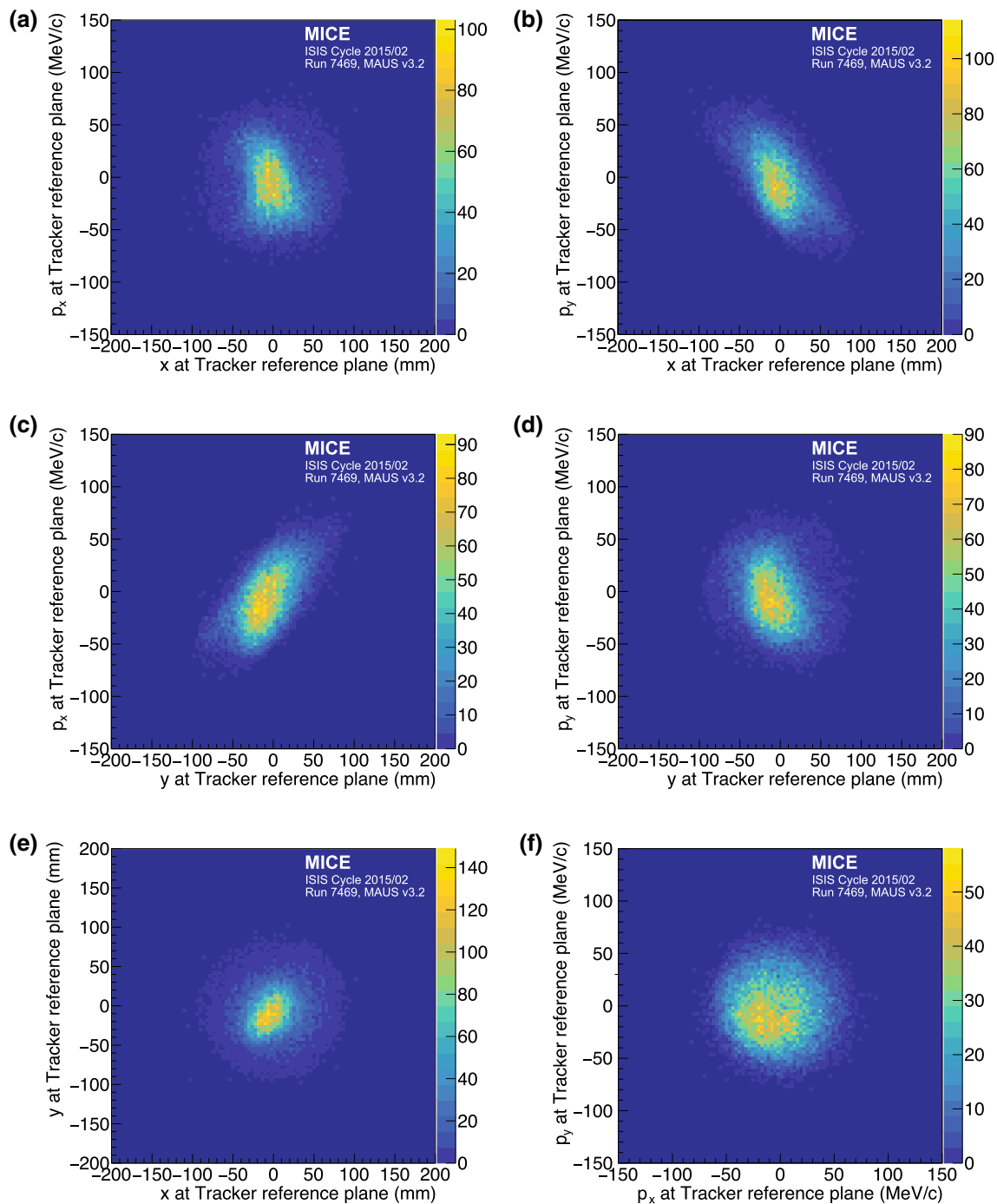


Fig. 6 Transverse phase space occupied by selected muons transported through the MICE Muon Beam line to the reference plane of the upstream tracker. **a** (x, p_x), **b** (x, p_y), **c** (y, p_x), **d** (y, p_y), **e** (x, y), and **f** (p_x, p_y)

from the nominal emittance were added in quadrature separately to obtain the total positive and negative systematic uncertainty. Sources of correlated uncertainties are discussed below.

7.4.2 Correlated systematic uncertainties

Some systematic uncertainties are correlated with the total momentum, p . For example, the measured value of p dictates the momentum bin to which a muon is assigned for the emittance calculation. The uncertainty on the emittance reconstructed in each bin has been evaluated by allowing the

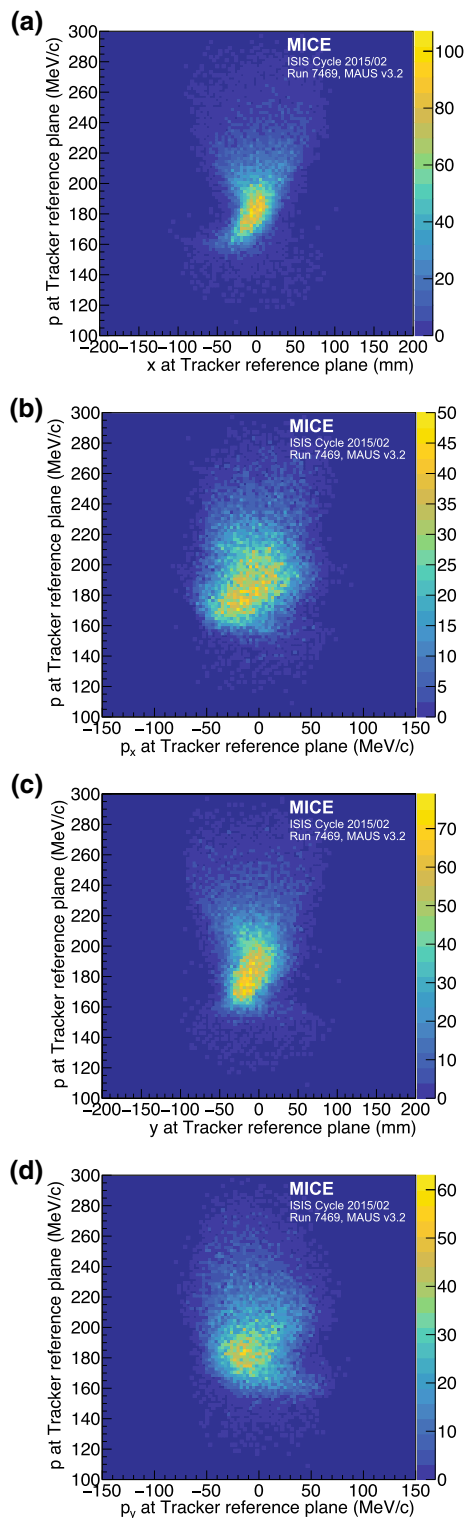


Fig. 7 The effect of dispersion, the dependence of the components of transverse phase space on the momentum, p , is shown at the reference surface of the upstream tracker: **a**) (x, p); **b**) (p_x, p); **c**) (y, p); **d**) (p_y, p)

momentum of each muon to fluctuate around its measured value according to a Gaussian distribution of width equal to

the measurement uncertainty on p . In Table 3 this uncertainty is listed as ‘Binning in p ’.

A second uncertainty that is correlated with total momentum is the uncertainty on the reconstructed x , p_x , y , and p_y . The effect on the emittance was evaluated with the same procedure used to evaluate the uncertainty due to binning in total momentum. This is listed as ‘Tracker resolution’ in Table 3.

Systematic uncertainties correlated with p are primarily due to the differences between the model of the apparatus used in the reconstruction and the hardware actually used in the experiment. The most significant contribution arises from the magnetic field within the tracking volume. Particle tracks are reconstructed assuming a uniform solenoidal field, with no fringe-field effects. Small non-uniformities in the magnetic field in the tracking volume will result in a disagreement between the true parameters and the reconstructed values. To quantify this effect, six field models (one optimal and five additional models) were used to estimate the deviation in reconstructed emittance from the true value under realistic conditions. Three families of field model were investigated, corresponding to the three key field descriptors: field scale, field alignment, and field uniformity. The values of these descriptors that best describe the Hall-probe measurements were used to define the optimal model and the uncertainty in the descriptor values were used to determine the 1σ variations.

7.4.3 Field scale

Hall-probes located on the tracker provided measurements of the magnetic field strength within the tracking volume at known positions. An optimal field model was produced with a scale factor of 0.49% that reproduced the Hall-probe measurements. Two additional field models were produced which used scale factors that were one standard deviation, $\pm 0.03\%$, above and below the nominal value.

7.4.4 Field alignment

A field-alignment algorithm was developed based on the determination of the orientation of the field with respect to the mechanical axis of the tracker using coaxial tracks with $p_T \approx 0$ [41]. The field was rotated with respect to the tracker by 1.4 ± 0.1 mrad about the x axis and 0.3 ± 0.1 mrad about the y axis. The optimal field model was created such that the simulated alignment is in agreement with the measurements. Two additional models that vary the alignment by one standard deviation were also produced.

7.4.5 Field uniformity

A COMSOL [42] model of the field was used to generate the optimal model which includes the field generated by each coil

Table 3 Emittance together with the statistical and systematic uncertainties and biases as a function of mean total momentum, (p)

Source	190	200	210	220	230	240	250
Measured emittance (mm rad)	3.40	3.65	3.69	3.65	3.69	3.62	3.31
Statistical uncertainty	$\pm 3.8 \times 10^{-2}$	$\pm 4.4 \times 10^{-2}$	$\pm 5.0 \times 10^{-2}$	$\pm 5.8 \times 10^{-2}$	$\pm 7.0 \times 10^{-2}$	$\pm 8.4 \times 10^{-2}$	$\pm 9.2 \times 10^{-2}$
Beam selection:							
Diffuser aperture	4.9×10^{-2}	5.3×10^{-2}	4.9×10^{-2}	4.7×10^{-2}	4.2×10^{-2}	11.0×10^{-2}	4.4×10^{-2}
$\chi^2_{\text{DOF}} \leq 4$	-3.5×10^{-2}	-5.1×10^{-2}	-5.7×10^{-2}	-5.0×10^{-2}	-3.5×10^{-2}	-5.0×10^{-2}	-9.6×10^{-2}
Muon hypothesis	5.1×10^{-3}	2.0×10^{-3}	1.0×10^{-2}	4.1×10^{-3}	1.2×10^{-3}	5.5×10^{-3}	7.9×10^{-3}
	-4.8×10^{-3}	-1.3×10^{-3}	-1.8×10^{-3}	-3.3×10^{-3}	-2.8×10^{-4}	-6.5×10^{-3}	-4.7×10^{-4}
	4.5×10^{-3}	2.2×10^{-4}	6.4×10^{-3}	3.1×10^{-3}	1.4×10^{-3}	2.6×10^{-3}	1.3×10^{-3}
	-3.2×10^{-3}	-6.8×10^{-3}	-8.8×10^{-4}	-4.7×10^{-3}	-1.1×10^{-2}	-6.7×10^{-2}	-4.1×10^{-3}
Beam selection (Overall)	4.9×10^{-2}	5.3×10^{-2}	5.0×10^{-2}	4.7×10^{-2}	4.2×10^{-2}	1.1×10^{-1}	4.5×10^{-2}
	-3.6×10^{-2}	-5.2×10^{-2}	-5.8×10^{-2}	-5.0×10^{-2}	-3.9×10^{-2}	-8.4×10^{-2}	-9.6×10^{-2}
Binning in p	$\pm 1.8 \times 10^{-2}$	$\pm 2.1 \times 10^{-2}$	$\pm 2.3 \times 10^{-2}$	$\pm 2.9 \times 10^{-2}$	$\pm 3.5 \times 10^{-2}$	$\pm 4.3 \times 10^{-2}$	$\pm 5.2 \times 10^{-2}$
Magnetic field misalignment and scale:							
Bias	-1.3×10^{-2}	-1.4×10^{-2}	-1.5×10^{-2}	-1.6×10^{-2}	-1.6×10^{-2}	-1.7×10^{-2}	-1.6×10^{-2}
Uncertainty	$\pm 2.0 \times 10^{-4}$	$\pm 2.9 \times 10^{-4}$	$\pm 8.0 \times 10^{-4}$	$\pm 4.8 \times 10^{-4}$	$\pm 5.5 \times 10^{-4}$	$\pm 4.8 \times 10^{-4}$	$\pm 4.9 \times 10^{-4}$
Tracker resolution	$\pm 1.6 \times 10^{-3}$	$\pm 2.1 \times 10^{-3}$	$\pm 2.8 \times 10^{-3}$	$\pm 3.8 \times 10^{-3}$	$\pm 5.3 \times 10^{-3}$	$\pm 7.0 \times 10^{-3}$	$\pm 9.5 \times 10^{-3}$
Total systematic uncertainty	5.2×10^{-2}	5.7×10^{-2}	5.5×10^{-2}	5.6×10^{-2}	5.5×10^{-2}	11.7×10^{-2}	6.9×10^{-2}
	-4.0×10^{-2}	-5.6×10^{-2}	-6.2×10^{-2}	-5.8×10^{-2}	-5.2×10^{-2}	-9.5×10^{-2}	-11.0×10^{-2}
Corrected emittance (mm rad)	3.41	3.66	3.71	3.67	3.71	3.65	3.34
Total uncertainty	± 0.06	± 0.07	$+0.07$	± 0.08	± 0.09	$+0.14$	$+0.12$
			-0.08			-0.13	-0.14
Total uncertainty (%)	+1.90	+1.96	+2.01	+2.19	+2.40	+3.97	+3.47
	-1.63	-1.94	-2.15	-2.34	-2.37	-3.49	-4.30

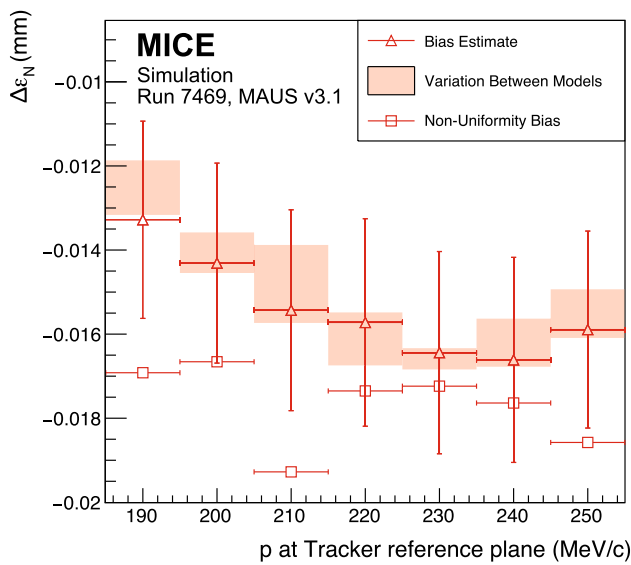


Fig. 8 The systematic bias and uncertainty on the reconstructed emittance under different magnetic field model assumptions. The bias estimate (open triangles) includes the non-uniformity bias (open squares). The variation between the models (see text) is indicated by the shaded bands

using the ‘as-built’ parameters and the partial return yoke. A simple field model was created using only the individual coil geometries to provide additional information on the effect of field uniformity on the reconstruction. The values for the simple field model were normalised to the Hall-probe measurements as for the other field models. This represents a significant deviation from the COMSOL model, but demonstrates the stability of the reconstruction with respect to changes in field uniformity, as the variation in emittance between all field models is small (less than 0.002 mm).

For each of the 5 field models, multiple 2000-muon ensembles were generated for each momentum bin. The deviation of the calculated emittance from the true emittance was found for each ensemble. The distribution of the difference between the ensemble emittance and the true emittance was assumed to be Gaussian with mean ε and variance $s^2 = \sigma^2 + \theta^2$, where σ is the statistical uncertainty and θ is an additional systematic uncertainty. The systematic bias for each momentum bin was then calculated as [43]

$$\Delta\varepsilon_N = \langle\varepsilon\rangle - \varepsilon_{\text{true}}, \tag{4}$$

where $\varepsilon_{\text{true}}$ is the true beam emittance in that momentum bin and $\langle\varepsilon\rangle$ is the mean emittance from the N ensembles. The systematic uncertainty was calculated assuming that the distribution of residuals of ε_i from the mean, $\langle\varepsilon\rangle$, satisfies a χ^2 distribution with $N - 1$ degrees of freedom,

$$\chi^2_{N-1} = \sum_i^N \frac{(\varepsilon_i - \langle\varepsilon\rangle)^2}{\sigma^2 + \theta^2}, \tag{5}$$

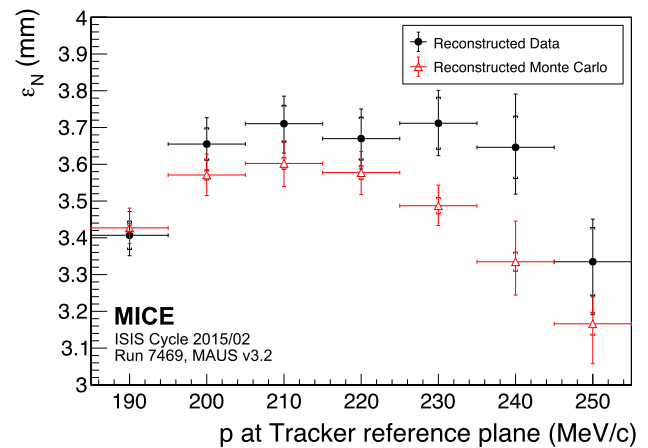


Fig. 9 Normalised transverse emittance as a function of total momentum, p , for data (black, filled circle) and reconstructed Monte Carlo (red, open triangle). The inner error bars show the statistical uncertainty. The outer error bars show the quadratic sum of the statistical and systematic uncertainties

and θ was estimated by minimising the expression $(\chi^2_{N-1} - (N - 1))^2$ [43].

The uncertainty, θ , was consistent with zero in all momentum bins, whereas the bias, $\Delta\varepsilon_N$, was found to be momentum dependent as shown in Fig. 8. The bias was estimated from the mean difference between the reconstructed and true emittance values using the optimal field model. The variation in the bias was calculated from the range of values reconstructed for each of the additional field models. The model representing the effects of non-uniformities in the field was considered separately due to the significance of the deviation from the optimal model.

The results show a consistent systematic bias in the reconstructed emittance of ≈ -0.015 mm that is a function of momentum (see Table 3). The absolute variation in the mean values between the models that were used was smaller than the expected statistical fluctuations, demonstrating the stability of the reconstruction across the expected variations in field alignment and scale. The effect of the non-uniformity model was larger but still demonstrates consistent reconstruction. The biases calculated from the optimal field model were used to correct the emittance values in the final calculation (Sect. 7.5).

7.5 Emittance

The normalised transverse emittance as a function of p is shown in Fig. 9. The emittance has been corrected for the systematic bias shown in Table 3. The uncertainties plotted are those summarised in Table 3, where the inner bars represent the statistical uncertainty and outer bars the total uncertainty. The emittance of the measured muon ensembles (black, filled circle) is approximately flat in the range

$195 \leq p \leq 245 \text{ MeV}/c$, corresponding to the design momentum of the experiment. The mean emittance in this region is $\approx 3.7 \text{ mm}$. The emittance of the reconstructed Monte Carlo is consistently lower than that of the data, and therefore gives only an approximate simulation of the beam.

8 Conclusions

A first particle-by-particle measurement of the emittance of the MICE Muon Beam was made using the upstream scintillating-fibre tracking detector in a 4 T solenoidal field. A total of 24,660 muons survive the selection criteria. The position and momentum of these muons were measured at the reference plane of the upstream tracking detector. The muon sample was divided into 10 MeV/c bins of total momentum, p , from 185–255 MeV/c to account for dispersion, chromaticity, and scraping in apertures upstream of the tracking detector. The emittance of the measured muon ensembles is approximately flat from $195 \leq p \leq 245 \text{ MeV}/c$ with a mean value of $\approx 3.7 \text{ mm}$ across this region.

The total uncertainty on this measurement ranged from $+1.9\%$ to $+3.5\%$, increasing with total momentum, p . As p increases, the number of muons in the reported ensemble decreases, increasing the statistical uncertainty. At the extremes of the momentum range, a larger proportion of the input beam distribution is scraped on the aperture of the diffuser. This contributes to an increase in systematic uncertainty at the limits of the reported momentum range. The systematic uncertainty introduced by the diffuser aperture highlights the need to study ensembles where the total momentum, p , is close to the design momentum of the beam line. The total systematic uncertainty on the measured emittance is larger than that on a future measurement of the ratio of emittance before and after an absorber. The measurement is sufficiently precise to demonstrate muon ionization cooling.

The technique presented here represents the first precise measurement of normalised transverse emittance on a particle-by-particle basis. This technique will be applied to muon ensembles up- and downstream of a low- Z absorber, such as liquid hydrogen or lithium hydride, to measure emittance change across the absorber and thereby to study ionization cooling.

Acknowledgements The work described here was made possible by grants from Department of Energy and National Science Foundation (USA), the Istituto Nazionale di Fisica Nucleare (Italy), the Science and Technology Facilities Council (UK), the European Community under the European Commission Framework Programme 7 (AIDA project, grant agreement no. 262025, TIARA project, grant agreement no. 261905, and EuCARD), the Japan Society for the Promotion of Science, the National Research Foundation of Korea (No. NRF-2016R1A5A1013277), and the Swiss National Science Foundation, in the framework of the SCOPES programme. We gratefully acknowledge all sources of support. We are grateful for the support given to us by the

staff of the STFC Rutherford Appleton and Daresbury Laboratories. We acknowledge the use of Grid computing resources deployed and operated by GridPP in the UK, <http://www.gridpp.ac.uk/>.

Data Availability Statement This manuscript has associated data in a data repository. [Authors' comment: The data that support the findings of this study are publicly available on the GridPP computing Grid via the data DOIs (the MICE unprocessed data: 10.17633/rd.brunel.3179644; the MICE reconstructed data: 10.17633/rd.brunel.5955850). Publications using the MICE data must contain the following statement: "We gratefully acknowledge the MICE collaboration for allowing us access to their data. Third-party results are not endorsed by the MICE collaboration and the MICE collaboration does not accept responsibility for any errors in the third-party's understanding of the MICE data."]

Open Access This article is distributed under the terms of the Creative Commons Attribution 4.0 International License (<http://creativecommons.org/licenses/by/4.0/>), which permits unrestricted use, distribution, and reproduction in any medium, provided you give appropriate credit to the original author(s) and the source, provide a link to the Creative Commons license, and indicate if changes were made. Funded by SCOAP³.

References

1. S. Geer, Phys. Rev. D **57**, 6989 (1998). <https://doi.org/10.1103/PhysRevD.57.6989>
2. M. Apollonio, et al., Oscillation physics with a neutrino factory (2002). [arXiv:hep-ph/0210192](https://arxiv.org/abs/hep-ph/0210192)
3. D.V. Neuffer, R.B. Palmer, Conf. Proc. C **940627**, 52 (1995)
4. R.B. Palmer, Rev. Accel. Sci. Tech. **7**, 137 (2014). <https://doi.org/10.1142/S1793626814300072>
5. M. Boscolo, M. Antonelli, O.R. Blanco-Garcia, S. Guiducci, S. Liuzzo, P. Raimondi, F. Collamati, Low emittance muon accelerator studies with production from positrons on target (2018). <https://doi.org/10.1103/PhysRevAccelBeams.21.061005>. [arXiv:1803.06696](https://arxiv.org/abs/1803.06696) [physics.acc-ph]
6. S.Y. Lee, *Accelerator Physics*, 3rd edn. (World Scientific Publishing Co, Singapore, 2012). <https://doi.org/10.1142/8335>
7. S. Schröder, R. Klein, N. Boos, M. Gerhard, R. Grieser, G. Huber, A. Karafillidis, M. Krieg, N. Schmidt, T. Kühl, R. Neumann, V. Balykin, M. Grieser, D. Habs, E. Jaeschke, D. Krämer, M. Kristensen, M. Music, W. Petrich, D. Schwalm, P. Sigray, M. Steck, B. Wanner, A. Wolf, Phys. Rev. Lett. **64**, 2901 (1990). <https://doi.org/10.1103/PhysRevLett.64.2901>
8. J.S. Hangst, M. Kristensen, J.S. Nielsen, O. Poulsen, J.P. Schiffer, P. Shi, Phys. Rev. Lett. **67**, 1238 (1991). <https://doi.org/10.1103/PhysRevLett.67.1238>
9. P.J. Channell, J. Appl. Phys. **52**(6), 3791 (1981). <https://doi.org/10.1063/1.329218>
10. J. Marriner, Nucl. Instrum. Methods A **532**, 11 (2004). <https://doi.org/10.1016/j.nima.2004.06.025>
11. V.V. Parkhomchuk, A.N. Skrinsky, Physics-Uspekhi **43**(5), 433 (2000)
12. A.N. Skrinsky, V.V. Parkhomchuk, Sov. J. Part. Nucl. **12**, 223 (1981) [**Fiz. Elem. Chast. Atom. Yadra** **12**,557 (1981)]
13. D. Neuffer, Conf. Proc. C **830811**, 481 (1983)
14. D. Neuffer, Part. Accel. **14**, 75 (1983)
15. The MICE collaboration, International MUON Ionization Cooling Experiment. <http://mice.iit.edu>. Accessed 4 Mar 2019
16. M. Apollonio et al., JINST **4**, P07001 (2009). <https://doi.org/10.1088/1748-0221/4/07/P07001>
17. J.B. Rosenzweig, *Fundamentals of Beam Physics* (Oxford University Press, Oxford, 2003)

18. C.N. Booth et al., JINST **8**, P03006 (2013). <https://doi.org/10.1088/1748-0221/8/03/P03006>
19. C.N. Booth et al., JINST **11**(05), P05006 (2016). <https://doi.org/10.1088/1748-0221/11/05/P05006>
20. M. Bogomilov et al., JINST **7**, P05009 (2012). <https://doi.org/10.1088/1748-0221/7/05/P05009>
21. D. Adams et al., Eur. Phys. J. C **73**(10), 2582 (2013). <https://doi.org/10.1140/epjc/s10052-013-2582-8>
22. M. Bogomilov et al., JINST **11**(03), P03001 (2016). <https://doi.org/10.1088/1748-0221/11/03/P03001>
23. R. Bertoni, Nucl. Instrum. Methods A **615**, 14 (2010). <https://doi.org/10.1016/j.nima.2009.12.065>
24. R. Bertoni, M. Bonesini, A. de Bari, G. Cecchet, Y. Karadzhov, R. Mazza, The construction of the MICE TOF2 detector (2010). <http://mice.iit.edu/micenotes/public/pdf/MICE0286/MICE0286.pdf>. Accessed 4 Mar 2019
25. L. Cremaldi, D.A. Sanders, P. Sonnek, D.J. Summers, J. Reidy Jr., I.E.E.E. Trans. Nucl. Sci. **56**, 1475 (2009). <https://doi.org/10.1109/TNS.2009.2021266>
26. M. Ellis, Nucl. Instrum. Methods A **659**, 136 (2011). <https://doi.org/10.1016/j.nima.2011.04.041>
27. F. Ambrosino, Nucl. Instrum. Methods A **598**, 239 (2009). <https://doi.org/10.1016/j.nima.2008.08.097>
28. R. Asfandiyarov et al., JINST **11**(10), T10007 (2016). <https://doi.org/10.1088/1748-0221/11/10/T10007>
29. D. Adams et al., JINST **10**(12), P12012 (2015). <https://doi.org/10.1088/1748-0221/10/12/P12012>
30. A. Dobbs, C. Hunt, K. Long, E. Santos, M.A. Uchida, P. Kyberd, C. Heidt, S. Blot, E. Overton, JINST **11**(12), T12001 (2016). <https://doi.org/10.1088/1748-0221/11/12/T12001>
31. S. Blot, *Proceedings 2nd International Particle Accelerator Conference (IPAC 11) 4–9 September 2011* (San Sebastian, 2011) <https://accelconf.web.cern.ch/accelconf/IPAC2011/papers/mopz034.pdf>. Accessed 4 Mar 2019
32. The MICE Collaboration, The MICE RAW Data. <https://doi.org/10.17633/rd.brunel.3179644> (MICE/Step4/07000/07469.tar)
33. T. Roberts, et al., G4beamline; a “Swiss Army Knife” for Geant4, optimized for simulating beamlines. <http://public.muonsinc.com/Projects/G4beamline.aspx>. Accessed 17 Sept 2018
34. D. Rajaram, C. Rogers, The mice offline computing capabilities (2014). <http://mice.iit.edu/micenotes/public/pdf/MICE0439/MICE0439.pdf> (MICE Note 439)
35. S. Agostinelli, Nucl. Instrum. Methods Phys. Res. A **506**, 250 (2003)
36. J. Allison et al., IEEE Trans. Nucl. Sci. **53**, 270 (2006). <https://doi.org/10.1109/TNS.2006.869826>
37. R. Brun, F. Rademakers, Nucl. Instrum. Methods A **389**, 81 (1997). [https://doi.org/10.1016/S0168-9002\(97\)00048-X](https://doi.org/10.1016/S0168-9002(97)00048-X)
38. J. Cobb, Statistical errors on emittance measurements (2009). <http://mice.iit.edu/micenotes/public/pdf/MICE341/MICE268.pdf>. Accessed 4 Mar 2019
39. J. Cobb, Statistical errors on emittance and optical functions (2011). <http://mice.iit.edu/micenotes/public/pdf/MICE341/MICE341.pdf>. Accessed 4 Mar 2019
40. J.H. Cobb, Statistical Errors on Emittance (2015, Private communication)
41. C. Hunt, Private communication Publication-in-progress
42. COMSOL Multiphysics software Webpage: <https://www.comsol.com>. Accessed 4 Mar 2019
43. L. Lyons, J. Phys. A Math. Gen. **25**(7), 1967 (1992). <http://stacks.iop.org/0305-4470/25/i=7/a=035>



Lattice design and expected performance of the Muon Ionization Cooling Experiment demonstration of ionization cooling

M. Bogomilov,¹ R. Tsenov,¹ G. Vankova-Kirilova,¹ Y. Song,² J. Tang,² Z. Li,³ R. Bertoni,⁴ M. Bonesini,⁴ F. Chignoli,⁴ R. Mazza,⁴ V. Palladino,⁵ A. de Bari,⁶ G. Cecchet,⁶ D. Orestano,⁷ L. Tortora,⁷ Y. Kuno,⁸ S. Ishimoto,⁹ F. Filthaut,¹⁰ D. Jokovic,¹¹ D. Maletic,¹¹ M. Savic,¹¹ O. M. Hansen,¹² S. Ramberger,¹² M. Vretenar,¹² R. Asfandiyarov,¹³ A. Blondel,¹³ F. Drielsma,¹³ Y. Karadzhov,¹³ G. Charnley,¹⁴ N. Collomb,¹⁴ K. Dumbell,¹⁴ A. Gallagher,¹⁴ A. Grant,¹⁴ S. Griffiths,¹⁴ T. Hartnett,¹⁴ B. Martlew,¹⁴ A. Moss,¹⁴ A. Muir,¹⁴ I. Mullacraane,¹⁴ A. Oates,¹⁴ P. Owens,¹⁴ G. Stokes,¹⁴ P. Warburton,¹⁴ C. White,¹⁴ D. Adams,¹⁵ R. J. Anderson,¹⁵ P. Barclay,¹⁵ V. Bayliss,¹⁵ J. Boehm,¹⁵ T. W. Bradshaw,¹⁵ M. Courthold,¹⁵ V. Francis,¹⁵ L. Fry,¹⁵ T. Hayler,¹⁵ M. Hills,¹⁵ A. Lintern,¹⁵ C. Macwaters,¹⁵ A. Nichols,¹⁵ R. Preece,¹⁵ S. Ricciardi,¹⁵ C. Rogers,¹⁵ T. Stanley,¹⁵ J. Tarrant,¹⁵ M. Tucker,¹⁵ A. Wilson,¹⁵ S. Watson,¹⁶ R. Bayes,¹⁷ J. C. Nugent,¹⁷ F. J. P. Soler,¹⁷ R. Gamet,¹⁸ G. Barber,¹⁹ V. J. Blackmore,¹⁹ D. Colling,¹⁹ A. Dobbs,¹⁹ P. Dornan,¹⁹ C. Hunt,¹⁹ A. Kurup,¹⁹ J.-B. Lagrange,^{19,*} K. Long,¹⁹ J. Martyniak,¹⁹ S. Middleton,¹⁹ J. Pasternak,¹⁹ M. A. Uchida,¹⁹ J. H. Cobb,²⁰ W. Lau,²⁰ C. N. Booth,²¹ P. Hodgson,²¹ J. Langlands,²¹ E. Overton,²¹ M. Robinson,²¹ P. J. Smith,²¹ S. Wilbur,²¹ A. J. Dick,²² K. Ronald,²² C. G. Whyte,²² A. R. Young,²² S. Boyd,²³ P. Franchini,²³ J. R. Greis,²³ C. Pidcott,²³ I. Taylor,²³ R. B. S. Gardener,²⁴ P. Kyberd,²⁴ J. J. Nebrensky,²⁴ M. Palmer,²⁵ H. Witte,²⁵ A. D. Bross,²⁶ D. Bowring,²⁶ A. Liu,²⁶ D. Neuffer,²⁶ M. Popovic,²⁶ P. Rubinov,²⁶ A. DeMello,²⁷ S. Gourlay,²⁷ D. Li,²⁷ S. Prestemon,²⁷ S. Virostek,²⁷ B. Freemire,²⁸ P. Hanlet,²⁸ D. M. Kaplan,²⁸ T. A. Mohayai,²⁸ D. Rajaram,²⁸ P. Snopok,²⁸ V. Suezaki,²⁸ Y. Torun,²⁸ Y. Onel,²⁹ L. M. Cremaldi,³⁰ D. A. Sanders,³⁰ D. J. Summers,³⁰ G. G. Hanson,³¹ and C. Heidt³¹

(The MICE collaboration)

¹*Department of Atomic Physics, St. Kliment Ohridski University of Sofia, Sofia 1164, Bulgaria*

²*Institute of High Energy Physics, Chinese Academy of Sciences, Beijing 100039, China*

³*Sichuan University, Sichuan Sheng 610000, China*

⁴*Sezione INFN Milano Bicocca, Dipartimento di Fisica G. Occhialini, Milano 20126, Italy*

⁵*Sezione INFN Napoli and Dipartimento di Fisica, Università Federico II, Complesso Universitario di Monte S. Angelo, Napoli 80126, Italy*

⁶*Sezione INFN Pavia and Dipartimento di Fisica, Pavia 27100, Italy*

⁷*INFN Sezione di Roma Tre and Dipartimento di Matematica e Fisica, Università Roma Tre, 00146 Roma, Italy*

⁸*Osaka University, Graduate School of Science, Department of Physics, Toyonaka, Osaka 565-0871, Japan*

⁹*High Energy Accelerator Research Organization (KEK), Institute of Particle and Nuclear Studies, Tsukuba 305-0801, Ibaraki, Japan*

¹⁰*Nikhef, Amsterdam, The Netherlands and Radboud University, Nijmegen 1098, The Netherlands*

¹¹*Institute of Physics, University of Belgrade, Belgrade 11080, Serbia*

¹²*CERN, Geneva 1217, Switzerland*

¹³*DPNC, Section de Physique, Université de Genève, Geneva 1205, Switzerland*

¹⁴*STFC Daresbury Laboratory, Daresbury, Cheshire WA4 4AD, United Kingdom*

¹⁵*STFC Rutherford Appleton Laboratory, Harwell Oxford, Didcot OX11 0QX, United Kingdom*

¹⁶*STFC Rutherford UK Astronomy Technology Centre, Royal Observatory, Edinburgh, Blackford Hill, Edinburgh EH9 3HJ, United Kingdom*

¹⁷*School of Physics and Astronomy, Kelvin Building, The University of Glasgow, Glasgow G12 8SU, United Kingdom*

¹⁸*Department of Physics, University of Liverpool, Liverpool L69 7ZE, United Kingdom*

¹⁹*Department of Physics, Blackett Laboratory, Imperial College London, London SW7 2BB, United Kingdom*

²⁰*Department of Physics, University of Oxford, Denys Wilkinson Building, Oxford OX1 3PJ, United Kingdom*

²¹*Department of Physics and Astronomy, University of Sheffield, Sheffield S10 2TN, United Kingdom*

²²*SUPA and the Department of Physics, University of Strathclyde, Glasgow G1 1XQ, United Kingdom and Cockcroft Institute, United Kingdom*

²³*Department of Physics, University of Warwick, Coventry CV4 7AL, United Kingdom*

²⁴*Brunel University, Uxbridge UB8 3PH, United Kingdom*

²⁵*Brookhaven National Laboratory, New York NY 11967, USA*

²⁶*Fermilab, Batavia, Illinois 60510, USA*

²⁷*Lawrence Berkeley National Laboratory, Berkeley, California 94720, USA*²⁸*Illinois Institute of Technology, Chicago, Illinois 60616, USA*²⁹*Department of Physics and Astronomy, University of Iowa, Iowa City, Iowa 52242, USA*³⁰*University of Mississippi, Oxford, Mississippi 38677, USA*³¹*University of California, Riverside, California 92521, USA*

(Received 30 January 2017; published 19 June 2017)

Muon beams of low emittance provide the basis for the intense, well-characterized neutrino beams necessary to elucidate the physics of flavor at a neutrino factory and to provide lepton-antilepton collisions at energies of up to several TeV at a muon collider. The international Muon Ionization Cooling Experiment (MICE) aims to demonstrate ionization cooling, the technique by which it is proposed to reduce the phase-space volume occupied by the muon beam at such facilities. In an ionization-cooling channel, the muon beam passes through a material in which it loses energy. The energy lost is then replaced using rf cavities. The combined effect of energy loss and reacceleration is to reduce the transverse emittance of the beam (transverse cooling). A major revision of the scope of the project was carried out over the summer of 2014. The revised experiment can deliver a demonstration of ionization cooling. The design of the cooling demonstration experiment will be described together with its predicted cooling performance.

DOI: [10.1103/PhysRevAccelBeams.20.063501](https://doi.org/10.1103/PhysRevAccelBeams.20.063501)

I. INTRODUCTION

Stored muon beams have been proposed as the source of neutrinos at a neutrino factory [1,2] and as the means to deliver multi-TeV lepton-antilepton collisions at a muon collider [3,4]. In such facilities the muon beam is produced from the decay of pions generated by a high-power proton beam striking a target. The tertiary muon beam occupies a large volume in phase space. To optimize the muon yield while maintaining a suitably small aperture in the muon-acceleration system requires that the muon beam be “cooled” (i.e., its phase-space volume reduced) prior to acceleration. A muon is short-lived, decaying with a lifetime of $2.2 \mu\text{s}$ in its rest frame. Therefore, beam manipulation at low energy ($\leq 1 \text{ GeV}$) must be carried out rapidly. Four cooling techniques are in use at particle accelerators: synchrotron-radiation cooling [5]; laser cooling [6–8]; stochastic cooling [9]; and electron cooling [10]. Synchrotron-radiation cooling is observed only in electron or positron beams, owing to the relatively low mass of the electron. Laser cooling is limited to certain ions and atomic beams. Stochastic cooling times are dependent on the bandwidth of the stochastic-cooling system relative to the frequency spread of the particle beam. The electron-cooling time is limited by the available electron density and the electron-beam energy and emittance. Typical cooling times are between seconds and hours, long compared with the muon lifetime. Ionization cooling proceeds by passing a muon beam through a material, the absorber, in which it

loses energy through ionization, and subsequently restoring the lost energy in accelerating cavities. Transverse and longitudinal momentum are lost in equal proportions in the absorber, while the cavities restore only the momentum component parallel to the beam axis. The net effect of the energy-loss/reacceleration process is to decrease the ratio of transverse to longitudinal momentum, thereby decreasing the transverse emittance of the beam. In an ionization-cooling channel the cooling time is short enough to allow the muon beam to be cooled efficiently with modest decay losses. Ionization cooling is therefore the technique by which it is proposed to cool muon beams [11–13]. This technique has never been demonstrated experimentally and such a demonstration is essential for the development of future high-brightness muon accelerators.

The international Muon Ionization Cooling Experiment (MICE) collaboration proposes a two-part process to perform a full demonstration of transverse ionization cooling. First, the “Step IV” configuration [14] will be used to study the material and beam properties that determine the performance of an ionization-cooling lattice. Second, a study of transverse-emittance reduction in a cooling cell that includes accelerating cavities will be performed.

The cooling performance of an ionization-cooling cell depends on the emittance and momentum of the initial beam, on the properties of the absorber material and on the transverse betatron function (β_{\perp}) at the absorber. These factors will be studied using the Step IV configuration. Once this has been done, “sustainable” ionization cooling must be demonstrated. This requires restoring energy lost by the muons as they pass through the absorber using rf cavities. The experimental configuration with which the MICE collaboration originally proposed to study ionization cooling was presented in [15]. This configuration was revised to accelerate the timetable on which a demonstration of ionization cooling could be delivered and to reduce

*j.lagrange@imperial.ac.uk

cost. This paper describes the revised lattice proposed by the MICE collaboration for the demonstration of ionization cooling and presents its performance.

II. COOLING IN NEUTRINO FACTORIES AND MUON COLLIDERS

At production, muons occupy a large volume of phase space. The emittance of the initial muon beam must be reduced before the beam is accelerated. A neutrino factory [16] requires the transverse emittance to be reduced from 15–20 mm to 2–5 mm. A muon collider [17] requires the muon beam to be cooled in all six phase-space dimensions; to achieve the desired luminosity requires an emittance of ~ 0.025 mm in the transverse plane and ~ 70 mm in the longitudinal direction [18,19].

Ionization cooling is achieved by passing a muon beam through a material with low atomic number (Z), in which it loses energy by ionization, and subsequently accelerating the beam. The rate of change of the normalized transverse emittance, ε_{\perp} , is given approximately by [12,20,21]:

$$\frac{d\varepsilon_{\perp}}{dz} \simeq -\frac{\varepsilon_{\perp}}{\beta^2 E_{\mu}} \left\langle \frac{dE}{dz} \right\rangle + \frac{\beta_{\perp} (13.6 \text{ MeV}/c)^2}{2\beta^3 E_{\mu} m_{\mu} X_0}; \quad (1)$$

where z is the longitudinal coordinate, βc is the muon velocity, E_{μ} the energy, $\langle \frac{dE}{dz} \rangle$ the mean rate of energy loss per unit path-length, m_{μ} the mass of the muon, X_0 the radiation length of the absorber and β_{\perp} the transverse betatron function at the absorber. The first term of this equation describes “cooling” by ionization energy loss and the second describes “heating” by multiple Coulomb scattering. Equation (1) implies that the equilibrium emittance, for which $\frac{d\varepsilon_{\perp}}{dz} = 0$, and the asymptotic value of $\frac{d\varepsilon_{\perp}}{dz}$ for large emittance are functions of muon-beam energy.

In order to have good performance in an ionization-cooling channel, β_{\perp} needs to be minimized and $X_0 \langle \frac{dE}{dz} \rangle$

maximised. The betatron function at the absorber is minimized using a suitable magnetic focusing channel (typically solenoidal) [22,23] and $X_0 \langle \frac{dE}{dz} \rangle$ is maximized using a low- Z absorber such as liquid hydrogen (LH_2) or lithium hydride (LiH) [24].

III. THE MUON IONIZATION COOLING EXPERIMENT

The muons for MICE come from the decay of pions produced at an internal target dipping directly into the circulating proton beam in the ISIS synchrotron at the Rutherford Appleton Laboratory (RAL) [25,26]. A beam line of 9 quadrupoles, 2 dipoles and a superconducting “decay solenoid” collects and transports the momentum-selected beam into the experiment [27]. The small fraction of pions that remain in the beam may be rejected during analysis using the time-of-flight hodoscopes and Cherenkov counters that are installed in the beam line upstream of the experiment [28]. A diffuser is installed at the upstream end of the experiment to vary the initial emittance of the beam. Ionization cooling depends on momentum through β , E_{μ} and $\langle \frac{dE}{dz} \rangle$ as shown in Eq. (1). It is therefore proposed that the performance of the cell be measured for momenta in the range 140 MeV/ c to 240 MeV/ c [15].

A. The configuration of the ionization-cooling experiment

The configuration proposed for the demonstration of ionization cooling is shown in Fig. 1. It contains a cooling cell sandwiched between two spectrometer-solenoid modules. The cooling cell is composed of two 201 MHz cavities, one primary (65 mm) and two secondary (32.5 mm) LiH absorbers placed between two superconducting “focus-coil” (FC) modules. Each FC has two separate windings that can be operated either with the same or in opposed polarity.

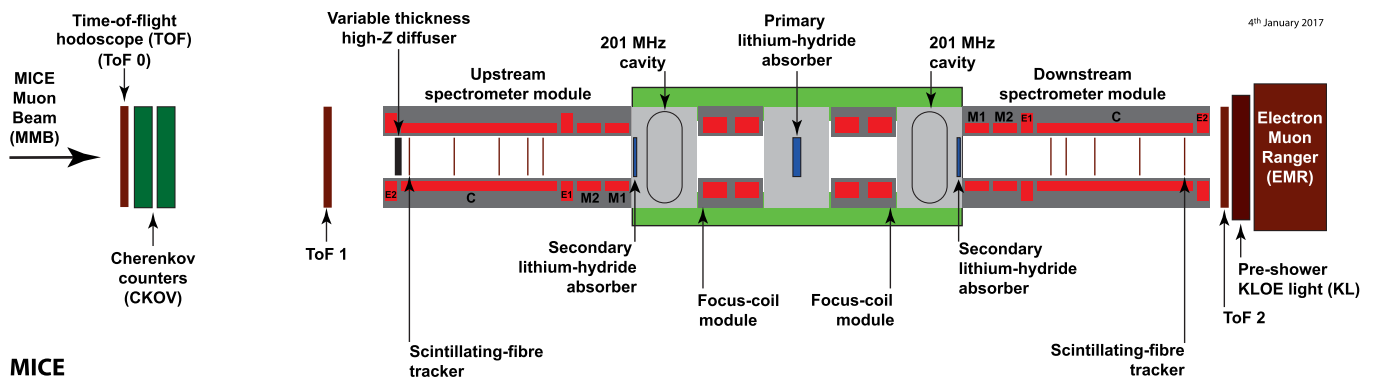


FIG. 1. Layout of the lattice configuration for the cooling demonstration. The red rectangles represent the solenoids. The individual coils in the spectrometer solenoids are labeled E1, C, E2, M1 and M2. The ovals represent the rf cavities and the blue rectangles the absorbers. The various detectors (time-of-flight hodoscopes [29,30], Cherenkov counters [31], scintillating-fibre trackers [32], KLOE Light (KL) calorimeter [27,33], electron muon ranger [34]) used to characterize the beam are also represented. The green-shaded box indicates the cooling cell.

The emittance is measured upstream and downstream of the cooling cell using scintillating-fiber tracking detectors [32] immersed in the uniform 4 T magnetic field provided by three superconducting coils (E1, C, E2). The trackers are used to reconstruct the trajectories of individual muons at the entrance and exit of the cooling cell. The reconstructed tracks are combined with information from instrumentation upstream and downstream of the spectrometer modules to measure the muon-beam emittance at the upstream and downstream tracker reference planes. The instrumentation upstream and downstream of the spectrometer modules serves to select a pure sample of muons. Time-of-flight hodoscopes are used to determine the time at which the muon crosses the rf cavities. The spectrometer-solenoid magnets also contain two superconducting “matching” coils (M1, M2) that are used to match the optics between the uniform field region and the neighboring FC.

The secondary LiH absorbers (SAs) are introduced between the cavities and the trackers to minimize the exposure of the trackers to “dark-current” electrons originating from the rf cavities. Experiments at the MuCool Test Area (MTA) at Fermilab [35] have observed that the rate of direct x-ray production from the rf cavities can be managed to ensure it does not damage the trackers [36]. The SAs are introduced to minimize the exposure of the trackers to energetic dark-current electrons that could produce background hits. The SAs are positioned between the trackers and the cavities such that they can be removed to study the empty channel. The SAs increase the net transverse-cooling effect since the betatron functions at these locations are small.

Retractable lead radiation shutters will be installed on rails between the spectrometer solenoids and the rf modules to protect the trackers against dark-current induced radiation during cavity conditioning. The SAs will be mounted on a rail system similar to that which will be used for the lead shutters and will be located between the cavities and the lead shutters. Both mechanisms will be moved using linear piezoelectric motors that operate in vacuum and magnetic field. The design of both the radiation shutter and the movable SA inside the vacuum chamber is shown in Fig. 2.

The rf cavities are 201 MHz “pillbox” resonators, 430 mm in length, operating in the TM_{010} mode with large diameter apertures to accommodate the high emittance beam. The apertures are covered by thin (0.38 mm) beryllium windows to define the limits for the accelerating rf fields whilst minimizing the scattering of muons. The cavity is excited by two magnetic-loop couplers on opposite sides of the cavity. At the particle rate expected in MICE there is no beam-loading of the rf fields. An effective peak field of 10.3 MV/m is expected for a drive power of 1.6 MW to each cavity. This estimate was used to define the gradient in the simulations described below.

The original configuration of the MICE cooling cell described in [15] was composed of three focus-coil modules, each of which housed a liquid-hydrogen absorber, and two,

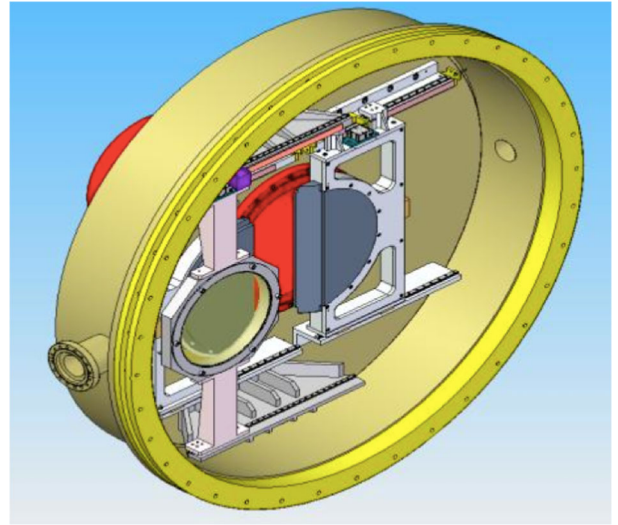


FIG. 2. Design of the movable frame for the secondary absorber (front) and the lead radiation shutter (back). The half discs of the lead shutter (grey) can be seen together with the rails (white) inside the vacuum chamber (yellow).

four-cavity, linac modules. Each linac module incorporated a large, superconducting “coupling coil” to transport the beam. The configuration described in this paper was developed to simplify the lattice described in [15] such that the coupling coils are not required and acceleration is provided by two single-cavity modules. The revision of the magnetic lattice substantially reduces the technical risks associated with the implementation of the experiment since all of the superconducting solenoids required to transport and focus the beam have been commissioned on the beam line. Further, by reducing the number of cavities from eight to two and reconfiguring the rf-power-distribution system the cost of implementing the experiment has been reduced and the timetable on which the experiment can be mounted has been advanced. The present configuration was optimized to maximize its cooling performance as described in Sec. IV. The performance of the optimized lattice, though reduced compared to that described in [15], is sufficient for the principle of ionization-cooling to be demonstrated (see Sec. VI).

IV. LATTICE DESIGN

A. Design parameters

The lattice has been optimized to maximize the reduction in transverse emittance. The optimum is obtained by matching the betatron function to a small value in the central absorber while minimizing its maximum values in the FC modules; limiting the size of the betatron function in the FCs helps to reduce the influence of nonlinear terms in the magnetic-field expansion. The matching accounts for the change in energy of the muons as they pass through the cooling cell by adjusting currents in the upstream and

downstream FCs and in the matching coils in the spectrometer solenoids independently while maintaining the field in the tracking volumes at 4 T. In this configuration, it is also possible to keep the betatron function relatively small at the position of the secondary absorbers whilst maintaining an acceptable beam size at the position of the cavities.

Chromatic aberrations caused by the large momentum spread of the beam ($\sim 5\%$ rms) lead to a chromatic mismatch of the beam in the downstream solenoid unless the phase advance across the cooling cell (i.e., the rate of rotation of the phase-space ellipse) is chosen appropriately. The phase advance of the cell is obtained by integrating the inverse of the beta-function along the beam axis from the reference plane in the upstream spectrometer-solenoid to the reference plane in the downstream spectrometer-solenoid. Such a mismatch reduces the effective transverse-emittance reduction through the chromatic decoherence that results from the superposition of beam evolutions for the different betatron frequencies that result from the range of momenta in the beam. For beams with a large input emittance, spherical aberrations may lead to phase-space filamentation. The chromatic and spherical aberrations were studied by tracking samples of muons through the lattice using the ‘‘MICE Analysis User Software’’ (MAUS, see Sec. V). The betatron-function and emittance evolution of a 200 MeV/ c beam with the

TABLE I. General parameters of the initial beam conditions used in the simulations.

Parameter	Value
Particle	muon μ^+
Number of particles	10000
Longitudinal position [mm]	-4612.1
Central energy (140 MeV/ c settings) [MeV]	175.4
Central energy (200 MeV/ c settings) [MeV]	228.0
Central energy (240 MeV/ c settings) [MeV]	262.2
Transverse Gaussian distribution:	
α_{\perp}	0
β_{\perp} (140 MeV/ c settings) [mm]	233.5
ε_{\perp} (140 MeV/ c settings) [mm]	4.2
β_{\perp} (200 MeV/ c settings) [mm]	339.0
ε_{\perp} (200 MeV/ c settings) [mm]	6.0
β_{\perp} (240 MeV/ c settings) [mm]	400.3
ε_{\perp} (240 MeV/ c settings) [mm]	7.2
Longitudinal Gaussian distribution:	
Longitudinal emittance [mm]	20
Longitudinal β [ns]	11
Longitudinal α	-0.7
rms momentum spread (140 MeV/ c settings)	4.8%
rms time spread (140 MeV/ c settings) [ns]	0.40
rms momentum spread (200 MeV/ c settings)	4.0%
rms time spread (200 MeV/ c settings) [ns]	0.34
rms momentum spread (240 MeV/ c settings)	3.6%
rms time spread (240 MeV/ c settings) [ns]	0.31

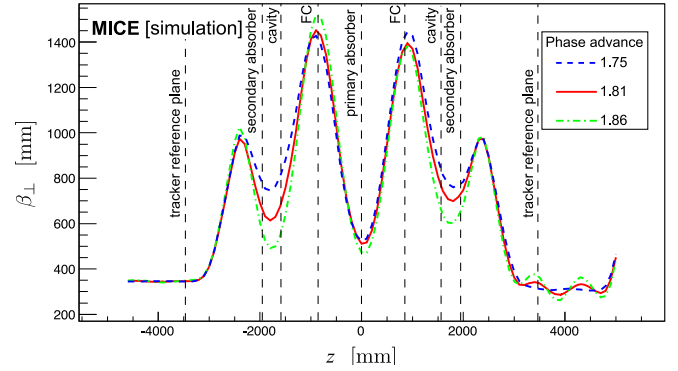


FIG. 3. Transverse 4D beta-function versus longitudinal coordinate z in the cooling-demonstration lattice for 200 MeV/ c settings with a phase advance of $2\pi \times 1.75$ (dashed blue line), $2\pi \times 1.81$ (solid red line) and $2\pi \times 1.86$ (dot-dashed green line). The vertical dashed lines with labels show the positions of the tracker reference planes and the centers of the absorbers, rf cavities, and focus coil modules.

initial parameters given in Table I are shown, for different phase advances, in Figs. 3 and 4, respectively. The phase advance of $2\pi \times 1.81$ showed the largest transverse-emittance reduction and was therefore chosen. The lattice parameters for this phase advance are presented in Table II.

The currents that produce the optimum magnetic lattice were obtained using the procedure described above for three momentum settings: 140 MeV/ c , 200 MeV/ c , and 240 MeV/ c . The magnetic field on axis for each of these settings is shown in Fig. 5. The fields in the downstream FC and spectrometer are opposite to those in the upstream FC and spectrometer, the field changing sign at the primary absorber. Such a field flip is required in an ionization cooling channel to reduce the build-up of canonical angular momentum [37]. The currents required to produce the magnetic fields shown in Fig. 5 are listed in Table III. All currents are within the proven limits of operation for the

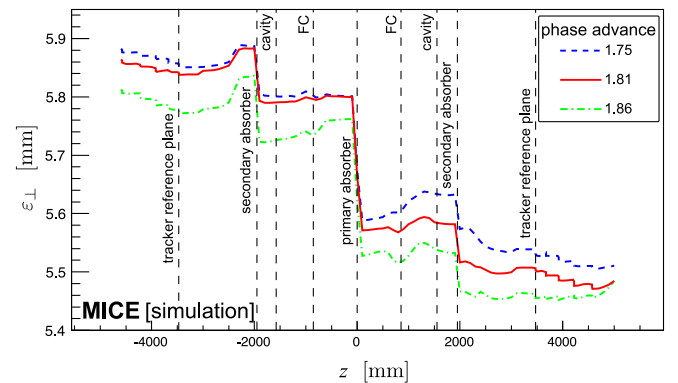


FIG. 4. 4D emittance evolution in the cooling-demonstration lattice for 200 MeV/ c settings with a phase advance of $2\pi \times 1.75$ (dashed blue line), $2\pi \times 1.81$ (solid red line) and $2\pi \times 1.86$ (dot-dashed green line). The vertical dashed lines with labels show the positions of the tracker reference planes and the centers of the absorbers, rf cavities, and focus coil modules.

TABLE II. Parameters of the cooling-demonstration lattice. $L_{SS \rightarrow FC}$ is the distance between the center of the spectrometer solenoid and the center of the neighboring FC, $L_{FC \rightarrow FC}$ the distance between the centers of the FCs, and $L_{RF \text{ module} \rightarrow FC}$ the distance between the rf module and the neighboring FC.

Parameter	Value
Length $L_{SS \rightarrow FC}$ [mm]	2607.5
Length $L_{FC \rightarrow FC}$ [mm]	1678.8
Length $L_{rf \text{ module} \rightarrow FC}$ [mm]	784.0
rf Gradient [MV/m]	10.3
Number of rf cavities	2
Number of primary absorbers	1
Number of secondary absorbers	2

individual coil windings. The magnetic forces acting on the coils have been analyzed and were found to be acceptable. Configurations in which there is no field flip can also be considered.

Figure 6 shows matched betatron functions versus longitudinal position for beams of different initial momentum. These betatron functions are constrained, within the fiducial-volume of the trackers, by the requirements on the Courant-Snyder parameters $\alpha_{\perp} = 0$ and $\beta_{\perp} = \frac{2p_z}{eB_z}$ (where p_z is the mean longitudinal momentum of the beam, e the elementary charge and B_z the longitudinal component of the magnetic field). A small betatron-function “waist” in the central absorber is achieved. Betatron-function values at relevant positions in the different configurations are summarized in Table IV.

V. SIMULATION

Simulations to evaluate the performance of the lattice have been performed using the official MICE simulation

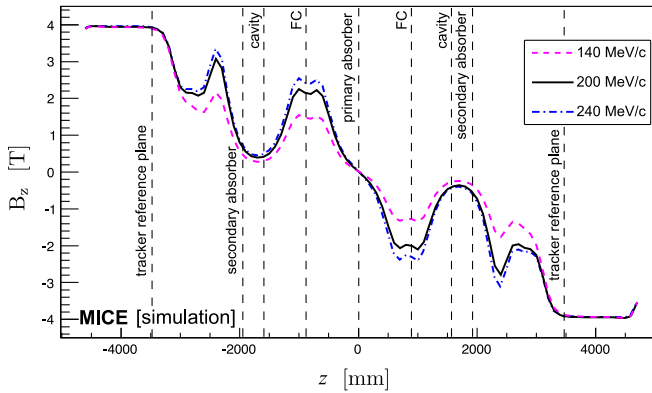


FIG. 5. Magnetic field B_z on-axis versus the longitudinal coordinate z for the cooling-demonstration lattice design for 200 MeV/c (solid black line), 140 MeV/c (dashed purple line), and 240 MeV/c (dot-dashed blue line) settings. The vertical dashed lines with labels show the positions of the tracker reference planes and the centres of the absorbers, rf cavities, and focus coil modules.

TABLE III. Coil currents used for 140 MeV/c, 200 MeV/c, and 240 MeV/c lattice settings.

Coil	140 MeV/c Lattice [A]	200 MeV/c Lattice [A]	240 MeV/c Lattice [A]
Upstream E2	+253.00	+253.00	+253.00
Upstream C	+274.00	+274.00	+274.00
Upstream E1	+234.00	+234.00	+234.00
Upstream M2	+126.48	+155.37	+163.50
Upstream M1	+175.89	+258.42	+280.72
Upstream FC-coil 1	+54.14	+79.35	+89.77
Upstream FC-coil 2	+54.14	+79.35	+89.77
Downstream FC-coil 1	-47.32	-74.10	-85.35
Downstream FC-coil 2	-47.32	-74.10	-85.35
Downstream M1	-140.43	-231.60	-261.71
Downstream M2	-100.12	-149.15	-159.21
Downstream E1	-234.00	-234.00	-234.00
Downstream C	-274.00	-274.00	-274.00
Downstream E2	-253.00	-253.00	-253.00

and reconstruction software MAUS (MICE Analysis User Software) [38]. In addition to simulation, MAUS also provides a framework for data analysis. MAUS is used for offline analysis and to provide fast real-time detector reconstruction and data visualisation during MICE running. MAUS uses GEANT4 [39,40] for beam propagation and the simulation of detector response. ROOT [41] is used for data visualisation and for data storage.

Particle tracking has been performed for several configurations. The parameters of the initial beam configurations used for the simulations are summarized in Table I.

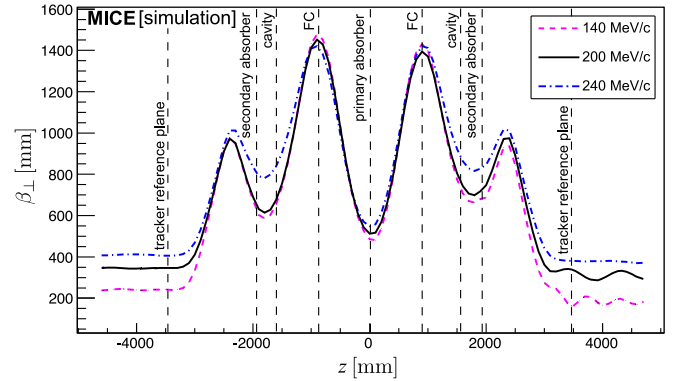


FIG. 6. β_{\perp} versus the longitudinal coordinate z for 200 MeV/c (solid black line), 140 MeV/c (dashed purple line) and 240 MeV/c (dot-dashed blue line) in the cooling-demonstration lattice. The vertical dashed lines with labels show the positions of the tracker reference planes and the centers of the absorbers, rf cavities, and focus coil modules.

TABLE IV. Beta-function values at relevant positions for an initial beam at 140 MeV/c, 200 MeV/c, and 240 MeV/c in the cooling-demonstration lattice design.

Parameter	Value for 140 MeV/c	Value for 200 MeV/c	Value for 240 MeV/c
β_{\perp} at primary absorber [mm]	480	512	545
β_{\perp} at upstream secondary absorber [mm]	660	710	840
β_{\perp} at downstream secondary absorber [mm]	680	740	850
$\beta_{\perp \text{ max}}$ at FC [mm]	1480	1450	1430

The simulation of the beam starts at a point between the diffuser and the first plane of the tracker. The beam is generated by a randomizing algorithm with a fixed seed. The number of particles launched for each simulation is a compromise between the statistical uncertainty required ($\approx 1\%$) and computing time. Each cavity is simulated by a TM₀₁₀ ideal cylindrical pillbox with a peak effective gradient matched to that expected for the real cavities. The reference particle is used to set the phase of the cavities so that it is accelerated “on crest.” The initial distributions defined in Table I are centred on the reference particle in both time and momentum. Table V lists the acceptance criteria applied to all analyses presented here. Trajectories that fail to meet the acceptance criteria are removed from the analysis.

The normalized transverse emittance is calculated by taking the fourth root of the determinant of the four-dimensional phase-space covariance matrix [20,21]. The MICE collaboration plans to take data such that the statistical uncertainty on the relative change in emittance for a particular setting is 1%. The MICE instrumentation was designed such that the systematic uncertainty related to the reconstruction of particle trajectories would contribute at the $\sim 0.3\%$ level to the overall systematic uncertainty [15]; such uncertainties would thus be negligible.

VI. PERFORMANCE

Figure 7 shows the evolution of the mean energy of a muon beam as it traverses the lattice. Beams with initial normalised transverse emittance $\epsilon_{\perp} = 4.2$ mm,

TABLE V. Acceptance criteria for analysis.

Parameter	Acceptance condition
Particle	muon μ^+
Transmission: pass through two planes	$z = -4600$ mm and $z = 5000$ mm
Radius at $z = -4600$ mm	≤ 150.0 mm
Radius at $z = 5000$ mm	≤ 150.0 mm

$\epsilon_{\perp} = 6$ mm, and $\epsilon_{\perp} = 7.2$ mm for initial muon beam momenta of 140 MeV/c, 200 MeV/c, and 240 MeV/c respectively are shown. The initial normalized transverse emittance is chosen such that the geometrical emittance of the three beams is the same. A 200 MeV/c muon passing through two 32.5 mm thick secondary LiH absorbers and one 65 mm thick primary LiH absorber loses an energy of 18.9 MeV. Including losses in the scintillating-fiber

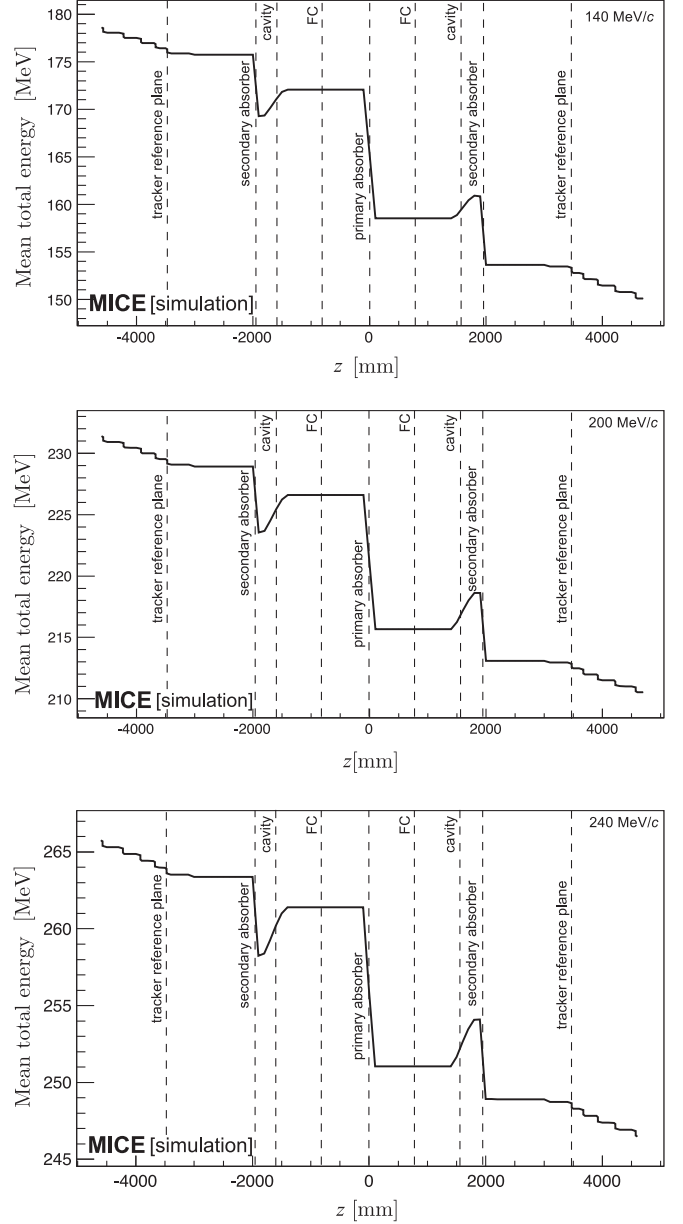


FIG. 7. Mean energy of the beam versus longitudinal coordinate (z) in the cooling-demonstration lattice. Top: the 140 MeV/c configuration for initial emittance $\epsilon_{\perp} = 4.2$ mm. Middle: the 200 MeV/c configuration for initial emittance $\epsilon_{\perp} = 6$ mm. Bottom: the 240 MeV/c configuration for initial emittance $\epsilon_{\perp} = 7.2$ mm. The vertical dashed lines with labels show the positions of the tracker reference planes, and the centers of the absorbers, rf cavities, and focus coil modules.

trackers and windows, this increases to 24.3 MeV. The accelerating gradient that can be achieved in each of the two cavities is constrained by the available rf power and is insufficient to replace all the lost energy. Therefore, a comparison of beam energy with and without acceleration is required. With acceleration an energy

deficit of $\langle \Delta E \rangle = 19$ MeV will be observed. This measurable difference will be used to extrapolate the measured cooling effect to that which would pertain if all the lost energy were restored.

The evolution of normalized transverse emittance across the lattice is shown in Fig. 8. The beam is subject to nonlinear effects in regions of high β_{\perp} , which cause the normalized transverse emittance to grow, especially in the 140 MeV/c configuration. This phenomenon can be seen in three different regions of the lattice: a moderate increase in emittance is observed at $z \approx -2500$ mm and $z \approx 1000$ mm while a larger increase is observed at $z \approx 3000$ mm. The nonlinear effects are mainly chromatic in origin, since they are greatly lessened when the initial momentum spread is reduced. This is illustrated for the 140 MeV/c case for which the evolution of normalized emittance for beams with an rms momentum spread of 6.7 MeV/c and 2.5 MeV/c are shown. Nonetheless, in all cases a reduction in emittance is observed between the upstream and downstream trackers ($z = \pm 3473$ mm). The lattice is predicted to achieve an emittance reduction between the tracker reference planes of $\approx 8.1\%$, $\approx 5.8\%$ and $\approx 4.0\%$ in the 140 MeV/c, 200 MeV/c, and 240 MeV/c cases, respectively. A reduction as large as $\approx 10\%$ can be reached in the 140 MeV/c configuration with an rms momentum spread of 1.4%.

The transmission of the cooling-demonstration lattice for beams of mean momentum 140 MeV/c, 200 MeV/c, and 240 MeV/c is shown in Fig. 9. Transmission is computed as the ratio of the number of particles that satisfy the acceptance criteria observed downstream of the cooling cell divided by the number that enter the cell. This accounts

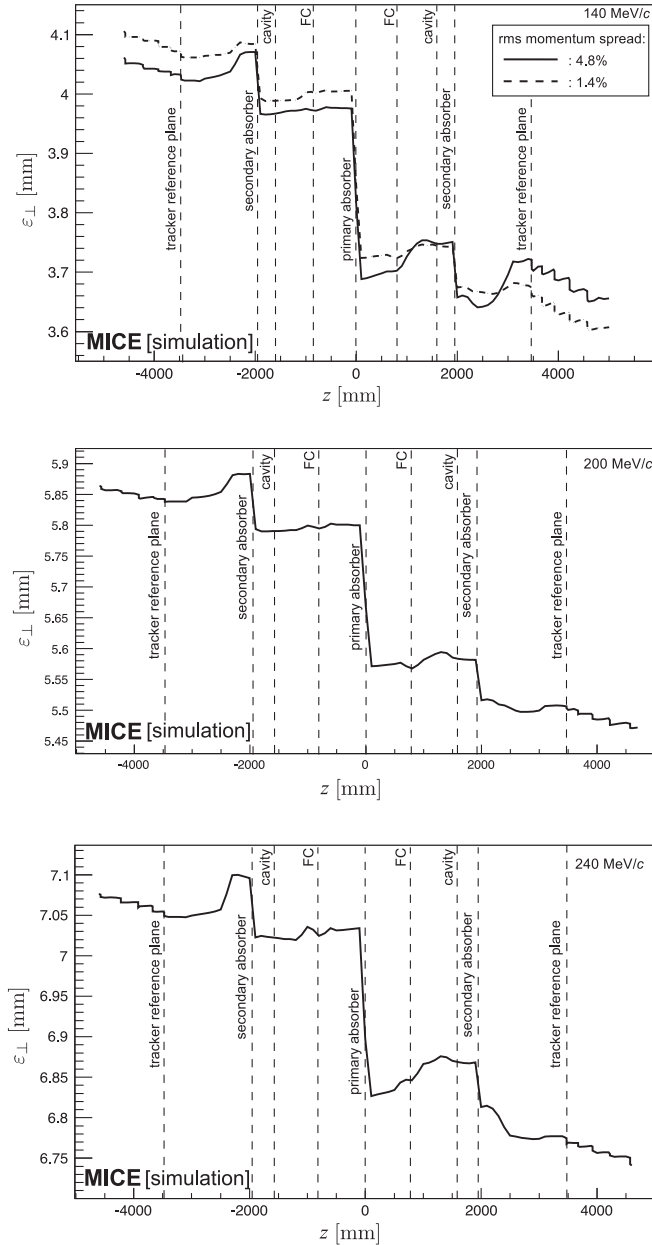


FIG. 8. Emittance variation versus the longitudinal coordinate (z) for the cooling-demonstration lattice design. Top: 140 MeV/c beam with initial $\epsilon_{\perp} = 4.2$ mm with an rms momentum spread of 6.7 MeV/c (rms spread 4.8%, solid line) and 2.5 MeV/c (rms spread 1.8%, dashed line). Middle: 200 MeV/c beam with initial $\epsilon_{\perp} = 6$ mm (rms spread 4.0%). Bottom: 240 MeV/c beam with initial $\epsilon_{\perp} = 7.2$ mm (rms spread 3.6%). The vertical dashed lines with labels show the positions of the tracker reference planes, and the centers of the absorbers, rf cavities, and focus coil modules.

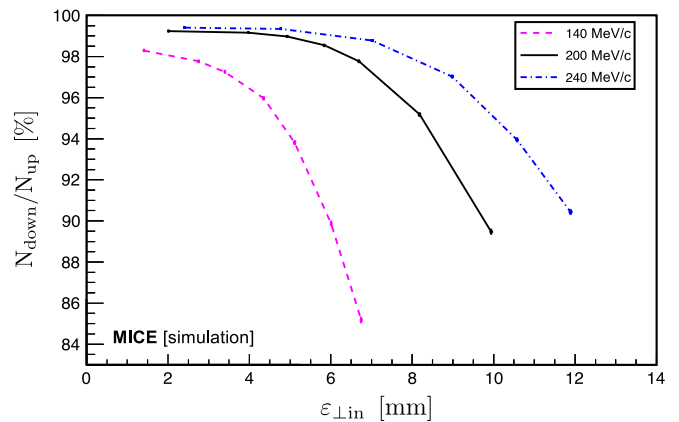


FIG. 9. Transmission (defined as the ratio of good muons observed downstream of the cooling cell, N_{down} , to those observed upstream, N_{up}) in percent versus initial emittance ($\epsilon_{\perp,\text{in}}$) for the cooling-demonstration lattice. The transmission of the 140 MeV/c, 200 MeV/c, and 240 MeV/c lattices are shown as the purple-dashed, solid black, and dot-dashed blue lines respectively. The error bars indicate the statistical precision that would be achieved using a sample of 100,000 muons.

for decay losses and implies that, in the absence of scraping or acceptance losses, the maximum transmission for beams of mean momentum 140 MeV/c, 200 MeV/c, and 240 MeV/c is 98.9%, 99.2%, and 99.5%, respectively. The lattice delivers transmission close to the maximum for 200 MeV/c and 240 MeV/c beams with input emittance below ≈ 5 mm and ≈ 7 mm, respectively. For beams of larger input emittance, the transmission gradually decreases with increasing initial emittance due to the scraping of high amplitude muons. The beam is subject to chromatic effects in regions of high β_{\perp} , which causes nonlinear emittance growth and limits the transmission. The behavior of the transmission for the various beam energies results from the different geometrical emittance values of the beam for the same initial normalised emittance and the energy dependence of the energy loss and scattering in the material through which the beam passes.

The fractional change in normalized transverse emittance with respect to the input emittance for beams of mean momentum 140 MeV/c, 200 MeV/c, and 240 MeV/c is shown in Fig. 10. The different values of the equilibrium emittance and the asymptote at large emittance for each momentum are clearly visible in Fig. 10. A maximum cooling effect of 15%, 8%, and 6% can be observed for beams with 140 MeV/c, 200 MeV/c, and 240 MeV/c, respectively.

The performance of the configuration proposed here is comparable to that described in [15]. In the ‘‘Step V’’ configuration, that incorporated two liquid-hydrogen absorbers each placed within a focus-coil module capable of providing a value β_{\perp} smaller than that which can be achieved with the present lattice, the maximum cooling effect with an input momentum and emittance of

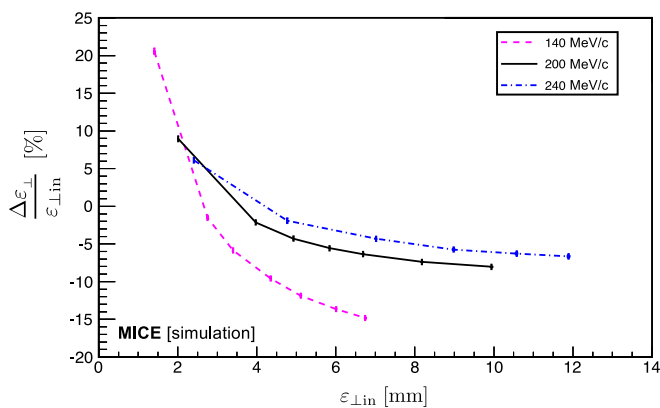


FIG. 10. Fractional change in emittance versus initial emittance ($\epsilon_{\perp, \text{in}}$) for the cooling-demonstration lattice design measured at the tracker reference planes. The fractional change in emittance of the 140 MeV/c, 200 MeV/c, and 240 MeV/c lattices are shown as the purple-dashed, solid black, and dot-dashed blue lines, respectively. The error bars indicate the statistical precision that would be achieved using a sample of 100,000 muons.

200 MeV/c and 10 mm respectively, was $\sim 10\%$. Figures 9 and 10 show the statistical uncertainties that will result from the reconstruction of a sample of 100,000 muons [42] with the configuration proposed in this paper. The instrumentation was specified to ensure that no single source of systematic uncertainty would contribute more than one third of the statistical uncertainty on the fractional change in emittance [15]. All of the instrumentation has been commissioned on the beam-line and performs to specification. The emittance-change evolution presented in Fig. 10 can therefore be measured with high significance.

VII. CONCLUSION

An experiment by which to demonstrate ionization cooling has been described that is predicted by simulations to exhibit cooling over a range of momentum. The demonstration is performed using lithium-hydride absorbers and with acceleration provided by two 201 MHz cavities. The equipment necessary to mount the experiment is either in hand (the superconducting magnets and instrumentation), or at an advanced stage of preparation. The configuration of the demonstration of ionization cooling has been shown to deliver the performance required for the detailed study of the ionization-cooling technique.

The demonstration of ionization cooling is essential to the future development of muon-based facilities that would provide the intense, well characterized low-emittance muon beams required to elucidate the physics of flavor at a neutrino factory or to deliver multi-TeV lepton-antilepton collisions at a muon collider. The successful completion of the MICE programme would therefore herald the establishment of a new technique for particle physics.

ACKNOWLEDGMENTS

The work described here was made possible by grants from the Science and Technology Facilities Council (UK), the Department of Energy and National Science Foundation (USA), the Istituto Nazionale di Fisica Nucleare (Italy), the Bulgarian Academy of Sciences, the Chinese Academy of Sciences, the Dutch National Science Foundation, the Ministry of Education, Science and Technological Development of the Republic of Serbia, the European Community under the European Commission Framework Programme 7 (AIDA project, Grant Agreement No. 262025, TIARA project, Grant Agreement No. 261905, and EuCARD), the Japan Society for the Promotion of Science and the Swiss National Science Foundation in the framework of the SCOPES programme. We gratefully acknowledge all sources of support. We are grateful to the support given to us by the staff of the STFC Rutherford Appleton and Daresbury Laboratories. We acknowledge the use of Grid computing resources deployed and operated by GridPP in the UK, <http://www.gridpp.ac.uk/>.

- [1] S. Geer, Neutrino beams from muon storage rings: Characteristics and physics potential, *Phys. Rev. D* **57**, 6989 (1998).
- [2] M. Apollonio *et al.*, Oscillation Physics with a Neutrino Factory, [arXiv:hep-ph/0210192](https://arxiv.org/abs/hep-ph/0210192).
- [3] D. V. Neuffer and R. B. Palmer, A high-energy high-luminosity $\mu^+\mu^-$ collider in *Proceedings of the Fourth European Particle Accelerator Conference EPAC 94, London, England* (World Scientific, River Edge, NJ, 1994), p. 52.
- [4] R. B. Palmer, Muon colliders, *Rev. Accel. Sci. Technol.* **07**, 137 (2014).
- [5] S. Y. Lee, *Accelerator Physics*, 3rd ed., edited by S. Y. Lee (World Scientific, Singapore, 2012).
- [6] S. Schröder *et al.*, First laser cooling of relativistic ions in a storage ring, *Phys. Rev. Lett.* **64**, 2901 (1990).
- [7] J. S. Hangst, M. Kristensen, J. S. Nielsen, O. Poulsen, J. P. Schiffer, and P. Shi, Laser cooling of a stored ion beam to 1 mK, *Phys. Rev. Lett.* **67**, 1238 (1991).
- [8] P. J. Channell, Laser cooling of heavy ion beams, *J. Appl. Phys.* **52**, 3791 (1981).
- [9] J. Marriner, Stochastic cooling overview, *Nucl. Instrum. Methods Phys. Res., Sect. A* **532**, 11 (2004).
- [10] V. V. Parkhomchuk and A. N. Skrinsky, Electron cooling: 35 years of development, *Phys. Usp.* **43**, 433 (2000).
- [11] A. N. Skrinsky and V. V. Parkhomchuk, Cooling methods for beams of charged particles, *Fiz. Elem. Chastits At. Yadra* **12**, 557 (1981) [*Sov. J. Part. Nucl.* **12**, 223 (1981)].
- [12] D. Neuffer, Principles and applications of muon cooling, in *Proceedings, 12th International Conference on High-Energy Accelerators, HEACC 1983: Fermilab, Batavia, 1983*, Vol. C830811 (Fermi National Accelerator Laboratory, Batavia, 1983), p. 481–484.
- [13] D. Neuffer, Principles and applications of muon cooling, *Part. Accel.* **14**, 75 (1983).
- [14] D. Rajaram and V. C. Palladino, The status of MICE Step IV, in *Proceedings, 6th International Particle Accelerator Conference (IPAC 2015): Richmond, Virginia, USA, 2015* (JACoW, Geneva, 2015), p. 4000.
- [15] MICE Collaboration, MICE: An International Muon Ionization Cooling Experiment, <http://mice.iit.edu/micenotes/public/pdf/MICE0021/MICE0021.pdf> (2003), MICE Note 21.
- [16] M. Apollonio *et al.* (ISS Accelerator Working Group Collaboration), Accelerator design concept for future neutrino facilities, *J. Instrum.* **4**, P07001 (2009).
- [17] C. M. Ankenbrandt *et al.*, Status of muon collider research and development and future plans, *Phys. Rev. ST Accel. Beams* **2**, 081001 (1999).
- [18] M. M. Alsharoa *et al.* (Neutrino Factory and Muon Collider Collaboration), Recent progress in neutrino factory and muon collider research within the Muon collaboration, *Phys. Rev. ST Accel. Beams* **6**, 081001 (2003).
- [19] R. B. Palmer, J. S. Berg, R. C. Fernow, J. C. Gallardo, H. G. Kirk, Y. Alexahin, D. Neuffer, S. A. Kahn, and D. Summers, A complete scheme of ionization cooling for a muon collider, in *Proceedings of the 22nd Particle Accelerator Conference, PAC-2007, Albuquerque, NM* (IEEE, New York, 2007), p. 3193.
- [20] G. Penn and J. S. Wurtele, Beam Envelope Equations for Cooling of Muons in Solenoid Fields, *Phys. Rev. Lett.* **85**, 764 (2000).
- [21] C. Rogers, Ph.D. dissertation, Imperial College of London, 2008.
- [22] D. Stratakis and R. B. Palmer, Rectilinear six-dimensional ionization cooling channel for a muon collider: A theoretical and numerical study, *Phys. Rev. ST Accel. Beams* **18**, 031003 (2015).
- [23] D. Neuffer, H. Sayed, T. Hart, and D. Summers, Final Cooling for a High-Energy High-Luminosity Lepton Collider, [arXiv:1612.08960](https://arxiv.org/abs/1612.08960).
- [24] A. V. Tollestrup and J. Monroe, Fermi National Accelerator Laboratory Technical Report No. FERMILAB-MUCOOL-176, 2000.
- [25] C. N. Booth *et al.*, The design, construction and performance of the MICE target, *J. Instrum.* **8**, P03006 (2013).
- [26] C. N. Booth *et al.*, The design and performance of an improved target for MICE, *J. Instrum.* **11**, P05006 (2016).
- [27] M. Bogomilov *et al.* (MICE Collaboration), The MICE Muon Beam on ISIS and the beam-line instrumentation of the Muon Ionization Cooling Experiment, *J. Instrum.* **7**, P05009 (2012).
- [28] D. Adams *et al.* (MICE Collaboration), Characterisation of the muon beams for the Muon Ionisation Cooling Experiment, *Eur. Phys. J. C* **73**, 2582 (2013).
- [29] R. Bertoni *et al.*, The design and commissioning of the MICE upstream time-of-flight system, *Nucl. Instrum. Methods Phys. Res., Sect. A* **615**, 14 (2010).
- [30] R. Bertoni, M. Bonesini, A. de Bari, G. Cecchet, Y. Karadzhev, and R. Mazza, The construction of the MICE TOF2 detector, <http://mice.iit.edu/micenotes/public/pdf/MICE0286/MICE0286.pdf> (2010).
- [31] L. Cremaldi, D. A. Sanders, P. Sonnek, D. J. Summers, and J. Reidy, Jr., A Cherenkov radiation detector with high density aerogels, *IEEE Trans. Nucl. Sci.* **56**, 1475 (2009).
- [32] M. Ellis *et al.*, The design, construction and performance of the MICE scintillating fibre trackers, *Nucl. Instrum. Methods Phys. Res., Sect. A* **659**, 136 (2011).
- [33] F. Ambrosino *et al.*, Calibration and performances of the KLOE calorimeter, *Nucl. Instrum. Methods Phys. Res., Sect. A* **598**, 239 (2009).
- [34] R. Asfandiyarov *et al.*, The design and construction of the MICE Electron-Muon Ranger, *J. Instrum.* **11**, T10007 (2016).
- [35] M. Leonova *et al.*, MICE cavity installation and commissioning/operation at MTA, in *Proceedings, 6th International Particle Accelerator Conference (IPAC 2015): Richmond, Virginia, USA, 2015* (JACoW, Geneva, 2015), p. 3342–3344.
- [36] Y. Torun *et al.*, Final commissioning of the MICE RF module prototype with production couplers, in *Proceedings, 7th International Particle Accelerator Conference (IPAC 2016): Busan, Korea, 2016* (JACoW, Geneva, 2016), p. 474.
- [37] R. C. Fernow and R. B. Palmer, Solenoidal ionization cooling lattices, *Phys. Rev. ST Accel. Beams* **10**, 064001 (2007).
- [38] C. D. Tunnell and C. T. Rogers, MAUS: MICE Analysis User Software, in *Proceedings of the 2nd International Particle Accelerator Conference, San Sebastián, Spain* (EPS-AG, Spain, 2011), p. 850.

-
- [39] S. Agostinelli *et al.* (GEANT4 Collaboration), GEANT4: A simulation toolkit, *Nucl. Instrum. Methods Phys. Res., Sect. A* **506**, 250 (2003).
- [40] J. Allison *et al.*, Geant4 developments and applications, *IEEE Trans. Nucl. Sci.* **53**, 270 (2006).
- [41] R. Brun and F. Rademakers, ROOT: An object oriented data analysis framework, *Nucl. Instrum. Methods Phys. Res., Sect. A* **389**, 81 (1997).
- [42] C. Hunt, Ph.D. dissertation, Imperial College of London, 2017.

Forecasting hourly particulate matter concentrations based on the advanced multivariate methods

M. Perišić¹ · D. Maletić¹ · S. S. Stojić² · S. Rajšić¹ · A. Stojić¹

Received: 22 April 2016/Revised: 11 July 2016/Accepted: 19 November 2016
© Islamic Azad University (IAU) 2016

Abstract In this study, several multivariate methods were used for forecasting hourly PM₁₀ concentrations at four locations based on SO₂ and meteorological data from the previous period. According to the results, boosted decision trees and multi-layer perceptrons yielded the best predictions. The forecasting performances were similar for all examined locations, despite the additional PM₁₀ spatio-temporal analysis showed that the sites were affected by different emission sources, topographic and microclimatic conditions. The best prediction of PM₁₀ concentrations was obtained for industrial sites, probably due to the simplicity and regularity of dominant pollutant emissions on a daily basis. Conversely, somewhat weaker forecast accuracy was achieved at urban canyon avenue, which can be attributed to the specific urban morphology and most diverse emission sources. In conclusion to this, the integration of advanced multivariate methods in air quality forecasting systems could enhance accuracy and provide the basis for efficient decision-making in environmental regulatory management.

Keywords Air quality · Environmental pollution · Regulatory management · Supervised learning algorithms

Introduction

Over the last century, changes in emission sources, methane concentrations and climate have affected atmospheric composition and led to the significant increase in the levels of particulate matter (PM) and gaseous pollutants, particularly in developing countries (Fang et al. 2013). According to recent estimates, about 3.5 million cardiopulmonary deaths annually and globally can be attributed to exposure to anthropogenic PM_{2.5}, and the projections are that this number could double by 2050 (Lelieveld et al. 2015). In addition to stringent abatement measures, the accurate and reliable prediction of air pollutant episodes and establishment of an early public warning system is of vital importance for the increase in life expectancy and reduction of health care expenditures.

Despite the fact that significant progress has been made through integration of different scientific approaches, modeling of air pollution data remains a challenge, due to complexity and non-linear nature of atmospheric phenomena and processes (Pai et al. 2013). The variety of techniques and tools described in the literature for air quality forecasting covers simple empirical approaches, statistical approaches including artificial neural networks and fuzzy logic methods, and physically-based approaches including deterministic methods and ensemble and probabilistic methods (Zhang et al. 2012). The deterministic approach mostly refers to meteorological and chemical transport models, such as sophisticated Community Air Quality Modelling System (CMAQ) for prediction of air quality index at locations with no real-time measurements.

Editorial responsibility: An-Lei Wei.

Electronic supplementary material The online version of this article (doi:10.1007/s13762-016-1208-8) contains supplementary material, which is available to authorized users.

✉ M. Perišić
mirjana.perisic@ipb.ac.rs

¹ Institute of Physics Belgrade, University of Belgrade, Pregrevica 118, 11080 Belgrade, Serbia

² Singidunum University, Danijelova 32, 11010 Belgrade, Serbia

The chemical transport models were first used in Germany for air quality forecasting purposes, and soon many other developed countries became aware of the benefits of such implementation and launched the centralized air quality forecasting systems based on different tools, from simple empirical to online-coupled meteorology and chemistry models. While deterministic models don't require a large quantity of observational data, they do demand sufficient knowledge and understanding of pollutant emission sources, transport and atmospheric reactions and transformations under the planetary boundary layer (Feng et al. 2015). Since crucial knowledge in this area is often limited and some processes are too complex to be presented within a model, deterministic models are computationally expensive and time-consuming for routine predictions and often employ approximations and simplifications that lead to strong biases and inaccuracy, thus making the forecasts useless for timely management of critical situations (Cobourn 2010; Russo and Soares 2014).

Over the last decade, the parametric or non-parametric statistical approaches have been proposed as a more economical alternative for discovering the underlying site-specific dependencies between pollutant concentrations and potential predictors (Feng et al. 2015). The most commonly examined were artificial neural networks, based on artificial neurons or nodes capable of learning relationships between the routinely-measured pollutant data and selected predictors through embedded functions and data from the previous period (Fernando et al. 2012). Unlike deterministic models, artificial neural networks provide more accurate air quality forecasts, whereas their major disadvantages are associated with "black box" nature and poor generalization performance (Moustris et al. 2013). Furthermore, both statistical and deterministic approaches show satisfactory or good performance in forecasting concentrations closer to average values, whereas the prediction of extreme pollution events is more challenging.

As summarized by Zhang et al. (2012), the integration of advanced statistical methods in future air quality forecasting systems could considerably reduce forecasting biases and further enhance accuracy. In our previous study, MVA methods were successfully applied for forecasting the contributions of industry and vehicle exhaust to volatile organic compound (VOC) levels in the urban area, with smallest relative forecast error of only 6% (Stojić et al. 2015a). In this study, we compared the performance of twelve advanced multivariate (MVA) methods for PM₁₀ forecasting relying on meteorological data and SO₂ concentrations. The analysis was based on a multi-year dataset collected at four different locations, affected by traffic or

industry emissions. The herein employed MVA classification and regression methods belong to the supervised learning algorithms designed within Toolkit for Multivariate Analysis (TMVA; Hoecker et al. 2007) within the ROOT framework (Brun and Rademakers 1997), for extracting the maximum available information from the extensive data in high-energy physics.

Materials and methods

The analyzed dataset comprising 5-year (2011–2015) hourly concentrations of PM₁₀, SO₂ and meteorological data (atmospheric pressure, temperature, humidity, wind speed and direction), was obtained from the automatic monitoring stations within the Institute of Public Health network, at four different sites (Fig. 1, Supplementary Material). In the urban area, mostly affected by vehicle-exhaust emissions, measurements were conducted at the Institute of Public Health and New Belgrade, the sites characterized as being urban canyon avenue (UCA) and urban boulevard (UB), respectively, due to their topographic configuration. In the area influenced by emissions from fossil fuel burning for industry and heating operations, the data were collected in Obrenovac and Grabovac, the sites corresponding to urban industry (UI) and rural industry (RI), respectively. The measurements at industrial sites were incomplete due to severe floods that affected the area in 2014. The concentrations of PM₁₀ and SO₂ were measured by means of referent beta-ray attenuation (Thermo FH 62-IR) sampler and referent sampling device Horiba APSA 360, respectively. The meteorological data were obtained by using Lufft WS500-UMB Smart Weather Sensor. The accuracy and precision of detection methods are provided in Stojic et al. (2016).

The analyses of daily, weekly, seasonal and annual dynamics, trend (Pretty 2015) and periodicity were performed by means of Openair (Carslaw and Ropkins 2012) and Lomb (Ruf 1999) packages within the Statistical Software Environment R (Team 2012). The relationships between pollutant concentrations and wind characteristics were investigated by the use of bivariate polar plot and bivariate cluster analyses within the Openair package. The contribution of local emission sources, background and transport to the observed PM₁₀ pollution was analyzed using the 72-h air mass back trajectories and trajectory sector analysis (TSA) as described in Stojić et al. (2016).

The following MVA methods were used for PM₁₀ forecasting: Boosted decision trees (BDT, BDTG, BDTMitFisher), Artificial Neural Network Multilayer

Perceptron (MLP), MLP with Bayesian Extension (MLPBNN), Support Vector Machine (SVM), k-nearest neighbor (KNN), Linear Discriminant (LD), Boosted Fisher Discriminant (BoostedFisher), Multidimensional Probability Density Estimator Range Search Method (PDERS), Predictive Learning via Rule Ensembles (Rule-Fit) and Function Discriminant Analysis (FDA). All methods were used for both classification and regression. The five-year dataset was divided into two equal subsets, each consisting of PM₁₀ concentrations and input data (meteorological and SO₂). One subset was used for method trainings, either to differentiate between high and low importance indicators for PM₁₀ concentrations (classification), or to determine an approximation of the underlying functional behavior defining PM₁₀ concentrations (regression). The other subset was utilized for method performance testing.

Results and discussion

Previous studies aimed at investigating the origin and spatio-temporal distribution of different pollutant species converge on the conclusion that poor air quality presents an important health risk factor in Belgrade area (Perišić et al. 2015; Stojić et al. 2015b). In the previous years, the mean annual PM₁₀ concentrations in Belgrade area were in the range from 39.74 to 62.32 µg m³, whereas the exceedances of the proposed air quality guideline value of 50 µg m³ were registered during 20.5–42.2% of total number of days (Stanišić Stojić et al. 2016).

Specifics of measurement sites

In order to examine the MVA forecasting performances, PM₁₀ observational data from four measurement sites affected by different emission sources were collected and analyzed (Fig. 1, Supplementary Material). The two locations defined as urban were affected by traffic emissions throughout the year. However, specific microclimatic conditions associated with contrasting urban morphology between UCA and UB plays an important role in spatial distribution of particles. The presence of tall buildings along both sides of the canyon avenue induces a complex wind flow that does not enhance the pollutant dispersion due to terrain configuration, but it facilitates suspension, particularly fine PM fraction (Vardoulakis et al. 2003). Furthermore, frequent congestions in the canyon avenue compared to free flowing traffic in the wide boulevard contributed to higher PM₁₀ concentrations at UCA

throughout the year, with the exception of winter season, when the air quality at UB was additionally affected by fuel burning from the neighboring heating plant.

The herein presented industrial locations were affected either by fuel burning emissions only (RI), or by emissions from both industrial activities and vehicle exhaust (UI). Within the range of 15–20 km in NW/N and SE/S direction around the two industrial sites, the strong emission sources including three thermal power plants, four open-pit mines of high-sulfur lignite and several coal ash disposal sites are located.

As can be seen, the highest mean PM₁₀ concentration for the entire period was registered at UI (Table 1, Supplementary Material), which was partly driven by extreme pollutant loadings in 2012 (Fig. 2, Supplementary Material). It should be noted that the PM₁₀ variations at two industrial locations exhibited similar pattern, only with less significant deviations at rural site, which points to the prevalence of the same emission sources.

Daily mean PM₁₀ exceedances (>50 µg m⁻³) were commonly observed, whereas the episodes of extreme pollutant levels were registered only at UI (Fig. 3, Supplementary Material). The winter PM₁₀ concentrations were considerably higher at all examined locations, which can be partly attributed to heating operations, but also to lower planetary boundary layer (PBL) height in winter season. Unsurprisingly, the lowest PM₁₀ levels for the entire period were observed at rural site, particularly during spring and summer season, with the values of 29.15 and 32.09 µg m⁻³ being registered, respectively. Conversely, the highest concentrations in warm season were measured at UCA, the only site predominately affected by traffic. The differences between the summer and winter concentrations were relatively small at UCA and RI, whereas the inter-seasonal variations at two other sites exposed to the emissions from two strong sources were almost two times higher.

In Fig. 4, Supplementary Material, daily, weekly and seasonal PM₁₀ variations are displayed. Accordingly, the lowest concentrations were registered in May and June, probably due to intense precipitations. The particle resuspension processes and atmospheric photochemical reactions in dry summer months starting from July, led to the rising pollutant levels, particularly at industrial sites in the vicinity of ash disposals. The accumulation of particles during working days was followed by a significant decrease at the weekend at two locations dominated by vehicle exhaust emissions, whereas the weekday/weekend difference was not observed at UI and RI sites. As regards diurnal PM₁₀ variations, the same pattern was detected at all locations: daytime levels tended to be low with the exception of

morning and afternoon rush hours, whereas the pronounced increase in nighttime concentrations could be attributed to stable atmospheric conditions and shallow PBL.

According to bivariate and cluster analysis, the average contributions of the surrounding emission sources were dominant at all locations (Fig. 1), particularly at UCA (59.5 $\mu\text{g m}^{-3}$), due to limited pollutant dispersion, and UI (73.1 $\mu\text{g m}^{-3}$), which has been directly exposed to emissions from the thermal plant which produces more than 50% of electricity for the Serbian market. The UCA is located in the central city area and thus, the polluted air masses were observed to come from all directions, whereas at UB, the impact of heating plant emissions from S and intersections with intensive traffic coming from E can be noted. In the case of industrial locations, local sources appeared to be particularly significant during the heating season, whereas in spring and summer, both UI and RI were affected by emissions from ash disposals and lignite mining sites in NW/N and SE/S. The dynamics of cluster contributions on a daily, weekly and seasonal basis are shown in Fig. 5, Supplementary Material. As can be seen, local emissions, corresponding to cluster 4 at industrial sites, exhibited extremely regular daily variations, which suggests the prominent role of anthropogenic sources. The rush hour peaks were noticeable only in the variations of locally-emitted PM_{10} concentrations at UCA (cluster 4), since the site has been dominated by traffic emissions.

The analysis was also performed to determine the impact of local emissions, transported pollution and background on the air quality at examined locations. According to TSA results, the estimated share of background was highest at rural site (48%), whereas the contribution of local production was the most significant factor (43%) for PM_{10} concentrations at UI, as previously shown by bivariate and cluster analysis.

Upon the presented analysis, we have reached the conclusion that the selected locations are substantially different in terms of air quality and factors closely associated with it, including micro-climatic conditions, topographic features and proximity of strong sources. This was considered a prerequisite for examining the dependency between the efficiency of MVA methods for air quality forecasting and site characteristics.

Classification MVA methods

As previously mentioned, the 5-year dataset, including PM_{10} and SO_2 concentrations, and meteorological data, was divided into two subsets equal in size, used for training and testing of MVA methods, respectively. In order to account for seasonal, *i.e.* weekday/weekend variations, two new variables were introduced for classification purposes: Yearreal is a quotient of the ordinal number of a day and total number of days per year, while Weekreal represents

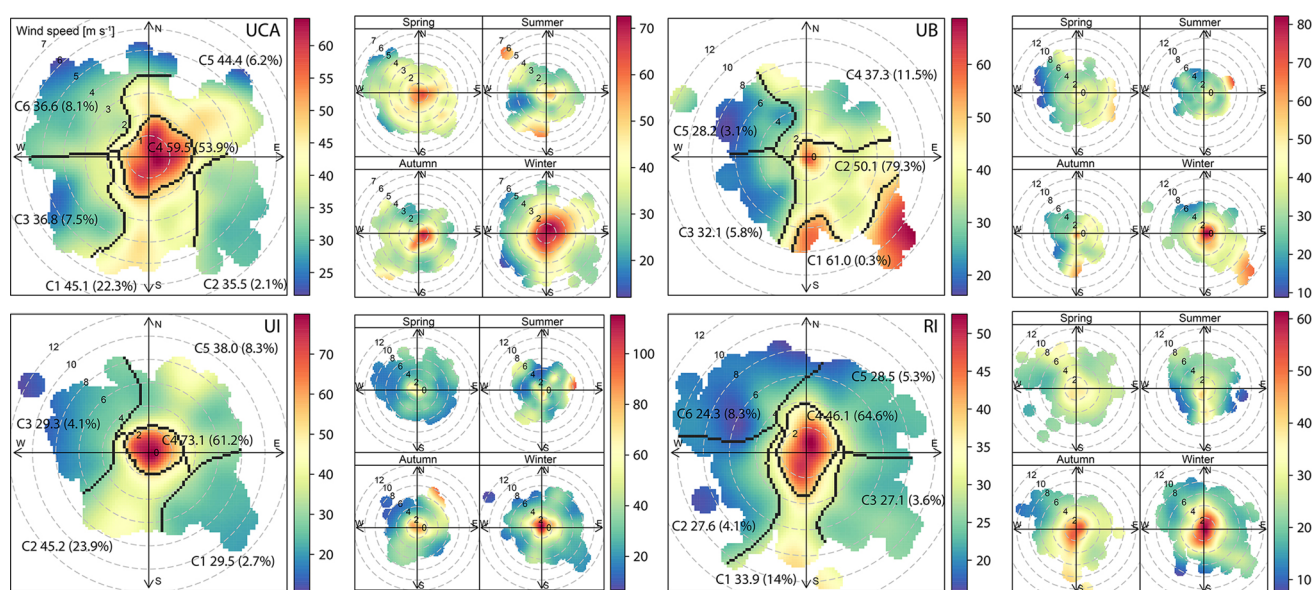


Fig. 1 The relationship between PM_{10} concentrations and wind characteristics: bivariate cluster plot [frequency (%) and average contributions ($\mu\text{g m}^{-3}$)] for the entire period (*left*) and seasonal variations ($\mu\text{g m}^{-3}$) (*right*)

the quotient of the ordinal number of a day and number 7. Correlation and mutual information of input variables and the observed PM₁₀ mass concentrations for all sampling sites are presented in Table 1.

For the purposes of classification, the PM₁₀ levels above 50 µg m⁻³ are considered to require the increased level of caution, whereas those exceeding 100 µg m⁻³ are considered extremely high—alarm triggering values, both of which are chosen as arbitrary limits. The estimation of classification method performances by using the Receiver Operating Characteristic (ROC) curve is presented in

Table 1 Correlation (C) and mutual information (MI) of input variables (P, pressure; T, temperature; Rh, relative humidity; ws, wind speed; Yearreal, day of year; Weekreal, day of week) and measured PM₁₀ concentrations at all sampling sites

Variable	UCA		UB		UI		RI	
	C	MI	C	MI	C	MI	C	MI
P	0.18	1.31	0.26	0.97	0.20	1.49	0.29	1.26
T	0.21	1.40	0.30	1.21	0.28	1.69	0.22	1.39
Rh	0.24	1.47	0.24	1.29	0.22	1.86	0.19	1.60
ws	0.29	1.39	0.25	0.82	0.26	1.57	0.32	1.18
SO ₂	0.25	1.63	0.09	1.39	0.20	1.87	0.32	1.59
Yearreal	0.04	1.49	0.05	1.31	0.09	1.86	0.12	1.53
Weekreal	0.02	0.12	0.03	0.11	0.02	0.18	0.02	0.14

Fig. 2. The highest separation between background and predicted PM₁₀ concentrations was observed when PM₁₀ classifier value of 100 µg m⁻³ was taken into account (Fig. 3), whereas somewhat poorer results were obtained for 50 µg m⁻³, which suggests that including additional meteorological or pollutant variables as input data might further enhance classification performance.

The comparison of the results by evaluating signal and background efficiencies revealed that certain MVA methods are capable of classifying the PM₁₀ levels which are considered to require a high degree of caution (Table 2, left). The results showed that BDTG and MLP exhibit the best results for all examined locations. Signal and background separation was most efficiently performed for RI and UB, and to a somewhat lower extent for UCA.

Regression MVA methods

Regression MVA methods were applied to interpret the relationships between pollutant concentrations and the examined input data. Similar to classification methods, BDTG and MLP exhibited the most satisfying performances with absolute and relative errors presented in Table 2, right. The MVA method performance was best for PM₁₀ loadings at industrial sites, around 25%, while the forecast quality could be clearly seen at RI location, Fig. 4. It can be assumed that more accurate air quality forecasts can be

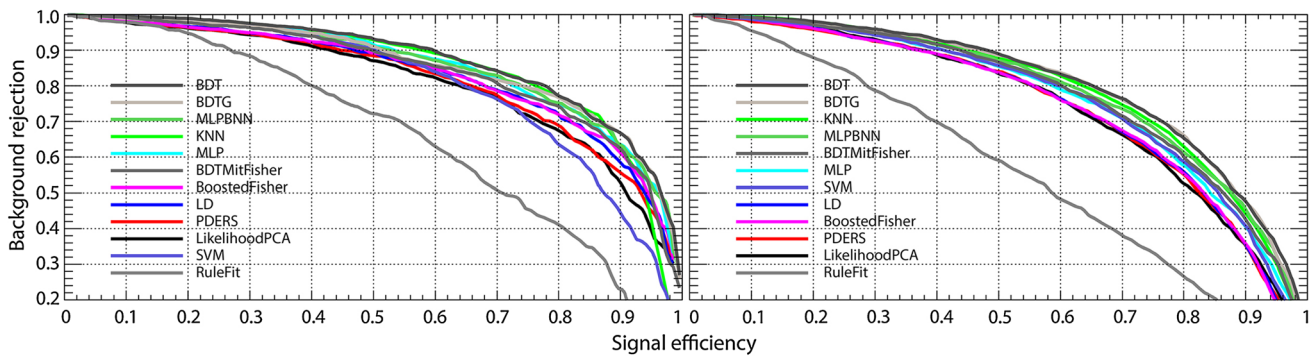


Fig. 2 ROC curves for MVA classification methods with PM₁₀ classifier value of 100 µg m⁻³ (left) and 50 µg m⁻³ (right) for all sampling sites

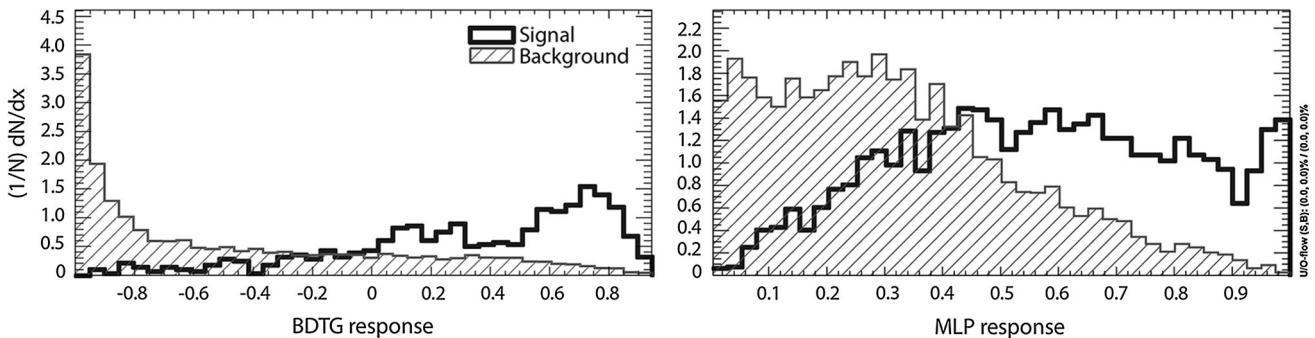


Fig. 3 MVA classification method response for PM₁₀ classifier value of 100 µg m⁻³ (left) and 50 µg m⁻³ (right) for UCA site

Table 2 The comparison of best performing methods for ROC, separation and significance values for all measurement sites (left) and absolute ($\mu\text{g m}^{-3}$) and relative (%) errors of the best performing regression methods (right)

Sampling site	Method	Classification			Regression	
		ROC	Separation	Significance	Absolute error	Relative error
UCA	BDTG	0.806	0.282	0.883	17.2	29.6
	MLP	0.772	0.226	0.755	21.8	37.5
UB	BDTG	0.868	0.408	1.12	13.9	26.8
	MLP	0.841	0.352	1.015	17.4	33.5
UI	BDTG	0.855	0.379	1.059	15.6	24.6
	MLP	0.826	0.323	0.956	24.0	37.9
RI	BDTG	0.867	0.412	1.172	10.6	25.2
	MLP	0.837	0.345	0.962	15.1	36.0

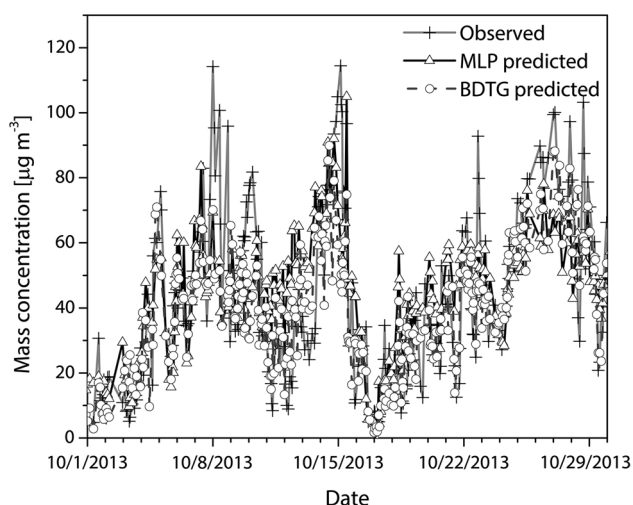


Fig. 4 The comparison of time series of the observed and best performing MVA-predicted PM_{10} concentrations ($\mu\text{g m}^{-3}$) at RI site

achieved at the locations such as RI, which are affected by less significant number of emission sources. Furthermore, the simplicity and regularity of dominant pollutant emissions on a daily, weekly and seasonal basis, as registered at UI location, as well as minor deviations from the commonly observed pollutant loadings, which is particularly evident for air quality forecasting at rural site, are probably the additional factors associated with forecast accuracy.

Conversely, the weakest MVA method performance was derived for PM_{10} concentrations at UCA, probably because the urban morphology of the canyon avenue represents the additional factor modifying the pollutant levels in a less predictable manner. Furthermore, the emission sources in the central city zone are diverse and primarily refer to traffic congestions and intense atmospheric reactions that take place in stagnant conditions of the canyon street. Moreover, they also relate to local fireboxes in residential area where lignite is burned

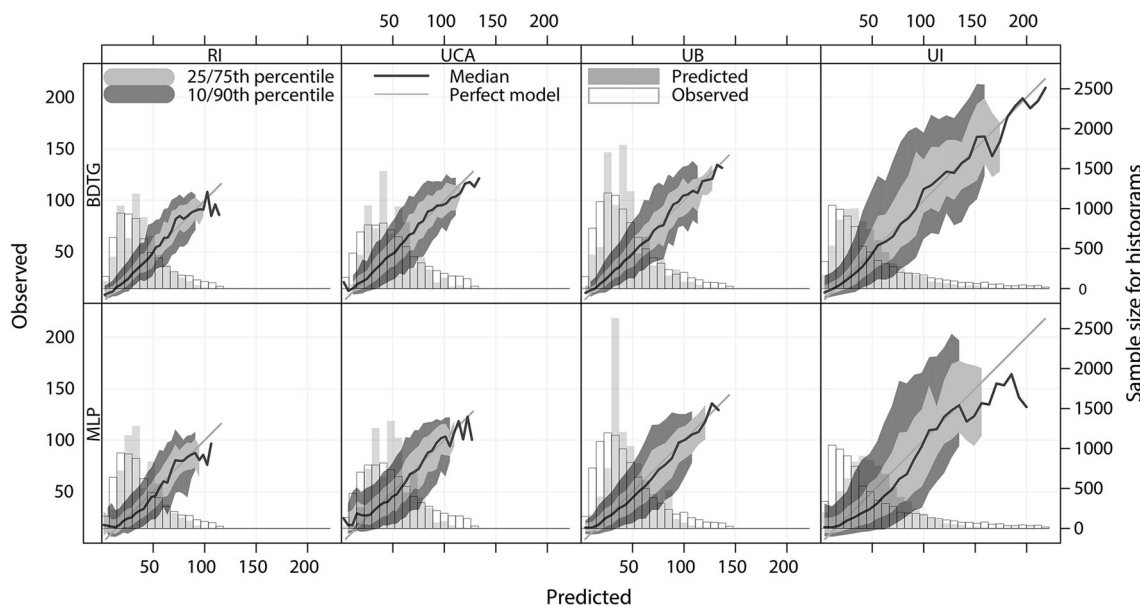


Fig. 5 The comparison of the observed and best performing MVA-predicted PM_{10} mass concentrations ($\mu\text{g m}^{-3}$)

during autumn and winter season and local manufactures that are associated with pollutant emissions highly variable in time and intensity.

As can be seen in Fig. 5, the PM₁₀ time series evaluated by means of MVA regression methods correlated very well with the observed concentrations at all sampling sites. Mutual information obtained for BDTG-predicted and the observed PM₁₀ mass concentrations were 0.71, 0.7, 0.65 and 0.64 for RI, UB, UCA and UI, respectively. This suggests that significant input variables were used for the forecasting process. In addition, it could be noted that their distributions are relatively well.

Although the other MVA methods employed in the present study generated similar results when being used for classification, they generated the significant PM₁₀ forecast errors when being used for regression, at least based on the observed input variables. The herein presented errors are mostly in compliance with the findings of our previous study, aimed at forecasting the contributions from traffic and industry to the observed VOC concentrations in the urban area, which suggests that both PM and VOC, as important air quality indicators, can be predicted using the MVA methods.

Conclusion

In this study, the performances of MVA methods for forecasting PM₁₀ concentrations and prediction of related health-damaging events were evaluated on the basis of datasets from traffic- and industry-affected locations with substantial differences in air quality, which has also been verified through additional analyses. The results of both classification and regression methods were rather promising, particularly considering the fact that the presented forecast accuracy referred to hourly concentrations. The quality of the prediction might be partly dependent on microclimatic conditions, topographic characteristics, presence of strong emission sources and other site characteristics, as well as on the input data. All that implies that the selection of additional or different variables could enhance the method forecasting performances. The importance of accurate air quality forecasts as part of the management system is reflected in the potential applications, including health alerts for susceptible categories, operational planning, as well as amendment of pollutant time-series and reduction of regular monitoring expenditures.

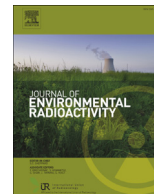
Acknowledgements This study was carried out as part of the Project No. III43007, III41011 and OI171002, financed by the Ministry of Education, Science and Technological Development of the Republic of Serbia for the period 2011–2016.

References

- Brun R, Rademakers F (1997) ROOT—an object oriented data analysis framework. *Nucl Instrum Methods A* 389:81–86
- Carslaw DC, Ropkins K (2012) Openair—an R package for air quality data analysis. *Environ Model Softw* 27:52–61
- Cobourn WG (2010) An enhanced PM_{2.5} air quality forecast model based on nonlinear regression and back-trajectory concentrations. *Atmos Environ* 44:3015–3023
- Fang Y, Mauzerall DL, Liu J, Fiore AM, Horowitz LW (2013) Impacts of 21st century climate change on global air pollution-related premature mortality. *Clim Change* 121:239–253
- Feng X, Li Q, Zhu Y, Hou J, Jin L, Wang J (2015) Artificial neural networks forecasting of PM_{2.5} pollution using air mass trajectory based geographic model and wavelet transformation. *Atmos Environ* 107:118–128
- Fernando HJS, Mammarella MC, Grandoni G, Fedele P, Di Marco R, Dimitrova R, Hyde P (2012) Forecasting PM₁₀ in metropolitan areas: efficacy of neural networks. *Environ Pollut* 163:62–67
- Hoecker A, Speckmayer P, Stelzer J, Therhaag J, Von Toerne E, Voss H, Backes M, Carli T, Cohen O, Christov A, Dannheim D, Danilowski K, Henrot-Versille S, Jachowski M, Kraszewski K, Krasznahorkay A, Kruk M, Mahalalel Y, Ospanov R, Prudent X, Robert A, Schouten D, Tegenfeldt F, Voigt A, Voss K, Wolter M, Zemla A (2007) TMVA users guide—toolkit for multivariate data analysis, PoSACAT 040. <http://arxiv.org/abs/physics/0703039>. Accessed 14 June 2015
- Lelieveld J, Evans JS, Fnais M, Giannadaki D, Pozzer A (2015) The contribution of outdoor air pollution sources to premature mortality on a global scale. *Nature* 525:367–371
- Moustris KP, Larissi IK, Nastos PT, Koukouletsos KV, Paliatsos AG (2013) Development and application of artificial neural network modeling in forecasting PM₁₀ levels in a Mediterranean city. *Water Air Soil Pollut* 224:1–11
- Pai TY, Hanaki K, Chiou RJ (2013) Forecasting hourly roadside particulate matter in Taipei County of Taiwan based on first-order and one-variable grey model. *CLEAN Soil Air Water* 41:737–742
- Perišić M, Stojić A, Stojić SS, Šoštarić A, Mijić Z, Rajšić S (2015) Estimation of required PM₁₀ emission source reduction on the basis of a 10-year period data. *Air Qual Atmos Health* 8:379–389
- Pretty R (2015) TheilSen {openair} tests for trends using Theil–Sen estimates. <http://www.inside-r.org/packages/cran/openair/docs/TheilSen>. Accessed 12 Dec 2015
- Ruf T (1999) The Lomb-Scargle periodogram in biological rhythm research: analysis of incomplete and unequally spaced time-series. *Biol Rhythm Res* 30:178–201
- Russo A, Soares AO (2014) Hybrid model for urban air pollution forecasting: a stochastic spatio-temporal approach. *Math Geosci* 46:75–93
- Stanišić Stojić S, Stanišić N, Stojić A, Šoštarić A (2016) Single and combined effects of air pollutants on circulatory and respiratory system-related mortality in Belgrade, Serbia. *J Toxicol Environ Health A* 79:17–27
- Stojić A, Maletić D, Stojić SS, Mijić Z, Šoštarić A (2015a) Forecasting of VOC emissions from traffic and industry using classification and regression multivariate methods. *Sci Total Environ* 521:19–26
- Stojić A, Stojić SS, Mijić Z, Šoštarić A, Rajšić S (2015b) Spatio-temporal distribution of VOC emissions in urban area based on receptor modeling. *Atmos Environ* 106:71–79
- Stojić A, Stanišić Stojić S, Reljin I, Čabarkapa M, Šoštarić A, Perišić M, Mijić Z (2016) Comprehensive analysis of PM₁₀ in Belgrade urban area on the basis of long term measurements. *Environ Sci Pollut Res*. doi:10.1007/s11356-016-6266-4



- Team RC (2012) R: a language and environment for statistical computing. <http://cran.case.edu/web/packages/dplR/vignettes/timeseries-dplR.pdf>. Accessed 10 June 2015
- Vardoulakis S, Fisher BE, Pericleous K, Gonzalez-Flesca N (2003) Modelling air quality in street canyons: a review. *Atmos Environ* 37:155–182
- Zhang Y, Bocquet M, Mallet V, Seigneur C, Baklanov A (2012) Real-time air quality forecasting, part I: history, techniques, and current status. *Atmos Environ* 60:632–655



Correlation analysis of the natural radionuclides in soil and indoor radon in Vojvodina, Province of Serbia



S. Forkapic^{a,*}, D. Maletić^b, J. Vasin^c, K. Bikit^a, D. Mrdja^a, I. Bikit^a, V. Udovičić^b, R. Banjanac^b

^a University of Novi Sad, Faculty of Sciences, Department of Physics, Laboratory for Radioactivity and Dose Measurements, 21000 Novi Sad, Serbia

^b Institute of Physics Belgrade, University of Belgrade, Belgrade, Serbia

^c Institute of Field and Vegetable Crops, 21000 Novi Sad, Serbia

ARTICLE INFO

Article history:

Received 8 November 2015

Received in revised form

8 July 2016

Accepted 21 July 2016

Available online 29 July 2016

Keywords:

Radon

Soil characteristics

Correlative and multivariate analysis

ABSTRACT

The most dominant source of indoor radon is the underlying soil, so the enhanced levels of radon are usually expected in mountain regions and geology units with high radium and uranium content in surface soils. Laboratory for radioactivity and dose measurement, Faculty of Sciences, University of Novi Sad has rich databases of natural radionuclides concentrations in Vojvodina soil and also of indoor radon concentrations for the region of Vojvodina, Northern Province of Serbia. In this paper we present the results of correlative and multivariate analysis of these results and soil characteristics in order to estimate the geogenic radon potential. The correlative and multivariate analysis were done using Toolkit for Multivariate Analysis software package TMVA package, within ROOT analysis framework, which uses several comparable multivariate methods for our analysis. The evaluation ranking results based on the best signal efficiency and purity, show that the Boosted Decision Trees (BDT) and Multi Layer Preceptor (MLP), based on Artificial Neural Network (ANN), are multivariate methods which give the best results in the analysis. The BDTG multivariate method shows that variables with the highest importance are radionuclides activity on 30 cm depth. Moreover, the multivariate regression methods give a good approximation of indoor radon activity using full set of input variables. On several locations in the city of Novi Sad the results of indoor radon concentrations, radon emanation from soil, gamma spectrometry measurements of underlying soil and geology characteristics of soil were analyzed in detail in order to verify previously obtained correlations for Vojvodina soil.

© 2016 Elsevier Ltd. All rights reserved.

1. Introduction

It is well known that radon and their short lived progenies have the most impact to the population effective dose from radioactive sources (UNSCEAR, 2008). Recent epidemiological studies show that the radiation risk due to radon exists on concentrations that were considered negligible (WHO, 2009). In most European countries radon mapping has been carried out and the results are summing in the publications of Joint Research Centre of European Commission (JRC EC) which coordinates of the project of European Natural Radioactivity Atlas (De Cort et al., 2011). Therefore, all member states (including candidate countries) must propose the

reference level of radon in dwellings and working places and identify radon priority areas with high radon potential according to EU directive (EURATOM, 2013). There are two different concepts in definition of radon potential: the first one relative to number of houses with indoor radon concentrations above the reference value (depends of construction types, living habits and meteorology) and the other one geogenic radon potential relative to local geophysical parameters (radon concentration in soil and the permeability of soil) (Gruber et al., 2013). Geogenic radon emanates from radium and uranium rich minerals into the soil pore space and it migrates through the soil by diffusion and convection due to the gradient in concentrations. Geogenic radon potential (GRP) therefore describes radon in the subsurface soil as the main contributor to radon buildup in houses and in contrast to indoor radon potential (IRP) it is independent on human influence and temporally constant over a geological timescale. In the lack of soil gas radon and soil gas permeability measurements, our first steps toward the geogenic

* Corresponding author. University of Novi Sad, Faculty of Sciences, Department of Physics, Trg Dositeja Obradovića 4, 21000 Novi Sad, Serbia.

E-mail address: sofija@df.uns.ac.rs (S. Forkapic).

radon map are to find correlations between available radio-geochemical data and indoor radon concentration measurements in order to predict radon prone areas and validate geogenic prognosis.

In Serbian Northern Province Vojvodina several indoor radon surveys were performed in the period of four years from 2002 to 2005 by Laboratory for radioactivity and dose measurement, Faculty of Sciences, University of Novi Sad (Forkapić et al., 2007). The same laboratory during this period carried out radioactivity monitoring of soil on 50 different locations in Vojvodina region (Bikit et al., 2005) in cooperation with the Institute of Field and Vegetable Crops who determined the geochemical soil characteristics, mechanical composition and content of total N, CaCO₃ and available phosphorus P₂O₅ and potassium K₂O. The locations were

selected in a way to proportionally represent all geomorphological units (Koščal et al., 2005): two mountains, four loess plateaus, three loess terraces, four alluvial plains, two sandstone terrains and all soil types (IUSS, 2014): Chernozem, Vertisol, Fluvisol, Cambisol, Planosol, Solonchak and Solonetz. The influence of clay and humus content and humidity of soil on radon adsorption to the soil grains were discussed and analyzed using correlative and multivariate analysis with indoor radon concentrations.

The demand for detailed analyses of large amount of data in high-energy physics resulted in wide and intense development and usage of multivariate methods. Many of multivariate methods and algorithms for classification and regression are already integrated into the analysis framework ROOT (Brun and Rademakers, 1997), more specifically, into the Toolkit for Multivariate analysis (TMVA)

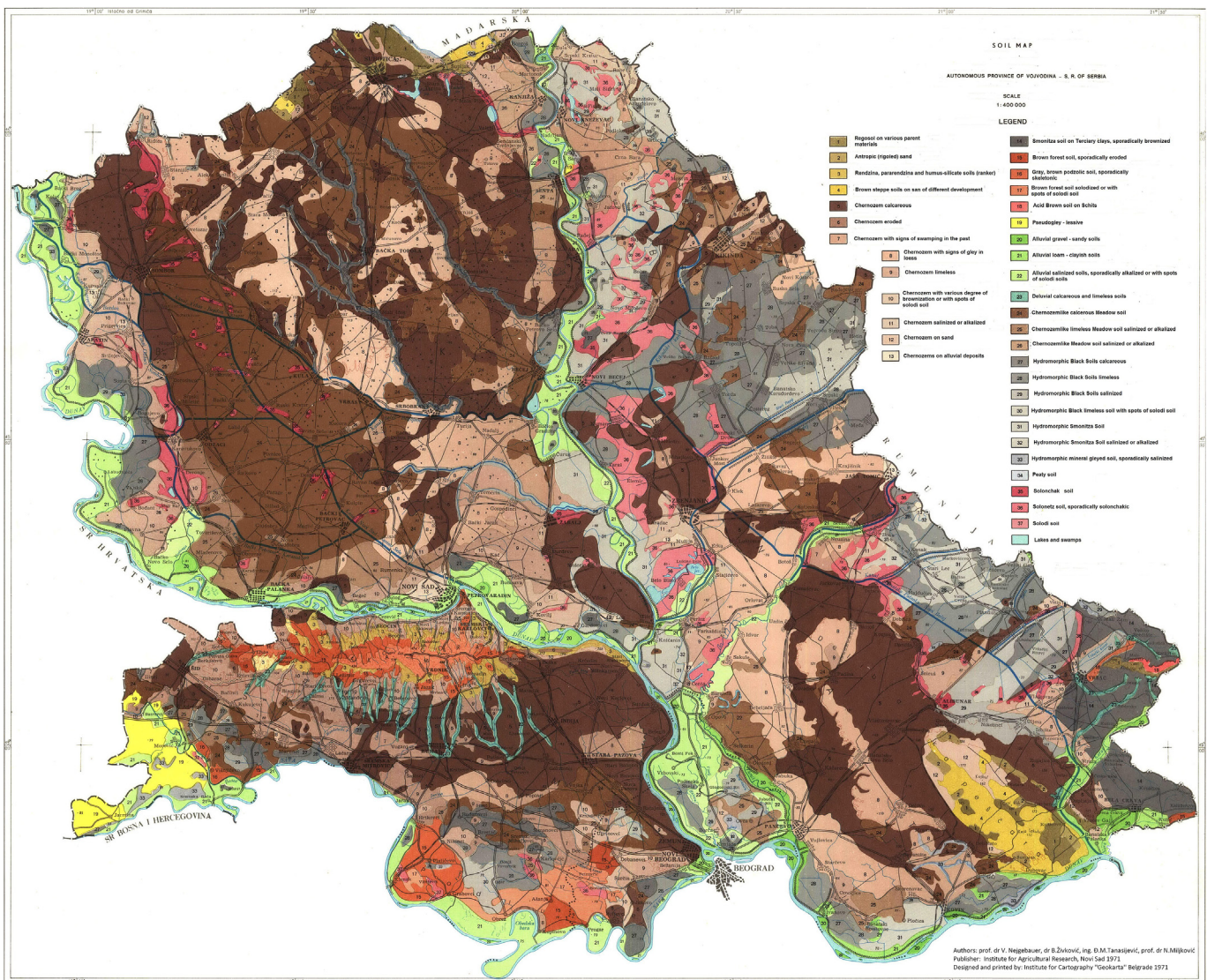


Fig. 1. Soil map of Vojvodina Province (Nejezbauer et al., 1971): 1 – Regosol on various parent materials; 2 – Antropic (rigoled) sand; 3 – Rendzina, pararendzina and humus-silicate soils (ranker); 4 – Brown steppe soils on sand of different development; 5 – Chernozem calcareous; 6 – Chernozem eroded; 7 – Chernozem with signs of swamping in the past; 8 – Chernozem with signs of clay in loess; 9 – Chernozem limeless; 10 – Chernozems with various degree of brownization or with spots of solodi soil; 11 – Chernozem salinized or alkalized; 12 – Chernozem on sand; 13 – Chernozems on alluvial deposits; 14 – Smonitza soil on Tertiary clays, sporadically brownized; 15 – Brown Forest soil, sporadically eroded; 16 – Gray, brown podzolic soil sporadically skeletal; 17 – Brown Forest soil solodized or with spots of solodi soil; 18 – Acid Brown Soil on Schits; 19 – Pseudogley – lessive; 20 – Alluvial gravel – sandy soils; 21 – Alluvial loam – clayish soils; 22 – Alluvial salinized soils, sporadically alkalized or with spots of solodi soils; 23 – Deluvial calcareous and limeless soils; 24 – Chernozemlike calcareous Meadow Soil; 25 – Chernozemlike limeless Meadow Soil salinized or alkalized; 26 – Chernozemlike Meadow soil salinized or alkalized; 27 – Hydromorphic Black Soils calcareous; 28 – Hydromorphic Black Soils limeless; 29 – Hydromorphic Black Soils salinized; 30 – Hydromorphic Black limeless soil with spots of solodi soil; 31 – Hydromorphic Smonitza Soil; 32 – Hydromorphic Smonitza Soil salinized or alkalized; 33 – Hydromorphic mineral gleyed soil, sporadically salinized; 34 – Peaty Soil; 35 – Solonchak Soil; 36 – Solonetz soil, sporadically solonchakic; 37 – Solodi Soil.

(Hoecker et al., 2007). Institute of Physics Belgrade used these multivariate methods to create, test and apply all available classifiers and regression methods implemented in the TMVA in order to find the method that would be the most appropriate and yield maximum information on the dependence of radon concentrations on the multitude of input variables.

The first step is to calculate and rank the correlation coefficients between all the variables involved, what will help in setting up and testing the framework for running the various multivariate methods contained in the TMVA. Although these correlation rankings will later be superseded by method-specific variable rankings, they are useful at the beginning of the analysis.

The next step is to use and compare the multivariate methods in order to find out which one is best suited for classification (division) of indoor radon concentrations into what would be considered acceptable and what would be considered increased concentration.

In order to be able to use the multivariate classification, the set of input events used, have to be split into those the correspond to

the signal (the indoor radon concentrations that are considered increased) and to the background (consisting of indoor radon concentrations that are declared acceptable). This splitting of the set of input events is for the purposes of this preliminary analysis performed at the limiting value of 120 Bq/m³. This value is used for classification analyses, and is selected because this splitting ensures maximum employment of multivariate comparison methods, and this particular value reflects the fact that in our test case the statistics on higher radon concentration values are lower. The method of multivariate regression, however, does not require preliminary splitting of input events, and is therefore a more general one. Main aim is to find out which method can, if any, on the basis of input variables only, give an output that would satisfactorily close match the observed variations of indoor radon concentrations.

In this paper we proposed and analyzed the application of multivariate techniques developed at CERN for experiments with particle physics for correlation analysis of experimental indoor radon data and soil characteristics. Obtained results were verified

Table 1
Classification of soil types for 50 locations of sampling.

No	Locality	Soil type (national classification) (Škorić et al., 1985)	Soil group (FAO-WRB) (IUSS, 2014)
1	Horgoš	Arenosol	Protic ARENOSOL (Calcic, Aridic)
2	Palić	Solonchak	Haplic SOLONCHAK (Siltic)
3	Žednik	Chernozem	Calcic CHERNOZEM (Loamic, Pachic)
4	Aleksa Santić	Chernozem	Haplic CHERNOZEM (Loamic, Pachic)
5	Tornjoš	Chernozem	Gleyic CHERNOZEM (Loamic, Pachic)
6	Gakovo	Chernozem	Haplic CHERNOZEM (Loamic, Pachic)
7	Kula	Chernozem	Calcic, Gleyic CHERNOZEM (Loamic, Pachic)
8	Becej	Humoglej	Mollic Oxigleyic GLEYSOL (Clayic)
9	Srbobran	Chernozem	Calcic, Gleyic CHERNOZEM (Loamic, Pachic)
10	Srpski Miletić	Chernozem	Gleyic CHERNOZEM (Loamic, Pachic)
11	Bogojevo	Humoglej – marsh swamp soil	Mollic Oxigleyic GLEYSOL (Loamic)
12	Nadalj	Chernozem	Gleyic CHERNOZEM (Loamic, Pachic)
13	Ruski Krstur	Chernozem	Gleyic CHERNOZEM (Loamic, Pachic)
14	Parage	Chernozem	Gleyic CHERNOZEM (Loamic, Pachic)
15	Rimski Šančevi	Chernozem	Haplic CHERNOZEM (Clayic, Pachic)
16	Žabalj	Chernozem	Gleyic CHERNOZEM (Loamic, Pachic)
17	Maglić	Chernozem	Gleyic CHERNOZEM (Loamic, Pachic)
18	Kač	Fluvisol	Gleyic FLUVISOL (Loamic, Salic)
19	Bačko Novo Selo	Fluvisol	Gleyic FLUVISOL (Loamic)
20	Banatsko Arandelovo	Humoglej – marsh swamp soil	Mollic Oxigleyic GLEYSOL (Clayic)
21	Sanad	Fluvisol	Stagnic FLUVISOL (Clayic)
22	Crna Bara – Čoka	Chernozem	Gleyic CHERNOZEM (Clayic, Pachic)
23	Kikinda	Chernozem	Haplic CHERNOZEM (Clayic, Pachic)
24	Rusko Selo	Humoglej – marsh swamp soil	Mollic Oxigleyic GLEYSOL (Clayic)
25	Torda	Humoglej – marsh swamp soil	Mollic Oxigleyic GLEYSOL (Clayic)
26	Kumane	Solonetz	Gleyic, Salic SOLONETZ (Clayic)
27	Begejci	Chernozem	Gleyic CHERNOZEM (Clayic, Pachic)
28	Zrenjanin	Chernozem	Calcic CHERNOZEM (Clayic, Pachic)
29	Boka	Solonetz	Haplic SOLONETZ (Clayic)
30	Orlovat	Chernozem	Gleyic CHERNOZEM (Loamic, Pachic)
31	Vršacki Ritovi	Humoglej – marsh swamp soil	Mollic Oxigleyic GLEYSOL (Clayic)
32	Kozjak	Chernozem	Gleyic CHERNOZEM (Loamic, Pachic)
33	Ilandža	Humoglej – marsh swamp soil	Mollic Oxigleyic GLEYSOL (Clayic)
34	Idvor	Chernozem	Gleyic CHERNOZEM (Clayic, Pachic)
35	Padina	Chernozem	Haplic CHERNOZEM (Loamic, Pachic)
36	Vršac	Eutric Cambisol	Eutric CAMBISOL (Clayic)
37	Crepaja	Chernozem	Haplic CHERNOZEM (Loamic, Pachic)
38	Deliblato	Chernozem	Haplic CHERNOZEM (Arenic, Pachic)
39	Bavanište	Chernozem	Haplic CHERNOZEM (Loamic, Pachic)
40	Petrovaradin	Eutric Cambisol	Eutric CAMBISOL (Clayic)
41	Šid	Chernozem	Haplic CHERNOZEM (Loamic, Pachic, Stagnic)
42	Rivica	Chernozem	Haplic CHERNOZEM (Clayic, Pachic)
43	Ruma	Chernozem	Haplic CHERNOZEM (Clayic, Pachic)
44	Indija	Chernozem	Haplic CHERNOZEM (Loamic, Pachic)
45	Morović	Pseudoglej	Gleyic, Fluvic, Luvic PLANOSOL (Loamic)
46	Višnjicevo	Pseudoglej	Gleyic, Fluvic, Luvic PLANOSOL (Loamic)
47	Sremska Mitrovica	Chernozem	Haplic CHERNOZEM (Clayic, Pachic)
48	Popinci	Chernozem	Gleyic CHERNOZEM (Clayic, Pachic)
49	Donji Tovarnik	Humoglej – marsh swamp soil	Mollic Oxigleyic GLEYSOL (Clayic)
50	Kupinovo	Fluvisol	Haplic FLUVISOL (Loamic)



Fig. 2. The RAD7 complete for soil gas measurements (Durridge, 2014).

Table 2
Correlation coefficients between indoor radon concentration and input variables.

Number	Parameter	Correlation coefficient
1	Elevation	+0.11
2	pH	0
3	CaCO ₃	-0.03
4	Humus	+0.15
5	Total N	+0.13
6	P ₂ O ₅	-0.01
7	K ₂ O	+0.01
8	Coarse sand	-0.08
9	Fine sand	-0.19
10	Powder	+0.16
11	Clay	+0.17
12	Ra-226 30 cm	+0.27
13	U-238 30 cm	+0.17
14	Th-232 30 cm	+0.22
15	K-40 30 cm	+0.10
16	U-238 surface	-0.17
17	Ra-226 surface	+0.04
18	Th-232 surface	0
19	K-40 surface	+0.02
20	Cs-137 surface	-0.17

and discussed on measured soil gas data for Novi Sad districts.

2. Study area

Vojvodina region is located in the Pannonian Basin of Central Europe. The choice of sampling locations was made on the basis of the presence of certain soil types (Škorić et al., 1985) on the Pedological Map of Vojvodina (Nejgebauer et al., 1971) which is shown on Fig. 1. The observed soil types were classified in Table 1 according to the FAO-WRB classification (IUSS, 2014). The dominant soil type at the examined area is Chernozem. Parent material (geological substrate) for this type of soil, and for the largest part of the surface of Vojvodina, is loess – loose sedimentary rock deposited by wind-accumulation in the Pleistocene (during interglacial periods).

3. Materials and methods

Indoor radon mapping of Vojvodina Province was performed using the etched track detectors CR39 on about 3000 locations in ground floor rooms during three years from 2002 to 2005. The time of exposure was 90 days during the winter seasons, from December

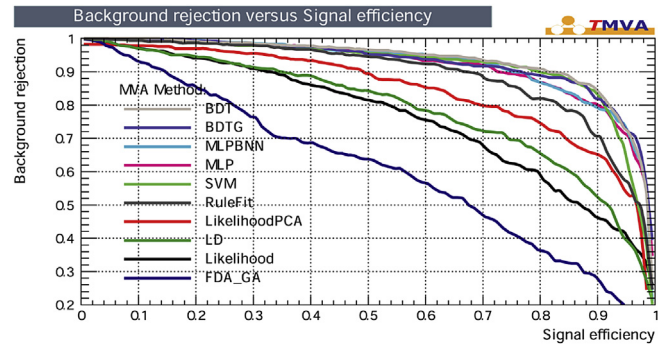


Fig. 3. Receiver operating characteristic (ROC) for all Multivariate methods used for classification of indoor radon concentration using climate variables. It shows that BDT and MLP methods are the best ones for radon.

to March. The etching and counting of tracks were performed by Radosys Company. For this study the average indoor radon concentrations in the nearest village or city to locations of soil sampling were calculated and used in correlation analysis. The results of intercomparison of radon CR-39 detector systems conducted in CLOR's accredited calibration laboratory and quality control data of commercially available Hungarian RadoSys systems are presented and discussed in (Mamont-Ciesla et al., 2010).

For radioactivity measurements from each location of an approximately area 10×10 m, 10 subsamples of soil were collected, mixed and homogenized. The soil was sampled from the surface layer (0–10 cm). For chemical analysis soil was sampled by agro-chemical probe to a depth of 30 cm. Soil samples were dried at 105 °C to constant mass. After that all mechanical contaminants, mainly small stone peaces and plant material were removed. Dried soil samples were homogenized as fine powder and measured in cylindrical geometry 62 mm \times 67 mm on the cap of HPGe detector. Typical mass of samples was 200 g–300 g and measurement time was 80 ks. Activity concentrations of radionuclides gamma emitters were determined by the method of low-level gamma spectrometry on actively and passively shielded germanium detectors with maximal background reduction. Detector calibrations and quality control measurements were done with certified reference material in cylindrical geometry type CBSS2 supplied by Czech Metrology Institute. Every year laboratory participates with accepted results in world-wide open proficiency tests for gamma spectrometry organized by IAEA Reference Materials Group, Terrestrial Environment Laboratory. The gamma spectra were acquired and analyzed using the Canberra Genie 2000 software. The program calculates the activity concentration of an isotope from all prominent gamma lines after peaked background subtraction. All measurement uncertainties are presented at 95% confidence level. A special procedure developed in the Novi Sad laboratory was used for the determination of the ²³⁸U activity concentration from gamma-lines of the first progeny of this radionuclide, ²³⁴Th (Bikit et al., 2003).

pH-value was measured in the suspension of soil with water (10 g: 25 cm³) by pH meter PHM62 standard- Radiometar Copenhagen. Content of humus was determined according to method of Tjurin. The total nitrogen content was determined by Kjeldahl on the system for digestion and titration Tacator. The available phosphorus and potassium were measured using the extraction with ammonium lactate. For soil characterization purposes, removal of organic matter by H₂O₂ and of carbonates by HCl was carried out. Then, the sample is shaken with a dispersing agent and sand is separated from clay and powder with a 63 μ m sieve. The sand is fractionated by dry sieving, and by the pipette method the clay and powder fractions are determined (IUSS, 2014). Particle size in the soil

Table 3

Evaluation results ranked by best signal efficiency and purity (area) It shows that BDT and MLP methods are the best ones for radon. @B is part of Background events classified as Signal events.

MVA method	Signal efficiency at bkg eff.(error):				Separation	Significance
	@B = 0.01	@B = 0.10	@B = 0.30	ROC-integ		
BDT	0.212(16)	0.814(16)	0.959(08)	0.932	0.609	1.614
BDTG	0.243(17)	0.767(17)	0.966(07)	0.927	0.611	1.676
MLPBNN	0.224(17)	0.754(17)	0.957(08)	0.922	0.600	1.579
MLP	0.228(17)	0.728(18)	0.955(08)	0.919	0.577	1.540
SVM	0.211(16)	0.797(16)	0.938(09)	0.918	0.587	1.611
RuleFit	0.162(15)	0.671(19)	0.906(12)	0.891	0.482	1.263
LikelihoodPCA	0.000(00)	0.491(20)	0.845(14)	0.843	0.404	1.099
LD	0.047(08)	0.348(19)	0.744(18)	0.789	0.271	0.806
Likelihood	0.031(07)	0.328(19)	0.674(19)	0.764	0.208	0.589
FDA_GA	0.031(07)	0.147(14)	0.363(19)	0.611	0.093	0.353

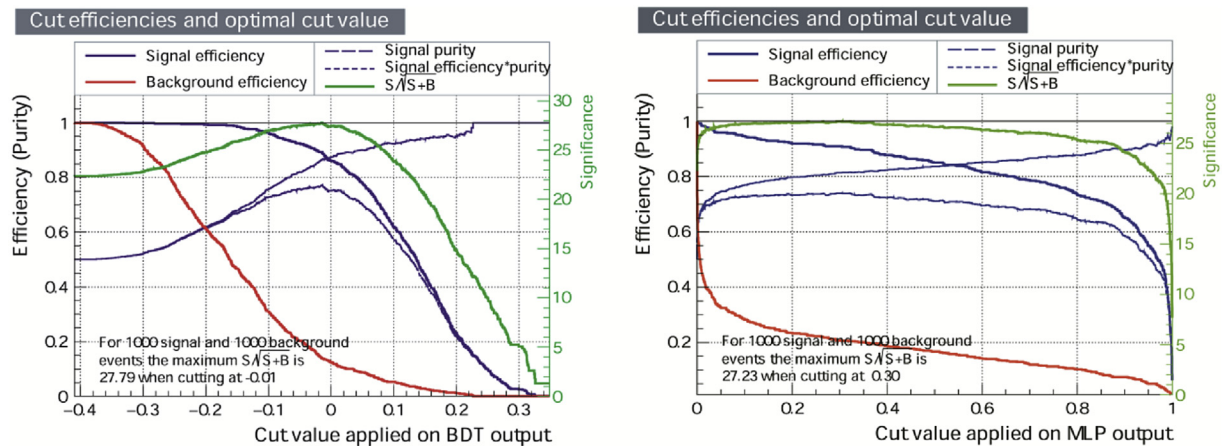


Fig. 4. Cut efficiency and optimal cut value of BDT (left) and MLP (right) classification MVA method for indoor radon concentration.

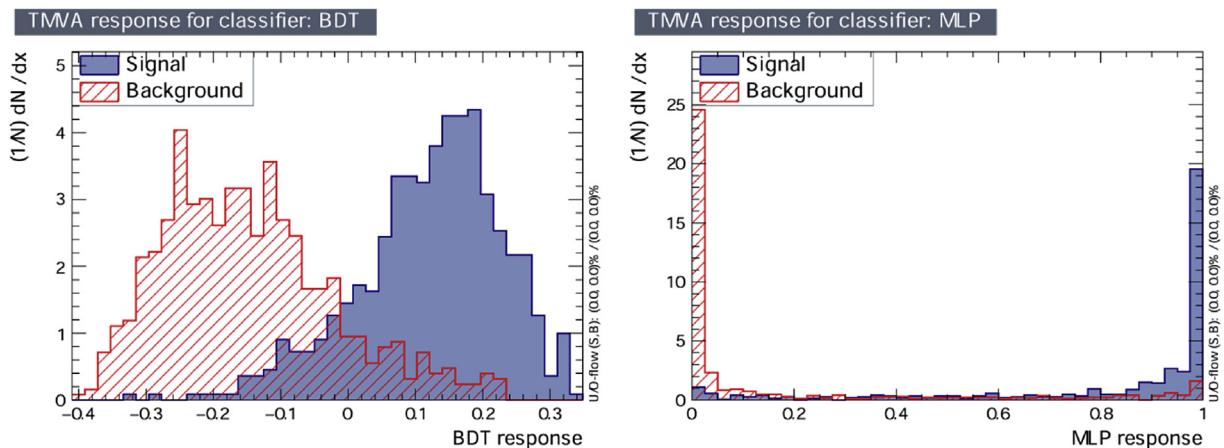


Fig. 5. Distribution of BDT and ANN MLP classification method outputs for input signal and background events.

samples was determined by the pipette method with sodium pyrophosphate as peptizing agent. Based on particle size analysis the following fractions were determined according to IUSS classification: coarse sand (0.2–2 mm), fine sand (0.02–0.2 mm), powder (0.002–0.02 mm) and clay (<0.002 mm).

Soil gas radon activity concentration was measured in situ by RAD7 alpha-spectrometer (DURRIDGE Company) with stainless soil gas probe using grab protocol (Fig. 2). While pumping, the air flow rate is about 0.7 l/min and therefore 3.5 l of soil gas is extracted from the soil at the depth of 70 cm. The last calibration of used

device was performed in radon chamber at the accredited trial metrological Lab. SUJCHBO Kamenna, Czech Republic. Calibration laboratory is traceable to PTB Braunschweig, Germany. After that calibration laboratory participated with RAD7 device in the 2015 NRPI Intercomparison of Radon gas Measurement Instruments with satisfactory results ($|\text{zeta score}| < 2$ – Report number NRPI REG 01-2016, January 2016).

The Toolkit for Multivariate Analysis (TMVA) provides a ROOT-integrated environment for the processing, parallel evaluation and application of multivariate classification and multivariate

Table 4
Variable importance for BDTG MVA method for indoor radon.

BDTG rank	Variable	Variable importance $\times 10^{-2}$
1	Total N	6.490
2	U-238 30 cm	6.425
3	K-40 30 cm	6.040
4	Th-232 30 cm	5.495
5	Humus	5.490
6	K ₂ O	5.406
7	Clay	5.360
8	U-238 surface	5.218
9	Fine	5.116
10	CaCO ₃	5.081
11	P ₂ O ₅	5.003
12	Cs-137 surface	4.715
13	Ra-226 30 cm	4.656
14	Elevation	4.595
15	K-40 surface	4.509
16	pH	4.435
17	Ra-226 surface	4.188
18	Powder	4.082
19	Th-232 surface	4.026
20	Coarse	3.671

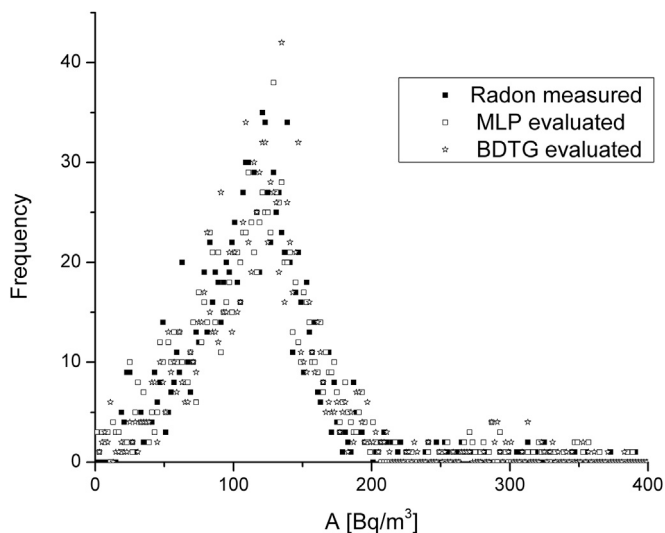


Fig. 6. Distribution of indoor radon concentrations and outputs from MLP Multivariate regression method's evaluation for of indoor radon concentration.

regression methods. All multivariate methods in TMVA belong to the family of “supervised learning” algorithms. They make use of training events, for which the desired output is known, to determine the mapping function that either describes a decision boundary (classification) or an approximation of the underlying functional behavior defining the target value (regression). The two most important Multivariate methods for our purposes are “Boosted Decision Trees” (BDT) and “Artificial Neural Networks” (ANN).

Boosted Decision Trees (BDT) have been successfully used in High Energy Physics analysis for example by the MiniBooNE experiment (Hai-Jun et al., 2005). In BDT, the selection is done on a majority vote on the result of several decision trees. However, the advantage of the straightforward interpretation of the decision tree is lost.

An Artificial Neural Network (ANN) (Rojas, 1996) is most generally speaking any simulated collection of interconnected neurons, with each neuron producing a certain response at a given set of input signals. ANNs in TMVA belong to the class of Multilayer Perceptrons (MLP), which are feed-forward neural networks.

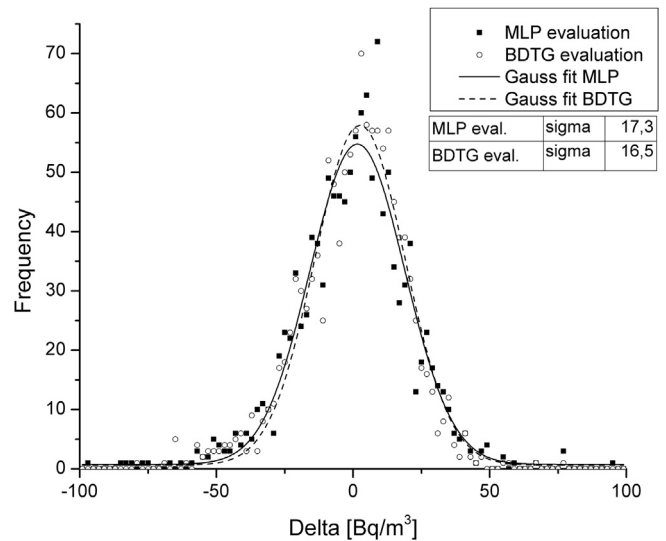


Fig. 7. Distributions of differences of outputs from MLP Multivariate regression method and measured indoor radon concentrations.

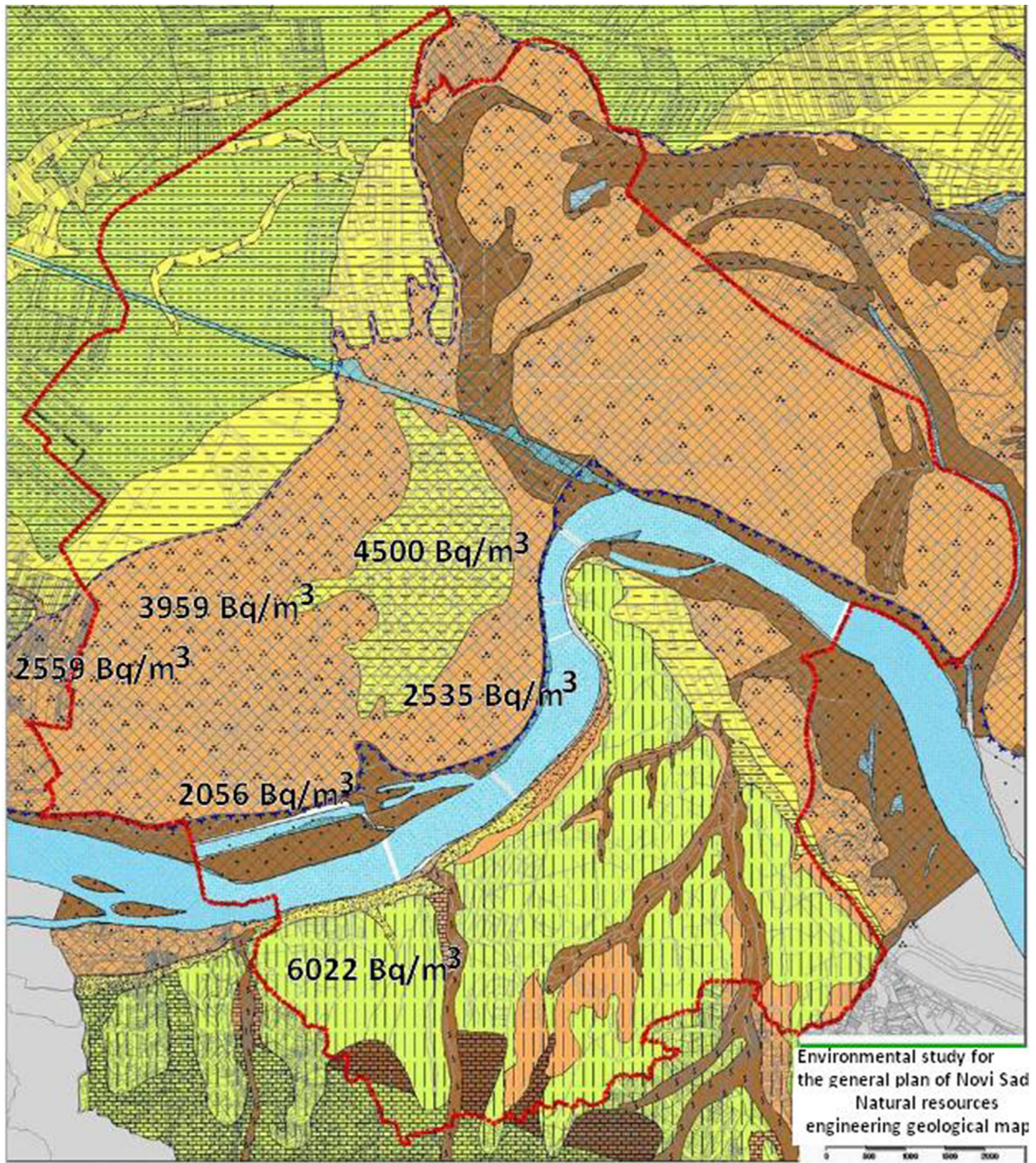
4. Results and discussion

Table 2 shows linear correlation coefficients, which tells us how big is the correlation of input variable and indoor radon concentration. We can notice that radon is more correlated to radioisotopes at depth of 30 cm.

In order to use MVA methods, the sample has to have significant statistics. Since set intended to be used in this analysis does not have enough statistics, we artificially increased the sample by introducing of copy of same sample events, but with modified values of input and measured radon concentrations multiplying initial value with $1 +$ random Gaussian values with sigma $1/10$. We are using the input events (set of soil sample properties and radionuclides activity in 30 cm depth and on surface) to train, test and evaluate the 12 multivariate methods implemented in TMVA. The graph presenting the “Receiver operating characteristic” (ROC) for each multivariate method (Fig. 3) may be considered as the most indicative in comparing the different methods used for classification of radon concentrations using climate variables. On this graph one can read the dependence of background rejection on signal efficiency. The best method is the one that holds maximum value of background rejection for highest Signal efficiency (Table 3), i.e. the best method has ROC curve closest to the upper right corner on the graph presented in Fig. 3. It turns out that the method best suited for our purpose is the Boosted Decision Trees (BDT) method. This means that BDT gives most efficient classification of input events. This is seen in Fig. 4, which shows the distribution of BDT classification method outputs for input signal and background events. The second best method is the implementation of ANN Multilayer Perceptrons (MLP).

In Fig. 4, one can see the values of signal and background efficiency and significance. Significance, calculated as $N(\text{Signal})/\sqrt{N(\text{Signal})+N(\text{Background})}$, can be used as the value for comparison of various multivariate methods, and also for comparison of method efficiencies for different sets of input variables.

Fig. 5 shows the distribution of BDT classification method outputs for input signal and background events. These figures again demonstrate that classification methods work well i.e. that the separation of signal and background works very good. Also, the significance value for BDT is higher for higher cut values for splitting of input events. Interestingly, it appears that other multivariate



Lithological classification

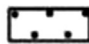



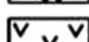

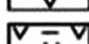
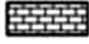
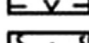
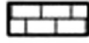
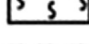

	contemporary riverbanks fine sandy		loess clay
	older riverbanks sandy clay		unchanged loess
	sediments old lakes and swamps rich in organic matter		Delluvial gravel-sandy clay
	sediments of new swamps		Tertiary (clay, marl, conglomerates, clays, sands)
	sediments of loess valley		Mesozoic flysch
	redeposited loess		Eruptive rocks

Fig. 8. Lithological map of Novi Sad city (Obrknežev et al., 2009) with maximal soil gas radon activity concentrations measured in six parts of the city.

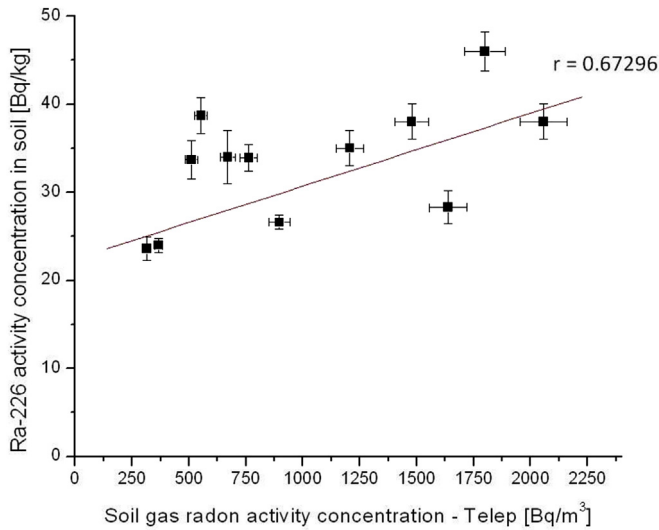


Fig. 9. Correlation between radium activity concentrations in the soil and soil gas activity concentrations for Telep district.

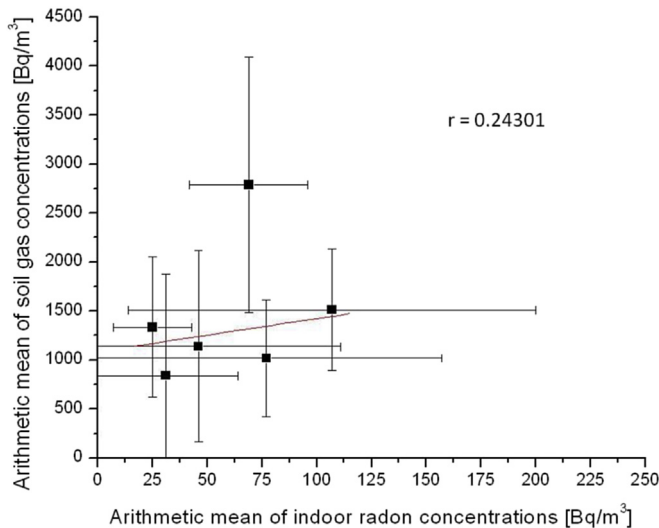


Fig. 10. Correlations between arithmetic means of soil gas concentrations and indoor radon activity concentrations with standard deviations (error bars) for six districts of Novi Sad city.

methods also give better results under these new conditions.

Ranking of the BDTG input variables (Table 4) is derived by counting how often the variables are used to split decision tree nodes, and by weighting each split occurrence by the separation it has achieved and by the number of events in the node. As seen from Table 4, besides Total N, radionuclides on 30 cm depth appears to be the most important variables for indoor radon.

Regression is the approximation of the underlying functional behavior defining the target value. We tried to find the best regression method that will give output values (predicted indoor radon concentration) closest to the actual concentrations that corresponds to specific input variables. The best multivariate regression method is found to be BDT, and the second one is MLP, same as in case of multivariate classifiers. Fig. 6 presents the distribution of indoor radon concentrations and outputs from the MLP multivariate regression method evaluation of radon concentration using all input variables.

To best way to estimate the quality of the method is to look at the differences between the output values from MLP multivariate regression method and the values of measured indoor radon concentrations (Fig. 7). The figure indicates the good predictive power of multivariate regression methods as applied for prediction of variations of indoor radon concentrations based on full set of input variables.

In the city of Novi Sad Laboratory for dose and radioactivity measurements performed soil gas measurements by active device RAD7 coupled with soil gas probe on about 100 locations divided in 6 districts of the city. In order to verify previously obtained correlations we analyzed in detail all available parameters: radionuclide contents of the soil, average indoor radon concentrations in each district, maximal and average soil gas concentrations for each district and geomorphologic units. Results are shown on Figs. 8–10 and in Table 5. Indoor radon concentrations were measured by gamma spectrometry method using charcoal canisters for radon adsorption. The MDA for this technique of indoor radon measurement is about 2 Bq/m³ and the measurement uncertainty depends on count rates in post radon gamma lines, detector efficiency and charcoal water gain.

The effects of radium activity concentrations in deep layers of examined soil to indoor radon concentrations were analyzed through linear correlations and the results are shown on Figs. 9 and 10. We used Pearson correlation coefficient based on a comparison of the actual impact of observed variables to one another in relation to the maximum potential impact of the two variables (1) and obtained almost high positive correlation between radium activity concentrations in soil and soil gas concentrations ($r = 0.67296$) and low positive correlation between arithmetic means of soil gas concentrations and indoor radon activity concentrations ($r = 0.24301$).

$$r = \frac{\sum_i x_i y_i - \frac{1}{n} \sum_i x_i \sum_i y_i}{\sqrt{\left[\sum_i y_i^2 - \left(\frac{1}{n} \right) \left(\sum_i y_i \right)^2 \right] \left[\sum_i x_i^2 - \left(\frac{1}{n} \right) \left(\sum_i x_i \right)^2 \right]}} \quad (1)$$

5. Conclusion

In the paper the possibility of multivariate analysis application for radon potential estimation is described in detailed. The most appropriate multivariate method of analysis of indoor radon measurements is selected from a wide spectrum of multivariate methods developed for data analysis in high-energy physics and implemented in the Toolkit for Multivariate Analysis software package. The evaluation ranking results based on the best signal efficiency and purity, show that the Boosted Decision Trees (BDT) and Multi Layer Perceptron (MLP), based on Artificial Neural Network (ANN), are multivariate methods which give the best results in the analysis. Further multivariate analysis results give insight into the dependence of indoor radon concentrations with other radionuclides activity both 30 cm underground and on surface during the time of measurements, as well as soil properties variables. The BDTG multivariate method shows that variables with the highest importance are radionuclides activity in deep layers compared with the activity of surface layer, but also the humus and clay content (Table 4). Moreover, the multivariate regression methods give a good approximation of indoor radon activity using full set of input variables.

This study showed that radiogeochimical data are useful to generate maps of radon priority areas. We confirmed the assumption that the soil types which contain the highest content of clay

Table 5

Comparison of available data for each analyzed district of Novi Sad city with the description of geomorphologic unit and the number of samples that were considered. Numbers in brackets are the standard deviations for the average values and the measurement uncertainties for measured values in the range column.

City district (Geomorphologic unit)	Average of soil gas concentrations [Bq/m ³]	Range of soil gas concentrations [Bq/m ³]	Average of indoor radon concentrations [Bq/m ³]	Range of indoor radon concentrations [Bq/m ³]	Average of Ra-226 concentrations in soil [Bq/kg]	Range of Ra-226 concentrations in soil [Bq/kg]
Telep (Contemporary riverbanks, fine sandy) 13 samples	1020(596)	315(16) –2056(105)	77(80)	4(2)–313(8)	33(7)	23,6(13)–46,0(22)
Detelinara (Loess clay) 29 samples	1138(976)	312(17) –4500(220)	46(65)	4(2)–345(14)	30(7)	14,1(14)–45(2)
Liman (Older riverbanks, sandy clay) 17 samples	1334(715)	230(12) –2535(130)	25(18)	6(2)–74(5)	27(7)	14,9(14)–40,5(21)
Veternik (Older riverbanks, sandy clay) 16 samples	1512(616)	104(7)–2559(132)	107(93)	34(4)–276(8)	32(5)	22,3(14)–41(2)
Novo Naselje (Older riverbanks, sandy clay) 19 samples	840(1033)	122(8)–3959(198)	31(33)	4(2)–92(6)	31(6)	19(2)–44(2)
Sremska Kamenica (Unchanged loess) 14 samples	2787(1306)	1582(80) –6022(302)	69(27)	38(4)–110(6)	36(7)	19,9(16)–43,5(17)

and humus best adsorb and retain radon which is reflected in elevated soil gas radon concentrations and higher geogenic radon potential. This conclusion could be used for selection of locations for planning radon permeability measurements. The best correlation of radon concentrations with total nitrogen amount in the soil is very interested result and it will be studied in next research.

The results of detailed analysis of databases for radon and soil radioactivity measurements for the city of Novi Sad validated geogenic prognosis that soil gas radon concentrations mostly depend on geomorphologic units and litologic distribution in study area. Good agreement of radium content in soil samples and radon soil gas activity concentrations obtained.

The multivariate regression methods used gives as a result a "mapped" functional behavior of indoor radon and input variables. Using this "mapped" function, the search for radon priority areas is straightforward. The best performing multivariate methods identified most important variables, and help with simplification of "mapped" function which then requires smaller number of input variables. Further analysis of "mapped" function can point to which are the most important mechanisms for increase of indoor radon concentrations.

So the multivariate methods can be used in identifying the most significant variables, help identify radon priority areas, and help with physics analysis of processes of radon emanation.

Acknowledgements

The authors acknowledge the financial support of the Provincial Secretariat for Environmental Protection and Sustainable Development (grant number 401-00088/2003) and Ministry of Science, Technology and Development of Serbia within the projects: Nuclear Methods Investigations of Rare Processes and Cosmic Rays (grant number 171002) and Biosensing Technologies and Global System for Continuous Research and Integrated Management (grant number 43002).

References

- Bikit, I., et al., 2003. Simple method for depleted uranium determination. *Jpn. J. Appl. Phys.* 42, 5269–5273.
- Bikit, I., et al., 2005. Radioactivity of the soil in Vojvodina (northern province of Serbia and Montenegro). *J. Environ. Radioact.* 78, 11–19.
- Brun, R., Rademakers, F., 1997. Root – an object oriented data analysis framework. *Nucl. Inst. Meth. Phys. Res. A* 389, 81.
- De Cort, M., et al., 2011. Towards a European atlas of natural radiation: goal, status and future perspectives. *Radioprotection* 46, 737–743.
- Durrige, 2014. RAD7 Radon Detector User Manual, Revision 7.26. DURRIDGE Company. <http://www.durrige.com/documentation/RAD7Manual.pdf>.
- EURATOM, 2013. Council Directive 2013/59/EURATOM of 5 December 2013 Laying Down Basic Safety Standards for Protection against the Dangers Arising from Exposure to Ionising Radiation, and Repealing Directives 89/618/Euratom, 90/641/Euratom, 96/29/Euratom, 97/43/Euratom and 2003/122/Euratom, Article 74 Indoor Exposure to Radon. <http://eur-lex.europa.eu/LexUriServ/LexUriServ.do?uri=OJ:L:2014:013:0001:0073:EN:PDF>.
- Forkapic, S., et al., 2007. Indoor radon in rural dwellings of the south-Pannonian region. *Radiat. Prot. Dosim.* 123, 378–383.
- Gruber, V., et al., 2013. The European map of geogenic radon potential. *J. Radiol. Prot.* 33, 51–60.
- Hai-Jun, Y., et al., 2005. Studies of boosted decision trees for MiniBooNE particle identification. *Nucl. Instrum. Meth. A* 555, 370–385. <http://arxiv.org/abs/physics/0508045>.
- Hoecker, A., et al., 2007. TMVA – Toolkit for Multivariate Data Analysis. *PoS ACAT* 040, arXiv:physics/070303.
- IUSS Working Group WRB, 2014. World reference base for soil resources 2014. In: *International Soil Classification System for Naming Soils and Creating Legends for Soil Maps*. World Soil, 106. FAO, Rome.
- Košćal, M., et al., 2005. Geomorphological Map of Vojvodina with Legends. Geozavod – Gemini, Beograd.
- Mamont-Ciešla, K., et al., 2010. Intercomparison of radon CR-39 detector systems conducted in CLOR's calibration chamber. *Nukleonika* 55 (4), 598–593.
- Nejgebauer, V., et al., 1971. The Pedological Map of Vojvodina (R 1 : 50.000). Institute for Agricultural Research, Novi Sad.
- Obrknežev, R., et al., 2009. The Study of Environmental Protection in the City of Novi Sad, Public Enterprise "Urbanizam". Department of Urban Planning, Novi Sad.
- Rojas, R., 1996. *Neural Networks*. Springer-Verlag, Berlin.
- Skorić, A., et al., 1985. Classification of soils in Yugoslavia, academy of Sciences and arts of Bosnia and Herzegovina special editions, book LXXVIII, Sarajevo.
- UNSCEAR, 2008. Ionizing Radiation: Sources and Effects, UNSCEAR 2008 REPORT, VOLUME II. United Nations, New York. http://www.unscear.org/unscear/en/publications/2008_1.html.
- WHO, 2009. In: *Handbook on Indoor Radon – a Public Health Perspective*. www.who.int/ionizing_radiation/env/radon/en/imdex1.html.

MAUS: the MICE analysis user software

To cite this article: R. Asfandiyarov *et al* 2019 *JINST* **14** T04005

View the [article online](#) for updates and enhancements.

Recent citations

- [Demonstration of cooling by the Muon Ionization Cooling Experiment](#)



IOP | ebooks™

Bringing you innovative digital publishing with leading voices to create your essential collection of books in STEM research.

Start exploring the collection - download the first chapter of every title for free.

MUON ACCELERATORS FOR PARTICLE PHYSICS — MUON

MAUS: the MICE analysis user software

R. Asfandiyarov,^a R. Bayes,^b V. Blackmore,^c M. Bogomilov,^d D. Colling,^c A.J. Dobbs,^c F. Drielsma,^a M. Drews,^h M. Ellis,^c M. Fedorov,^e P. Franchini,^f R. Gardener,^g J.R. Greis,^f P.M. Hanlet,^h C. Heidt,ⁱ C. Hunt,^c G. Kafka,^h Y. Karadzhov,^a A. Kurup,^c P. Kyberd,^g M. Littlefield,^g A. Liu,^j K. Long,^{c,n} D. Maletic,^k J. Martyniak,^c S. Middleton,^c T. Mohayai,^{h,j} J.J. Nebrensky,^g J.C. Nugent,^b E. Overton,^l V. Pec,^l C.E. Pidcott,^f D. Rajaram,^{h,1} M. Rayner,^m I.D. Reid,^g C.T. Rogers,ⁿ E. Santos,^c M. Savic,^k I. Taylor,^f Y. Torun,^h C.D. Tunnell,^m M.A. Uchida,^c V. Verguilov,^a K. Walaron,^b M. Winter^h and S. Wilbur^l

^aDPNC, section de Physique, Université de Genève, Geneva, Switzerland

^bSchool of Physics and Astronomy, Kelvin Building, The University of Glasgow, Glasgow, U.K.

^cDepartment of Physics, Blackett Laboratory, Imperial College London, London, U.K.

^dDepartment of Atomic Physics, St. Kliment Ohridski University of Sofia, Sofia, Bulgaria

^eRadboud University of Nijmegen, Netherlands

^fDepartment of Physics, University of Warwick, Coventry, U.K.

^gBrunel University, Uxbridge, U.K.

^hPhysics Department, Illinois Institute of Technology, Chicago, IL, U.S.A.

ⁱUniversity of California, Riverside, CA, U.S.A.

^jFermilab, Batavia, IL, U.S.A.

^kInstitute of Physics, University of Belgrade, Serbia

^lDepartment of Physics and Astronomy, University of Sheffield, Sheffield, U.K.

^mDepartment of Physics, University of Oxford, Denys Wilkinson Building, Oxford, U.K.

ⁿSTFC Rutherford Appleton Laboratory, Harwell Oxford, Didcot, U.K.

E-mail: durga@fnal.gov

ABSTRACT: The Muon Ionization Cooling Experiment (MICE) collaboration has developed the MICE Analysis User Software (MAUS) to simulate and analyze experimental data. It serves as the primary codebase for the experiment, providing for offline batch simulation and reconstruction as well as online data quality checks. The software provides both traditional particle-physics functionalities such as track reconstruction and particle identification, and accelerator physics functions, such as calculating transfer matrices and emittances. The code design is object orientated, but has a top-level structure based on the Map-Reduce model. This allows for parallelization to support live data reconstruction during data-taking operations. MAUS allows users to develop in

¹Corresponding author.

either Python or C++ and provides APIs for both. Various software engineering practices from industry are also used to ensure correct and maintainable code, including style, unit and integration tests, continuous integration and load testing, code reviews, and distributed version control. The software framework and the simulation and reconstruction capabilities are described.

KEYWORDS: Data reduction methods; Simulation methods and programs; Software architectures (event data models, frameworks and databases); Accelerator modelling and simulations (multi-particle dynamics; single-particle dynamics)

ARXIV EPRINT: [1812.02674](https://arxiv.org/abs/1812.02674)

Contents

1	Introduction	1
1.1	The MICE experiment	1
1.2	Software requirements	3
2	MAUS	3
2.1	Code design	3
2.2	Data structure	6
2.2.1	Physics data	6
2.2.2	Top level data organization	10
2.3	Data flow	10
2.4	Testing	10
3	Monte Carlo	12
3.1	Beam generation	12
3.2	Geant4	12
3.3	Geometry	13
3.4	Tracking, field maps and beam optics	14
3.5	Detector response and digitization	15
4	Reconstruction	15
4.1	Time of flight	15
4.2	Scintillating-fiber trackers	16
4.3	KL calorimeter	17
4.4	Electron-muon ranger	17
4.5	Cherenkov	18
4.6	Global reconstruction	18
4.6.1	Global track matching	18
4.6.2	Global PID	18
4.7	Online reconstruction	19
5	Summary	19

1 Introduction

1.1 The MICE experiment

The Muon Ionization Cooling Experiment (MICE) sited at the STFC Rutherford Appleton Laboratory (RAL) has delivered the first demonstration of muon ionization cooling [1] — the reduction of the phase-space of muon beams. Muon-beam cooling is essential for future facilities based on

muon acceleration, such as the Neutrino Factory or Muon Collider [2, 3]. The experiment was designed to be built and operated in a staged manner. In the first stage, the muon beamline was commissioned [4] and characterized [5]. A schematic diagram of the configuration used to study the factors that determine the performance of an ionization-cooling channel is shown in figure 1. The MICE experiment was operated such that muons passed through the experiment one at a time. The experiment included instrumentation to identify particle species (the particle-identification detectors, PID) [6–11] and to measure the phase-space coordinates of each muon. An ensemble of muons that was representative of the muon beam was then assembled using the measured coordinates. The techniques used to reconstruct the ensemble properties of the beam are described in [12] and the first observation of the ionization-cooling of a muon beam is presented in [1].

The configuration shown in figure 1 was used to study the factors that determine the performance of an ionization-cooling channel and to observe for the first time the reduction in transverse emittance of a muon beam.

The MICE Muon Beam line is described in detail in [4]. There are 5 different detector systems present on the beamline: time-of-flight (TOF) scintillators [6], threshold Cherenkov (Ckov) counters [13], scintillating-fiber trackers [14], a sampling calorimeter (KL) [8, 9], and the Electron Muon Ranger (EMR) — a totally active scintillating calorimeter [10, 11]. The TOF, Ckov, KL and EMR detectors are used for particle identification (PID), and the scintillating-fiber trackers are used to measure position and momentum. The TOF detector system consists of three detector stations, TOF0, TOF1 and TOF2, each composed of two orthogonal layers of scintillator bars. The TOF system determines PID via the time-of-flight between the stations. Each station also provides a low-resolution image of the beam profile. The Ckov system consists of two aerogel threshold Cherenkov stations, CkovA and CkovB. The KL and EMR detectors, the former using scintillating fibers embedded in lead sheets, and the latter scintillating bars, form the downstream calorimeter system.

The tracker system consists of two scintillating-fiber detectors, one upstream of the MICE cooling cell, the other downstream, in order to measure the change in emittance across the cooling cell. Each detector consists of 5 stations, each station having 3 fiber planes, allowing precision measurement of momentum and position to be made on a particle-by-particle basis.

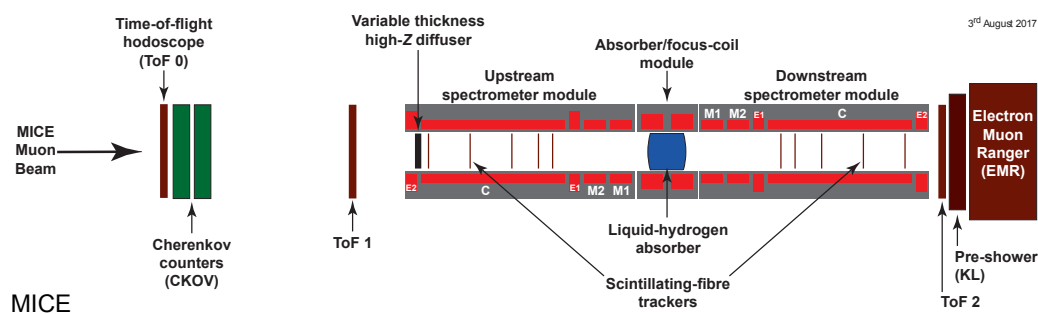


Figure 1. Schematic diagram of the MICE experiment. The red rectangles represent the coils of the spectrometer solenoids and focus-coil module. The individual coils of the spectrometer solenoids are labelled E1, C, E2, M1 and M2. The various detectors (time-of-flight hodoscopes (TOF0, TOF1) [6], Cherenkov counters [13], scintillating-fiber trackers [14], KLOE-Light (KL) calorimeter [7, 8], and Electron Muon Ranger (EMR) [10, 11]) are also represented.

1.2 Software requirements

The MICE software must serve both the accelerator-physics and the particle-physics needs of the experiment. Traditional particle-physics functionality includes reconstructing particle tracks, identifying them, and simulating the response from various detectors, while the accelerator-physics aspect includes the calculation of transfer matrices and Twiss parameters and propagating the beam envelopes. All of these items require a detailed description of the beamline, the geometries of the detectors, and the magnetic fields, as well as functionality to simulate the various detectors and reconstruct the detector outputs. MICE aims to measure the change in emittance to 1%, which imposes requirements on the performance of the track reconstruction, particle identification and measurements of scattering widths. In addition, the computational performance of the software was also important in order to ensure that the software can reconstruct data with sufficient speed to support live online monitoring of the experiment.

2 MAUS

The MICE Analysis User Software (MAUS) is the collaboration's simulation, reconstruction, and analysis software framework. MAUS provides a Monte Carlo (MC) simulation of the experiment, reconstruction of tracks and identification of particles from simulations and real data, and provides monitoring and diagnostics while running the experiment.

Installation is performed via a set of shell scripts with SCons [15] as the tool for constructing and building the software libraries and executables. The codebase is maintained with GNU Bazaar [16], a distributed version control system, and is hosted on Launchpad [17], a website that provides functionalities to host and maintain the software repository. MAUS has a number of dependencies on standard packages such as Python, ROOT [18] and Geant4 [19] which are built as "third party" external libraries during the installation process. The officially supported platform is Scientific Linux 6 [20] though developers have successfully built on CentOS [21], Fedora [22], and Ubuntu [23] distributions.

Each of the MICE detector systems, described in section 1.1, is represented within MAUS. Their data structures are described in section 2.2 and their simulation and reconstruction algorithms in sections 3 and 4. MAUS also provides "global" reconstruction routines, which combine data from individual detector systems to identify particle species by the likelihood method and perform a global track fit. These algorithms are also described in section 4.

2.1 Code design

MAUS is written in a mixture of Python and C++. C++ is used for complex or low-level algorithms where processing time is important, while Python is used for simple or high-level algorithms where development time is a more stringent requirement. Developers are allowed to write in either Python or C++ and Python bindings to C++ are handled through internal abstractions. In practice, all the reconstruction modules are written in C++ but support is provided for legacy modules written in Python.

MAUS has an Application Programming Interface (API) that provides a framework on which developers can hang individual routines. The MAUS API provides MAUS developers with a well-defined environment for developing reconstruction code, while allowing independent development of the back-end and code-sharing of common elements, such as error handling.

The MAUS data processing model is inspired by the Map-Reduce framework [24], which forms the core of the API design. Map-Reduce, illustrated in figure 2 is a useful model for parallelizing data processing on a large scale. A *map* process takes a single object as an input, transforms it, and returns a new object as the output (in the case of MAUS this input object is the *spill* class, see section 2.2).

A module is the basic building block of the MAUS API framework. Four types of module exist within MAUS:

1. **Inputters** generate input data either by reading data from files or over a network, or by generating an input beam;
2. **Mappers** modify the input data, for example by reconstructing signals from detectors, or tracking particles to generate MC hits;
3. **Reducers** collate the mapped data and provide functionality that requires access to the entire data set; and
4. **Outputters** save the data either by streaming over a network or writing to disk.

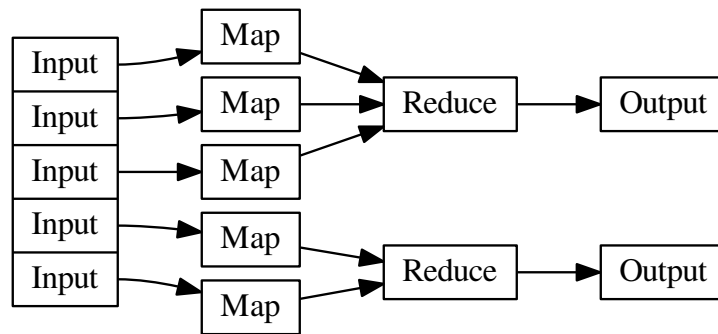


Figure 2. A Map-Reduce framework.

Each module type follows a common, extensible, object-orientated class hierarchy, shown for the case of the *map* and *reduce* modules in figure 3.

There are some objects that sit outside the scope of this modular framework but are nevertheless required by several of the modules. For instance, the detector geometries, magnetic fields, and calibrations are required by the reconstruction and simulation modules, and objects such as the electronics-cabling maps are required in order to unpack data from the data acquisition (DAQ) source, and error handling functionality is required by all of the modules. All these objects are accessed through a static singleton *globals* class.

MAUS has two execution concepts. A *job* refers to a single execution of the code, while a *run* refers to the processing of data for a DAQ run or MC run. A job may contain many runs. Since data are typically accessed from a single source and written to a single destination, *inputters* and *outputters* are initialized and destroyed at the beginning and end of a job. On the other hand, *mappers*

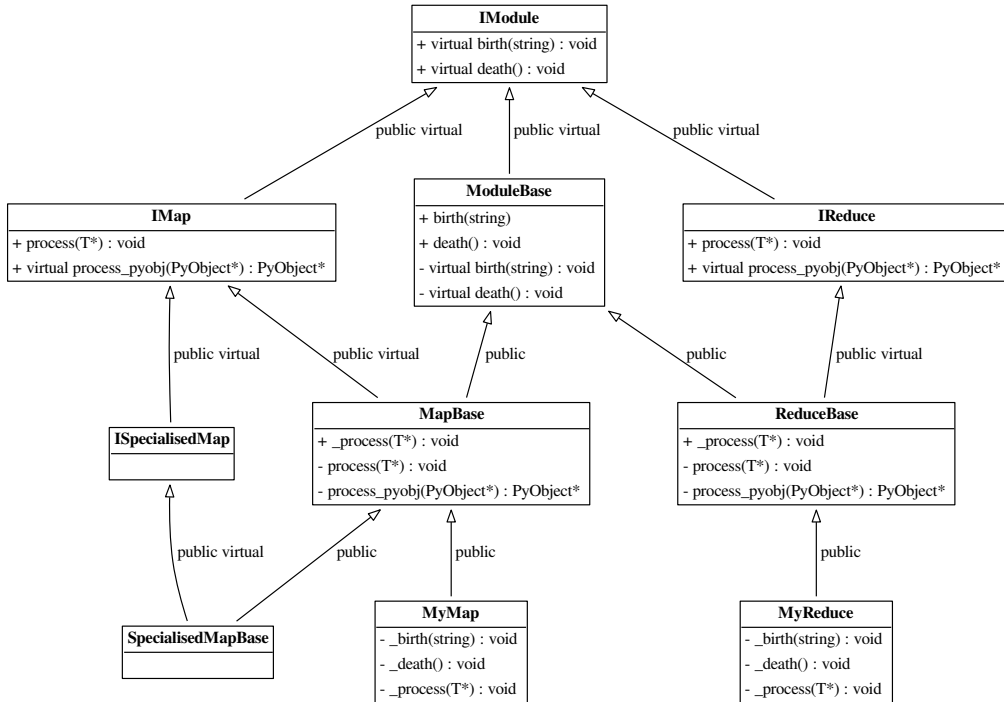


Figure 3. The MAUS API class hierarchy for Map and Reduce modules. The input and output modules follow related designs. T represents a templated argument. “+” indicates the introduction of a virtual void method, defining an interface, while “-” indicates that a class implements that method, fulfilling that aspect of the interface. The `process_pyobj` functions are the main entry points for Python applications, and `process` the entry points for C++ applications. The framework can be extended as many times as necessary, as exemplified by the “SpecialisedMap” classes.

and *reducers* are initialized at the beginning of a run in order to allow run-specific information such as electronics cabling maps, fields, calibrations and geometries to be loaded.

The principal data type in MAUS, which is passed from module to module, is the *spill*. A single spill corresponds to data from the particle burst associated with a dip of the MICE target [4]. A spill lasts up to ~ 3 ms and contains several DAQ triggers. Data from a given trigger define a single MICE *event*. In the language of the Input-Map-Reduce-Output framework, an *Input* module creates an instance of spill data, a *Map* module processes the spill (simulating, reconstructing, etc.), a *Reduce* module acts on a collection of spills when all the *mappers* finish, and finally an *Output* module records the data to a given file format.

Modules can exchange spill data either as C++ pointers or JSON [25] objects. In Python, the data format can be changed by using a converter module, and in C++ *mappers* are templated to a MAUS data type and an API handles any necessary conversion to that type (see figure 3).

Data contained within the MAUS data structure (see section 2.2) can be saved to permanent storage in one of two formats. The default data format is a ROOT [18] binary and the secondary format is JSON. ROOT is a standard high-energy physics analysis package, distributed with MAUS, through which many of the analyses on MICE are performed. Each spill is stored as a single entry in a ROOT TTree object. JSON is an ASCII data-tree format. Specific JSON parsers are available — for example, the Python *json* library, and the C++ *JsonCpp* [26] parser come prepackaged with MAUS.

In addition to storing the output from the *map* modules, MAUS is also capable of storing the data produced by *reducer* modules using a special *Image* class. This class is used by *reducers* to store images of monitoring histograms, efficiency plots, etc. *Image* data may only be saved in JSON format.

2.2 Data structure

2.2.1 Physics data

At the top of the MAUS data structure is the spill class which contains all the data from the simulation, raw real data and the reconstructed data. The spill is passed between modules and written to permanent storage. The data within a spill is organized into arrays of three possible event types: an *MCEvent* contains data representing the simulation of a single particle traversing the experiment and the simulated detector responses; a *DAQEvent* corresponds to the real data for a single trigger; and a *ReconEvent* corresponds to the data reconstructed for a single particle event (arising either from a Monte Carlo(MC) particle or a real data trigger). These different branches of the MAUS data structure are shown diagrammatically in figures 4–9.

The sub-structure of the MC event class is shown in figure 5. The class is subdivided into events containing detector hits (energy deposited, position, momentum) for each of the MICE detectors (see section 1.1). The event also contains information about the primary particle that created the hits in the detectors.

The sub-structure of the reconstruction event class is shown in figure 6. The class is subdivided into events representing each of the MICE detectors, together with the data from the trigger, and data for the global event reconstruction. Each detector class and the global-reconstruction class has several further layers of reconstruction data. This is shown in figures 7–9.

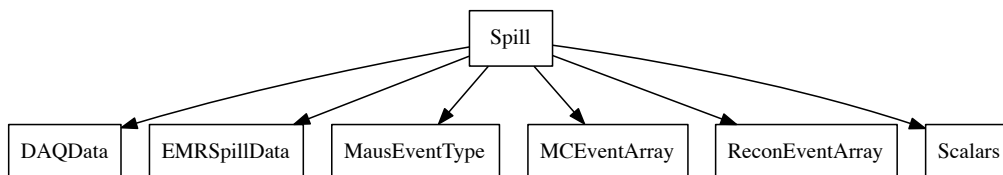


Figure 4. The MAUS output structure for a spill event. The label in each box is the name of the C++ class.

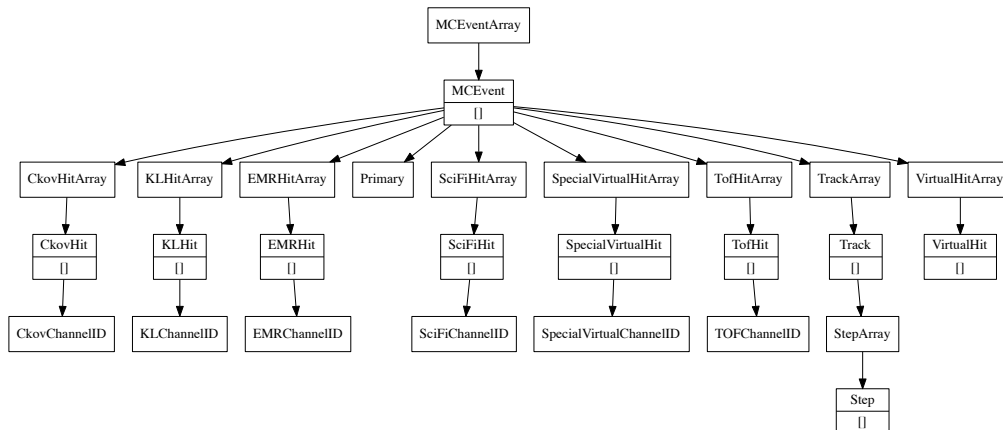


Figure 5. The MAUS data structure for MC events. The label in each box is the name of the C++ class and [] indicates that child objects are array items.

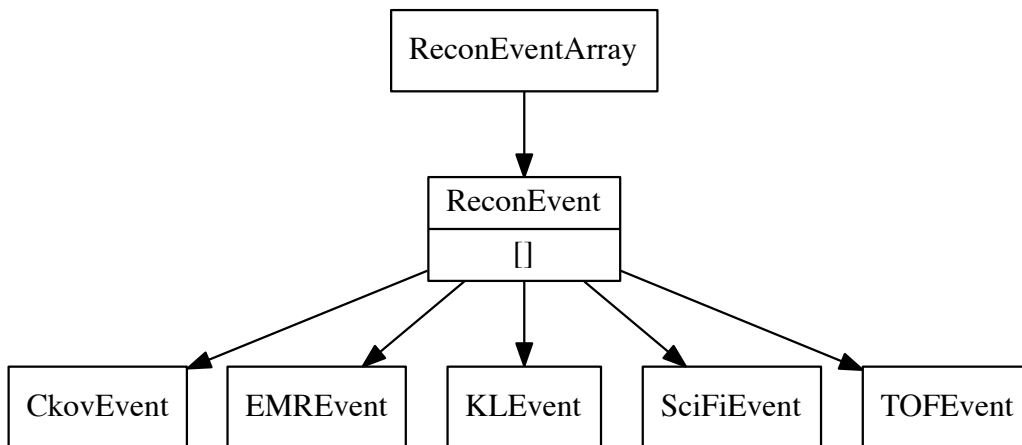


Figure 6. The MAUS data structure for reconstructed events. The label in each box is the name of the C++ class.

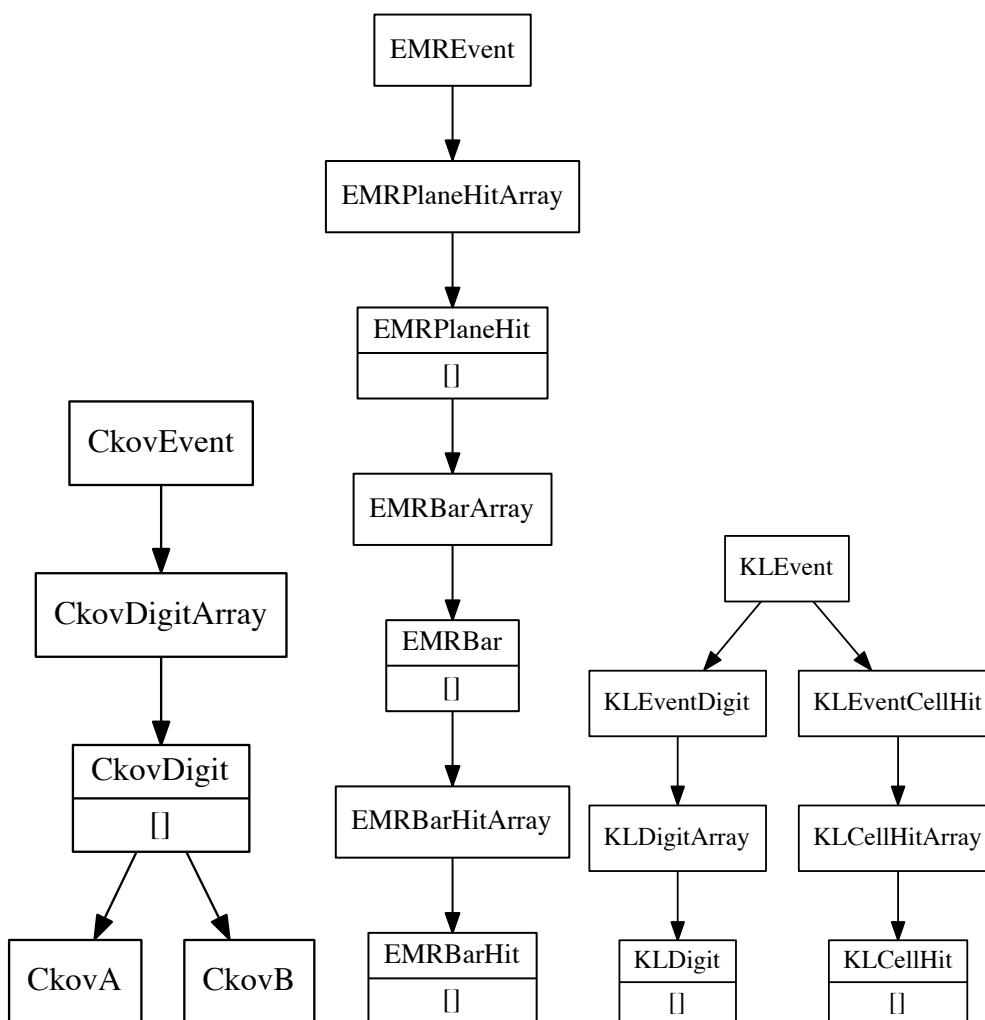


Figure 7. The MAUS data structure for CKOV (left), EMR (middle) and KL (right) reconstructed events. The label in each box is the name of the C++ class [] indicates that child objects are array items.

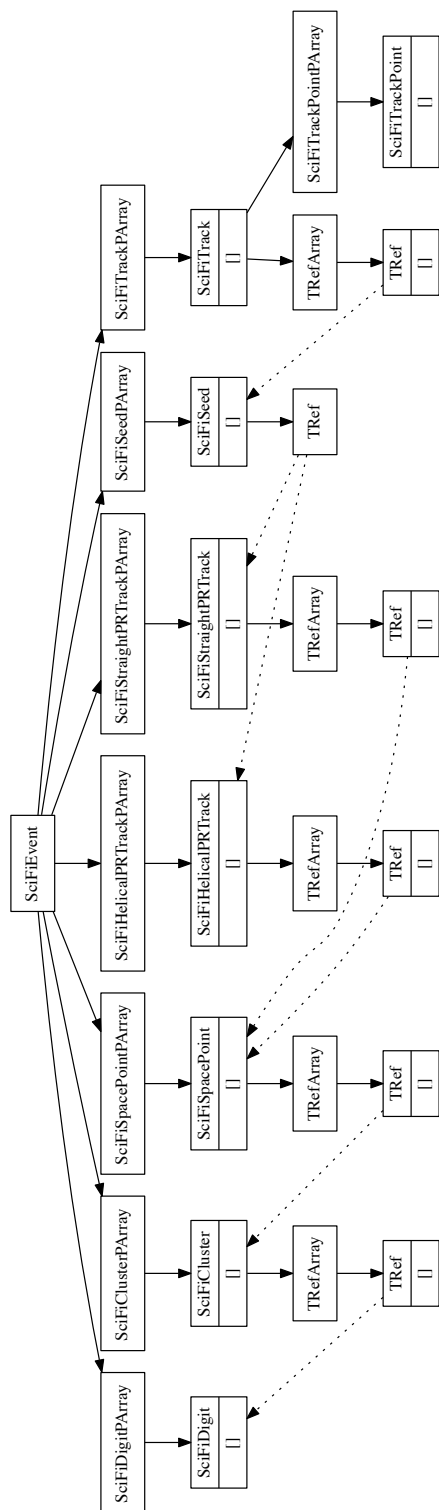


Figure 8. The MAUS data structure for the tracker. The label in each box is the name of the C++ class and [] indicates that child objects are array items.

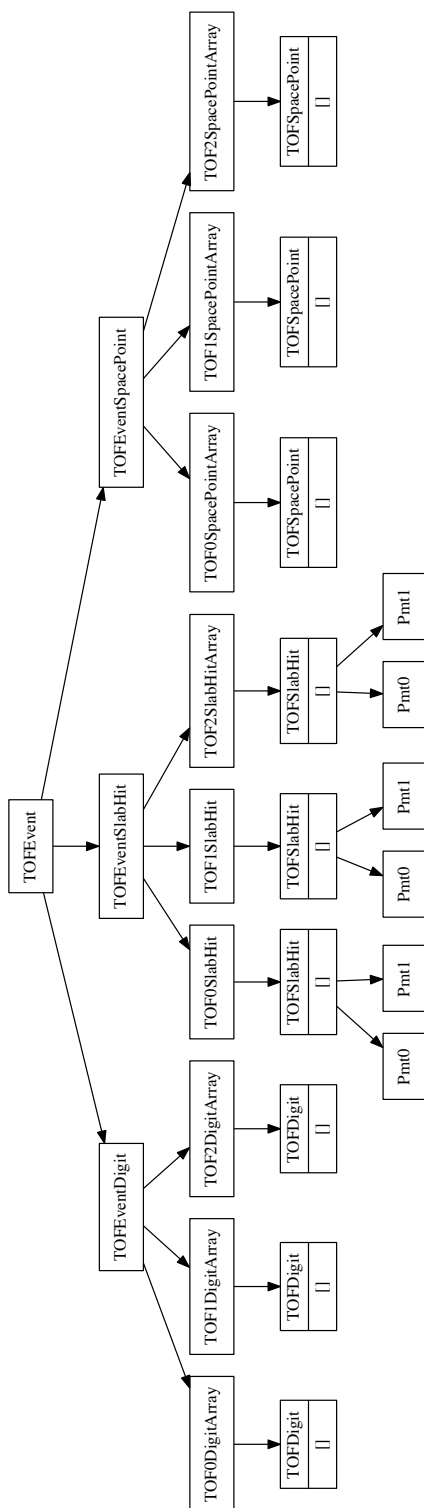


Figure 9. The MAUS data structure for the TOFs. The label in each box is the name of the C++ class and [] indicates that child objects are array items.

2.2.2 Top level data organization

In addition to the spill data, MAUS also contains structures for storing supplementary information for each run and job. These are referred to as *JobHeader* and *JobFooter*, and *RunHeader* and *RunFooter*. The *JobHeader* and *JobFooter* represent data, such as the MAUS release version, associated with the start and end of a job, and the *RunHeader* and *RunFooter* represent data, such as the geometry and calibrations associated with a run, associated with the start and end of a run. These are saved to the output along with the spill.

In order to interface with ROOT, particularly in order to save data in the ROOT format, thin wrappers for each of the top level classes, and a templated base class, were introduced. This allows the ROOT TTree, in which the output data is stored (see section 2.2.1), to be given a single memory address to read from. The wrapper for Spill is called *Data*, while for each of *RunHeader*, *RunFooter*, *JobHeader* and *JobFooter*, the respective wrapper class is just given the original class name with “Data” appended, e.g., *RunHeaderData*. The base class for each of the wrappers is called *MAUSEvent*. The class hierarchy is illustrated in figure 10.

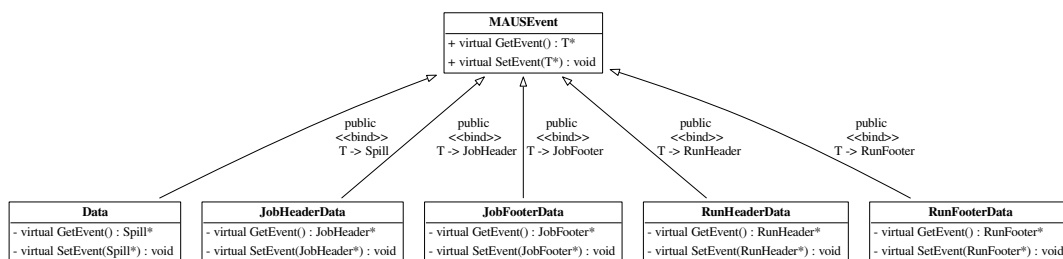


Figure 10. Class hierarchy for the wrappers and base class of the top-level classes of the MAUS data structure.

2.3 Data flow

The MAUS data-flow, showing the reconstruction chain for data originating from MC or real data, is depicted in figure 11. Each item in the diagram is implemented as an individual module. The data flow is grouped into three principal areas: the simulation data flow used to generate digits (electronics signals) from particle tracking; the real data flow used to generate digits from real detector data; and the reconstruction data flow which illustrates how digits are built into higher level objects and converted to parameters of interest. The reconstruction data flow is the same for digits from real data and simulation. In the case of real data, separate input modules are provided to read either directly from the DAQ, or from archived data stored on disk. A *reducer* module for each detector provides functionality to create summary histograms.

2.4 Testing

MAUS has a set of tests at the unit level and the integration level, together with code-style tests for both Python and C++. Unit tests are implemented to test a single function, while integration tests operate on a complete workflow. Unit tests check that each function operates as intended

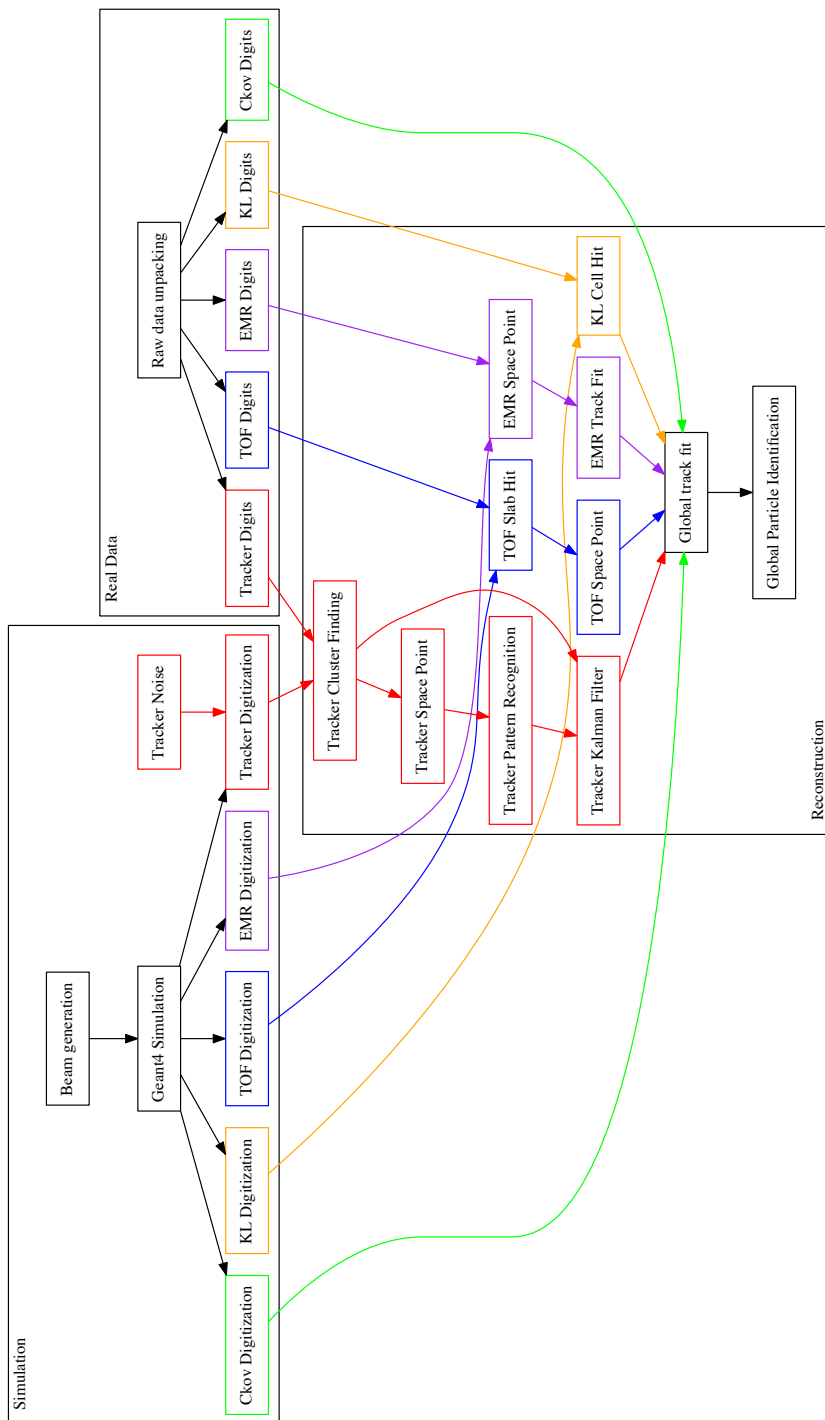


Figure 11. Data flow for the MAUS project. The data flow is color-coded by detector: Ckov — green, EMR — purple, KL — orange, TOF — blue, Tracker — red.

by the developer. Tests are run automatically for every version committed to the repository and results show that a high level of code coverage has been achieved. Integration tests allow the overall performance of the code to be checked against specifications. The MAUS team provides unit test coverage that executes 70–80 % of the total code base. This level of coverage typically results in a code that performs the major workflows without any problems.

The MAUS codebase is built and tested using a Jenkins [27] continuous integration environment deployed on a cluster of servers. Builds and tests of the development branch are automatically triggered when there is a change to the codebase. Developers are asked to perform a build and test on a personal branch of the codebase using the test server before requesting a merge with the development trunk. This enables the MAUS team to make frequent clean releases. Typically MAUS works on a 4–8 week major-release cycle.

3 Monte Carlo

The Monte Carlo simulation of MICE encompasses beam generation, geometrical description of detectors and fields, tracking of particles through detectors and digitization of the detectors' response to particle interactions.

3.1 Beam generation

Several options are provided to generate an incident beam. Routines are provided to sample particles from a multivariate Gaussian distribution or generate ensembles of identical particles (pencil beams). In addition, it is possible to produce time distributions that are either rectangular or triangular in time to give a simplistic representation of the MICE time distribution. Parameters, controlled by data-cards, are available to control random seed generation, relative weighting of particle species and the transverse-to-longitudinal coupling in the beam. MAUS also allows the generation of a polarized beam.

Beam particles can also be read in from an external file created by G4Beamline [28] — a particle-tracking simulation program based on Geant4, or ICOOL [29] — a simulation program that was developed to study the ionization cooling of muon beams, as well as files in user-defined formats. In order to generate beams which are more realistic taking into account the geometry and fields of the actual MICE beamline, we use G4Beamline to model the MICE beamline from the target to a point upstream of the second quad triplet (upstream of Q4). The beamline settings, e.g., magnetic field strengths and number of particles to generate, are controlled through data-cards. The magnetic field strengths have been tuned to produce beams that are reasonably accurate descriptions of the real beam. Scripts to install G4beamline are shipped with MAUS.

Once the beam is generated, the tracking and interactions of particles as they traverse the rest of the beamline and the MICE detectors are performed using Geant4.

3.2 Geant4

A drawing of the MICE Muon Beam line [4] is shown in figure 12. It consists of a quadrupole triplet (Q123) that captures pions produced when the MICE target intersects the ISIS proton beam, a pion-momentum-selection dipole (D1), a superconducting solenoid (DS) to focus and transport the particles to a second dipole (D2) that is used to select the muon-beam momentum, and a transport

channel composed of a further two quadrupole triplets (Q456 and Q789). As described in the next section, the positions and apertures of the beamline magnets were surveyed and are reproduced in the geometry along with windows and materials in the path of the muon beams. The Geant4 simulation within MAUS starts 1 m downstream of the second beamline dipole magnet D2. Geant4 bindings are encoded in the Simulation module. Geant4 groups particles by run, event and track. A Geant4 run maps to a MICE spill; a Geant4 event maps to a single inbound particle from the beamline; and a Geant4 track corresponds to a single particle in the experiment.

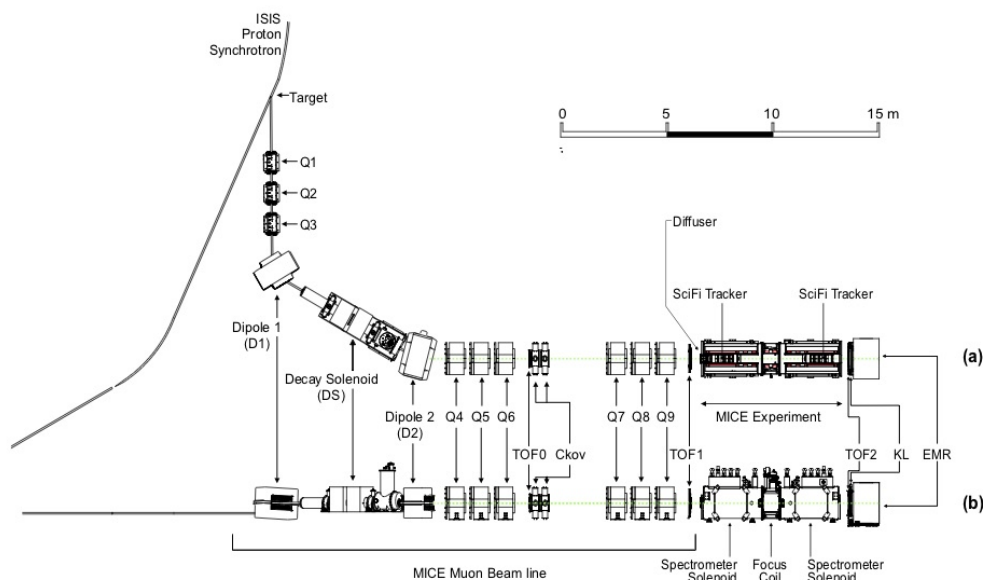


Figure 12. (a) Top and (b) side views of the MICE Muon Beamline, its instrumentation, and the experimental configuration. A titanium target dipped into the ISIS proton synchrotron and the resultant spill of particles was captured with a quadrupole triplet (Q1–3) and transported through momentum-selecting dipoles (D1, D2). The quadrupole triplets (Q4–6, Q7–9) transported particles to the upstream spectrometer module. The time-of-flight of particles, measured between TOF0 and TOF1, was used for particle identification.

Geant4 provides a variety of reference physics processes to model the interactions of particles with matter. The default process in MAUS is “*QGSP_BERT*” which causes Geant4 to model hadron interactions using a Bertini cascade model up to 10 GeV/c [30]. MAUS provides methods to set up the Geant4 physical processes through user-controlled data-cards. Finally, MAUS provides routines to extract particle data from the Geant4 tracks at user-defined locations.

3.3 Geometry

MAUS uses an online Configuration Database to store all of its geometries. These geometries have been extracted from CAD drawings which are updated based on the most recent surveys and technical drawings available. The CAD drawings are translated to a geometry-specific subset of XML, the Geometry Description Markup Language (GDML) [31] prior to being recorded in the configuration database through the use of the FastRAD [32] commercial software package.

The GDML formatted description contains the beamline elements and the positions of the detector survey points. Beam-line elements are described using tessellated solids to define the

shapes of the physical volumes. The detectors themselves are described using an independently generated set of GDML files using Geant4 standard volumes. An additional XML file is appended to the geometry description that assigns magnetic fields and associates the detectors to their locations in the GDML files. This file is initially written by the geometry maintainers and formatted to contain run-specific information during download.

The GDML files can be read via a number of libraries in Geant4 and ROOT for the purpose of independent validation. The files are in turn translated into the MAUS-readable geometry files either by accessing directly the data using a python extension or through the use of EXtensible Stylesheet Language Transformations (XSLT) [33].

3.4 Tracking, field maps and beam optics

MAUS tracking is performed using Geant4. By default, MAUS uses 4th order Runge-Kutta (RK4) for tracking, although other routines are available. RK4 has been shown to have very good precision relative to the MICE detector resolutions, even for step sizes of several cm.

In a solenoid focussing lattice a cylindrically symmetric beam can be described by the 4D RMS beam emittance ε_N and optical parameters β_\perp and β'_\perp , its derivative with respect to z . β_\perp is related to the variance of the position of particles x by [34]:

$$\beta_\perp = \frac{p_z \text{Var}(x)}{\varepsilon_N m c}; \quad (3.1)$$

where m is the particle mass, c is the speed of light, and p_z is the beam longitudinal momentum. In the approximation that particles travel near to the solenoid axis, transport of the beam envelope can be performed by integration of the differential equation:

$$2\beta_\perp \beta''_\perp - (\beta'_\perp)^2 + 4\beta_\perp^2 \kappa^2 - 4(1 + \mathcal{L})^2 = 0. \quad (3.2)$$

Transport of individual particles can be performed using numerical integration of the Lorentz force law. Alternately transport can be performed by calculating a transfer map \mathbf{M} defined by:

$$\vec{u}_{ds} = \mathbf{M} \vec{u}_{us}; \quad (3.3)$$

where \vec{u}_{us} and \vec{u}_{ds} are the upstream and downstream transverse phase space vectors $\vec{u} = (x, p_x, y, p_y)$. MAUS can calculate the transfer map at arbitrary order by transporting a handful of particles and fitting to a multidimensional polynomial in \vec{u} .

Electromagnetic field maps are implemented in a series of overlapping regions. The world volume is divided into a number of voxels, and the field maps that impinge on each voxel is stored in a list. At each tracking step, MAUS iterates over the list of fields that impinge on the voxels within which the particle is stepping. For each field map, MAUS transforms to the local coordinate system of the field map, and calculates the field. The field values are transformed back into the global coordinate system, summed, and passed to Geant4. The voxelization enables the simulation of long accelerators without a performance penalty.

Numerous field types have been implemented within the MAUS framework. Solenoid fields can be calculated numerically from cylindrically symmetric 2D field maps, by taking derivatives of an on-axis solenoidal field or by using the sum of fields from a set of cylindrical current sheets.

The use of field maps enables the realistic reproduction of the MICE apparatus, while a derivatives-based approach enables the exclusion of different terms in the higher order parts of the transfer map [35]. Multipole fields can be calculated from a 3D field map, or by taking derivatives from the usual multipole expansion formulae. Linear, quadratic and cubic interpolation routines have been implemented for field maps. Pillbox fields can be calculated by using the Bessel functions appropriate for a TM010 cavity or by reading a cylindrically symmetric field map.

The transport algorithms have been compared with each other and experimental data and show agreement at linear order [36] in \vec{u} . Work is ongoing to study the effect of aberrations in the optics, indicated by non-linear terms in the transfer map relationship. These aberrations can cause distortion of the beam leading to emittance growth, which has been observed in the tails of the MICE beam. The tracking in MAUS has been benchmarked against ICOOL, G4Beamline, and MaryLie [37], demonstrating good agreement. The routines have been used to model a number of beamlines and rings, including a neutrino factory front-end [38].

3.5 Detector response and digitization

The modeling of the detector response and electronics enables MAUS to provide data used to test reconstruction algorithms and estimate the uncertainties introduced by detectors and their readout.

The interaction of particles in materials is modeled using Geant4. For each detector, a “sensitive detector” class processes Geant4 hits in active detector volumes and stores hit information such as the volume that was hit, the energy deposited and the time of the hit. Each detector’s digitization routine then simulates the response of the electronics to these hits, modeling processes such as the photo-electron yield from a scintillator bar, attenuation in light guides and the pulse shape in the electronics. The data structure of the outputs from the digitizers are designed to match the output from the unpacking of real data from the DAQ.

4 Reconstruction

The reconstruction chain takes as its input either digitized hits from the MC or DAQ digits from real data. Regardless, the detector reconstruction algorithms, by requirement and design, operate the same way on both MC and real data.

4.1 Time of flight

There are three time-of-flight detectors in MICE which serve to distinguish particle type. The detectors are made of plastic scintillator and in each station there are orthogonal x and y planes with 7 or 10 slabs in each plane.

Each Geant4 hit in the TOF is associated with a physical scintillator slab. The energy deposited by a hit is first converted to units of photo-electrons. The photo-electron yield from a hit accounts for the light attenuation corresponding to the distance of the hit from the photomultiplier tube (PMT) and is then smeared by the photo-electron resolution. The yields from all hits in a given slab are then summed and the resultant yield is converted to ADC counts.

The time of the hit in the slab is propagated to the PMTs at either end of the slab. The propagated time is then smeared by the PMT’s time resolution and converted to TDC counts. Calibration

corrections based on real data are then added to the TDC values so that, at the reconstruction stage, they can be corrected just as is done with real data.

The reconstruction proceeds in two main steps. First, the slab-hit-reconstruction takes individual PMT digits and associates them to reconstruct the hit in the slab. If there are multiple hits associated with a PMT, the hit which is earliest in time is taken to be the real hit. Then, if both PMTs on a slab have fired, the slab is considered to have a valid hit. The TDC values are converted to time and the hit time and charge associated with the slab hit are taken to be the average of the two PMT times and charges respectively. In addition, the product of the PMT charges is also calculated and stored. Secondly, individual slab hits are used to form space-points. A space-point in the TOF is a combination of x and y slab hits. All combinations of x and y slab hits in a given station are treated as space-point candidates. Calibration corrections, stored in the Configurations Database, are applied to these hit times and if the reconstructed space-point is consistent with the resolution of the detector, the combination is said to be a valid space-point. The TOF has been shown to provide good time resolutions at the 60 ps level [6].

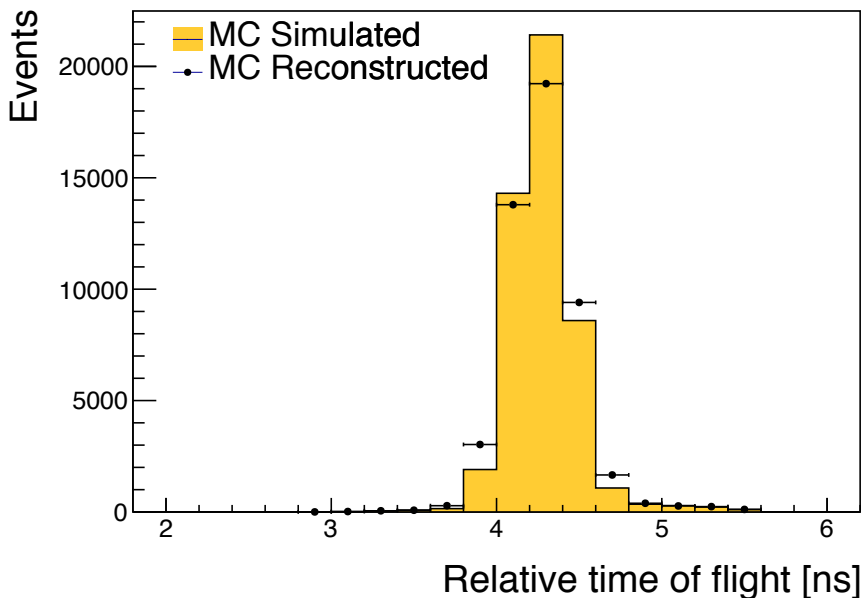


Figure 13. Relative time of flight between TOF0 and TOF1. The yellow histogram represents true MC events and the solid markers represent the same sample reconstructed with MAUS.

4.2 Scintillating-fiber trackers

The scintillating-fiber trackers are the central piece of the reconstruction. As mentioned in section 1.1, there are two trackers, one upstream and the other downstream of an absorber, situated within solenoidal magnetic fields. The trackers measure the emittance before and after particles pass through the absorber.

The tracker software algorithms and performance are described in detail in [39]. Digits are the most basic unit fed into the main reconstruction module, each digit representing a signal from one channel. Digits from adjacent channels are assumed to come from the same particle and are grouped to form clusters. Clusters from channels which intersect each other, in at least two planes from the

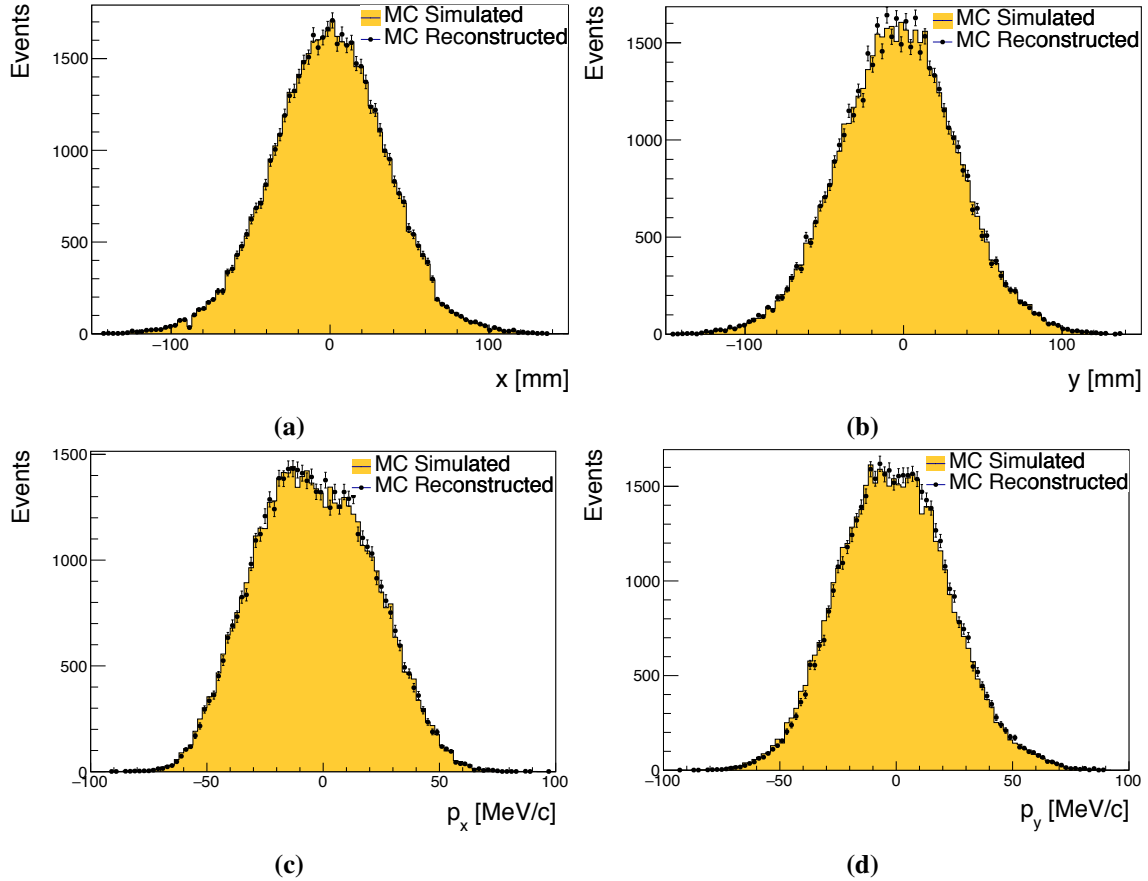


Figure 14. Position and momentum distributions of muons reconstructed at upstream tracker station nearest to the absorber: a) x , b) y , c) p_x , d) p_y . The yellow histograms represent true MC simulations, and the markers represent the MC sample reconstructed using MAUS.

same station, are used to form space-points, giving x and y positions where a particle intersected a station. Once space-points have been found, they are associated with individual tracks through pattern recognition (PR), giving straight or helical PR tracks. These tracks, and the space-points associated with them, are then sent to the final track fit. To avoid biases that may come from space-point reconstruction, the Kalman filter uses only reconstructed clusters as input.

4.3 KL calorimeter

Hit-level reconstruction of the KL is implemented in MAUS. Individual PMT hits are unpacked from the DAQ or simulated from MC and the reconstruction associates them to identify the slabs that were hit and calculates the charge and charge-product corresponding to each slab hit. The KL has been used successfully to estimate the pion contamination in the MICE muon beamline [9].

4.4 Electron-muon ranger

Hit-level reconstruction of the EMR is implemented in MAUS. The integrated ADC count and time over threshold are calculated for each bar that was hit. The EMR reconstructs a wide range of

variables that can be used for particle identification and momentum reconstruction. The software and performance of the EMR are described in detail in [10].

4.5 Cherenkov

The CKOV reconstruction takes the raw flash-ADC data, subtracts pedestals, calculates the charge and applies calibrations to determine the photo-electron yield.

4.6 Global reconstruction

The aim of the Global Reconstruction is to take the reconstructed outputs from individual detectors and tie them together to form a global track. A likelihood for each particle hypothesis is also calculated.

4.6.1 Global track matching

Global track matching is performed by collating particle hits (TOFs 0, 1 and 2, KL, Ckovs) and tracks (Trackers and EMR) from each detector using their individual reconstruction and combining them using a RK4 method to propagate particles between these detectors. The tracking is performed outwards from the cooling channel — i.e., from the upstream tracker to the TOF0 detector, and from the downstream tracker to the EMR detector. Track points are matched to form tracks using an RK4 method. Initially this is done independently for the upstream and downstream sections (i.e., either side of the absorber). As the trackers provide the most accurate position reconstruction, they are used as starting points for track matching, propagating hits outwards into the other detectors and then comparing the propagated position to the measured hit in the detector. The acceptance criterion for a hit belonging to a track is an agreement within the detector’s resolution with an additional allowance for multiple scattering. Track matching is currently performed for all TOFs, KL and EMR.

The RK4 propagation requires the mass and charge of the particle to be known. Hence, it is necessary to perform track matching using a hypothesis for each particle type (muons, pions, and electrons). Tracks for all possible PID hypotheses are then passed to the Global PID algorithms.

4.6.2 Global PID

Global particle identification in MICE typically requires the combination of several detectors. The time-of-flight between TOF detectors can be used to calculate velocity, which is compared with the momentum measured in the trackers to identify the particle type. For all events but those with very low transverse momentum (p_t), charge can be determined from the direction of helical motion in the trackers. Additional information can be obtained from the CKOV, KL and EMR detectors. The global particle identification framework is designed to tie this disparate information into a set of hypotheses of particle types, with an estimate of the likelihood of each hypothesis.

The Global PID in MAUS uses a log-likelihood method to identify the particle species of a global track. It is based upon a framework of PID variables. Simulated tracks are used to produce probability density functions (PDFs) of the PID variables. These are then compared with the PID variables for tracks in real data to obtain a set of likelihoods for the PIDs of the track.

The input to the Global PID is several potential tracks from global track matching. During the track matching stage, each of these tracks was matched for a specific particle hypothesis. The Global PID then takes each track and determines the most likely PID following a series of steps:

1. Each track is copied into an intermediate track;
2. For each potential PID hypothesis p , the log-likelihood is calculated using the PID variables;
3. The track is assigned an object containing the log-likelihood for each hypothesis; and
4. From the log-likelihoods, the confidence level, C.L., for a track having a PID p is calculated and the PID is set to the hypothesis with the best C.L.

4.7 Online reconstruction

During data taking, it is essential to visualize a detector's performance and have diagnostic tools to identify and debug unexpected behavior. This is accomplished through summary histograms of high and low-level quantities from detectors. The implementation is through a custom multi-threaded application based on a producer-consumer pattern with thread-safe FIFO buffers. Raw data produced by the DAQ are streamed through a network and consumed by individual detector *mappers* described in section 3. The reconstructed outputs produced by the *mappers*, are in turn consumed by the *reducers*. The *mappers* and *reducers* are distributed among the threads to balance the load. Finally, outputs from the *reducers* are written as histogram images. Though the framework for the online reconstruction is based on parallelized processing of spills, the reconstruction modules are the same as those used for offline processing. A lightweight tool based on Django [40] provides live web-based visualization of the histogram images as and when they are created. Typical data rates during experimental operations were ~ 300 MB/s. The average event rate varied, depending on the configuration of the beamline, with the maximum instantaneous rate being ~ 150 kHz. MAUS performance matched the data rates and online reconstruction happened virtually "live" with the reconstructed outputs available instantly allowing collaborators to monitor the quality of the data being acquired.

5 Summary

The MICE collaboration has developed the MAUS software suite to simulate the muon beamline, simulate the MICE detectors, and reconstruct both simulated and real data. The software also provides global track-matching and particle-identification capabilities. Simplified programming interfaces and testing environments enable productive development. MAUS has been successfully used to reconstruct data online during data collection. In addition, MAUS is routinely used to perform reconstruction of the entire MICE data volume on batch production systems. MICE has collected ~ 15 TB of raw data and a full reconstruction of the data is performed with each released version of MAUS. The batch systems are also used to perform compute-intensive simulations with various configurations of the beamline and the cooling channel.

Acknowledgments

The work described here was made possible by grants from Department of Energy and National Science Foundation (U.S.A.), the Istituto Nazionale di Fisica Nucleare (Italy), the Science and Technology Facilities Council (U.K.), the European Community under the European Commission Framework Programme 7 (AIDA project, grant agreement no. 262025, TIARA project, grant

agreement no. 261905, and EuCARD), the Japan Society for the Promotion of Science and the Swiss National Science Foundation, in the framework of the SCOPES programme. We gratefully acknowledge all sources of support. We are grateful to the support given to us by the staff of the STFC Rutherford Appleton and Daresbury Laboratories. We acknowledge the use of Grid computing resources deployed and operated by GridPP [41] in the U.K.

References

- [1] MICE collaboration, *First Demonstration of Ionization Cooling in MICE*, in *Proceedings of the International Particle Accelerator Conference*, Vancouver, Canada, 29 April–May 4 2018, pp. 5035–5040.
- [2] IDS-NF collaboration, *International design study for the neutrino factory: Interim design report*, 2011.
- [3] S. Geer, *Muon Colliders and Neutrino Factories*, *Annu. Rev. Nucl. Part. Sci.* **59** (2009) 345.
- [4] MICE collaboration, *The MICE Muon Beam on ISIS and the beam-line instrumentation of the Muon Ionization Cooling Experiment*, 2012 *JINST* **7** P05009 [[arXiv:1203.4089](#)].
- [5] MICE collaboration, *Characterisation of the muon beams for the Muon Ionisation Cooling Experiment*, *Eur. Phys. J. C* **73** (2013) 2582 [[arXiv:1306.1509](#)].
- [6] MICE collaboration, *The design and commissioning of the MICE upstream time-of-flight system*, *Nucl. Instrum. Meth. A* **615** (2010) 14 [[arXiv:1001.4426](#)].
- [7] KLOE collaboration, *The KLOE electromagnetic calorimeter*, *Nucl. Instrum. Meth. A* **494** (2002) 326.
- [8] F. Ambrosino et al., *Calibration and performances of the KLOE calorimeter*, *Nucl. Instrum. Meth. A* **598** (2009) 239.
- [9] MICE collaboration, *Pion Contamination in the MICE Muon Beam*, 2016 *JINST* **11** P03001 [[arXiv:1511.00556](#)].
- [10] MICE collaboration, *Electron-Muon Ranger: performance in the MICE Muon Beam*, 2015 *JINST* **10** P12012 [[arXiv:1510.08306](#)].
- [11] R. Asfandiyarov et al., *The design and construction of the MICE Electron-Muon Ranger*, 2016 *JINST* **11** T10007 [[arXiv:1607.04955](#)].
- [12] MICE collaboration, *First particle-by-particle measurement of emittance in the Muon Ionization Cooling Experiment*, *Eur. Phys. J. C* **79** (2019) 257 [[arXiv:1810.13224](#)].
- [13] L. Cremaldi, D.A. Sanders, P. Sonnek, D.J. Summers and J. Reidy, Jr, *A Cherenkov Radiation Detector with High Density Aerogels*, *IEEE Trans. Nucl. Sci.* **56** (2009) 1475 [[arXiv:0905.3411](#)].
- [14] M. Ellis et al., *The Design, construction and performance of the MICE scintillating fibre trackers*, *Nucl. Instrum. Meth. A* **659** (2011) 136 [[arXiv:1005.3491](#)].
- [15] <https://scons.org>.
- [16] <https://bazaar.canonical.com>.
- [17] <https://launchpad.net>.
- [18] R. Brun and F. Rademakers, *ROOT: An object oriented data analysis framework*, *Nucl. Instrum. Meth. A* **389** (1997) 81.
- [19] GEANT4 collaboration, *GEANT4: A Simulation toolkit*, *Nucl. Instrum. Meth. A* **506** (2003) 250.

- [20] <https://scientificlinux.org>.
- [21] <https://centos.org>.
- [22] <https://getfedora.org>.
- [23] <https://ubuntu.com>.
- [24] J. Dean and S. Ghemawat, *MapReduce: Simplified data processing on large clusters*, in *Proceedings of OSDI04*, San Francisco, CA, U.S.A., 2004, pp. 137–150.
- [25] <https://json.org>.
- [26] <https://github.com/open-source-parsers/jsoncpp>.
- [27] <https://jenkins-ci.org>.
- [28] T.J. Roberts and D.M. Kaplan, *G4BeamLine programme for matter dominated beamlines*, in *Proceedings of the Particle Accelerator Conference*, Albuquerque, NM, U.S.A., 25–29 June 2007, pp. 3468–3470.
- [29] R.C. Fernow, *Icool: A simulation code for ionization cooling of muon beams*, in *Proceedings of the Particle Accelerator Conference*, New York, NY, U.S.A., 27 March–2 April 1999, pp. 3020–3022.
- [30] J. Apostolakis et al., *Geometry and physics of the geant4 toolkit for high and medium energy applications*, *Radiat. Phys. Chem.* **78** (2009) 859.
- [31] R. Chytracek, J. McCormick, W. Pokorski and G. Santin, *Geometry description markup language for physics simulation and analysis applications.*, *IEEE Trans. Nucl. Sci.* **53** (2006) 2892.
- [32] <https://fastrad.net>.
- [33] <https://www.w3.org/standards/xml/transformation>.
- [34] G. Penn and J.S. Wurtele, *Beam envelope equations for cooling of muons in solenoid fields*, *Phys. Rev. Lett.* **85** (2000) 764.
- [35] R. Ryne and C. Rogers, *Nonlinear effects in the MICE step iv lattice*, MICE-NOTE-461, 2015.
- [36] S.C. Middleton, *Characterisation of the MICE experiment*, Ph.D. Thesis, Imperial College London (2018).
- [37] R.D. Ryne et al., *Recent progress on the MARYLIE/IMPACT beam dynamics code*, in *Proceedings of the 9th International Computational Accelerator Physics Conference*, Chamonix, France, 2–6 October 2006, pp. 157–159.
- [38] C.T. Rogers, D. Stratakis, G. Prior, S. Gilardoni, D. Neuffer, P. Snopok et al., *Muon front end for the neutrino factory*, *Phys. Rev. ST Accel. Beams* **16** (2013) 040104.
- [39] A. Dobbs, C. Hunt, K. Long, E. Santos, M.A. Uchida, P. Kyberd et al., *The reconstruction software for the MICE scintillating fibre trackers*, 2016 *JINST* **11** T12001 [[arXiv:1610.05161](https://arxiv.org/abs/1610.05161)].
- [40] <https://www.djangoproject.com>.
- [41] <https://www.gridpp.ac.uk>.

MULTIYEAR INDOOR RADON VARIABILITY IN A FAMILY HOUSE – A CASE STUDY IN SERBIA

by

**Vladimir I. UDOVIČIĆ^{1*}, Dimitrije M. MALETIĆ¹, Radomir M. BANJANAC¹,
Dejan R. JOKOVIĆ¹, Aleksandar L. DRAGIĆ¹, Nikola B. VESELINOVIĆ¹,
Jelena Z. ŽIVANOVIĆ¹, Mihailo R. SAVIĆ¹, and Sofija M. FORKAPIĆ²**

¹Institute of Physics, University of Belgrade, Belgrade, Serbia

²Department of Physics, Faculty of Science, University of Novi Sad, Novi Sad, Serbia

Scientific paper

<http://doi.org/10.2298/NTRP1802174U>

The indoor radon behavior has complex dynamics due to the influence of the large number of different parameters: the state of indoor atmosphere (temperature, pressure, and relative humidity), aerosol concentration, the exchange rate between indoor and outdoor air, construction materials, and living habits. As a result, indoor radon concentration shows variation, with the usual periodicity of one day and one year. It is well-known that seasonal variation of the radon concentration exists. It is particularly interesting to investigate indoor radon variation at the same measuring location and time period, each year, due to estimation of individual annual dose from radon exposure. The long-term indoor radon measurements, in a typical family house in Serbia, were performed. Measurements were taken during 2014, 2015, and 2016, in February and July, each year. The following measuring techniques were used: active and charcoal canisters methods. Analysis of the obtained results, using multivariate analysis methods, is presented.

Key words: radon variability, multivariate regression analysis, multi-seasonal radon measurements, indoor radon

INTRODUCTION

The research of the dynamics of radon in various environments, especially indoors, is of great importance in terms of protection against ionizing radiation and in designing of measures for its reduction. Published results and development of many models to describe the behavior of indoor radon, indicates the complexity of this research, especially with models for prediction of the variability of radon [1-3]. This is because the variability of radon depends on a large number of variables such as local geology, permeability of soil, building materials used for the buildings, the state of the indoor atmosphere (temperature, pressure and relative humidity), aerosol concentration, the exchange rate between indoor and outdoor air, construction materials, as well as the living habits of people. It is known that the indoor radon concentration variation has periodicity of one day and one year. It is also well-known that the seasonal variation of the radon concentration exists. This is why it is particularly interesting to investigate indoor radon variation at the same measuring location and time period, year after

year, in order to estimate the individual annual dose from radon exposure. In that sense, we performed long-term indoor radon measurements in a typical family house in Serbia. Measurements were taken during the 2014, 2015, and 2016, in February and July, each year. We used the following measuring techniques: active and charcoal canisters methods. The detailed analysis of the obtained results using multivariate analysis (MVA) methods is presented in this paper.

First, MVA methods were tested on the radon variability studies in the Underground Low Background Laboratory in the Institute of Physics, Belgrade [4, 5]. Several climate variables: air temperature, pressure, and humidity were considered. Further advance was made by using all the publicly available climate variables monitored by nearby automatic meteorological station. In order to analyze the dependence of radon variation on multiple variables, multivariate analysis needs to be used. The goal was to find an appropriate method, out of the wide spectrum of multivariate analysis methods that are developed for the analysis of data from high-energy physics experiments, to analyze the measurements of variations of radon concentrations in indoor spaces. Previous

* Corresponding author; e-mail: udovicic@ipb.ac.rs

analysis were done using the maximum of 18 climate parameters and use and comparison of 8 different multivariate methods. In this paper the number of variables is reduced to the most important ones and new derived variables, like vapor pressure, simple modeled solar irradiance and simple modeled precipitation, which were introduced in the multivariate analysis.

INDOOR RADON MEASUREMENTS METHODS

Depending on the integrated measurement time, methods of measurement of the indoor radon concentrations may be divided into long-term and short-term ones. The device for the performed short-term radon measurements is SN1029 radon monitor (manufactured by the Sun Nuclear Corporation, NRSB approval-code 31822) with the following characteristics: the measurement range from 1 Bqm^{-3} to 99.99 kBqm^{-3} , accuracy equal to $+25 \%$, sensitivity of $0.16 \text{ counts hour per Bqm}^{-3}$. The device consists of two diffused junction photodiodes as the radon detector which is furnished with sensors for temperature, barometric pressure, and relative humidity. The sampling time was set to 2 h. The method for Charcoal Canister used is: EERF Standard Operating Procedures for Radon-222 Measurement Using Charcoal Canisters [6], also used by major laboratories which conduct radon measurements in Serbia [7]. Exposure time of the charcoal canisters was 48 h. The connection between short term and long term measurements has attracted some interest previously [8].

The family house, selected for the measurements and analysis of variations of radon concentrations, is a typical house in Belgrade residential areas, with requirement of existence of cellar. House is built on limestone soil. Radon measurements were carried out in the living room of the family house, which is built of standard materials (brick, concrete, mortar) and isolated with styrofoam. During the period of measurements (winter-summer 2014, 2015, and 2016), the house was naturally ventilated and air conditioning was used in heating mode at the beginning of the measurement period. During the winter period measurements, the electrical heating was used in addition to air conditioning. Measured radon concentrations, room temperature (T_{id}), atmospheric pressure (P_{id}) and relative humidity (H_{id}) inside the house, were obtained using radon monitor. Values of meteorological variables, in the measurement period, were obtained from an automatic meteorological station, located near the house in which the measurement was performed. We used the following meteorological variables: external air temperature (T), also at height of 5cm, pressure (P) and humidity (H), solar irradiation, wind speed, precipitation, temperature of the soil at depths of 10 cm, 20 cm and 50 cm. The natural ventilation routine was not monitored. Since the ventilation is of

crucial importance for the level of radon indoors [9], Multivariate regression analysis was used mainly for winter periods.

MULTIVARIATE REGRESSION ANALYSIS

In many fields of physics, especially in high-energy physics, there is the demand for detailed analyses of a large amount of data. For this purpose, the data analysis environment ROOT [10], is developed. ROOT is modular scientific software framework, which provides all the functionalities needed to deal with big data processing, statistical analysis, visualization and storage. A specific functionality gives the developed Toolkit for Multivariate Analysis (TMVA) [11]. The TMVA provides an environment for the processing, parallel evaluation and application of multivariate regression techniques.

TMVA is used to create, test and apply all available regression multivariate methods, implemented in ROOT, in order to find methods which are the most appropriate and yield maximum information on the dependence of indoor radon concentrations on the multitude of meteorological variables. Regression methods are used to find out which regression method can, if any, on the basis of input meteorological variables only, give an output that would satisfactorily close match the observed variations of radon concentrations. The output of usage of multivariate regression analysis methods has mapped functional behavior, which can be used to evaluate the measurements of radon concentrations using input meteorological variables only. All the methods make use of training events, for which the desired output is known and is used for training of Multivariate regression methods, and test events, which are used to test the MVA methods outputs.

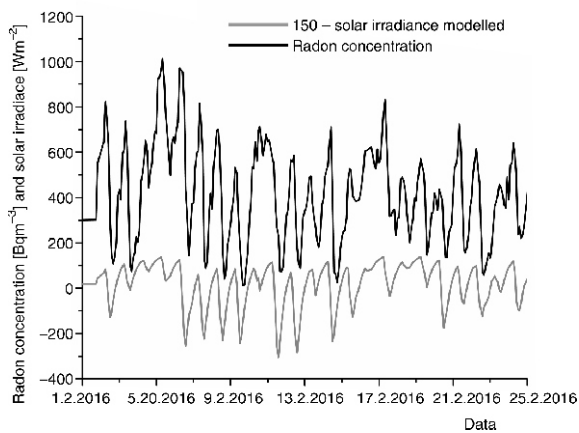
RESULTS

Measurements were performed during February and July in 2014, 2015, and 2016 using radon monitor and charcoal canister measurements. The descriptive results are summarized in tab. 1. The measurements using radon monitor and charcoal canisters are in good agreement.

Previous work done by researchers from the Low Background Laboratory, Institute of Physics, Belgrade, using the MVA analysis in search of connections between radon concentration and meteorological variables, included only one period of measurement, February or July 2014 [4]. Now the MVA analysis is using all the measured data February/July 2014-2016. New variables introduced in MVA analysis are modeled solar irradiance, modeled precipitation and vapor

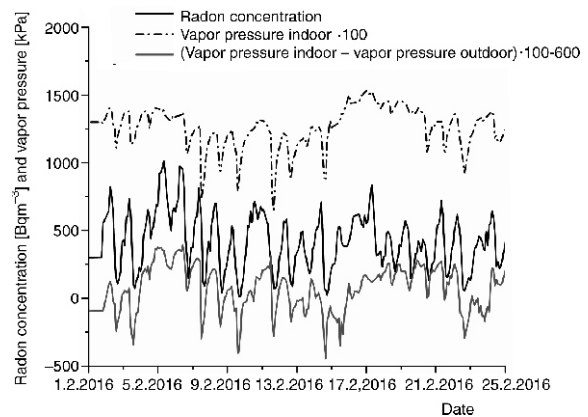
Table 1. Descriptive results of February and July 2014, 2015, and 2016 measurements, using radon monitor and charcoal canisters (only in February)

Results of measurements	2014		2015		2016	
	Feb.	July	Feb.	July	Feb.	July
Minimal radon activity using radon monitor [Bqm^{-3}]	15	0	28	0	12	3
Maximal radon activity using radon monitor [Bqm^{-3}]	1000	286	915	88	1013	262
Median radon activity using radon monitor [Bqm^{-3}]	418	25	524	22	412	28
Arithmetic mean of radon activity using radon monitor (standard deviation) [Bqm^{-3}]	402 (216)	40 (41)	508 (207)	27 (18)	423 (214)	39 (32)
Room temperature using radon monitor (standard deviation) [$^{\circ}\text{C}$]	20.4 (0.8)	24.7 (0.9)	21.2 (0.6)	24.9 (0.8)	22.3 (0.6)	24.6 (0.8)
Relative humidity using radon monitor (standard deviation) [%]	67.4 (5.7)	67.8 (4.8)	68.2 (4.8)	51.5 (4.7)	64.0 (6.4)	58.9 (7.5)
Radon activity using charcoal canister (standard deviation) [Bqm^{-3}]	432 (10)	/	518 (6)	/	407 (5)	/

**Figure 1. Modeled solar irradiance in comparison with measured radon concentration during February 2016**

pressure. In order to make use of intensity of solar irradiance during the whole day and night, the solar irradiance is modeled so that it includes 80 % of solar irradiance value from the previous measurement (previous hour) with addition of solar irradiance value for the actual hour of measurement (fig. 1). The value of 80 % is chosen so that the modeled solar irradiation has the best correlation with the radon measurements. Similar model of precipitation was used in this analysis. The next new variable is vapor pressure. The vapor pressure variable is calculated using the slope $s(T)$, of the relationship between saturation vapor pressure and air temperature and is given by [12, 13], so that the vapor pressure equals relative humidity times saturation vapor pressure, fig. 2.

Before the start of training of Multivariate regression methods using TMVA toolkit in ROOT, the description of input meteorological variables is performed, mainly by looking into inter-correlations of input variables and their connections with the measured radon concentrations. The MVA is using all the measured data. Table 2 presents the meteorological variables and their module value of correlation with the measured radon concentrations (target), which is indicative in finding linear dependence of radon mea-

**Figure 2. Vapor pressure in comparison with measured radon concentration during February 2016**

surements and input variables. The second column in tab. 2 presents us with correlation ratio values which indicate if there are some functional dependence (not only linear) between input variables and radon concentration, and the last column presents the mutual information which indicates if there is a non-functional dependence of input variables and radon measurements [11].

From tab. 2 it can be noticed that linear correlated values are not the only ones which can be used in MVA analysis, for example variable solar irradiance has high mutual information with the radon measurements.

In the data preparation for MVA training the whole dataset is consisting of many events. An event includes time of measurement, radon measurement and meteorological variables. The dataset is randomly split in two halves, one half of the events will be used for training of multivariate regression methods, and the other half of events for testing of methods, mainly to compare the measured and MVA evaluated values for radon concentration.

It turns out that the methods best suited for our purpose is the Boosted Decision Trees (BDT) method. This means that BDT gives the smallest difference be-

Table 2. Input variable rank and values for correlation, correlation ratio and mutual information, all with the measured radon concentrations (target) for February and July 2014-2016 measurements

Variable	Correlation with target		Correlation ratio		Mutual information	
	Rank	Value	Rank	Value	Rank	Value
Soil temperature depth 20 cm [°C]	1	0.87	1	0.60	13	1.48
Soil temperature depth 50 cm [°C]	2	0.86	2	0.57	14	1.31
Soil temperature depth 10 cm [°C]	3	0.82	3	0.54	9	1.84
Temperature outdoor [°C]	4	0.82	5	0.53	8	1.85
Vapor indoor – vapor od [mbar]	5	0.81	9	0.41	11	1.73
Temperature od – temperature id [°C]	6	0.80	4	0.53	6	1.92
Temperature height 5 cm [°C]	7	0.77	8	0.48	7	1.91
Vapor od [mbar]	8	0.76	10	0.41	5	1.92
Temperature id [°C]	9	0.75	7	0.49	17	1.16
Solar irradiance [Wm ⁻²]	10	0.61	6	0.50	2	2.23
Humidity indoor [%]	11	0.45	11	0.26	1	2.26
Humidity outdoor [%]	12	0.31	13	0.20	10	1.76
Air pressure outdoor [mbar]	13	0.27	17	0.07	12	1.55
Wind speed [ms ⁻¹]	14	0.22	16	0.01	16	1.28
Air pressure indoor [mbar]	15	0.17	18	0.04	15	1.31
Humidity od – Humidity id [%]	16	0.10	14	0.19	4	2.11
Precipitation [Lm ⁻²]	17	0.01	15	0.19	18	1.13
Vapor indoor [mbar]	18	0.002	12	0.02	3	2.17

tween the measured radon concentration from test sample and the evaluation of value of radon concentration using input variables only. This can be seen in fig. 3, which shows the distribution of BDT and BDTG regression method outputs (evaluated values) in comparison with the measured radon concentration during February 2016.

Since TMVA has 12 different regression methods implemented, only some of those will give useful results when evaluating the radon concentration measurements. Table 4 summaries the results of MVA analysis. It shows the MVA methods RMS of difference of evaluated and measured radon concentration. Also, tab. 4 shows the mutual information of measured and MVA evaluated radon concentration. Besides

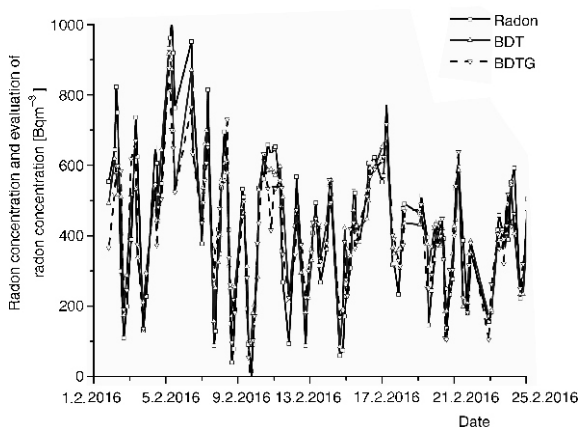


Figure 3. Comparison of MVA evaluated radon concentration and measured one from the test sample of events during February 2016

BDT, the Multi-Layer Perceptron (MLP) [10], an implementation of Artificial Neural Network multivariate method, also gives good results.

The MVA regression analysis results in mapped functional behavior and, as opposed to possible existence of theoretical modeling, which is independent of the number of measurements, MVA depends on the number of events. More events, the better mapped function we get as a result. In this sense, if the number of measurements is not great, multivariate analysis can be used only as help, to indicate which variables are more important to be used in theoretical modeling, for comparison of mapped and modeled functions, and modeled function test.

CONCLUSION

Indoor radon variation at one location in the same periods (February and July), was investigated for three years. Long-term indoor radon measurements show intense seasonal variation. The results obtained with different measuring methods are in good agreement. The radon behavior in the house is almost the same and shows good reproducibility year by year. The small variations in the year by year dynamics are originated mostly from the variations in meteorological variables during winter seasons and mostly due to ventilation habits during summer season. Ventilation habits were not monitored nor taken into account in MVA regression analysis. The preliminary results using multivariate analysis methods in TMVA are shown. Main output of Multivariate regression analy-

Table 3. Input variable correlation with the measured radon concentrations for February and July 2016

Correlation with target			
February 2016		July 2016	
Variable	Value	Variable	Value
Vapor id-vapor od [mbar]	0.58	Soil temperature depth 20 cm [°C]	0.46
Humidity id [%]	0.54	Soil temperature depth 50 cm [°C]	0.42
Vapor id [mbar]	0.52	Solar irradiance	0.32
Solar irradiance [Wm ⁻²]	0.48	Temperature id [°C]	0.30
Temperature od – temperature id [°C]	0.46	Soil temperature depth 10 cm [°C]	0.24
Temperature [°C]	0.44	Temperature od [°C]	0.21
Soil temperature depth 10 cm [°C]	0.43	Humidity od [%]	0.20
Soil temperature depth 20 cm [°C]	0.42	Humidity id [%]	0.19
Humidity [%]	0.38	Air pressure [mbar]	0.17
Temperature height 5 cm [°C]	0.32	Precipitation [Lm ⁻²]	0.17
Temperature id [°C]	0.29	Temperature od – temperature id [°C]	0.16
Air pressure od [mbar]	0.23	Air pressure id [mbar]	0.16
Air pressure id [mbar]	0.21	Humidity od – humidity id [%]	0.14
Soil temperature depth 50 cm [°C]	0.20	Wind speed [ms ⁻²]	0.13
Precipitation [Lm ⁻²]	0.19	Temperature height 5 cm [°C]	0.12
Humidity od – humidity id [%]	0.15	Vapor id [mbar]	0.06
Vapor od [mbar]	0.08	Vapor od [mbar]	0.03
Wind speed [ms ⁻¹]	0.05	Vapor id – vapor od [mbar]	0.02

Table 4. RMS of MVA method's evaluation error and mutual information; February/July 2014-2016

MVA method	RMS [Bqm ⁻³]	Mutual information
BDT	85.5	1.477
BDTG	92.1	1.614
MLP	101	1.401

sis is the initial version of *mapped* function of radon concentration dependence on multitude of meteorological variables. Simplification of MVA methods can be made by choosing only the most important input variables and exclude the other variables.

ACKNOWLEDGEMENTS

The authors acknowledge the financial support of the Ministry of Science, Technology and Development of Serbia within the projects: Nuclear Methods Investigations of Rare Processes and Cosmic Rays (grant number 171002) and Biosensing Technologies and Global System for Continuous Research and Integrated Management (grant number 43002).

AUTHORS' CONTRIBUTIONS

The idea for this paper came as a result of discussions of V. I. Udovičić, R. M. Banjanac, D. R. Joković, A. L. Dragić, and D. M. Maletić. Gathering climate data and MVA analysis was done by D. M. Maletić and V. I. Udovičić. Performed indoor radon measurements were done by V. I. Udovičić and S. M. Forkapić. Writing of the paper was done by D. M. Maletić and V. I. Udovičić. A. L. Dragić gave idea about using MVA

methods in cosmic and radon measurements. N. B. Veselinović and M. R. Savić analyzed and validated climate data. J. Z. Živanović helped with MVA analysis. D. R. Joković helped with data analysis and paper technical preparation.

REFERENCES

- [1] Collignan, B., *et al.*, Development of a Methodology to Characterize Radon Entry in Dwellings, *Building and Environment*, 57 (2012), Nov., pp. 176-183
- [2] Li, F., Baixeras, C., The RAGENA Dynamic Model of Radon Generation, Entry and Accumulation Indoors, *Science of the Total Environment*, 307 (2003), 1-3, pp. 55-69
- [3] Jelle, B. P., *et al.*, Development of a Model for Radon Concentration in Indoor Air, *Science of the Total Environment*, 416 (2012), Jan., pp. 343-350
- [4] Maletić, D., *et al.*, Comparison of Multivariate Classification and Regression Methods for Indoor Radon Measurements, *Nucl Technol Radiat*, 29 (2014), 1, pp. 17-23
- [5] Udovičić, V., *et al.*, Radon Problem in an Underground Low-Level Laboratory, *Radiation Measurements*, 44 (2009), 9-10, pp. 1009-1012
- [6] ***, EPA 520/5-87-005, Gray D.J, Windham S.T, United States Environmental Protection Agency, Montgomery, 1987
- [7] Živanović, M. Z., *et al.*, Radon Measurements with Charcoal Canisters, *Nucl Technol Radiat*, 31 (2016), 1, pp. 65-72
- [8] Stojanovska, Z., *et al.*, Prediction of Long-Term Indoor Radon Concentrations Based on Short-Term Measurements, *Nucl Technol Radiat*, 32 (2017), 1, pp. 77-84
- [9] Nikolić, M. D., *et al.*, Modelling Radiation Exposure in Homes from Siporex Blocks by Using Exhalation Rates of Radon, *Nucl Technol Radiat*, 30 (2015), 4, pp. 301-305
- [10] Brun, R., Rademakers, F., ROOT – An Object Oriented Data Analysis Framework, *Nucl. Inst. Meth. in Phys. Res., A* 389 (1997), 1-2, pp. 81-86

- [11] Hoescker, A., et al., TMVA – Toolkit for Multivariate Data Analysis, PoS ACAT 040, arXiv:physics/070303, 2007
- [12] Murray, F. W., On the Computation of Saturation Vapor Pressure, *J. Applied Meteorology*, 6 (1967), 1, pp. 203-204

- [13] Tetens, O., About Some Meteorological Aspects (in German), *Z. Geophys*, 6 (1930), pp. 207-309

Received on October 6, 2018

Accepted on June 8, 2018

**Владимир И. УДОВИЧИЋ, Димитрије М. МАЛЕТИЋ, Радомир М. БАЊАНАЦ,
Дејан Р. ЈОКОВИЋ, Александар Л. ДРАГИЋ, Никола Б. ВЕСЕЛИНОВИЋ,
Јелена З. ЖИВАНОВИЋ, Михаило Р. САВИЋ, Софија М. ФОРКАПИЋ**

**СТУДИЈА СЛУЧАЈА ВИШЕГОДИШЊЕ ВАРИЈАБИЛНОСТИ РАДОНА
У ПОРОДИЧНОЈ КУЋИ У СРБИЈИ**

Понашање радона у затвореном простору има сложену динамику због утицаја великог броја различитих параметара који утичу на његову варијабилност: метеоролошких (температура, притисак и релативна влажност), концентрације аеросола, брзине размене између унутрашњег и спољашњег ваздуха, грађевинских материјала и животних навика. Као резултат, концентрација радона у затвореним просторијама показује варијацију, уз стандардну периодичност од једног дана и једне године. Годишња варијабилност је добро позната сезонска варијација концентрације радона. Посебно је интересантно пратити вишегодишње варијације концентрације радона на истој мерној локацији и временском периоду, пре свега због процене индивидуалних годишњих доза од изложености радону. У типичној породичној кући у Србији извршена су дуготрајна мерења радона у дневном боравку. Мерења су рађена током 2014, 2015, и 2016. године, у фебруару и јулу, сваке године. Коришћене су следеће мерне технике: активна и метода коришћења угљених канистера. Добијени резултати анализирани су коришћењем мултиваријантне регресионе анализе.

Кључне речи: варијабилност радона, мултиваријантна регресиона анализа, радон у затвореним просторијама, вишегодишње мерење радона



First steps towards national radon action plan in Serbia

Vladimir Udovičić,
Dimitrije Maletić,
Maja Eremić Savković,
Gordana Pantelić,
Predrag Ujić,
Igor Čeliković,
Sofija Forkapić,
Dragoslav Nikezić,
Vladimir M. Marković,
Vesna Arsić,
Jovana Ilić

Abstract. Radon problem has a special attention in many countries in the world and the most of them have established national radon programmes. The radon issues in Serbia have not been approached in a systematic and organized way. Currently, there are many research groups and institutions working in radon field, and it is a good basis to integrate all these activities into a comprehensive national programme to define the strategic objectives and action plan for the next few years. Also, Serbia as a candidate for membership in the EU is obliged to harmonize its legislation, including the field of radiation protection in which the radon issues has an important role. In this report, a brief history of radon research, present status and plans for the future activity on radon issues in Serbia are presented. Regarding the long-term plans, the establishment and implementation of the Radon Action Plan with the primary goal of raising awareness about the harmful effects of public exposure to radon and implementing a set of measures for its reduction. In that sense, the synergy between the national, regional and local organizations responsible for public health and radiation protection must be achieved.

Key words: radon • action plan • survey

V. Udovičić[✉], D. Maletić
Institute of Physics Belgrade,
University of Belgrade,
118 Pregrevica Str., 11080 Belgrade, Serbia,
E-mail: udovicic@ipb.ac.rs

M. Eremić Savković
Serbian Radiation Protection and Nuclear Safety Agency,
Belgrade, Serbia

G. Pantelić, P. Ujić, I. Čeliković
Vinča Institute of Nuclear Sciences,
University of Belgrade,
Belgrade, Serbia

S. Forkapić
Department of Physics,
Faculty of Science,
University of Novi Sad,
Novi Sad, Serbia

D. Nikezić, V. M. Marković
Faculty of Science,
University of Kragujevac,
Kragujevac, Serbia

V. Arsić, J. Ilić
Serbian Institute of Occupational Health
“Dr Dragomir Karajović”,
Belgrade, Serbia

Received: 4 January 2016
Accepted: 31 March 2016

Introduction

Radon is a noble, naturally occurring radioactive gas. Radon contribute to almost 50% of the overall high-effective annual dose to the population received from all sources of natural radioactivity. Harmful effects of radon has been proven in a large number of epidemiological studies [1]. The latest recommendation of the International Atomic Energy Agency (IAEA) [2] and Directive EC [3] relating to the field of radiation protection, radon problem got more space and importance because the World Health Organization (WHO) has identified radon as the second biggest cause of cancer lung [4]. In addition, radon is included in the ranks of major pollutants of indoor air [5]. Current knowledge about the mechanisms by which radon is harmful to human health are reflected primarily in harmful, radioactive radon progeny fact. In fact, radon progenies are attached to the aerosol particles from the air and such radioactive particles enter the body through inhalation. These radioactive aerosols deposited in the lungs emit alpha radiation. The harmful activity can be seen in disorders of the cellular structure of DNA, causing the development of cancer cells. Consequently, radon problem has been addressed seriously, and in a number of countries, national radon programme is established, which is basically a multidisciplinary nature and requires the involve-

ment of a large number of experts, researchers involved in radiation physics, geo sciences, chemistry, biology to specialist in various fields of medicine. In that sense, the group of radon professionals decide to start working on establishing and developing national radon programme in Serbia. In this paper, a brief history of radon research, present status and plans for the future activity on radon issues in Serbia are presented.

International framework

The regulations related to the exposure of the population to radon and its progenies are different worldwide. Based on the researches and a large number of epidemiological studies done in the recent past, the new standards and recommendations have to be incorporated into the national legislation regarding radon issues. Basically, a new approach to the radon issue is to introduce the concept of the reference level (not as strict boundaries between safe and dangerous concentrations of radon, but the annual average indoor radon concentration above which it is necessary to take measures to reduce radon). It differs from action level (the radon concentration above which, if it is found that the measured concentration is greater than defined, gives recommendations to take measures for its reduction). The new concept is incorporated in two new documents. One is developed at the International Atomic Energy Agency (IAEA) [2]. In this new BSS (international Basic Safety Standards), radon is placed in several topics, but the most important is requirements of 50 (Requirement 50: Public exposure because of radon indoors). It defines the reference level, in dwellings of high occupational factors, which must not exceed $300 \text{ Bq}\cdot\text{m}^{-3}$. Assuming equilibrium factor for radon 0.4 and the annual occupational factors of 7000 h, the reference level of $300 \text{ Bq}\cdot\text{m}^{-3}$ corresponds to an annual effective dose of 10 mSv, with dose conversion factor (DCF) of 7.5 mSv per WLM (working level month). The request 52 (Requirement 52: Exposure in workplaces) defines the reference level for radon in workplaces of $1000 \text{ Bq}\cdot\text{m}^{-3}$. As the occupation factor for 2000 h with the same factor to balance radon of 0.4 leads to the same effective annual dose of 10 mSv. Important conclusions are based on the collected data and performed radon risk maps, the country has to decide and implement adequate control of the indoor radon, to inform the public and other stakeholders and, finally, to establish and implement Radon Action Plan (RAP).

The second document is EU Directive 2013/59 [3]. In the article 74: Indoor exposure to radon, writes the similar as in the new BSS, accept that the reference level shall not exceed $300 \text{ Bq}\cdot\text{m}^{-3}$ for the all indoor environment, living and workplaces. Article 105 defines RAP to be developing in member states: The action plan shall take into account the issues set out in Annex XVIII and be updated on a regular basis. Annex XVIII defined 14 items to consider in preparing the national RAP. In the case of Serbia, the first steps towards RAP are described in the next section.

National radon action plan in Serbia

Serbia did not have a systematic approach to the radon problem. In this sense, there were individual initiatives and research activities dealing with radon:

University of Novi Sad, Faculty of Science, Department of Physics, Chair of Nuclear Physics, Novi Sad

Radon mapping of Autonomous Province of Vojvodina [6], long-term and short-term measurements of radon concentration in soil, water and air using passive devices, active device RAD7, exhalation and diffusion measurements [7], charcoal canisters with gamma spectrometric analysis [8].

University of Belgrade, Vinča Institute of Nuclear Sciences, ECE Lab Belgrade

Department for Nuclear and Plasma Physics

Mapping radon and thoron throughout south-eastern Serbia, Kosovo and Metohija parts of western Serbia [9, 10] by using different passive devices; electrochemical etch track detectors in a specially designed and built in laboratory [11]; developing method for radon and thoron exhalation from building material [12]; radon measurement campaigns in the schools and houses in the Sokobanja municipality [13].

Radiation and Environmental Protection Department

Active charcoal detectors are used for testing the concentration of radon in dwellings. The method of measurement is based on radon adsorption on coal and measurement of gamma radiation of radon daughters according to US EPA protocol. Based on this EPA procedure and national and international intercomparison, the laboratory developed a set of procedures for charcoal detector exposure and measurement [14, 15].

University of Belgrade, Institute of Physics Belgrade, Low-Background Laboratory for Nuclear Physics

Radon monitoring in the underground low-background laboratory with the passive and active devices [16]; radon laboratory for chemical etching of the track detectors and automatic counting of the tracks by optical microscopy [17]; modelling of the indoor radon behaviour [18].

Institute of Occupational Health of Serbia "Dr Dragomir Karajović", Center for Radiological Protection, Belgrade

Radon measurements using charcoal canisters with gamma spectrometric analysis, radon monitoring in

schools and kindergartens in the city of Belgrade from 1991 [19] and radon measurements campaigns in schools and kindergartens in Belgrade from 2010 [20].

**University of Kragujevac, Faculty of Science
Kragujevac, Institute of Physics**

Radon measurement using passive devices with chemical treatment of the track detectors and automatic scanning of the developed detectors; modelling of the behaviour of indoor radon [21]; dosimetric modelling of the effects of the inhalation of radon and its progeny in the lung [22].

Based on the great experience of research related to radon, the group of radon professionals organized Radon Forum in May 2014 and made a decision to start work on RAP in Serbia. The responsibility for the establishment and implementation of RAP is on national regulatory body: Serbian Radiation Protection and Nuclear Safety Agency (SRPNA). We started with Internet radon forum (www.cosmic.ipb.ac.rs/radon_forum), which provides an opportunity for radon professionals in Serbia to meet and discuss radon activities and plans. Also, SRPNA formed a ‘radon working group’ that will manage RAP. The organization chart of the institutions involved in RAP is shown in Fig. 1.

- Short-term plans (to the end of 2015) include
- carrying out initial representative national indoor radon survey for this purpose,
 - developing communication strategy (first basic information leaflet on radon to accompany the measurement explaining the purpose of the measurement, Internet site: <http://cosmic.ipb.ac.rs/radon/index.html>; public relation; etc.).

First national indoor radon survey in Serbia

As a first step in RAP, it is the national radon survey in Serbia planned to be done in 2015. In the cooperation with IAEA, SRPNA through radon working

group made the design of the first national radon survey in Serbia. It is well known that regarding the objective of the indoor radon survey, there are two types of survey:

- population-weighted survey by measuring indoor radon levels in randomly selected homes (to estimate the distribution of radon public exposures),
- geographically based survey where homes are randomly selected to obtain a minimum density of measurements per area unit chosen, e.g., a grid square, an administrative unit (to identify radon prone areas, radon map).

Every radon survey needs to check the representativeness (e.g. compare certain parameters in the actual sample with corresponding values in the last census). A carefully designed survey can, in principle, meet the requirements and objectives of both the types of surveys. In the case of Serbia, we choose a stratified (target population is partitioned into separated groups – STRATA) sampling design. We defined STRATA according to the administrative divisions of Serbia into districts.

In principle, our design model can be described as follows:

- SRPNA, in cooperation with the IAEA through the national project SRB9003 – Enhancing the Regulatory Infrastructure and Legislative System,
- Expert mission on National Radon Trial Survey and Raising Awareness of Key Stakeholders held in SRPNA, Belgrade, 2–4 February 2015,
- Equipment: Leasing of 6000 track-etched indoor radon detectors; the distribution of detectors across the Serbian territory should be the responsibility of SRPNA,

and relevant ministries began with the national programme for indoor radon measurements in dwellings and flats in Serbia. The aim of this programme is to determine the radiological exposure risk to radon in residential areas because of the inhalation of this gas as well as to locate areas in Serbia with high concentrations, areas with high radon potential. Within the working group on radon, the division of

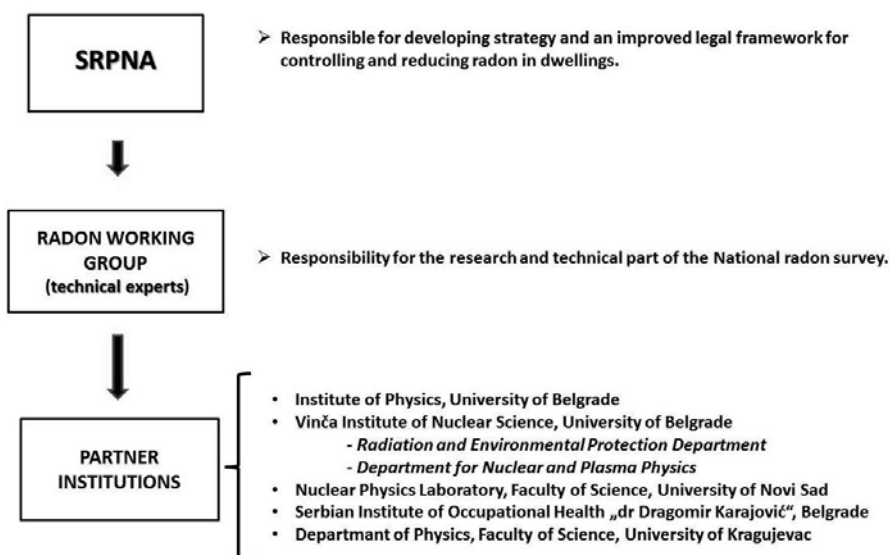


Fig. 1. Organization chart of the institutions involved in RAP.

responsibilities of individual institutions in a given set of administrative regions was established. All owners of houses and apartments (who wish to participate in the project), with the aim of determining the concentration of radon, filled predefined questionnaire on the Web site dedicated to radon in Serbia (<http://cosmic.ipb.ac.rs/radon/index.html>). In this way, they expressed interest to participate in the project. In total, 6000 detectors have been distributed during October 2015 and will be exposed in houses and apartments for six months (till April 2016). Afterwards, the detectors will be sent to an authorized laboratory to be processed, and consequently, we should get data for the first national map radon risk in Serbia. The measurement results will be presented to the owners of houses and apartments that are used for the measurement. Based on these results, in cases where radon concentration exceeds current intervention level of 200 Bq·m⁻³ for new developments or 400 Bq·m⁻³ for existing facilities, the whole set of measures that could result in a reduction of the radon concentrations and thus reduce the risk of getting lung cancer will be recommended. Additionally, all data collected for the whole of Serbia will enable the determination of the national reference level for radon. During the realization of the national programme for indoor radon measurements, we plan to perform communication strategy (first basic information leaflet on radon to accompany the measurement explaining the purpose of the measurement, internet site, public relation, public education, etc.).

Conclusions

World Health Organization declared radon as the second most important cause of getting lung cancer. Radon problem being addressed seriously, and in a number of countries, there are established national radon programme. Serbia started work on RAP in 2014, with the first step of preparing, and performed the national indoor radon survey in Serbia, planned to be done in 2015. The responsibility for the establishment and implementation of RAP is on national regulatory body: Serbian Radiation Protection and Nuclear Safety Agency. The results of national radon survey serves to evaluate the existing exposure situation and to define the next steps in establishing and developing RAP in Serbia. Also, the Serbian experience in efforts to have systematic approach to the radon issues, described in this paper, may be useful to the other countries who wish to establish their own RAP.

References

1. Darby, S., Hill, D., Auvinen, A., Barros-Dios, J. M., Baysson, H., Bochicchio, F., Deo, H., Falk, R., Forastiere, F., Hakama, M., Heid, I., Kreienbrock, L., Kreuzer, M., Lagarde, F., Mäkeläinen, I., Muirhead, C., Oberaigner, W., Pershagen, G., Ruano-Ravina, A., Ruosteenoja, E., Schaffrath Rosario, A., Tirmarche,

- M., Tomáscaronek, L., Whitley, E., Wichmann, H.-E., & Doll, R. (2005). Radon in homes and risk of lung cancer: collaborative analysis of individual data from 13 European case-control studies. *Brit. Med. J.*, *330*, 223–227.
2. International Atomic Energy Agency. (2011). *Radiation protection and safety of radiation sources: International basic safety standards Interim edition. General safety requirements Part 3*. Vienna: IAEA. Retrieved from http://www-pub.iaea.org/MTCD/publications/PDF/p1531interim_web.pdf.
3. Council of the European Union. (2014). *Council Directive 2013/59/EURATOM of 5 December 2013 laying down basic safety standards for protection against the dangers arising from exposure to ionising radiation, and repealing Directives 89/618/Euratom, 90/641/Euratom, 96/29/Euratom, 97/43/Euratom and 2003/122/Euratom*. (Official Journal of the European Union 2014; L13). Retrieved from <http://www.srbatom.gov.rs/srbatom/doc/eu-direktive/2013%2059%20eng.pdf>.
4. World Health Organization. (2009). *WHO handbook on indoor radon: a public health perspective*. Retrieved from http://www.who.int/ionizing_radiation/env/radon/en/index1.html.
5. World Health Organization. (2010). *WHO guidelines for indoor air quality: selected pollutants*. Retrieved from <http://www.who.int/indoorair/publications/9789289002134/en/index.html>.
6. Forkapić, S., Bikit, I., Slivka, J., Čonkić, Lj., Vesković, M., Todorović, N., Varga, E., Mrda, D., & Hulber, E. (2006). Indoor radon in rural dwellings of the South-Pannonian region. *Radiat. Prot. Dosim.*, *123*(3), 378–383.
7. Nikolov, J., Todorovic, N., Bikit, I., Petrovic Pantic, T., Forkapic, S., Mrda, D., & Bikit, K. (2014). Radon in thermal waters in South-East part of Serbia. *Radiat. Prot. Dosim.*, *160*(1/3), 239–243.
8. Todorović, N., Bikit, I., Vesković, M., Krmar, M., Mrda, D., Forkapić, S., Hansman, J., Nikolov, J., & Bikit, K. (2014). Radioactivity in the indoor building environment in Serbia. *Radiat. Prot. Dosim.*, *158*(2), 208–215.
9. Žunić, Z. S., Yarmoshenko, I. V., Veselinović, N., Zhukovsky, M. V., Ujić, P., Čeliković, I., Mc Laughlin, J. P., Simopoulos, S. E., Birovljev, A., Fujimoto, K., Paridaens, J., Trotti, F., Tokonami, S., Olko, P., Kozak, K., Bochicchio, F., Ramola, R., Mietelski, J. W., Jakupi, B., Milić, G., Ciotoli, G., Kelleher, K., Budzanowski, M., Sahoo, S. K., Vanmarcke, H., & Waligorski, M. P. R. (2009). Identification and assessment of elevated exposure to natural radiation in Balkan region (Serbia). *Radioprotection*, *44*, 919–925.
10. Žunić, Z. S., Janik, M., Tokonami, S., Veselinović, N., Yarmoshenko, I. V., Zhukovsky, M., Ishikawa, T., Ramola, R. C., Ciotoli, G., Jovanović, P., Kozak, K., Mazur, J., Celiković, I., Ujić, P., Onischenko, A., Sahoo, S. K., & Bochicchio, F. (2009). Field experience with soil gas mapping using Japanese passive radon/thoron discriminative detectors for comparing high and low radiation areas in Serbia (Balkan region). *J. Radiat. Res.*, *50*(4), 355–361.
11. Zunic, Z. S., Ujić, P., Nadderđ, L., Yarmoshenko, I. V., Radanović, S. B., Komatina Petrović, S., Čeliković, I., Komatina, M., & Bossew, P. (2014). High variability of indoor radon concentrations in uraniumiferous bedrock areas in the Balkan region. *Appl. Radiat. Isot.*, *94*, 328–337.
12. Ujić, P., Čeliković, I., Kandić, A., & Žunić, Z. (2008). Development of method for radon/thoron exhalation measurement. *Radiat. Meas.*, *43*(8), 1396–1401.

13. Bohicchio, F., Žunić, Z. S., Carpentieri, C., Antignani, S., Venoso, G., Carelli, V., Cordedda, C., Veselinović, N., Tollefsen, T., & Bossew, P. (2014). Radon in indoor air of primary schools: a systematic survey to evaluate factors affecting radon concentration levels and their variability. *Indoor Air*, 24, 315–326.
14. Pantelić, G., Živanović, M., Eremić Savković, M., & Forkapić, S. (2013). Radon concentration inter-comparison in Serbia. In Ž. Knežević, M. Majer, & I. Krajcar-Bronić (Eds.), *Proceedings of the Ninth Symposium of the Croatian Radiation Protection Association, 10–12. April 2013, Krk, Croatia* (pp. 193–198). Zagreb: CRPA.
15. Pantelić, G., Eremić Savković, M., Živanović, M., Nikolić, J., Rajačić, M., & Todorović, D. (2014). Uncertainty evaluation in radon concentration measurement using charcoal canister. *Appl. Radiat. Isot.*, 87, 452–455.
16. Udovičić, V., Aničin, I., Joković, D., Dragić, A., Banjanac, R., Grabež, B., & Veselinović, N. (2011). Radon time-series analysis in the Underground Low-Level Laboratory in Belgrade, Serbia. *Radiat. Prot. Dosim.*, 145(2/3), 155–158.
17. Banjanac, R., Dragić, A., Grabež, B., Joković, D., Markushev, D., Panić, B., Udovičić, V., & Aničin, I. (2006). Indoor radon measurements by nuclear track detectors: Applications in secondary schools. *Facta Universitatis*, 4, 93–100.
18. Maletić, D., Udovičić, V., Banjanac, R., Joković, D., Dragić, A., Veselinović, N., & Filipović, J. (2014). Comparison of multivariate classification and regression methods for indoor radon measurements. *Nucl. Technol. Radiat. Prot.*, 29, 17–23.
19. Eremić-Savković, M., Pantelić, G., Tanasković, I., Vuletić, V., & Javorina, Lj. (2002). Concentration of radon in apartments on the territory of Belgrade in period 1997–2001. *Arch. Toxicol. Kinet. Xenobiot. Metab.*, 10(1/2), 195–197.
20. Arsić, V., Ilić, J., Bogojević, S., Tanasković, I., Eremić-Savković, M., & Javorina, Lj. (2014). Assessment of the effective radon dose, measured in schools and kindergartens in Belgrade during 2012 and 2013. In *Proceedings of Second East European Radon Symposium (SEERAS), May 27–30, 2014, Niš, Serbia* (pp. 17–20).
21. Stevanovic, N., Markovic, V., & Nikezic, D. (2010). Relationship between deposition and attachment rates in Jacobi room model. *J. Environ. Radioact.*, 101(5), 349–352.
22. Jovanovic, B., Nikezic, D., & Stevanovic, N. (2011). Applied mathematical modeling for calculating the probability of the cell killing per hit in the human lung. *J. Radioanal. Nucl. Chem.*, 290(3), 607–613.



The use of multivariate analysis of the radon variability in the underground laboratory and indoor environment

Jelena Filipović,
Dimitrije Maletić,
Vladimir Udovičić,
Radomir Banjanac,
Dejan Joković,
Mihailo Savić,
Nikola Veselinović

Abstract. The paper presents results of multivariate analysis of variations of radon concentrations in the shallow underground laboratory and a family house, depending on meteorological variables only. All available multivariate classification and regression methods, developed for data analysis in high-energy physics and implemented in the toolkit for multivariate analysis (TMVA) software package in ROOT, are used in the analysis. The result of multivariate regression analysis is a mapped functional behaviour of variations of radon concentration depending on meteorological variables only, which can be used for the evaluation of radon concentration, as well as to help with modelling of variation of radon concentration. The results of analysis of the radon concentration variations in the underground laboratory and real indoor environment, using multivariate methods, demonstrated the potential usefulness of these methods. Multivariate analysis showed that there is a potentially considerable prediction power of variations of indoor radon concentrations based on the knowledge of meteorological variables only. In addition, the online system using the resulting mapped functional behaviour for underground laboratory in the Institute of Physics Belgrade is implemented, and the resulting evaluation of radon concentrations are presented in this paper.

Key words: multivariate analysis • radon variability

Introduction

The research of the dynamics of radon in various environments, especially indoors, is of great importance in terms of protection against ionizing radiation and in designing of measures for its reduction. Research of radioactive emanations (of radon (^{222}Rn) and thoron (^{220}Rn)) are in the domain of radiation physics, but since a few decades ago, subject of radioactive emanation involves many other scientific disciplines, thus giving a multidisciplinary character to this research. Published results and development of many models to describe the behaviour of indoor radon indicate the complexity of this research, especially with models for the prediction of the variability of radon, simply because the variability depends on large number of variables. Large number of factors (such as local geology, permeability of soil, building materials used to build the buildings as well as the habits of people) impact the variation of radon, and therefore, it is important to study their correlation. In this paper, the results of correlative analysis of indoor radon and meteorological variables are presented. Furthermore, the results of multivariate classification and regression analysis is presented. More details of this study can be found in [1].

Indoor radon variation depends significantly on large number of factors, which include the local ge-

J. Filipović, D. Maletić, V. Udovičić✉, R. Banjanac,
D. Joković, M. Savić, N. Veselinović
Institute of Physics Belgrade,
University of Belgrade,
118 Pregrevica Str., 11080 Belgrade, Serbia,
E-mail: udovicic@ipb.ac.rs

Received: 4 January 2016
Accepted: 24 March 2016

ology, soil permeability, building materials, lifestyle characteristics and meteorological variables. In order to analyse the dependence of radon variation on multiple variables, multivariate analysis needs to be used.

The demand for detailed analyses of large amount of data in high-energy physics resulted in wide and intense development and usage of multivariate methods. Many of multivariate methods and algorithms for classification and regression are already integrated into the analysis framework ROOT [2], more specifically, into the toolkit for multivariate analysis (TMVA [3]). Multivariate analysis toolkit is used to create, test and apply all available classifiers and regression multivariate methods implemented in the TMVA in order to find methods that are the most appropriate and yield maximum information on the dependence of indoor radon concentrations on the multitude of meteorological variables. Classification methods are used to find out if it is possible to classify radon concentrations into low and high concentrations, using arbitrary cut value for radon concentrations. Regression methods are used as a next step with a goal to find out which regression method can, if any, on the basis of input meteorological variables only, give an output that would satisfactorily close match the observed variations of radon concentrations. The output of usage of multivariate regression analysis methods is mapped functional behaviour, which can be used to evaluate the measurements of radon concentrations using input meteorological variables only. The prediction of radon concentrations can be an output of mapped function when the prediction of input meteorological variables exists.

Short-term radon measurements in laboratory and real environment

Depending on the integrated measurement time, methods of measurement of radon concentrations in air may be divided into long-term and short-term ones. For the measurements of radon concentration presented in this paper, the SN1029 radon monitor (manufactured by the Sun Nuclear Corporation, NRSB approval-code 31822) has been used as active, short-term measurement device. The device consists of two diffused junction photodiodes as a radon detector and is furnished with sensors for temperature, barometric pressure and relative humidity. The user can set the measurement intervals from 30 min to 24 h. It was set to record simultaneously the radon concentration, temperature, atmospheric pressure and relative humidity.

For the purposes of determining the best multivariate methods to use in the analysis, the results are obtained using radon monitor are from measurements in two locations, the Low-Background Laboratory for Nuclear Physics in the Institute of Physics in Belgrade and in a family house.

The underground Low-Background Laboratory for Nuclear Physics is selected for measurement and analysis because routine measurements in this labo-

ratory require low levels of radon concentration with minimum temporal variations. Low-background laboratory is located on the right bank of the river Danube in the Belgrade borough of Zemun, on the grounds of the Institute of Physics. The ground level portion of the laboratory, at 75 m above sea level, is situated at the foot of a vertical loess cliff, about 10 m high. The underground part of the laboratory, useful area of 45 m², is dug into the foot of the cliff. Underground laboratory is surrounded with 30-cm thick concrete wall. The overburden of the underground laboratory is thus about 12 m of loess soil. Significant efforts are being made to contain the low radon concentration within the laboratory. The underground laboratory is completely lined with a hermetically sealed, 1-mm thick aluminium foil. The ventilation system maintains the overpressure of 2 mbar, so as to prevent radon diffusion from the soil. Fresh air entering the laboratory is passed through a two-stage filtering system. The first stage is a mechanical filter for dust removal. The second one is a battery of coarse and fine charcoal active filters. The concentration of radon is kept at an average value of about 10 Bq/m³.

In the Low-Background Laboratory for Nuclear Physics, radon concentrations were measured in period from 2008 to 2011 and continued later on periodically about a couple of months each year. Measurements of meteorological variables used in the analysis were recorded since 2008 and are taken from the meteorological station located 4 km from the laboratory. Measurements of radon concentrations, room temperature, atmospheric pressure and relative humidity inside the laboratory were obtained using radon monitor. The results obtained from the measurements of radon concentrations and their influence on gamma and cosmic ray measurements in the laboratory were published in several articles in international scientific journals [4–6].

The family house selected for the measurements and analysis of variations of radon concentrations is a typical house in Belgrade residential areas, with requirement of existence of cellar. House is built on limestone soil. Radon measurements were carried out in the living room of the family house, which is built of standard materials (brick, concrete, mortar) and isolated with styrofoam. During the period of measurements (spring–summer), the house was naturally ventilated and air conditioning was used in heating mode at the beginning of the measurement period. During the winter period measurements, the electrical heating was used in addition to air conditioning. Measured radon concentrations, room temperature, atmospheric pressure and relative humidity inside the house were obtained using radon monitor. Values of meteorological variables in measurement period were obtained from an automatic meteorological station located 400 m from the house in which the measurement was performed. We used the following meteorological variables: external air temperature, pressure and humidity, solar radiation, wind speed at a height of 10 m above ground, precipitation, evaporation and temperature and humidity of the soil at a depth of 10, 20, 30 and 50 cm.

Correlation and regression analysis of the results

All multivariate methods implemented in the TMVA are used in our search. All multivariate methods in TMVA belong to the family of 'supervised learning' algorithms [1]. All methods make use of training events, for which the desired output is known, to determine the mapping function that either describes a decision boundary (classification) or an approximation of the underlying functional behaviour defining the target value (regression). Every MVA methods see the same training and test data. The two best performing multivariate methods for our purposes are boosted decision trees (BDT) and artificial neural networks (ANN).

The determination of correlation coefficients between measured radon concentration and meteorological variables serves as a good tool for identifying the variables with strongest correlation, which are not excluded from the analysis later on. Also, correlation coefficient tables gives a good overview of input data and their intercorrelations. In Fig. 1, the correlation matrix of linear correlation coefficients as an overview of intercorrelations of measured radon concentration and all input meteorological variables are shown for underground laboratory. The input variables in case of analysis of underground laboratory are atmospheric pressure, temperature and humidity in laboratory (P_{mm}, T_{mm}, H_{mm}) and outdoor (P, T, H) and differences in measured values of pressure ($P - P_{mm}$), temperature ($T - T_{mm}$) and humidity ($H - H_{mm}$) in laboratory and outdoor. Input meteorological variables in case of family house are the same as the list of measured meteorological variables from nearby meteorological station, with the addition of differences in temperature ($T - T_{mm}$) and humidity ($H - H_{mm}$) from indoor and outdoor values, where indoor measurements results were obtained using radon monitor.

Multivariate methods within the package TMVA in ROOT can search for best multivariate approximation of functional behaviour for the classification function of radon concentration depending on meteorological variables. In the analysis, several mul-

Linear correlation coefficients in %

Radon	17	4	25	14	5	1	13	5	-14	100
H-H _{mm}	-81	13	-73	-94	10	79	-94	-8	100	-14
P-P _{mm}	9	-15	13	1	15			100	-8	5
T-T _{mm}	80	-14	77	99	-14	-68	100		-94	13
H	-43	3	-18	-65	3	100	-68		79	1
P	-4	95	-12	-13	100	3	-14	15	10	5
T	86	-13	80	100	-13	-65	99	1	-94	14
H _{mm}	84	-17	100	80	-12	-18	77	13	-73	25
P _{mm}	-7	100	-17	-13	95	3	-14	-15	13	4
T _{mm}	100	-7	84	86	-4	-43	80	9	-81	17

T_{mm} P_{mm} H_{mm} T P H $T - T_{mm}$ $P - P_{mm}$ $H - H_{mm}$ $Radon$

Fig. 1. Correlation matrix with linear correlation coefficients as an overview of radon and meteorological variables intercorrelations in case of the Low-Background Laboratory for Nuclear Physics.

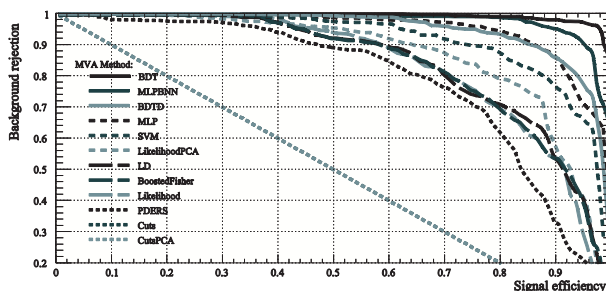


Fig. 2. ROC curve for all multivariate methods in case of house measurements.

tivariate methods were tested, and best performed method was BDT. This can be seen by presenting the receiver operating characteristics (ROC) curve for all tested multivariate methods in case of house measurements (Fig. 2). The BDT method has the highest value of integrated ROC function.

BDT has proven to be the most effective method for the classification of radon concentrations in case of data obtained from the house as well as those obtained from measurements in the Low-Background Laboratory for Nuclear Physics.

The next step in the analysis is the regression analysis, which is the way of finding a mapped function behaviour of dependence of radon concentrations and meteorological input variables. The regression analysis was done using the TMVA packages, already used in classification analysis, and for the same set of measured radon concentration and meteorological variables in underground laboratory and a family house in Serbia. Multivariate method BDT was found to be the best suited for regression analysis also, as was the case in classification analysis.

The data of measured radon concentration in house and BDT evaluated values, using only the values of meteorological variables, without the knowledge of measured values (i.e. in the testing set of multivariate analysis), is presented for comparison in Fig. 3.

One of the possible application of having resulting mapped function, given by multivariate regression analysis, is to have prediction of radon concentration values (evaluated) based on meteorological variables alone. The online application of the regression multivariate analysis can be imple-

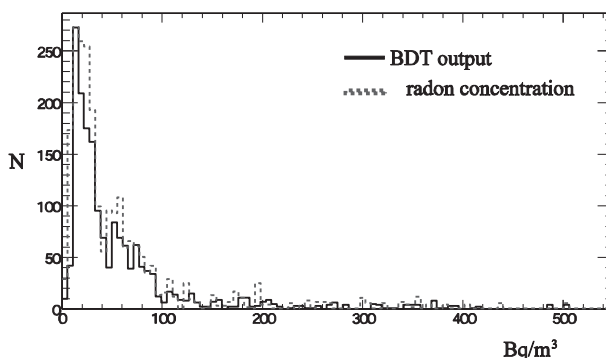


Fig. 3. BDT evaluated (predicted) values of radon concentrations based on meteorological variables using regression analysis within TMVA packages in house (left) and measured values (right).

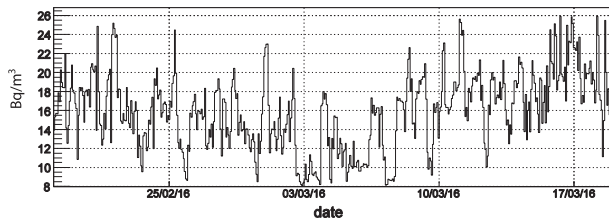


Fig. 4. BDT evaluated (predicted) values of radon concentration, based on meteorological variables alone of underground laboratory posted online and updated daily.

mented, as the one posted online for evaluation (and prediction) based on meteorological variables alone (Fig. 4).

Limitation of multivariate methods

As the multivariate methods used in the analysis are ‘supervised learning’ algorithms, the performance of the main result of multivariate analysis, the resulting mapped functional behaviour, depends on learning process. Limitation of multivariate analysis in the analysis of radon dependence on meteorological variables are coming from small number of measurements used in learning process, unlike the great number of measurements in high-energy physics experiments. As the next logical step in multivariate analysis presented in this paper should be inclusion of variables such as local geology, permeability of soil, building materials used to build the buildings as well as the habits of people, the requirement for efficient multivariate analysis is to have many measurements in many different houses. Many measurements would help to get good mapped functional behaviour, as opposed to possible existence of theoretical modelling that is independent on number of measurements. In this sense, if the number of measurements is not great, multivariate analysis can be used only as hell to indicate which variables are more important to be used in theoretical modelling, for comparison of mapped and modelled functions, and modelled function test. Another important limitation of multivariate analysis is that no ‘straightforward’ interpretation of mapped functional behaviour is possible, or simply, the mapped function is a ‘black box’. This comes from the fact that the error minimization in learning algorithms, while mapping the functional behaviour, is an important part in learning process.

Conclusions

The paper presents the results of multivariate analysis of variations of radon concentrations in the shallow underground laboratory and a family house, depending on meteorological variables only. This test of multivariate methods, implemented in the

TMVA software package, applied to the analysis of the radon concentration variations connection with meteorological variables in underground laboratory (with ventilation system turned on and off) and typical house in Serbia, demonstrated the potential usefulness of these methods. It appears that the method can be used for the prediction of the radon concentrations, on the basis of predicted meteorological variables. The next step in multivariate analysis presented in this paper should be inclusion of variables such as local geology, permeability of soil, building materials used to build the buildings as well as the habits of people. The requirement for efficient multivariate analysis is to have many measurements in many different houses, which makes multivariate method very useful only when having many measurement, for instance, during radon mapping campaigns. Many measurements would help to get good mapped functional behaviour, as opposed to possible existence of theoretical modelling that is independent on number of measurements. Generally, multivariate analysis can be used to help indicate which variables are more important to be used in theoretical modelling, furthermore, for comparison of mapped and modelled functions, and modelled function test.

Another usage of the results of classification multivariate analysis presented in this paper is the implementation of online warning system for possible increased radon concentration in family houses based on meteorological variables only.

References

1. Maletić, D., Udovičić, V., Banjanac, R., Joković, D., Dragić, A., Veselinović, N., & Filipović, J. (2014). Comparison of multivariate classification and regression methods for indoor radon measurements. *Nucl. Technol. Radiat. Prot.*, 29, 17–23.
2. Hoecker, A., Speckmayer, P., Stelzer, J., Therhaag, J., Von Toerne, E., & Voss, H. (2007). TMVA – Toolkit for Multivariate Data Analysis. *PoS ACAT 040*. arXiv:physics/070303.
3. Brun, R., & Rademakers, F. (1997). ROOT – An Object Oriented Data Analysis Framework. *Nucl. Instrum. Methods Phys. Res. Sect. A-Accel. Spectrom. Dect. Assoc. Equip.* 389(1/2), 81–86.
4. Udovičić, V., Grabež, B., Dragić, A., Banjanac, R., Joković, D., Panić, B., Joksimović, D., Puzović, J., & Aničin, I. (2009). Radon problem in an underground low-level laboratory. *Radiat. Meas.*, 44, 1009–1012.
5. Udovičić, V., Aničin, I., Joković, D., Dragić, A., Banjanac, R., Grabež, B., & Veselinović, N. (2011). Radon time-series analysis in the Underground Low-Level Laboratory in Belgrade, Serbia. *Radiat. Prot. Dosim.*, 145(2/3), 155–158.
6. Banjanac, R., Udovičić, V., Dragić, A., Joković, D., Maletić, D., Veselinović, N., & Grabež, B. (2013). Daily variations of gamma-ray background and radon concentration. *Rom. J. Phys.*, 58(Suppl.), S14–S21.

10. Прилози

RAD2014 - BEST PAPERS AWARDS

<http://www.rad2014.elfak.rs/bestpapers.php>



The Second International Conference on Radiation and Dosimetry in Various Fields of Research
www.rad2014.elfak.rs

MAY 27 - 30, 2014 | FACULTY OF ELECTRONIC ENGINEERING | NIŠ | SERBIA



Gold sponsor


Silver sponsor


Awards – RAD 2014 Conference and SEERAS Symposium

The winners are awarded by not paying the conference fee for the next RAD Conference. Moreover, a Certificate will be given to the winners at the next RAD Conference.

Since we had two events with a large number of participants and a lot of high-quality papers, we have decided to give 5 awards – 2 for the best oral contributions, 1 for the best poster contribution and 2 for the best student contributions (one for oral and one for poster).

Awards for the best oral contribution go to:

Jorge Sampaio
for the contribution:
J. Sampaio, M^a. Conceição Abreu, P. Sousa, Scatter fraction with simulations. revisiting radiation scatter in x-ray imaging
and
Mikhail Zhukovsky
for the contribution:
M. Rogozina, M. Zhukovsky, A. Ekidin, M.Vasyanovich, Thoron decay products size distribution in Monazite Storage Facility

Award for the best poster contribution goes to:

Dimitrije Maletić
for the contribution:
D. M. Maletić, V. I. Udovičić, R. M. Banjanac, D. R. Joković, A. L. Dragić, N. B. Veselinović, J. Filipović, Correlative and multivariate analysis of increased radon concentration in underground laboratory

Awards for the best student contribution go to:

Karolina Krefft
for the contribution:
K. Krefft, B. Drogoszewska, J. Kamińska, M. Juniewicz, G. Wołakiewicz, I. Jakacka, B. Ciesielski, Application of EPR dosimetry in bone for verification of doses in radiotherapy patients
and
Ziyafer Gizem Portakal
for the contribution:
Z. G. Portakal, C. Tunali, A comparative treatment planning study of intensity modulated radiotherapy and 3-d conformal radiotherapy for head & neck cancer

We congratulate to all the nominees and to all the awarded contributions and participants, and are looking forward to see you at the next RAD Conference!

Nominations for:

I – Best oral contribution

1. T. Wysokinski, G. Okada, G. Belev, C. Koughia, A. Edgar, L. D. Chapman, J. Ueda, S. Tanabe, S. Kasap, QA dosimetry for the biomedical imaging and therapy facility at CLSI
2. A. Y. Kilcar, F. Z. Biber Muftuler, H. Enginar, E. I. Medine, V. Tekin, P. Unak, A novel brain imaging agent including Alzheimer's disease diagnosis potential: ^{99m}Tc-BIOQUIN-HMPO
3. A. Esposito, B. Caccia, C. Andenna, GEANT4 simulation of a helical tomotherapy unit
4. G. Žauhar, S. Jurković, Đ. Smilović Radojčić, D. Dobravac, Testing of ultrasound trasducers by use of thermocromic tile
5. B. Obryk, P. Bilski, K. Hodyr, P. Mika, High-level TL dosimetry for high-temperature environment
6. M. Cuijić, J. Petrović, M. Đorđević, R. Dragović, S. Dragović, The radiological hazard due to



Rad 2015
SEERAS
NEWS
WELCOME
ABOUT CONFERENCE
FIRST CALL
TOPICS
RAD 2012
VENUE | CONTACT
APL
ABSTRACTS
TITLE LIST
SCHEDULE
PROGRAM
STATISTICS
PAPERS
IMPORTANT DATES
SCIENTIFIC COMMITTEE
ORGANIZING COMMITTEE
INVITED LECTURES
FEE
WELCOME TO NIS
ACCOMMODATION
SHUTTLE SERVICE
VISAS
REGISTRATION
SPONSORS & EXHIBITORS
CONFERENCE MATERIALS
BEST PAPER AWARDS
GALLERY
GUESTBOOK
PROJECT PROPOSALS
LINKS & EVENTS
PARTICIPANTS



Way to go, Dimitrije!

R^G

With new reads,
your research items
Were the **most read**
research items from
your institution

Achieved in 2020:

January 6, 13, 27, February 3

Achieved in 2019:

December 2, 9, 23, 30

November 4, 11, 18, 25

October 7, 21, 28,

September 2, 9, 16, 23, 30,

August 5, 12, 19, July 29,

June 3, 10, May 13, 20, 27,

Apr 1, 8, 15, 22,

Mar 4, 11, 18, 25,

Feb 5, 11, 18, 25, Jan 28

Achieved in 2018:

Jun 4, 11, 18,

May 11, 21, 28

With new reads, your research items were
the **most read** research items

from **Serbia**

Achieved in 2019

October 14,

July 1, 8, 15, 22,

June 17, 24,

May 6

Apr 29



Subject: Invitation to future MEMOs ...

From: "Long, Kenneth R" <k.long@imperial.ac.uk>

Date: 1/22/19, 5:48 PM

To: Maletic Dimitrije <maletic@ipb.ac.rs>, Kyberd Paul
<Paul.Kyberd@brunel.ac.uk>

CC: Dr Rogers Chris <Chris.Rogers@stfc.ac.uk>, Franchini Paolo
<p.franchini@warwick.ac.uk>

Dimitrije, Paul — Hi —

This is to invite you to future meetings of the MEMO — we meet once per month on a Tuesday at 15:30 UK time. The reason for the invite is that we need to be sure to address issues that arise related to the GRID processing as it affects MICE.

I hope you don't mind!

With best wishes ...

Ken

Kenneth Long

[EMail: K.Long@Imperial.AC.UK](mailto:K.Long@Imperial.AC.UK)

Mobile: work : +44-(0)7824 560302

home: +44-(0)7890-595138

MICE Experiment Management Office

Membership

- Spokesperson: K. Long (Chair)
- Deputy: A. Bross
- Experimental Integration Scientist: P. Hodgson
- Operations Coordinator: S. Boyd
- Physics Coordinator: C. Rogers
- Software and Computing Coordinator: D. Rajaram
- Co-opted:
 - Project Manager: C. Whyte
 - P. Kyberd, D. Maletic

MICE Experiment Management Office
Membership
Organisation
Mailing list
Meetings:
Reviews:
Documents:
Uplinks:

Organisation

- MEMO organigram: [MEMO.pdf](#)
- Operations organigram: [Ops.pdf](#)
- Software and computing organigram: [SWandC.pdf](#)
- Physics and analysis organigram: [Physics1.pdf](#)

Mailing list

- mice-memo_at_jiscmail.ac.uk

Meetings:

- 2019: joint MEMO/MIPO -- or MEMO alone
 - [2020-01-07](#)
 - [2019-07-23](#)
 - [2019-06-11](#)
 - [2019-03-12](#)
 - [2019-02-12](#)
 - [2019-01-22](#)
- [2018](#)
- [2017](#)
- [2016](#)
- [2015](#)
- [2014](#)
- [2013](#)

Reviews:

- **2017: Tracker s/w review:**
 - Meetings:
 - [Meeting 1, 2017-04-27](#)
 - [Meeting 2, 2017-05-26](#)
 - [Meeting 3, 2017-06-19](#)
 - [Meeting 4, 2017-07-19](#)
 - [Meeting 5, 2017-08-02](#)
 - [Meeting 6, 2017-08-16](#)
 - [Meeting 7, 2017-09-08](#)
 - [Meeting 8, 2017-11-01](#)
- [2016/17: Controls and monitoring review](#)

Documents:

- **2016:**
 - *MEMO 2016(01):* [MICE bimonthly project update 7](#)
- **2015:**
 - *MEMO 2015(01):* [Response to feedback from the RLSR panel and the MPB](#)

Uplinks:

[Back to Collaboration](#)

[Back to Governance](#)

[MEMO.pdf](#) (17.6 KB) Long, Kenneth, 29 May 2014 22:48

[Physics1.pdf](#) (41.9 KB) Long, Kenneth, 29 May 2014 23:03

[SWandC.pdf](#) (40.2 KB) Long, Kenneth, 29 May 2014 23:05

[Ops.pdf](#) (82.6 KB) Long, Kenneth, 29 May 2014 23:12

**DECISIONS
OF THE 4th JOINT COORDINATION COMMITTEE
OF THE MINISTRY OF EDUCATION, SCIENCE AND TECHNOLOGICAL
DEVELOPMENT
OF THE REPUBLIC OF SERBIA
AND THE JOINT INSTITUTE FOR NUCLEAR RESEARCH
8th February 2017, Dubna-Belgrade**

Participants from Serbia:

Dr. S. Petrović –Principal Research Fellow, Vinča Institute of Nuclear Sciences, Belgrade

Dr. Lj. Simić – Principal Research Fellow, Institute of Physics, Belgrade

Dr. M. Aničić Urošević – Senior Research Associate, Institute of Physics, Belgrade

Dr. Dimitrije Maletić – Senior Research Associate, Institute of Physics, Belgrade

Participants from JINR:

Prof. R. Lednicky – Vice Director

Prof. S. Pakuliak – Director of the University Centre

Dr. D. Kamanin – Deputy Chief Scientific Secretary

Dr. O. Culicov – Deputy Director, Frank Laboratory of Neutron Physics

Prof. V. Scuratov – Division Head, Laboratory of Nuclear Reactions

Mrs. Yu. Polyakova – Coordinator, Department of International Cooperation

On 8 February 2017, the session of the 4th Joint Coordination Committee (JCC) was held as the video conference, the participants were present in JINR, Dubna, and in Vinča Institute of Nuclear Sciences, Belgrade. During this meeting, the Committee discussed the status and the main tasks of the cooperation, financial issues and the next steps. The representatives from Serbia and JINR (hereinafter also referred to as the “Parties”) recorded as follows.

1. Prof. Lednicky made an introduction, and the Parties confirmed the list of JCC members:
 - D. Kamanin, S. Pakuliak and O. Culicov from the JINR side;
 - S. Petrović, D. Maletić and M. Aničić Urošević from the Serbian side.Prof. R. Lednicky as well as the State Secretary of Serbia will be considered as the Heads of the Parties being available.
2. The parties endorsed the roadmap of the development of cooperation to submit it subsequently to the Government of Serbia.
3. The Parties agreed to hold the forthcoming celebration of 10 Years JINR-Serbia cooperation on 15-17 March 2017 in Belgrade. The program will include participation in Russia-Serbia EXPO, launching of the roadmap, round table with the minister, lecture of JINR director at the Serbian academy of sciences etc. JINR will assign the representative delegation including the directorate of the JINR Laboratories and the project leaders, while Serbian part will provide with a program by 1 March 2017 and secure a quorum. The celebration should attract attention to the wide perspectives of the development of the cooperation between JINR and Serbian universities and research organizations.
4. The parties concluded that it is necessary to foster the new cooperation lines (IT, Radiobiology, gamma-activation). Both parties agreed to identify the respective experts on new cooperation lines by celebration or during it.

Одељење Друштва физичара Србије за научна истраживања и високо образовање

Одсеци Одељења НИВО ДФС

Братислав Обрадовић, председник, obrat@ff.bg.ac.rs
Горан Ђорђевић, потпредседник, gorandj@junis.ni.ac.rs

1. Одсек за квантну и математичку физику (7)

Милан Дамњановић, ФФ, председник, yqoq@afrodita.rcub.bg.ac.rs
Татјана Вуковић, ФФ, tanja37@afrodita.rcub.bg.ac.rs
Мирољуб Дугић, ПМФ Крагујевац, dugic@kg.ac.rs
Ненад Милојевић, ПМФ Ниш, nenad81@pmf.ni.ac.rs
Милан Пантић, ПМФ Нови Сад, mpantic@df.uns.ac.rs
Бранислав Цветковић, ИФ, branislav.cvetkovic@ipb.ac.rs
Далибор Чевизовић, Винча, cevizd@vinca.rs

2. Одсек за физику језгра, елементарних честица и основних интеракција (8)

Петар Аџић, ФФ, председник, adzic@ff.bg.ac.rs
Иванка Божовић-Јелисавчић, Винча, ibozovic@vinca.rs
Драгољуб Димитријевић, ПМФ Ниш, ddrag@pmf.ni.ac.rs
Димитрије Малетић, ИФ, dimitrije.maletic@ipb.ac.rs
Јована Николов, ПМФ Нови Сад, jovana.nikolov@df.uns.ac.rs
Воја Радовановић ФФ, rvoja@ff.bg.ac.rs
Светислав Савовић, ПМФ Крагујевац, savovic@kg.ac.rs
Ковиљка Станковић, ЕТФ, kstankovic@etf.bg.ac.rs

3. Одсек за астрономију и астрофизику (9)

Лука Поповић, АО, председник, lpopovic@aob.bg.ac.rs
Весна Борка Јовановић, Винча, vborka@vinca.rs
Драган Гајић, ПМФ Ниш, dgaja@junis.ni.ac.rs
Мирослав Мићић, АО, micic@aob.rs
Тијана Продановић, ПМФ Нови Сад, prodanvc@df.uns.ac.rs
Владимир Срећковић, ИФ, vladimir.sreckovic@ipb.ac.rs
Саша Симић, ПМФ Крагујевац, ssimic@kg.ac.rs
Зорица Цветковић, АО, zcvetkovic@aob.bg.ac.rs
Кристина Чајко, ПМФ Нови Сад,

4. Одсек за физику кондензоване материје и статистичку физику (9)

Антун Балаж, ИФ, председник, antun@ipb.ac.rs , antun.balaz@scl.rs
Наташа Бибић, Винча, natasabi@vinca.rs
Ивица Брадарич, Винча, bradaric@vinca.rs
Владимир Миљковић, ФФ, miljko@ff.bg.ac.rs
Милица Павков Хрвојевић, ПМФ Нови Сад, milica@df.uns.ac.rs
Јована Гојановић, ЕТФ, jovana@etf.bg.ac.rs
Ђорђе Спасојевић, ФФ, djordjes@ff.bg.ac.rs

Subject: URGENT REPLY DUE: a MICE contribution of yours at COOL 2017?

From: Vittorio Palladino <palladin@na.infn.it>

Date: 8/24/17, 3:54 PM

To: Mariyan.Bogomilov@CERN.CH, P.Hodgson@SHEFFIELD.AC.UK, Maletic Dimitrije <maletic@ipb.ac.rs>

CC: mauchida <m.a.uchida@imperial.ac.uk>, Ken Long <K.Long@Imperial.AC.UK>, Daniel Kaplan <kaplan@iit.edu>

Dear Dimitrije, Mariyan, Paul,

would you be in condition to be one of the four champions presenting MICE results at COOL 2017

<https://indico-jsc.fz-juelich.de/event/48/> ?

If so, would you have a preference for one of the three abstracts below?

The same three talks are being prepared for NuFact 2017 by C. Hunt, J. Nugent and F. Drielsma. So your task would not be so difficult. NB each of them will rehearse his talk at the MICE VC of Sep 7.

Our fourth presentation at COOL 2017 will precede these three and will be a general introduction to MICE also in preparation (by Melissa) for Sep 7.

Please reply literally as soon as possible. Especially if your answer had unfortunately to be negative.

Vittorio
for the MICE Speakers Bureau

- >
- > 2) Recent results from MICE on multiple Coulomb scattering and energy
- > loss
- >
- > Multiple coulomb scattering and energy loss are well known phenomena
- > experienced by charged particles as they traverse a material and
- > energy loss is a similarly well studied phenomenon for particles in
- > matter. However, from recent measurements by the MuScat
- > collaboration, it is known that the available simulation codes,
- > specifically GEANT4, overestimate the scattering of muons in low Z
- > materials. This is of particular interest to the Muon Ionization
- > Cooling Experiment (MICE) collaboration which has the goal of

COOL 2017

from Monday, 18 September 2017 at **08:30** to Friday, 22 September 2017 at **18:00** (Europe/Berlin)
at **Gustav-Stresemann-Institut, Bonn**

Langer Grabenweg 68 D-53175 Bonn

Description News:

- [Dieter-Möhl-Medal 2017 for Prof. Takeshi Katayama](#)
- [Dieter-Möhl-Medal 2017 for Dr. Markus Steck](#)
- [Dieter-Möhl-Award 2017 for Dr. Vsevolod Kamerzhiev](#)
- [Conference Photos](#)

Dear Colleagues,

we are delighted to invite you to join us for the 11th bi-annual COOL workshop on the 18th to 22nd of September 2017 at the Gustav-Stresemann-Institute Bonn. This year's workshop will be touching on topics from all across the field of beam cooling, including:

- electron cooling
- stochastic cooling
- muon cooling
- cooled beam dynamics
- new concepts and theoretical advancements in beam cooling
- facility status updates and beam cooling reviews

There will be lots of opportunity to gather and exchange thoughts, ideas and opinions in a relaxed environment. We would like to invite anyone from the field, accelerator physicists, engineers and students, to participate in this year's event. There will be oral presentations, both invited and contributed, as well as poster sessions during the week. Conference Proceedings will be published electronically on JACoW a couple of weeks after the workshop.

There will be an option for accommodation at the Gustav-Stresemann-Institut. If you would like to reserve a room there please indicate so during your registration. The price will be 73€ per person and night including breakfast. If you are arriving by car, there is parking available at the rate of 8€ per day for hotel guests. The workshop will also feature a banquet to facilitate informal exchange and gathering. Please let us know whether you would like to attend on the registration form.

The workshop fee will be 450€ per person. This will include the conference dinner as well as full board (lunch and dinner). It is to be paid in advance electronically. After registration you will be contacted by Forschungszentrum Jülich with instructions how to pay. Both credit card payment as well as bank transfer will be possible.

For those colleagues who need to apply for a visa we are happy to provide a letter of invitation on [request](#).

We hope to see you all in September.


The organisation committee.

Registration and abstract submission are now open.

Please register by September 8th. Abstracts are due September 8th and contributions to the proceedings must be submitted by September 18th.

Conference fee announced: 450€





Hotel rate announced: 73€ per person and night

Material: 






[Go to day](#)

Monday, 18 September 2017

10:00 - 11:00	Registration
11:00 - 11:30	Coffee Break
11:30 - 12:50	Registration
13:00 - 14:00	Lunch Break
14:00 - 16:00	Muon I
	Convener: Dieter Prasuhn
14:00	Welcome 20'
	Speaker: Dieter Prasuhn

- 14:20 **MICE muon ionization cooling – progress and first results** 50'
 Speaker: M.A. Uchida
 Material: [Slides](#) 
- 15:10 **Measurement of phase-space density evolution in MICE** 50'
 Speaker: D. Maletic
 Material: [Slides](#) 
- 16:00 - 16:30 Coffee Break
- 16:30 - 17:50 Muon II
 Convener: Yuhong Zhang
- 16:30 **Recent results from the study of emittance evolution in MICE** 40'
 Speaker: M.A. Uchida
 Material: [Slides](#) 
- 17:10 **Recent results from MICE on multiple Coulomb scattering and energy loss** 40'
 Speaker: D. Maletic
 Material: [Slides](#) 

Tuesday, 19 September 2017

- 09:00 - 11:00 E-Cooling I / L-Cooling
 Convener: Markus Steck
- 09:00 **Low Energy Cooler for NICA Booster** 40'
 Speaker: Alexander Bubley
 Material: [Slides](#) 
- 09:40 **Scaling Laser Cooling of Ion Beams towards High Beam Energies** 40'
 Speaker: M.H. Bussmann
 Material: [Slides](#) 
- 10:20 **Electron cooling at COSY – status and perspectives** 40'
 Speaker: Vsevolod Kamerzhiev
 Material: [Slides](#) 
- 11:00 - 11:30 Coffee Break
- 11:30 - 13:00 E-Cooling II
 Convener: Jürgen Dietrich
- 11:30 **The High Voltage cooler for NICA, Status and Ideas** 30'
 Speaker: Vladimir Borisovich Reva
 Material: [Slides](#) 
- 12:00 **Model Development for the Automated Setup of the 2 MeV Electron Cooler Transport Channel** 30'
 Speaker: Arthur Johannes Halama
 Material: [Slides](#) 
- 12:30 **Status of the Turbine Concept for Relativistic electron coolers** 30'
 Speaker: Kurt Aulenbacher
 Material: [Slides](#) 
- 13:00 - 14:00 Lunch Break
- 14:00 - 17:50 Poster
- 14:00 **Beam Tracking Studies of Electron Cooling in ELENA** 3h50'
 Speaker: Javier Resta-López
- 14:00 **Towards Laser Cooling of Relativistic $^{16}\text{O}^{5+}$ Ion Beams at the CSR** 3h50'
 Speaker: Hanbing Wang
- 14:00 **Muon Cooling Research at Fermilab** 3h50'
 Speaker: David Vincent Neuffer
- 14:00 **Stochastic cooling theory based on Langevin equations** 3h50'
 Speaker: Nikolay Shurkhno
- 14:00 **Emittance Measurement of Cooled Beams** 3h50'

Talk on bulk MC production at MPB ...

Subject: Talk on bulk MC production at MPB ...
From: Kenneth Long <k.long@imperial.ac.uk>
Date: 2/23/17, 9:06 AM
To: Dimitrije Maletic <maletic@ipb.ac.rs>
CC: Durga Rajaram <durga@fnal.gov>, Dr Chris Rogers
<Chris.Rogers@stfc.ac.uk>

Dimitrije,

I have been working on the agenda for teh next MICE Project Board (where we report on the project to the funders). One issue that they have pressed us on in the past is the MC processing. We're now OK with that thanks to your work to make batch production on the grid.

Would you be willing to explain the way we do the processing and demonstrate that this is not an issue for the MICE analysis? The talk will be at RAL on 07Mar17.

I do hope you will be able to do this!

K

Kenneth Long
*E*Mail: K.Long@Imperial.AC.UK
*M*obile: work : +44-(0)7824 560302
*h*ome: +44-(0)7890-595138

MICE Project Board and Resource Loaded Schedule Review, March 2017

[Back](#)

Documentation

- **Resource Loaded Schedule Review:**
 - [Resource Loaded Schedule, costs and risks to complete MICE](#)
- **MICE Project Board:**
 - [MICE report to the MICE Project Board](#)
- **Funding Agency Committee:**
 - <http://micewww.pp.rl.ac.uk/attachments/8384/Common-Fund.pdf>
- **Supporting documents:**
 - Step IV Hydrogen Project Plan: [170307_MICE_LH2_system_plan.mpp](#)
- **Recent reviews:**
 - [UK Cost-to-Completion Review](#)
 - [Meeting 28th June 2016 - Agenda and Files can be found with this link](#)
- **Responses to "homework questions":**
 - **Q1:** *MICE Muon Beam; simulation and tuning:*
 - *Please give an example of a comparison between simulation and measured data through the beamline from the target to the EMR.*
 - *What are the physical quantities used in the comparison? (Phase-space plots and what else?)*
 - *What are the parameters that are used in fitting the optics tuning data? (For example initial particle distribution, magnet settings, absorber settings, et cetera?)*
 - *How are the multiple Monte Carlo and other simulations integrated together? Why are the interface locations where they are?*
 - **Q1 Response:** C. Rogers, P. Franchini, D. Rajaram: [homework-question-1.pdf](#)
 - **Q2:** *What is the capability of U.S. members of the MICE collaboration to take part in the 2017/02 cycle (from September 19 to October 27) if such a data-taking run occurs? What would be the optimum (approximate) distribution between shifters and hardware experts?*
 - **Q2 Response:** M. Palmer: [MPB_Q2_Response.pdf](#)

[Back](#)

RLSR, MPB & FAC outline agendas - 07 & 08 March 2017

Venue: Conference Room 12/13, Building R68, RAL

Tuesday, 07 March 2017 and Wednesday, 08 March 2017

RLSR & MPB-11 outline agendas

07 March 2017			
09:00-09:20	RLSR closed session - introduction		
09:20-10:00	Project overview: 01-2017-03-07-Long.pptx	K. Long	30' + 10'
10:00-10:15	Coffee		15'
10:15-12:15	RLSR presentations & questions		
10:15-10:55	Project Manager's report: 02-2017-03-07-Whyte.pdf	C. Whyte	30' + 10'
10:55-11:20	Status of the liquid-hydrogen project: 03-2017-03-07-Bayliss.pdf	V. Bayliss	20' + 5'
11:20-11:55	Completion of the US construction project: 04-2017-03-07-Bross.pptx	A. Bross	25' + 10'
11:55-12:15	MICE project in the US; completion of efforts: 05-2017-03-07-Palmer.pptx	M. Palmer	15' + 5'
12:15-13:00	Lunch		
13:00-13:30	RLSR closed session session--critical findings		
13:30-15:00	MPB: Operations, software and computing		
13:30-13:55	Commissioning and operation: 06-2017-03-07-Hodgson.pdf	P. Hodgson	20' + 5'
13:55-14:20	Operation of the magnetic channel: 07-2017-03-07-Boehm.pdf	J. Boehm	20' + 5'
14:20-14:40	Bulk production of Monte Carlo: 08-2017-03-07-Maletic_v2.pptx	D. Maletic	15' + 5'
14:40-15:00	Software and computing overview: 09-2017-03-07-Rajaram.pdf	D. Rajaram	15' + 5'
15:00-15:15	Tea		
13:30-15:00	MPB: MICE Muon Beam and MICE experiment		
15:15-15:45	Tuning the MICE Muon Beam: 10-2017-03-07-Franchini.pdf	P. Franchini	25' + 5'
15:45-16:15	Detector performance: 11-2017-03-07-Overton.pdf	E. Overton	25' + 5'

dr Tijana Prodanovic

Professor of astrophysics @ Physics Department, Faculty of Sciences

Colloquium

Welcome to Astronomy and Physics Colloquium/Seminar Page!

Colloquia are held on Fridays at 14h, at the lecture room VII at the ground floor of the Physics Department.

15. mart 2019. 14:00, amfiteatar VII, Departman za fiziku

Др Марко Војиновић, Институт за физику Београд:

Квантна гравитација — шта, како и зашто

Конструкција теорије квантне гравитације (КГ) представља један од најфундаменталнијих проблема модерне теоријске физике. У овом предавању, даћемо увод и преглед разних приступа овом проблему, са конкретним циљем да на једноставан начин објаснимо (а) зашто хоћемо да квантујемо гравитацију, (б) шта тачно ту треба да се квантује, и (в) како то може да се изведе. Продискутоваћемо разна решена и нерешена питања везана за истраживање КГ. На крају ћемо дефинисати један конкретан модел КГ, као илустрацију једног од могућих приступа истраживању КГ.

23. novembar 2018. 14:00, amfiteatar V, Departman za fiziku

Prof. dr Dragutin Mihailović, Poljoprivredni fakultet, Novi Sad:

Fizika u potrazi za skrivenim strukturama

Kao po nekom pravilu, razvoj fizike zastane ispred zida za koji su se fizičari uvek nadali da će da se is-

rističe se Ljapunovljevi eksponenti i Kolmogorovljeva kompleksnost. na kraju će se ispitati ponašanje sistema jednačina za prognozu temperature na površini i u dubljem sloju zemljišta, proisteklog iz jednačine energijskog bilansa.

PETAK 4. decembar 2015. 14:00, amfiteatar V, Departman za fiziku

MSc Arpad Toth,

Departman za fiziku, Novi Sad: Simulacija protoka krvi kroz aneurizmu abdominalne aorte: nove mogućnosti

Klinički kriterijum za predviđanje rupture aneurizme abdominalne aorte (AAA) baziran je samo na dijametru AAA. Ovaj kriterijum ne uzima u obzir kompleksne hemodinačke sile koje deluju na zid AAA kao ni mehaničke osobine zida. U okviru našeg istraživanja pokušali smo da kroz četiri primera AAA dijagnostikovana kod muškaraca starijih od 65 godina pokažemo da trodimenzioni modeli krvnih sudova rekonstruisani na osnovu podataka dobijenih kompjuterizovanom tomografijom mogu dati mnogo bolja predviđanja rupture AAA. Za matematičko modelovanje i simulacije korišćena je računarska dinamika fluida. Na ovaj način smo bili u mogućnosti da pratimo dinamičko ponašanje protoka krvi u trodimenzionom prostoru. Rezultati simulacija provereni su doplerskom ultrazvučnom tehnikom. Validnost našeg modela potvrđena je dobrim slaganjem za vrednosti brzina protoka krvi dobijenih simulacijama i izmerenih doplerskom ultrazvučnom tehnikom. Nove informacije dali su nam i proračuni *Von Mises* napona što je još jedna od novih mogućnosti u proceni potencijalne rupture zida AAA.

PETAK 27. novembar 2015. 14:00, amfiteatar V, Departman za fiziku

dr Dimitrije Maletić,

Institut za fiziku, Beograd: Neutrinska i fizika kosmičkog zračenja korišćenjem relativističkih miona

U eksperimentima detekcije neutrina postoji problem slabe interakcije neutrina i detektora. Proces jonizacionog hladjenja relativističkih miona, koji se po prvi put ispituje na eksperimentu MICE, u Rutherford Appleton Laboratoriji u okolini Oksforda, Engleska, omogućiće da se višestruko poveća broj neutrina na neutrinским detektorima. Pored toga, proces jonizacionog hladjenja miona omogućiće razvoj kolajdera mnogo manjih dimenzija nego što su potrebne za ubrzanje elektrona ili protona. Saradnici Instituta za fiziku iz Beograda članovi su MICE kolaboracije.

Izučavanje fizike kosmičkog zračenja, u Niskofonskoj laboratoriji Instituta za fiziku u Beogradu, ko-

risti metod kontinualnog snimanja spektra i odbroja plastičnih scintilatora koji su indukovani prolaskom relativističkih miona kosmičkog zračenja kroz ove detektore. Prvenstveno se izučavaju promene odbroja dobijenih prolaskom miona iz kosmičkog zračenja i veza ovih promena sa aktivnošću Sunca. Beogradska mionska stanica je jedna od većeg broja svetskih stanica koja vrši monitorisanje intenziteta kosmičkog zračenja.

PETAK 20. novembar 2015. 14:00, amfiteatar V, Departman za fiziku

MSc Marko Pavlović

Katedra za astronomiju, Matematički fakultet, Beograd: Ubrzanje čestica na udarnim talasima i njihov uticaj na hidrodinamičku i radio-evoluciju ostataka supernovih

Ostaci supernove su objekti koji nastaju nakon eksplozije supernove. Materijal izbačen u eksploziji nastavlja život kroz interakciju sa okolnom medjuzvezdanom materijom hiljadama, pa čak i do milion godina nakon eksplozije. Ostaci supernovih su kosmički akceleratori, predstavljaju glavne izvore galaktičkih kosmičkih zraka. Ovi objekti ubrzavaju čestice do visokih energija u procesu koji nazivamo difuzno ubrzanje. Koriscenjem superkompjutera i kompleksnih magnetohidrodinamičkih kodova, modeliramo ostatke supernovih i proučavamo njihovu hidrodinamičku i radio evoluciju. Efikasno ubrzanje čestica na udarnim talasima modifikuje strukturu udarnog talasa i medjuzvezdanog magnetnog polja. Evolutivne trake ostataka supernovih koristeći buduci projekti kao sto su SKA i ALMA, za procenu mnogih parametara samih ostataka ali i okolne medjuzvezdane sredine.

PETAK 13. novembar 2015. 14:00, amfiteatar V, Departman za fiziku

dr Slobodan Radošević,

Departman za fiziku, Prirodno-matematički fakultet, Novi Sad: Primena lokalne $SU(2)$ algebre na opis spinskih sistema – za ili protiv

Sistemi lokalizovanih spinova (feromagnetni, antiferomagnetni itd.) su danas zanimljivi iz mnogo brojnih praktičnih i teorijskih razloga. Zbog toga je poželjno imati teorijske alate koje omogućavaju precizno i pouzdano predviđanje njihovih termodinamičkih karakteristika. Standardne metode koje se baziraju na direktnoj analizi lokalne $su(2)$ algebre, poput Monte-Karlo simulacija ili metoda jednačina kretanja, poseduju fundamentalni nedostatak usled odsustva jasno definisanih interakcija u sistemu što može da dovede do pogrešnih interpretacija dobijenih rezultata. Sa druge strane, metod efektivnih lagranžijana se zasniva na sistematskom uračunavanju interakcija između Nambu-